



Fondo Sociale Europeo - FSE  
Programma Operativo Nazionale 2000/06  
"Ricerca, Sviluppo tecnologico ed Alta Formazione  
nelle regioni dell'Obiettivo 1" - Misura 1.1 (F.S.E)



**Università degli Studi della Calabria**

**Dottorato di Ricerca in Ingegneria Chimica e dei Materiali**

**Tesi**

**Modellistica di membrane polimeriche “high performance”  
per separazione di gas**

**Settore Scientifico Disciplinare CHIM07 – Fondamenti chimici delle tecnologie**

*Supervisor*

Dr. Elena TOCCI

Dr. Giovanni GOLEMME

*Il Coordinatore del Corso di Dottorato*

Ch.mo Prof. Raffaele MOLINARI

*Candidato*

Luana De Lorenzo

Ciclo XXII

---

*A.A. 2008-2009*



Fondo Sociale Europeo - FSE  
Programma Operativo Nazionale 2000/06  
"Ricerca, Sviluppo tecnologico ed Alta Formazione  
nelle regioni dell'Obiettivo 1" - Misura 1.1 (F.S.E)



**Università degli Studi della Calabria**

**Dottorato di Ricerca in Ingegneria Chimica e dei Materiali**

**Tesi**

**Modellistica di membrane polimeriche "high performance"  
per separazione di gas**

Settore Scientifico Disciplinare CHIM07 – Fondamenti chimici delle tecnologie

*Supervisor*

Dr. Elena TOCCI

Dr. Giovanni GOLEMME

*Il Coordinatore del Corso di Dottorato*

Ch.mo Prof. Raffaele MOLINARI

*Candidato*

Luana De Lorenzo

Ciclo XXII

---

*A.A. 2008-2009*

*Ma guardate l'idrogeno tacere nel mare  
guardate l'ossigeno al suo fianco dormire:  
soltanto una legge che io riesco a capire  
ha potuto sposarli senza farli scoppiare.*

Fabrizio De Andrè - Un Chimico-1971

*(Questa copia della tesi di dottorato è stata stampata fronte retro nel rispetto dell'ambiente)*

## INTRODUZIONE GENERALE

### 1. Definizione del problema.

Vi è un notevole interesse verso lo studio del trasporto di piccole molecole attraverso membrane polimeriche, soprattutto a causa del gran numero di applicazioni in cui tale processo di trasporto svolge un ruolo importante.

Le membrane polimeriche sono principalmente utilizzate come :

- ✓ membrane per separazione.
- ✓ involucri plastici .

Queste due applicazioni richiedono membrane con caratteristiche completamente diverse. Per la prima applicazione è importante che il materiale polimerico sia altamente selettivo e sufficientemente permeabile, mentre per la seconda la membrana deve avere un'elevata resistenza a gas o a sapori-aromi.

L'interesse per tali applicazioni industriali ha stimolato lo sviluppo di modelli teorici per descrivere il processo di trasporto. Esiste un gran numero di modelli, ciascuno dei quali, tuttavia, manca di una corretta descrizione microscopica del processo di permeazione. Metodi di simulazione al computer e, in particolare, simulazioni di dinamica molecolare rappresentano uno strumento essenziale per ottenere un quadro più dettagliato di tali fenomeni. Una descrizione qualitativa dei processi descritti e infine le previsioni quantitative di permeabilità e selettività aprono la strada alla prospettiva di progettare membrane con specifiche caratteristiche. Al momento non siamo ancora nella fase delle previsioni. La maggior parte degli studi in questo momento sono interessati a descrivere la diffusione e il processo di permeazione e si limitano al confronto con i dati sperimentali ottenuti per membrane già esistenti.

La presente tesi descrive un progetto di ricerca in questo settore di rapida evoluzione.

### 2. Scopo della ricerca

L'obiettivo del progetto di ricerca oggetto della presente tesi di dottorato è quello di studiare le proprietà di trasporto di piccole molecole attraverso membrane polimeriche utilizzando metodi teorici di simulazione al fine di ottenere utili correlazioni struttura-proprietà.

Sono stati scelti per essere studiati con il metodo di Dinamica Molecolare (MD) due diversi tipi di materiali per le loro alte prestazioni come materiali di membrane per separazioni gassose.

In particolare, le simulazioni a livello atomistico sono state utilizzate per investigare:

- il processo di trasporto di gas e vapori e l'analisi strutturale di copolimeri gommosi puri e modificati caratterizzati da alta selettività per gas polar / non polari: la modifica *in situ* di

tali tipi di membrane con l'aggiunta di percentuali variabili di additivi chimici ne potenzia la permeabilità e la selettività per specifiche applicazioni in campo di separazione gassosa.

- le caratteristiche morfologiche di polimeri vetrosi ad elevato volume libero e altamente permeabili, recentemente utilizzati per separazioni di gas complicate (ad esempio, di olefine/paraffine o trattamento di gas naturale), attraverso la misura quantitativa della distribuzione del volume libero.

Al di là di una convalida reciproca tra dati sperimentali e teorici, una delle questioni più importanti della ricerca computazionale sui materiali di membrana è la simulazione multiscala, vale a dire il collegamento tra vari metodi di calcolo che si sviluppano in diverse scale di lunghezza e di tempo per prevedere le proprietà macroscopiche e il comportamento di fondamentali processi molecolari. L'idea alla base della modellazione multiscala è di facile comprensione: si calcolano informazioni più dettagliate su scale ridotte per passare a modelli meno dettagliati su scale superiori. L'obiettivo finale della modellazione multiscala è quindi di prevedere il comportamento macroscopico di un processo ingegneristico da principi primi, cioè, a partire dalla scala quantistica attraverso la trasmissione di informazioni in scala molecolare fino al processo.

Andando nella direzione di un approccio multidisciplinare e di interconnessione di metodi matematici di modellazione nel corso del progetto di ricerca simulazioni mesoscale (utilizzando la teoria dinamica del campo medio (DDFT) e la dinamica dissipativa delle particelle (DPD) tramite modelli molecolari *coarse-grained*) sono state effettuate per studiare la morfologia di copolimeri a blocchi di interesse nel settore della nanotecnologia.

### 3. Scelta dei polimeri

I materiali scelti sono:

- PEBAX® 2533: un copolimero ad alta percentuale di contenuto gommoso della serie di poli(amide-12b-etilenossido) nota con il nome di PEBAX.
- HYFLON®AD60X e HYFLON® AD80X: perfluoropolimeri vetrosi.

Entrambi i materiali sono comunemente utilizzati per la preparazione di membrane dense e sono caratterizzati da alte prestazioni nella separazione di gas.

### 4. Sommario della tesi

Capitolo 1: Membrane per la separazione di gas. Questo capitolo fornisce una panoramica generale sui diversi tipi di membrane polimeriche, con particolare attenzione alle membrane e ai processi di separazione gassosa. Vengono mostrati e descritti nel dettaglio le principali equazioni e i metodi di misura delle proprietà di trasporto dei gas attraverso membrane polimeriche.

Capitolo 2: Basi teoriche di simulazione molecolare. Questo capitolo descrive i principi di base della tecnica di Dinamica molecolare e i metodi usati per calcolare diffusività, solubilità e volume libero.

Capitolo 3: Proprietà di trasporto di membrane di poli(amide-12-b-etilenossido) (PEBAX); in questo capitolo viene descritto in dettaglio lo studio atomistico del meccanismo

di trasporto di gas polari-non polari attraverso membrane di poli (etere /ammide). Vengono inoltre fornite utili correlazioni struttura microscopica /proprietà di trasporto, sottolineando il ruolo delle selettività di diffusività e di solubilità per diverse specie penetranti.

Capitolo 4: Proprietà di trasporto dell'acqua in membrane modificate di PEBAX: questo capitolo descrive le indagini MD di proprietà di trasporto dell'acqua attraverso sistemi PEBAX modificati con diverse percentuali in peso di toluensulfonamide (KET). Vengono fornite inoltre utili correlazioni tra la struttura microscopica dei materiali oggetto di studio e le prestazioni di questi sistemi in termini di diffusività e solubilità dell'acqua sperimentalmente misurate.

Capitolo 5: Indagini molecolare delle proprietà di trasporto di gas e vapori in membrane di PEBAX modificate. Questo capitolo fornisce una dettagliata descrizione delle simulazioni atomistiche del trasporto di H<sub>2</sub>O, N<sub>2</sub>, O<sub>2</sub>, CO<sub>2</sub>, CH<sub>4</sub> attraverso i materiali oggetto di studio per valutare la selettività tra specifiche coppie di gas e il confronto con i dati sperimentali.

Capitolo 6: Simulazione mesoscala della morfologia e delle proprietà di trasporto in membrane di PEBAX. In questo capitolo viene descritta la procedura mesoscala usata per studiare la complessa morfologia del PEBAX®2533, con una breve descrizione dei metodi DDFT e DPD. Vengono presentati i risultati preliminari e delineate le prospettive future.

Capitolo 7: Analisi delle distribuzioni di volume libero in perfluoropolimeri amorfi. Questo capitolo fornisce una descrizione dettagliata della procedura MD per il calcolo del volume libero in films di amorfi perfluoropolimeri vetrosi di HYFLON®AD60x e AD80x e il confronto con i risultati ottenuti da vari metodi sperimentali.

La tesi termina con alcune considerazioni e conclusioni finali.

## GENERAL INTRODUCTION

### 1. Problem definition

There is a considerable interest in the study of the transport of small molecules across polymeric membranes, mainly because of the large number of applications in which this transport process plays a major role.

Polymeric membranes are mainly used as:

- ✓ separation membranes.
- ✓ barrier plastics.

These two applications require membranes with completely different properties. In the first application it is important that the polymeric material is highly selective and sufficiently permeable, while in the second application the membrane should have high resistance to gas and e.g. flavor-aroma molecules.

Such interest has stimulated the development of theoretical models to describe the transport process. There are a large number of models, all of which, however, lacks a complete microscopic description of the permeation process. Computer simulation methods and in particular molecular dynamics simulations are an essential tool to obtain a more detailed picture of these phenomena. A qualitative description of the underlying processes and eventually quantitative predictions of permeability and selectivity open the prospect to the design of membranes with tailored properties. At present we are not yet at the stage of predictions. Most studies at this moment are concerned with description of the diffusion and the permeation process and are restricted to comparison with existing membranes.

This thesis describes one study in this fast moving field of research.

### 2. Aim of the research

The aim of this research is to study the transport properties of small molecules through polymeric membranes using computer simulation methods and to obtain useful correlations with the microstructure properties.

Two different types of materials are been chosen to be investigated by Molecular Dynamics (MD) method due to the high performances for gas separation exhibited in the field of membrane technology.

In particular fully atomistic simulations have been used to study:

- ◆ Gases and vapour transport and structural analysis of pure and modified rubbery copolymer with high selectivity for polar/non polar gases; the modification *in situ* of these types of membranes by adding variable percentages of chemical additives led to an enhancement of specific surface and permeability properties.
- ◆ Morphological properties of high free volume glassy perfluoropolymers, recently used for challenging gas separations (e.g., olefin/paraffin or natural gas treatment), by quantitative measure of free volume distributions.



Beyond a reciprocal validation between experimental and theoretical data, one of the most important issue in computational materials research is the multiscale simulation, namely the bridging of length and time scales, and the linking of computational methods to predict macroscopic properties and behavior from fundamental molecular processes. The idea of multiscale modeling is straightforward: one computes information at a smaller (finer) scale and passes it to a model at a larger (coarser) scale by leaving out, i.e., coarse-graining, degrees of freedom. The ultimate goal of multiscale modeling is then to predict the macroscopic behavior of an engineering process from first principles, i.e., starting from the quantum scale and passing information into molecular scales and eventually to process scales.

Going in the direction of a multidisciplinary approach and interconnections of mathematical theoretical method in the present research Mesoscale simulations (Dynamic mean field theory (Mesodyn) and dissipative particle dynamics (DPD) utilizing coarse-grained molecular models) are been used for investigating the morphology of block copolymers for nanotechnological applications.

### 3. Choice of polymers

The chosen materials are:

- ◆ PEBAX<sup>®</sup>2533: an almost totally rubbery copolymer of the Poly(amide-12b-ethylene oxide) PEBAX series.
- ◆ Hyflon<sup>®</sup> AD60X and Hyflon AD80X: glassy perfluoropolymers.

Both the materials are commonly used in the preparation of dense membrane and exhibited high performance in the field of gas separation.

### 4. Outline of the thesis

Chapter 1: Membranes for gas separation. This chapter is a general overview about the different types of polymer membranes, with particular attention for the gas separation membranes and processes. The main equations related to the gas transport properties and their measurements are also shown and described.

Chapter 2: Theoretical basis of Molecular simulation; this chapter describes the basic principles of the technique of molecular dynamics and the method for calculating diffusivity, solubility and free volume.

Chapter 3: Transport properties of a copoly(amide-12-b-ethyleneoxide) (PEBAX) membrane; in this chapter a detailed fully-atomistic investigation of the separation of polar/non polar pair gas through co-poly(ether/amide) block membranes has been provided. An assessment of the structure/property relationships is included, highlighting the role of diffusivity and solubility selectivities for various penetrant species.

Chapter 4: Water Transport properties of modified PEBAX membranes: this chapter describes the MD investigations of water transport properties across PEBAX systems with different weight percentage of the additive toluensulphonamide (KET); useful correlations

between the microscopic structure of the materials object of study and the performances of these systems in terms of water diffusivity and solubility have been provided.

*Chapter 5: Molecular investigations of gas and vapours transport properties in modified PEBA<sup>X</sup> membrane:* in this chapter a fully atomistic study has been performed for simulating the transport of H<sub>2</sub>O, N<sub>2</sub>, O<sub>2</sub>, CO<sub>2</sub>, CH<sub>4</sub> for evaluating the selectivity between specific couple of gases and compared with experimental data.

*Chapter 6: Mesoscale Simulation of morphology and transport properties in PEBA<sup>X</sup> membrane:* in this chapter the mesoscale procedure used for the investigations of complex PEBA<sup>X</sup>2533 morphology has been described, with a briefly introduction of DDFT and DPD model equations; preliminary results and future perspectives have been discussed.

*Chapter 7: Analysis of the free volume distributions in amorphous glassy perfluoropolymers:* the present paper describes the MD procedure for the free volume investigation in amorphous glassy perfluoropolymer films of Hyflon<sup>®</sup>AD60x and AD80x; the theoretical data are compared with experimental ones obtained by several experimental techniques.

The thesis ends with some final remarks and conclusions.

## I. MEMBRANE FOR GAS SEPARATION

### 1. Basic Principles and Applications

Membrane gas separation process is an important unit operation widely employed in the chemical industries. Membrane-based gas separation offers a number of advantages compared to other traditional methods for certain applications.

Modern membrane engineering is an important way to implement the process intensification (PI) strategy by innovative design and process development methods aimed at decreasing production costs but also equipment size, energy utilization, and waste generation [1.1-1.5]. Membrane science and technology are recognized today as powerful tools in solving some important global problems, developing new industrial processes needed for a sustainable industrial growth. In seawater desalination, membrane operations or their combination in integrated systems are already a successful approach for solving the situation of fresh water demand in many regions of the world, at lower costs and minimum environmental impact. Membranes are a factor of 10 times more energetically efficient than thermal options for water desalination [1.6].

The major production cycles consume as much as 40-50% of the energy used just for separations, often carried out by inefficient thermally driven separation processes.

Membrane gas separation (GS) is a pressure-driven process with different industrial applications that represent only a small fraction of the potential applications in refineries and chemical industries.

Since 1980, when the serial production of commercial polymeric membrane was implemented, membrane GS has rapidly become a competitive separation technology. Differently from conventional separation unit operations (e.g., cryogenic distillation and adsorption processes), membrane GS does not require a phase change. Moreover, the absence of moving parts makes GS systems particularly suited for use in remote locations where reliability is critical; in addition, the small footprint makes them very attractive for remote applications such as offshore gas-processing platforms.

Table 1.1 lists the current status of membrane gas separation processes.

The established processes represent more than 80% of the current gas separation membrane market: nitrogen production from air, hydrogen recovery and air drying. All have been used on a large commercial scale for over 10 years with dramatic improvements in membrane selectivity, flux and process designs. The second group of applications is developing processes which include carbon dioxide separation from natural gas, organic vapour separation from air and nitrogen, and recovery of light hydrocarbons from refinery and petrochemical plant purge gases. These processes are being developed on a commercial scale, and the process performance has been improved with the development of better membranes and process designs. In addition, organic vapor separation membranes are currently being developed for petrochemical and refinery applications. The 'to be developed' membrane processes represent the future development of gas separation technology. Natural gas treatment by membranes is being carried out at field tests and early commercial stage by several companies. Another large potential application for membranes is the production of

oxygen-enriched air, and the market size is expected to depend largely on the properties of the membranes. [1.7]

Process	Application	Comments
<b>Established processes</b>		
Oxygen/nitrogen	Nitrogen from air	Processes are all well developed. Only incremental improvements in performance expected
Hydrogen/methane; hydrogen/nitrogen; hydrogen/carbon monoxide	Hydrogen recovery; ammonia plants and refineries	
Water/air	Drying compressed air	
<b>Developing processes</b>		
VOC/air	Air pollution control applications	Several applications being developed. Significant growth expected as the process becomes accepted
Light hydrocarbons from nitrogen or hydrogen	Reactor purge gas, petrochemical process streams, refinery waste gas	Application is expanding rapidly
Carbon dioxide/methane	Carbon dioxide from natural gas	Many plants installed but better membranes are required to change market economics significantly
<b>To be-developed processes</b>		
C <sub>3+</sub> hydrocarbons/methane	NGL recovery from natural gas	Field trials and demonstration system tests under way. Potential market is large
Hydrogen sulfide, water/methane	Natural gas treatment	Niche applications, difficult for membranes to compete with existing technology
Oxygen/nitrogen	Oxygen enriched air	Requires better membranes to become commercial. Size of ultimate market will depend on properties of membranes developed. Could be very large
Organic vapor mixtures	Separation of organic mixtures in refineries and petrochemical plants	Requires better membranes and modules. Potential size of application is large

**Table 1. 1 – Status of membrane gas separation processes**

Membrane processes are classified according to the driving force by which they achieve separation. The membrane can be simply defined as a permselective barrier that will favour the transport of one component over the others. The separation occurs as a result of the differences in permeabilities of the species through the membrane. In gas separation, when a gas mixture at a pressure higher than the other side contacts a membrane which is selectively permeable to one component of the feed mixture, that species will be enriched on the permeate side.

Table 1.2 lists commonly known means of separation along with their primary driving force and type of mechanism.

Process	Driving Force	Transport Mode
microfiltration	$\Delta p$	convection
ultrafiltration	$\Delta p$	convection
reverse osmosis	$\Delta C(\Delta \mu_i)$	diffusion
dialysis	$\Delta C(\Delta a)$	diffusion
gas separation	$\Delta p(\Delta f_i)$	diffusion
pervaporation	$\Delta p_i(\Delta f_i)$	diffusion
electrodialysis	$\Delta \varphi$	migration

*(p-hydrostatic pressure,  $\mu$ -chemical potential, C-concentration  
a-activity,  $p_i$ -partial pressure,  $f_i$ -fugacity,  $\varphi$ -electrical potential)*

**Table 1. 2-Various membrane separation processes and the corresponding driving forces.**

Types of membranes used today include nonporous (dense) and porous polymers, ceramic and metal films with symmetric or asymmetric structures, liquid films with selective carrier components, and electrically charged barriers [1.8].

The performance of a membrane is determined by several key properties:

- ◆ high selectivity and permeability;
- ◆ excellent chemical, thermal, and mechanical stability under the process operating conditions;
- ◆ low maintenance;
- ◆ good space efficiency;
- ◆ defect-free production.

Commercially, the most widely practiced separations using membranes include the separation of oxygen and nitrogen; the recovery of hydrogen from mixtures with larger components such as nitrogen, methane and carbon dioxide; and the removal of carbon dioxide from natural gas mixtures. For these separations, membranes with adequately high fluxes of the more permeable components (oxygen, hydrogen, and carbon dioxide, respectively) and sufficient selectivity have been developed. The membrane materials used in these separations

are glassy polymers, which derive high selectivity from their ability to separate gases based on differences in penetrant size

Membranes can be categorized according to their geometry, bulk structure, production method, separation regime, and application [1.9]. Hollow-fiber membranes are used commonly by industries due to their high surface area and compactness. Flat-sheet membranes are easy to produce and are used in laboratory experiments. In terms of structure, membranes can be separated into two groups; asymmetric and symmetric. This simply refers to the types of pores that can be found within the membrane. Symmetric membranes have pores which do not change in diameter significantly through the sheet. On the other hand, asymmetric membranes contain pores which increase in size from one side of the sheet to the other. The new membrane composites are good example of asymmetric membranes. They are made with a thin polymer film deposited onto a porous backing material. The separation is determined by the properties of the thin film while the mass transport or rate is dependent upon the porosity of the backing.

Different production methods can result in membranes with unique characteristics. Membranes are the result of pressing a powder into a porous film and then sintering, stretching an extruded polymer into a sheet, irradiating a thin film with nuclear particles and then etching in a bath (nucleation track), dissolving a polymer in a solvent and spreading into a film followed by precipitation (solution casting), contacting two monomers in two immiscible liquids (interfacial polymerization), or condensing gaseous monomers on a substrate layer through a stimulated plasma (plasma polymerization).

## 2. Transport through polymer membranes

### 2.1. *Fundamentals*

Three general transport mechanisms are commonly used to describe gas separations using membranes, as illustrated in Figure 2.2 [1.10]. They are Knudsen diffusion, molecular sieving, and solution-diffusion. As the name implies, the first type of separation is based on Knudsen diffusion and separation is achieved when the mean free paths of the molecules are large relative to the membrane pore radius. The separation factor from Knudsen diffusion is based on the inverse square root ratio of two molecular weights, assuming the gas mixture consists of only the two types of molecules. The process is limited to systems with large values for the molecular weight ratio, such as is found in H<sub>2</sub> separation. Due to their low selectivities, Knudsen diffusion membranes are not commercially attractive.

The molecular sieving mechanism describes the ideal condition for the separation of vapour compounds of different molecular sizes through a porous membrane. Smaller molecules have the highest diffusion rates. This process can happen only with sufficient driving force.

In other words, the upstream partial pressure of the "faster" gas should be higher than the downstream partial pressure.

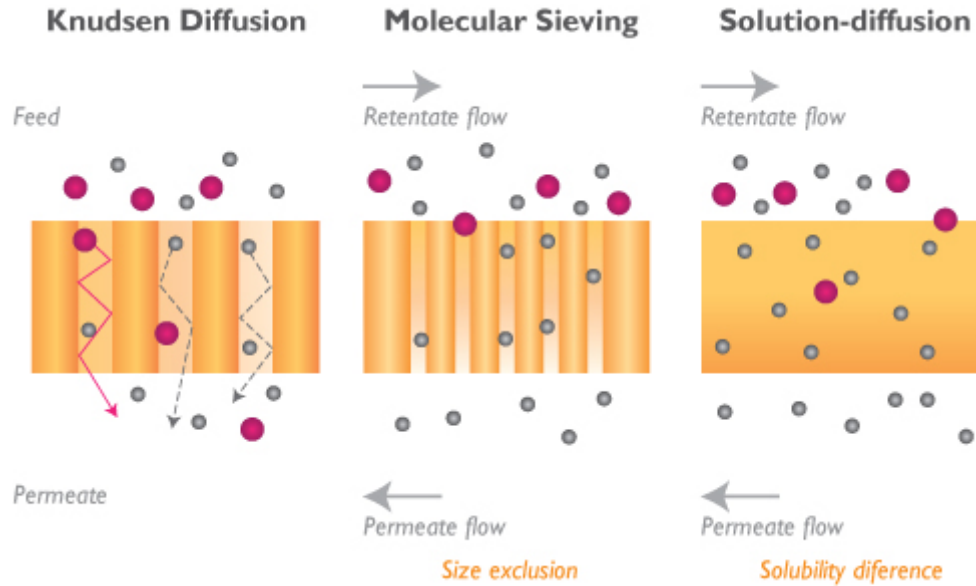


**Figure 1. 1 - General transport mechanisms for gas separations using membranes**

The main limitation is that condensable gases cause fouling, and alter the structure of the membrane; therefore, it is only feasible commercially in robust systems, such as those that use ultramicroporous carbon or hollow fibre glass membranes.

Solution-diffusion separation is based on both solubility and mobility factors. It is the most commonly used model in describing gas transport in non-porous membranes and it is applied in our studies. The details of this solution-diffusion model are given in the next section.

## **2.2. Solution Diffusion Model and Permeability Equations**

Gas permeation can be seen as a three-stage process in the solution-diffusion model:

1. adsorption and dissolution of gas at the polymer membrane interface.
2. diffusion of the gas in and through the bulk polymer.
3. desorption of gas into the external phase.

The first to use the term “solution-diffusion mechanism” was Graham [1.9] in 1866. He postulated that the penetrant leaves the external phase by dissolving in the membrane. It then undergoes molecular diffusion in the membrane, driven towards the downstream face by for example a concentration or pressure gradient, after which it evaporates again in the external phase. Thus the permeability coefficient  $P$ , defined by the ratio between the flux  $J$  of the permeant species and its concentration gradient  $\Delta c$  over the membrane of thickness  $d$ :

$$J = P \frac{\Delta c}{d} \quad (1.1)$$

is given by the product of the diffusion coefficient  $D$  and a solubility factor:

$$P = D \cdot S \quad (1.2)$$

A postulate of which the theoretical foundation will be shown next.

In the solution-diffusion model we consider an isothermal homogeneous stationary membrane in which particles at a position  $r$  are dissolved with a local concentration  $c(r)$ .

The particle flux  $J$  is assumed to behave in the regime of a linear irreversible process with the gradient of the chemical potential as the driving force. The flux is given by:

$$J(r) = c(r)v(r) \quad (1.3)$$

where  $v(r)$  is the average velocity of the dissolved particles. In the linear regime  $v(r)$  can be written as:

$$v(r) = \frac{1}{\xi} F = -\frac{1}{\xi} \nabla \mu(r) \quad (1.4)$$

where  $F$  is the thermodynamic force,  $\xi$  a friction coefficient  $\Delta\mu(r)$  and the chemical potential of the dissolved particles. The latter can be written as:

$$\mu(r) = \mu^0 + RT \ln c(r) + \mu_{ex}(r) \quad (1.5)$$

in which  $\mu^0$  is the standard chemical potential of the ideal gas phase based on unit molar concentration,  $c(r)$  is the local concentration and  $\mu_{ex}$  is the excess chemical potential of the dissolved species with respect to the ideal gas state. The previous equations give:

$$J(r) = -\frac{RT}{\xi} \nabla c(r) - \frac{c(r)}{\xi} \nabla \mu_{ex}(r) \quad (1.6)$$

Equating  $RT/\xi$  with the diffusion coefficient  $D$  eq. 1.6 can be written as:

$$J(r) = -D \exp\left(\frac{-\mu_{ex}(r)}{RT}\right) \cdot \nabla \left\{ c(r) \exp\left(\frac{\mu_{ex}(r)}{RT}\right) \right\} \quad (1.7)$$

Equation 2.7 is still general. We now consider a membrane with thickness  $d$  in the  $x$  direction and infinite dimensions in the  $yz$ -plane. The interfaces at  $x = 0$  are in contact with concentrations  $c_1$  and  $c_2$  ( $\Delta c = c_2 - c_1$ ) and we assume that an ideal gas phase is in equilibrium across both interfaces. Hence  $\mu$  is continuous at the interfaces.

Furthermore  $\mu_{ex}$  is assumed to be constant throughout the homogeneous membrane. This implies that any concentration dependence of  $\mu_{ex}$  is neglected. Thus:

$$\mu^0 + RT \ln c_1 = \mu^0 + RT \ln c(0) + \mu_{ex} \quad (1.8)$$

or

$$c(0) = c_1 \exp\left(\frac{-\mu_{ex}}{RT}\right) \quad (1.9)$$

Similarly



$$c(d) = c_2 \exp\left(\frac{-\mu_{ex}}{RT}\right) \quad (1.10)$$

If  $\mu_{ex}$  is constant then  $\Delta\mu_{ex}$  is zero. Then, for a stationary flux we find that according to equation 1.6,  $c(x)$  is a linear function of  $x$  and the gradient in equation (1.7) is equal to  $\frac{\{c(d) - c(0)\}}{d}$ . Equation (1.7) now reduces to:

$$J = -D \cdot S \frac{\Delta c}{d} \quad (1.11)$$

with:

$$S = \exp\left(\frac{-\mu_{ex}}{RT}\right) \quad (1.12)$$

Equation 1.11 expresses the solution-diffusion mechanism  $P$  is permeability of the gas defined as:

$$P = D \cdot S \quad (1.13)$$

The permeability is a product of the diffusivity and solubility coefficients. Thus, it can be seen that two parameters describe the solution-diffusion model: solubility and diffusivity. The permeability is a product of a thermodynamic factor (the solubility coefficient  $S$ ) and a kinetic parameter (the diffusion coefficient  $D$ ). In real systems, both diffusion and solubility coefficients may be a function of concentration. Selectivity is defined by the ratio of the individual gas permeabilities. Based on pure gas permeabilities, the "ideal selectivity" for gas species "A" and "B" can be defined as:

$$\alpha_{AB} = \frac{P_A}{P_B} = \left(\frac{D_A}{D_B}\right) \left(\frac{S_A}{S_B}\right) \quad (1.14)$$

which shows that the overall selectivity is determined by the differences in both the diffusivity and solubility coefficients, and measure the contributions of diffusivity and solubility aspects of the gas permeation, respectively.

Here,  $D_A/D_B$  is the ratio of the concentration-averaged diffusion coefficients of penetrants A and B, and is referred to as the membrane's "diffusivity selectivity".  $S_A/S_B$  is the ratio of solubility coefficients of penetrants A and B, and is called the "solubility selectivity". In typical gas separation applications, the downstream pressure is not negligible; however,  $\alpha_{AB}$  generally provides a convenient measure for assessing the relative ability of various polymers to separate gas mixtures. High permeability and high selectivity are the most important criteria in evaluating a membrane.

### **2.3. Performance of membranes for Gases separation: Robeson Plot**

Separation of gas mixtures employing polymeric membranes has been commercially utilized since the late 1970s. While the ability to separate gas mixtures was recognized much earlier, the commercial reality generated a significant amount of academic and industrial research activity. Membrane separation offers the advantage of low energy cost but has a high initial capital expense relative to the more established gas separation processes (e.g. adsorption and cryogenic distillation). With the increased cost of energy, membrane separation is reemerging as an economic option for various gas separations. Another area of emerging importance could be the recapture of CO<sub>2</sub> from industrial processes for reuse or sequestration, and the key separation (CO<sub>2</sub>/N<sub>2</sub>) for this area is included in the upper bound analysis. The key parameters for gas separation are the permeability of a specific component of the gas mixture and the separation factor. Moreover, robust (i.e., long-term and stable) materials are required to be applied in a membrane gas separation process. The gas separation properties of membranes depend upon:

- the material (permeability, separation factors),
- the membrane structure and thickness (permeance),
- the membrane configuration (e.g., flat, hollow fiber) and
- the module and system design.

Both membrane's permeability and selectivity influence the economics of a Gas Separation membrane process.

Permeability is the rate at which any compound permeates through a membrane; depends upon a thermodynamic factor (partitioning of species between feed phase and membrane phase) and a kinetic factor (e.g., diffusion in a dense membrane or surface diffusion in a microporous membrane).

The selectivity is the ability of a membrane to accomplish a given separation (relative permeability of the membrane for the feed species). Selectivity is a key parameter to achieve high product purity at high recoveries. Membrane for gas Separation has the potential to grow enormously if more selective membranes will become available.

Process design aspects for membrane gas separations were discussed recently in detail by Baker [1.12] different system configurations were described from an industrial point of view, together with the more suitable membrane system, depending on the selectivity of the membrane and on the target performance of the process considered. In multistage membrane systems there is a tradeoff between permeate composition and permeate pressure and therefore, recompression costs.

A key technical challenges exist. Achieving higher permselectivity and higher selectivity: The modern science material is focused on the preparation of new membrane materials that combines these requirements for specific gases separation applications.

It was recognized that these are trade-off parameters as the separation factor generally decreases with increasing permeability of the more permeable gas component.

This trade-off relationship was shown to be related to an upper bound relationship where the log of the separation factor versus the log of the higher permeability gas yielded a limit for

achieving the desired result of a high separation factor combined with a high permeability [1.6, 1.13] for polymeric membranes. The upper bound relationship was shown to be valid for a multitude of gas pairs including O<sub>2</sub>/N<sub>2</sub>, CO<sub>2</sub>/CH<sub>4</sub>, H<sub>2</sub>/N<sub>2</sub>, He/N<sub>2</sub>, H<sub>2</sub>/CH<sub>4</sub>, He/CH<sub>4</sub>, He/H<sub>2</sub>, H<sub>2</sub>/CO<sub>2</sub> and He/CO<sub>2</sub>. The upper bound relationship is expressed by:

$$P_i = k\alpha_{ij}^n \quad (1.15)$$

Where  $P_i$  is the permeability of the more permeable gas,  $\alpha_{ij}$  is the separation factor ( $P_i/P_j$ ) referred to as the “front factor” and  $n$  is the slope of the log–log plot of the noted relationship. Below this line on a plot of  $\log \alpha_{ij}$  versus  $\log P_i$ , virtually all the experimental data points exist. In spite of the intense investigation resulting in a much larger dataset than the original correlation, the upper bound position has had only minor shifts in position for many gas pairs.

Where more significant shifts are observed, they are almost exclusively due to data now in the literature on a series of perfluorinated polymers and involve many of the gas pairs comprising He. The shift observed is primarily due to a change in the front factor,  $k$ , whereas the slope of the resultant upper bound relationship remains similar to the prior data correlations.

As would be expected, the increased emphasis on membrane separation and the improved structure/property understanding from experimental studies and group contribution approaches has resulted in a number of observations equal to and exceeding the original upper bound. The comment in the original paper [1.6] “As further structure/property optimization of polymers based on solution/diffusion transport occurs, the upper bound relationship should shift slightly higher.

The slope of the line would, however, be expected to remain reasonably constant.” will be shown to be correct. The upper bound relationship is based on homogeneous polymer films and several approaches involving heterogeneous membranes have been demonstrated to easily exceed the upper bound. Surface modification is one method that clearly exceeds the upper bound limits as would be expected from the series resistance model as noted in an earlier paper [1.14]. UV surface modification [1.15], ion beam surface carbonization [1.16] and surface fluorination [1.17; 1.18] are among the viable surface modifications yielding such behavior.

Another approach initially proposed by Koros and co-workers [1.19] is typically referred to as a mixed matrix approach where selective molecular sieving structures are incorporated into a polymeric membrane. The mixed matrix approach has been reported in many studies [1.20-1.22] with results exceeding upper bound behavior. Another approach involving carbon molecular sieving membranes produced by carbonization of aromatic polymer membranes [1.23; 1.24] also yields permselective properties well above the upper bound relationships. Molecular sieve membranes with well defined uniform pore structure would, in essence, be considered to be the true upper bound limit for polymeric membranes. A recent paper on a novel approach to molecular sieving type structures [1.25] employed a solid-state thermal transformation of a polyimide to a benzoxazole-phenylene structure in the main chain yielding a material with remarkable CO<sub>2</sub>/CH<sub>4</sub> separation.

In the new upper bound published are considered the selectivity of CO<sub>2</sub>/N<sub>2</sub> for a very large series of polymers commercially in use: polymers containing poly(ethylene oxide) units have

interesting CO<sub>2</sub>/N<sub>2</sub> (polar-non polar gases) and the copolymer of the series PEBAX are very interesting for the high selectivity polar/non polar gases and high processability.

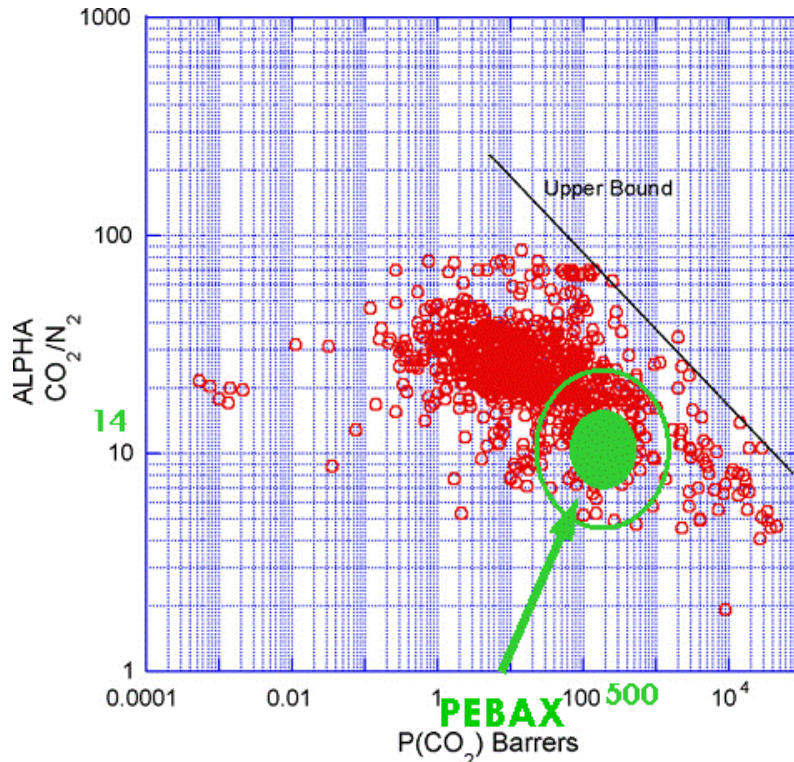


Figure 1. 2 - Robeson upper bond for the selectivity (ALPHA) CO<sub>2</sub>/N<sub>2</sub>.

### 3. Free Volume

Free volume (FV) is an extremely important characteristic of polymer materials which influences their properties, such as viscosity, diffusivity and permeability and, to some extent, the parameters of sorption thermodynamics and mechanical behavior. Because of its influence on transport properties, the concept of FV is extremely important for membranescience and technology. Some excellent reviews have been written by Yampolskii [1.26-1.28].

However, in contrast to other properties of polymers, free volume can be regarded as a complex physical object within polymers that can be characterized by size and size distribution of microcavities or free volume elements (FVEs) that form it, by topology and architecture of its nanostructure. Being initially formulated for the liquid state [1.29], it was extended to amorphous polymers that are either above or below the glass transition temperature (T<sub>g</sub>) [1.30-1.32]. At temperatures above T<sub>g</sub> one can distinguish in the free volume the “hole” component, characterized by zero energy expenditure for redistribution of FVE, and the interstitial component that becomes accessible to transport owing to energy fluctuations greater than kT. At temperatures below T<sub>g</sub>, yet another component of the free volume appears corresponding to the nonequilibrium thermodynamic state of glassy polymers [1.31,1.32].

Elaboration of additive incremental (group contribution) methods for inclusion of the effect of the chemical structure of the polymers on their properties became an important step

towards establishment of relations between the free volume using the van der Waals atomic radii and particular concepts of chain packing in polymers [1.33].

### 3.1. Definition of Free Volume

In the thermodynamic description of materials, it is generally distinguished between first and second order transitions [1.33]. The first order transitions are marked by a continuous free energy function of state variables (e.g. pressure  $p$  or temperature  $T$ ) which is discontinuous in the first partial derivatives with respect to the relevant state variables.

At a melting point, a typical first order transition, the Gibbs Free energy  $G$  is continuous, but there is a discontinuity in entropy  $S$ , volume  $V$  and enthalpy  $H$ :

$$\left(\frac{\partial G}{\partial T}\right)_p = -S \quad \left(\frac{\partial G}{\partial p}\right)_T = V \quad \left(\frac{\partial(G/T)}{\partial(1/T)}\right)_p = H \quad (1.16)$$

Second order transitions are classically defined [1.34] by discontinuities in the second partial derivatives of the free energy function while the function itself as well as the first partial derivatives  $S$ ,  $V$  or  $H$  are continuous, leading to discontinuities in the heat capacity  $C_p$ , compressibility  $\kappa$  and the thermal expansion coefficient  $\gamma$ :

$$\left(\frac{\partial S}{\partial T}\right)_p = -\frac{C_p}{T} \quad \left(\frac{\partial V}{\partial p}\right)_T = -\kappa V \quad \left(\frac{\partial H}{\partial T}\right)_p = C_p \quad \left(\frac{\partial V}{\partial T}\right)_p = -\gamma V \quad (1.17)$$

The nature of the glass transition is still the subject of discussions. Though it exhibits features of a second order transition, there is still disagreement whether it is purely kinetic or if it is a kinetic manifestation of an underlying thermodynamic transition [1.33]. However, when a liquid is cooled to form a glassy solid, it transforms from an equilibrium state (liquid) to a non equilibrium state (glass), and its appearance, i.e., the glass transition temperature  $T_g$ , is dependent on the rate or time scale of the experiment (see Figure 1.3), contradicting the definition of thermodynamic phase transitions. A way to determine the glass transition temperature  $T_g$  is provided by differential scanning calorimetry (DSC). Here, the heat flow of the sample to a reference is monitored and at the glass transition temperature  $T_g$  a step is observed that is caused by the discontinuity of the heat capacity  $C_p$ .

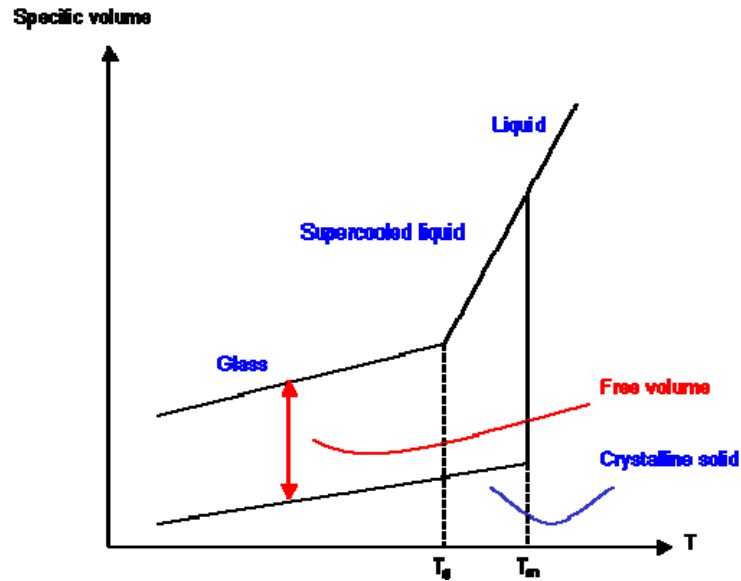


Figure 1.3 -Schematic diagram of volume definitions in polymers and temperature dependencies.

Above the glass transition temperature, glass forming amorphous polymers are in a liquid-like or rubbery state. At these temperatures, the enhanced molecular motion permits assemblies of polymer chain-segments to move in a coordinated manner, and hence allowing the material to flow [1.35] the degree of cooperative movement depending on temperature and molecular weight. The enhanced molecular mobility mutually depends on the presence of free volume which provides the space that is required for the rearrangement of the polymer segments to take place.

With decreasing temperature, the mobility of the polymer segments decreases and hence the specific volume  $V_{sp}$  of the polymer decreases according to the thermal expansion coefficient of the liquid state  $\gamma_l$ , see Figure 1.3. At the glass transition temperature, long range cooperative movement of polymer segments ceases, and while short-ranged rearrangements of individual mobile units of the polymer chain may still be possible, the restricted coordinated movement of the entangled macromolecular chains below the glass transition temperature turns the polymer into a solid glass, preserving the amorphous structure of the liquid or rubbery state.

Volume changes now follow the thermal expansion coefficient of the solid  $\gamma_s$ . The transition temperature  $T_g$  depends on the rate of cooling, as does the amount of frozen-in free volume. At slower rates, the glass transition temperature decreases and less free volume is conserved. Starting from the specific volume of the polymer  $V_{sp}$  different occupied volumes may be subtracted to give a measure of the *free volume*:

i)  $V_{sp} - V_{vdW}$ , the van der Waals volume of the polymer chains, gives the free volume at 0 K.

ii)  $V_{sp} - V_c$ , the volume of a hypothetical, close packed crystal, gives the excess free volume.

iii)  $V_{sp} - V_1$ , the extrapolated volume of an undercooled liquid, gives the amount of unrelaxed free volume.

Commonly glassy polymers are characterized with respect to the free volume by calculation of the *fractional free volume* using the method of Bondi [1.33]:

$$\Phi_{FV} = \frac{V_{free}}{V_{sp}} = 1 - 1.3 \frac{V_{vdW}}{V_{sp}} \quad (1.18)$$



## REFERENCES

- [1.1] P. Bernardo, E. Drioli, G. Golemme, *Ind. Eng. Chem. Res.* 48 (2009) 4638.
- [1.2] F. M. Dautzenberg, M. Mukherjee *Chem. Eng. Sci.* 56 (2001) 251.
- [1.3] W. J. Koros, Editorial. Three hundred volumes. *J. Membr. Sci.* 300 (2007) 1.
- [1.4] R. W. Baker, *Ind. Eng. Chem. Res.* 41 (2002) 1393.
- [1.5] H. Strathmann, *AIChE J.*, 47 (2001) 1077.
- [1.6] L. M. Robeson, *J. Membr. Sci.* 62 (1991) 165.
- [1.7] B. D. Freeman, *Macromolecules* 32 (1999) 375.
- [1.8] H. Strathmann, L. Giorno, E. Drioli, *An introduction to membrane science and technology*, Publisher CNR, Roma, ISBN 88-8080-063-9, 2006
- [1.9] B.D. Freeman, I. Pinnau, *Polymeric materials for gas separation*, in: B.D. Freeman, I. Pinnau (Eds.), *Polymer Membranes for Gas and Vapor Separation*, ACS Symposium Series 733, American Chemical Society, Washington, DC, 1999, p.1.
- [1.10] W.J. Koros and G.K. Fleming, *J. Membr. Sci.*, 83 (1993) 180.
- [1.11] R. W. Baker *Gas separation. In Membrane Technology and Applications*, 2nd ed.; John Wiley: Chichester UK, 2004; pp 287-335.
- [1.12] L.M. Robeson, *J. Membrane Sci.*, 320 (2008) 390.
- [1.13] L.M. Robeson, W.F. Burgoyne, M. Langsam, A.C. Savoca, C.F. Tien, *Polymer* 35 (1994) 4970.
- [1.14] K.K. Hsu, S.Nataraj, R.M. Thorogood, P.S. Puri, *J. Membr. Sci.* 79 (1993) 1.
- [1.15] J. Won, M.H. Kim, Y.S. Kang, H.C. Park, U.Y. Kim, S.C. Choi, S.K. Koh, *J. Appl. Polym. Sci.* 75 (2000) 1554.
- [1.16] J.D. LeRoux, D.R. Paul, J. Kampa, R.J. Lagow, *J. Membr. Sci.* 94 (1994) 121.
- [1.17] J.D. LeRoux, V.V. Teplyakov, D.R. Paul, *J. Membr. Sci.* 90 (1994) 55.
- [1.18] C.M. Zimmerman, A. Singh, W.J. Koros, *J. Membr. Sci.* 137 (1997) 145.
- [1.19] S. Husain, W.J. Koros, *J. Membr. Sci.* 288 (2007) 195.
- [1.20] T.-S. Chung, L.Y. Jiang, Y. Li, S. Kulprathipanja, *Prog. Polym. Sci.* 32 (2007) 483.
- [1.21] D. Sen, H. Kalipcilar, L. Yilmaz, *J. Membr. Sci.* 303 (2007) 194.
- [1.22] C.W. Jones, W.J. Koros, *Carbon* 32 (1994) 1419.
- [1.23] Y.K. Kim, H.B. Park, Y.M. Lee, *J. Membr. Sci.* 255 (2005) 265.
- [1.24] H.B. Park, C.H. Jung, Y.M. Lee, A.J. Hill, S.J. Pas, S.T. Mudie, E. Van Wagner, B.D. Freeman, D.J. Cookson, *Polymers with cavities tuned for fast selective transport of small molecules and ions*, *Science* 318 (2007) 254.
- [1.25] Y. Yampolskii, *Russian Chemical Reviews*, 2007, 76, 59-78 Chapter 2: Perfluoropolymer membranes and free volume in polymers
- [1.26] A. Y. Alentiev, Y. Yampolskii, V. P. Shantarovich, S. M. Nemser, N. A. Platè, *J. Membr. Sci.*, 126 (1997) 123.
- [1.27] A. Y. Alentiev, Y. Yampolskii, *J. Membr. Sci.*, 165 (2000) 201.
- [1.28] M. H. Cohen, D. Turnbull, *J. Chem. Phys.* 31 (1959) 1164.
- [1.29] D. Turnbull, M. H. Cohen, *J. Chem. Phys.* 34 (1961) 120.
- [1.30] J. S. Vrentas, J. L. Duda, in *Encyclopedia of Polymer Science and Engineering*, New York, Wiley 1986.



- [1.31] J. L. Duda, J. M. Zelinsky, Free-Volume Theory in Diffusion in Polymers, New York, Marcel Decker, 1996.
- [1.32] A. Bondi, Physical properties of Molecular Crystals, Liquids and Gases, N.Y., Wiley, 1968.
- [1.33] G. B. McKenna and S. L. Simon. The Glass Transition: Its Measurement and Underlying Physics. In S. Z. D. Cheng, editor, Applications to Polymers and Plastics, volume 3 of Handbook of Thermal Analysis and Calorimetry, book chapter 2. Elsevier Science B.V., 2002.
- [1.34] P. Ehrenfest. *Phase Proceedings of the Koninklke Akademie Van Wetenschappen Te Amsterdam*, 36 (1933) 153.
- [1.35] L. H. Sperling. Introduction to Physical Polymer Science. Wiley-Interscience, New York, 2001.

## II. THEORETICAL BASIS OF MOLECULAR SIMULATION

### 1. Introduction

The main goal of computational materials science is the rapid and accurate prediction of properties of new materials before their development and production. In order to develop new materials and compositions with designed new properties, it is essential that these properties can be predicted before preparation, processing, and characterization.

Polymers are complex macromolecules whose structure varies from the atomistic level of the individual backbone bond of a single chain to the scale of the radius of gyration, which can reach tens of nanometers. Polymeric structures in melts, blends and solutions can range from nanometer scales to microns, millimeters and larger. The corresponding time scales of the dynamic processes relevant for different materials properties span an even wider range, from femtoseconds to milliseconds, seconds or even hours in glassy materials, or for large scale ordering processes such as phase separation in blends.

Molecular modeling and simulation combines methods that cover a range of size scales in order to study material systems [2.1].

These range from the sub-atomic scales of quantum mechanics (QM), to the atomistic level of molecular mechanics (MM), molecular dynamics (MD) and Monte Carlo (MC) methods, to the micrometer focus of mesoscale modeling.

Quantum mechanical methods have undergone enormous advances in the past 10 years, enabling simulation of systems containing several hundred atoms. Molecular mechanics is a faster and more approximate method for computing the structure and behaviour of molecules or materials. It is based on a series of assumptions that greatly simplify chemistry, e.g., atoms and the bonds that connect them behave like balls and springs. The approximations make the study of larger molecular systems feasible, or the study of smaller systems, still not possible with QM methods, very fast. Using MM force fields to describe molecular-level interactions, MD and MC methods afford the prediction of thermodynamic and dynamic properties based on the principles of equilibrium and non-equilibrium statistical mechanics [2.2-2.6]. Mesoscale modeling uses a basic unit just above the molecular scale, and is particularly useful for studying the behaviour of polymers and soft materials. It can model even larger molecular systems, but with the commensurate trade-off in accuracy [2.7-2.9]. Furthermore, it is possible to transfer the simulated mesoscopic structure to finite elements modeling tools for calculating macroscopic properties for the systems of interest [2.10].

Figure 2.1 shows the class of models that are available at each single scale.

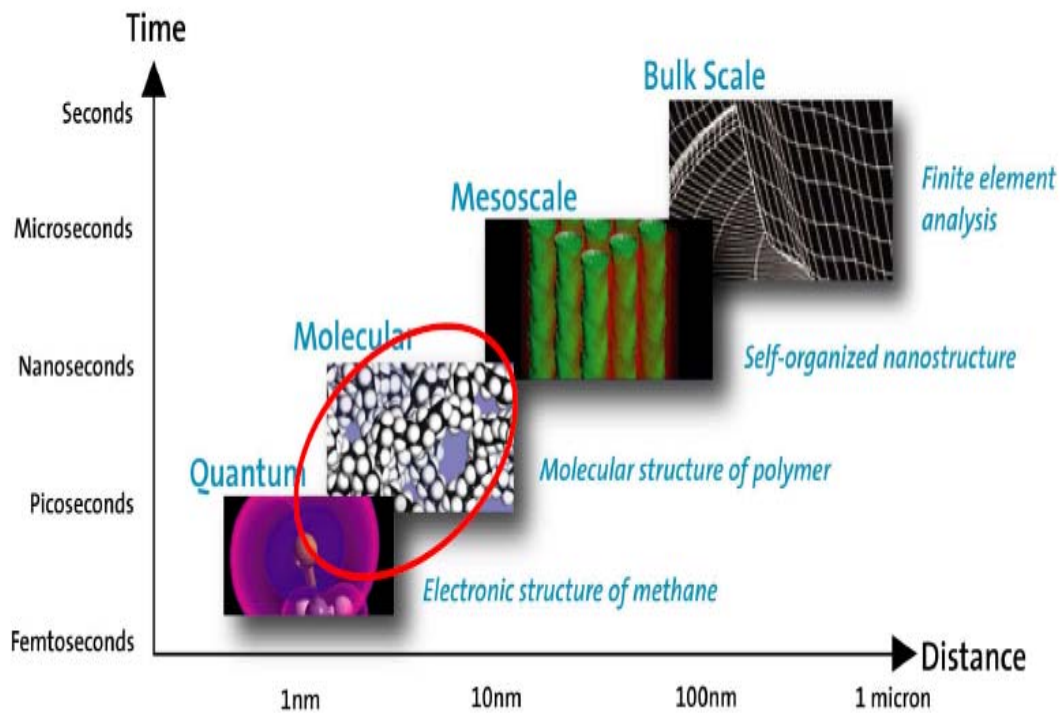


Figure 2. 1 – Multiscale molecular modeling: characteristic times and distances.

There are many levels at which modeling can be useful, ranging from the highly detailed ab initio quantum mechanics, through classical molecular modeling to process engineering modeling. These computations significantly reduce wasted experiments, allow products and processes to be optimized, and permit large numbers of candidate materials to be screened prior to production.

Over the last 20 years detailed atomistic molecular modeling techniques based on classical molecular mechanics have become a widely used method for the investigation of the molecular structure of membrane materials for gases separation based on amorphous polymers and the sorption and diffusion of low molecular weight penetrants in these materials [2.11]. The interest in development and application of molecular dynamics methodologies for the investigation of micro-structure of polymeric materials for gas separation is due to the fact that on the one hand major aspects of the small molecule membrane separation mechanisms are determined by the static structure on an atomistic scale and the dynamic behavior on a timescale ranging from picoseconds (ps) to nanoseconds (ns) of the separation system (membrane plus penetrants); it is impossible to get any direct experimental data about what is happening in these dimensions during the separation process.

To rectify this situation, better theoretical understanding of the transport mechanism and of the main factors which determine the permeability and permselectivity of dense amorphous polymers on a molecular level is clearly required. Furthermore, quantitative predictions of



$$U_{ij}(r_{ij}) = k_1(r_{ij} - r_{ij}^0)^2 + k_2(r_{ij} - r_{ij}^0)^3 + k_3(r_{ij} - r_{ij}^0)^4 \quad (\text{stretch})$$

$$U_{ijk}(\theta_{ijk}) = k_1(\theta_{ijk} - \theta_{ijk}^0)^2 + k_2(\theta_{ijk} - \theta_{ijk}^0)^3 + k_3(\theta_{ijk} - \theta_{ijk}^0)^4 \quad (\text{angle})$$

$$U_{ijkl}(\Phi_{i-l}) = k_1[1 - \cos(\Phi_{i-l} - \Phi_1^0)]^2 + k_2[1 - \cos(\Phi_{i-l} - \Phi_2^0)]^3 + k_3[1 - \cos(\Phi_{i-l} - \Phi_3^0)]^4 \quad (\text{torsion})$$

(2.2)

The force constants  $k_i$  and the equilibrium positions  $r_{ij}$ ,  $\theta_{ijk}$  and  $\Phi_{i-l}$  are based on results of quantum mechanics and constitute the integral part of the forcefield. The nonbonded interactions are expressed in the applied forcefield by a van derWaals term with a 9,6-potential and a coulomb-term:

$$U_{ij}(r_{ij}, q_i, q_j) = \left( \frac{A_{ij}}{r_{ij}^9} - \frac{B_{ij}}{r_{ij}^6} \right) + \frac{q_i q_j}{\epsilon_0 r_{ij}} \quad (\text{nonbonded})$$

(2.3)

where  $A_{ij}$  and  $B_{ij}$  are parameters describing the strength of the repulsive and attractive force,  $q_i$  and  $q_j$  are the partial charges of the interacting atoms and  $\epsilon_0$  is the vacuum permittivity. The forcefield is defined by the functional form (eqns. 2.2, 2.3) and a set of parameters  $k_i$ ,  $r_{ij}^0$ , . . . which are specific to types of atoms, i.e., account for different bonded states of the atoms.

For a given molecular structure, the force- field results in a potential energy surface, which can be evaluated with respect to local energy minima. These methods are known as molecular mechanics (MM) [2.14]. In the course of optimization, geometrically reasonable (static) structures can be obtained from the initially guessed geometry by varying the atom positions and minimizing the potential energy of the system.

It should be noticed that the evaluation of the nonbonded energy terms is the numerically most extensive part in molecular modeling calculations because these terms include contributions from each pair of atoms in a model. This leads to restrictions on the maximum possible size of a simulated membrane system (e. g. an amorphous polymer packing). The number of atoms  $N$  can not be much higher than 2000–10000 for typical transport simulations on modern workstations, while  $N$  may be up to about a factor of ten higher for selected simulations on currently available supercomputers.

## 2.2. Molecular dynamics (MD)

To perform molecular dynamics (MD) simulations, the forces that result from the forcefield and which act on each atom are applied to the system of finite temperature, i.e., finite kinetic energy  $E_{kin}$ .

Each of the  $N$  particles is assigned a random (Boltzmann) velocity vector  $r'_i$  so that the total kinetic energy of the system corresponds to the desired temperature  $T$ :

$$E_{kin} = \sum_{i=1}^n \frac{1}{2} m_i \dot{r}_i^2 = \frac{(3N-6)}{2} k_B T \quad (2.4)$$

Here  $(3N-6)$  is the number of degrees of freedom and  $k_B$  is the Boltzmann constant. In the course of a simulation, integration of the Newtonian equations of motion:

$$F_i = -\nabla_{r_i} U_i(r_1, \dots, r_N) = m_i \ddot{r}_i \quad (2.5)$$

leads to a new velocity of each particle which can be extrapolated over the time step  $\Delta t = 1$  fs of the simulation to determine the new coordinates  $r_i$ . The force  $F_i$ , acting on a particle  $i$  of mass  $m_i$ , results from the gradient of the potential energy  $U_i$  (see eq. 2.4) determined by the forcefield (eq. 2.1.)

Using Eq. (2.3-4) it is then possible to follow the motions of the atoms of a polymer matrix and the diffusive movement of imbedded small penetrant molecules at a given temperature over a certain interval of time. Eq. (2.4) represents a system of usually several thousand coupled differential equations of second order. It can be solved only numerically in small timesteps  $\Delta t$  [2.15-2.17]. The choice of the time step  $\Delta t$  results from the consideration that the fastest vibration of the system should be sufficiently resolved. In a typical IR-spectrum, the C-H-bond shows a characteristic peak at  $\nu(\text{C-H}) \approx 3000 \text{ cm}^{-1}$ , which corresponds to an oscillation period of  $\tau(\text{C-H}) \approx 10\text{fs}$ .

### 3. Condensed Phase Simulation

When simulating condensed-phase systems, it is necessary to build systems that can present the bulk of the simulated materials correctly. Therefore the size of the simulation cell must be large enough to be able to sample the configurational space of the properties of interest. On the other hand, the system size is also limited by computing power (about 10,000 atoms for molecular dynamics).

#### 3.1. Periodic Boundary Conditions

When taking a small system out of the bulk of simulated object, the same bulky environment has to be preserved to avoid unrealistic surface effect. The common approach is to use the periodic boundary conditions, in which the primary cell (parent cell) is surrounded on all sides by replica of itself (image cells) to form a three-dimensional infinite lattice. The atoms initially in the parent cell are parent atoms, while those initially in the image cells are image atoms. There is an image centering technique to control the constant atom number, i.e. whenever an atom migrates to the edge of the primary cell, it will appear in the adjacent image cell.

However, its image will enter the primary cell on the opposite side. Thus atoms may diffuse as far as they can during the course of the simulation instead of being confined in the small parent cell, and at the same time the number of atoms in the box is always constant. In an explicit image model a parent atom will interact with any image atoms (besides parent atoms) within the user-defined cutoff while implicit image model only counts the closest image atoms [2.18].

### 3.2. Amorphous Cell Construction

Polymer chain can adopt numerous conformations due to the existence of many rotatable bonds, whereas for small molecules, only limited number of conformations are accessible. Even a short polymer chain may have a few hundred rotatable bonds that give rise to millions of different conformers. This makes it difficult to sample all the conformations of a real polymer chain with a small simulation cell. It is almost impossible to find the “global” minimum energy conformation within such a large configuration space using energy minimization scheme. Also it is very time consuming if not impossible to equilibrate polymers with unrealistic initial structure by molecular dynamics. The interdependent RIS (Rotational Isomeric State) model has been proved to be an efficient and effective way to build a polymer chain of reasonable initial structure since condensed-phase polymer chain is known to be at unperturbed state. However, the conventional pair wise RIS model does not explicitly prohibit overlapping of atoms separated by a few backbone atoms away or atoms belonging to different molecules.

A method developed by Theodorou and Suter [2.19] takes advantage of the conventional RIS model while overcomes such limitations. In their method, a Monte Carlo type bond-by-bond construction scheme is employed to build a polymer backbone.

Usually amorphous cells are built at a relatively low initial density with ease and are compressed to the experimental density gradually using high-pressure NPT dynamics.

These cells generally need to be further refined to “equilibrate” the structure. The refinement adopted in present studies is an annealing procedure, which will heat up polymer cell step by step using high temperature NPT molecular dynamics, then cool it back to the original conditions. This procedure is particular useful for rubbery polymers that have a flexible backbone. High temperature dynamics may provide sufficient amount of energy for the polymer chains to overcome local energy barriers and reach “global” minimum energy conformation.

### 3.3. The Concept of Ensembles

In statistical thermodynamics, details of individual particles are usually not of great importance. On the contrary, for a realistic representation of thermodynamic behaviour, the expectancy of observable properties are regarded. This may be achieved by taking the mean value with respect to time or as the average of a number of configurations.

In molecular dynamics, the evolution of a system with respect to time is observed. Depending on the property under investigation, different ensembles are evaluated, i.e., different state-variables are held constant to observe the behaviour of others.

In the microcanonical ensemble the number of particles  $N$ , the total energy  $E$  and the volume of the simulation cell  $V$  are held constant. While keeping  $N$  and  $E$  constant is quite straightforward and needs no further explanation, the volume  $V$  of a system may be kept constant by periodic boundary conditions (see 3.1), forcing a particle that leaves the virtual simulation cell to enter on the opposite side by assigning the appropriate coordinates.



A canonical ensemble is characterized by constant  $N$ ,  $V$  and temperature  $T$ . The easiest way to control the temperature is to directly scale the particle velocities  $\dot{r}_i$ , whenever the system temperature  $T_{\text{sys}}$  leaves a predefined temperature window  $T_0 \pm \Delta T$ :

$$\dot{r}_{i,\text{now}} = \dot{r}_{i,\text{old}} \left( \frac{T_0}{T_{\text{sys}}} \right)^{\frac{1}{2}} \quad (2.6)$$

More refined methods like the Berendsen thermostat [2.20] are more commonly used because a temperature change per simulation time step leads to a more smooth progression of the temperature. In this work, molecular dynamics are applied to canonical ensembles as part of the equilibration steps in the packing procedure (see Chapter 3 section 1.3). and referred to as NVT -MD (according to the state variables  $N$ ,  $V$  and  $T$  that are kept constant).

If, at constant  $N$  and  $T$ , the pressure  $p$  is held constant instead of the volume  $V$  the ensemble is called isothermal-isobaric. The pressure is evaluated using the virial  $\Xi$  and kinetic energy  $E_{\text{kin}} \propto Nk_B T$  based on centers of mass [2.20]:

$$\Xi(t) = \frac{1}{2} \sum_{i < j} r_{ij}(t) F_{ij}(t) \quad (2.7)$$

It is controlled by changing the volume  $V$  of the simulation cell according to the relation:

$$pV = Nk_B T + \frac{2}{3} \langle \Xi \rangle \quad (2.8)$$

Molecular dynamics simulations of isothermal-isobaric ensembles (NpT -MD) are performed as final equilibration procedure of the packing models (see Chapter 3 section 1.3).

An ensemble of constant pressure, volume, temperature and chemical potential  $\mu$  is called grand canonical. Here, the number of particles  $N$  is allowed to fluctuate. This is achieved by randomly inserting or deleting molecules. The chemical potential of the molecules within the matrix is balanced with a reference chemical potential, e.g. that of a surrounding gas phase at corresponding pressure and temperature. Using a Monte Carlo algorithm, a new configuration is energetically evaluated and accepted if more favourable than the previous and otherwise rejected, allowing for thermal fluctuations using a temperature dependent Boltzmann factor. Grand Canonical Monte Carlo (GCMC) simulations are used in this work to calculate sorption equilibrium on static packing models for several pressures (chemical potentials) at constant volume and temperature to determine concentration-pressure isotherms which are referred to as GCMC-isotherms (see Section 4.3.1).

## 4. Simulation of gas transport properties

### 4.1. Calculation of diffusion coefficients

Gas diffusion coefficient ( $D$ ) is defined by Fick's first law (for isothermal diffusion) [2.21]



$$J_i = -D\nabla a_i \quad (2.9)$$

where  $J_i$  denotes the flux of particles of species  $i$  and  $a_i$  is its activity (usually we assume the activity equals the concentration). Fick's law holds in the case of thermal and mechanical equilibrium (constant  $T$  and  $p$ ).

From the microscopic point of view, the diffusion coefficient can be related to the autocorrelation function of particle velocity:

$$D = \frac{1}{3} \int_i \left\langle \left[ \sum_i v_i(0) \right] \left[ \sum_i v_i(t) \right] \right\rangle dt \quad (2.10)$$

if the diffusion species concentration is low and the interaction between these particles is a short-range interaction, Equation 2.9 can be simplified to

$$D = \frac{1}{3} \int_i \langle [v_i(t)] \cdot [v_i(0)] \rangle dt \quad (2.11)$$

which is known as the Green-Kubo relation for the diffusion coefficient.

This equation states that the diffusivity is given by the time integral of the single particle center-of-mass velocity autocorrelation function. Under the long-time condition, Equation 2.8 was shown to be equivalent to the Einstein equation:

$$D_\alpha = \frac{1}{6N_\alpha} \lim_{t \rightarrow \infty} \langle |\mathbf{r}_i(t) - \mathbf{r}_i(0)|^2 \rangle \quad (2.12)$$

Where  $N_\alpha$  is the number of diffusing molecules of type  $\alpha$ ,  $\mathbf{r}_i(0)$  and  $\mathbf{r}_i(t)$  are the initial and final positions of molecules (mass centres of particle  $i$ ) over the time interval  $t$ , and  $\langle |\mathbf{r}_i(t) - \mathbf{r}_i(0)|^2 \rangle$  is the mean square displacement (MSD) averaged over the possible ensemble. The Einstein relationship assumes a random-walk motion for the diffusing particles [2.22].

In this case,  $D_\alpha$  is linearly proportional to the MSD. For slow diffusing species, anomalous diffusion is sometime observed and characterized by:

$$\langle |\mathbf{r}_i(t) - \mathbf{r}_i(0)|^2 \rangle \propto t^n \quad (2.13)$$

where  $n < 1$  (for Einstein diffusion regime,  $n = 1$ ). At short dynamics time range, the MSD may be quadratic to time (i.e.  $n = 2$ ), this represents the occurrence of free flight of diffusing species. At sufficient long time (i.e. hydrodynamic limit), a transition from anomalous to Einstein diffusion ( $n = 1$ ) may be observed.

The resulted diffusion coefficient ( $D_\alpha$ ) is often called the tracer diffusion coefficient or the self-diffusion coefficient. It's a dynamic property under equilibrium state. While the diffusivities obtained from experiments ( $D_{ij}$ ) are often referred as transport coefficients. The relationship of these two diffusion coefficients in a two components (A, B) system is often expressed by Darken's equation [2.23, 2.24]:

$$D_{AB} = (D_A x_B + D_B x_A) \left( \frac{d \ln f_A}{d \ln f_B} \right) \quad (2.14)$$

when the penetrant concentration is low ( $x_A \rightarrow 0$ ), Equation 2.14 reduces to:

$$D_{AB} = D_A \quad (2.15)$$

The random walk behaviour of gas molecules in a polymer matrix can be simulated using NVT ensemble molecular dynamics simulations.

#### 4.2. TST method

The transition-state theory (TST) is a well-established methodology for the calculation of the kinetics of infrequent events in numerous physical systems. According to the TST method the gas transport mechanism across a dense polymer system is described as a series of activated jumps. For each transition, a “reaction trajectory” leading from a local energy minimum to another through a saddle point in the configuration space is tracked, and the transition rate constant is evaluated. According to the Gusev-Suter TST method [2.25, 2.26] a 3-dimensional (3-D) grid spacing of about Å is initially laid on the well-relaxed polymer packing cell.

Then a test particle in united atom representation with dimensions representative of the gas penetrant is inserted into the polymer matrix at each lattice point of the grid, and the resulting nonbonded intermolecular potential energy, between the inserted molecule and all polymer atoms, is calculated. The whole packing is separated into regions of free accessible volume (low-energy interactions) and regions of densely packed polymer (excluding volume, high interaction energy). The borders between each local minimum of the energy (sorption “microstate”) are defined as high-energy surfaces separating the local energy minima, using the grid construction. The rate coefficient for the jump from a microstate  $i$  to a microstate  $j$ , is:

$$k_{ij} = \frac{k_b T}{h} \frac{Q_{ij}}{Q_i} \quad (2.16)$$

where  $h$  is Plank’s constant, and  $Q_i$  and  $Q_{ij}$  are the partition functions of the molecule in microstate  $i$  and on the separating surface between microstates  $i$  and  $j$ , respectively. The partition function of a particle of mass  $m$ , localised in the microstate  $i$ , is :

$$Q_i = \left( \frac{2\pi m k_b T}{h^2} \right)^{\frac{2}{3}} \int_{V_i} e^{-U(\bar{X})/k_b T} dV \quad (2.17)$$

where  $V_i$  is the volume of the site  $i$  and  $U(\bar{X})$  is the interaction potential energy between a guest molecule at point  $\bar{X}$  and the host matrix atoms. The partition functions of the molecule on the separating surface between microstates  $i$  and  $j$ ,  $Q_{ij}$  are :

$$Q_{ij} = \frac{2\pi m k_b T}{h^2} \int_{\Omega_i} e^{-U(\bar{X})/k_b T} dS \quad (2.18)$$

where  $\Omega_{ij}$  and  $dS$  are the common crest surface separating sites  $i$  and  $j$  and the related surface element, respectively.

Gusev and Suter implemented the original TST method [2.25] taking into account the thermal vibrations of the polymer matrix [2.26, 2.27] with the assumption that the polymer atoms, in a sorption site, execute uncorrelated harmonic vibrations around their equilibrium positions to accommodate the guest molecules. These motions are small displacements,  $\Delta \mathbf{r}_i = \mathbf{r}_i - \langle \mathbf{r}_i \rangle$ , of each atom from their equilibrium position  $\langle \mathbf{r}_i \rangle$ , and are much shorter than the time elapsing between penetrant jumps. These assumptions may be considered valid only for the diffusion of small gas molecules such as (He, O<sub>2</sub>, N<sub>2</sub>, CH<sub>4</sub>); it is not appropriate for larger molecules (CO<sub>2</sub>) that may force the polymer atoms in the vicinity of the penetrant to undergo substantial local relaxations to accommodate the guest molecule.

The displacements  $\Delta \mathbf{r}_i$  follow a Gaussian probability density function such as:

$$W(\Delta \mathbf{r}_1, \Delta \mathbf{r}_2, \dots, \Delta \mathbf{r}_N) \propto \exp \left\{ - \sum_{i=1}^N \frac{\Delta \mathbf{r}_i^2}{2 \langle \Delta \mathbf{r}_i^2 \rangle} \right\} \quad (2.19)$$

where  $\langle \Delta \mathbf{r}_i^2 \rangle$  is the mean square displacement from the equilibrium position and  $\Delta^2$  is the “smearing factor”, a parameter for all atoms. Then a modified equilibrium Boltzmann-probability density  $\rho(\bar{X})$  of finding a solute can be written as:

$$\rho(\bar{X}) \propto \int d\{\Delta\} W\{\Delta\} \exp \left( - U(\bar{X}, \{\bar{x}\}) / k_b T \right) \quad (2.20)$$

where  $U(\bar{X}, \{\bar{x}\})$  is the interaction potential energy at the position  $\bar{X}$ . Considering the form of  $W(\Delta \mathbf{r}_1, \Delta \mathbf{r}_2, \dots, \Delta \mathbf{r}_N)$ , given the value of  $\Delta$ , the jump rate constants can be calculated through Eq. (2.16). The particle transition probability  $\rho_{ij}$  from site  $i$  to a particular adjacent site  $j$  is proportional to the rate constant  $k_{ij}$ :

$$\rho_{ij} = \tau_i k_{ij} \quad (2.21)$$

where  $\tau_i$  represents the mean residence time for the probe molecule at site  $i$ , given by:

$$\tau_i = \frac{1}{\sum_j k_{ij}} \quad (2.22)$$

Once the smearing factor and the corresponding jump probabilities are determined, the trajectory of the penetrant molecules are calculated by a Monte Carlo (MC) type procedure and the diffusivity is extracted from the slope of the mean square displacement (MSD) versus time at long times, when Fickian diffusion is established.

The TST procedure, as implemented in Gsnet and Gsdif [2.28] packages, gives different possibilities of defining the polymeric elastic fluctuations by fixing the average displacements of the matrix atoms. The smearing factor, in the present work, is defined by means of a self consistent MD calculation. For every penetrant particle 1000 trajectories were calculated for a

total diffusion time of  $10^{-4}$  second that is necessary to fulfil the criterion of establishment of Fickian diffusion, in order to determine the diffusion coefficient.

### 4.3. Calculation of solubility coefficients

#### 4.3.1 GCMC method

The solubility coefficients,  $S$ , were obtained from Gran Canonical Monte Carlo (GCMC) simulations by fitting the sorption isotherm obtained from every simulated box to a straight line through the origin and taking the slope to be the solubility coefficient. In this procedure, a Metropolis [2.29] algorithm is used to accept or reject an insertion and deletion of a sorbate molecule.

The probabilities of addition and deletion of a sorbate molecule are given as:

$$P_{add} = \min \left[ 1; \frac{1}{N_s + 1} \frac{pV}{k_b T} \exp \left( \frac{-\Delta U}{k_b T} \right) \right] \quad \text{and} \quad P_{del} = \min \left[ 1; \frac{N_s k_b T}{pV} \exp \left( \frac{-\Delta U}{k_b T} \right) \right] \quad (2.23)$$

where  $U$  is calculated from the sum of nonbonded (i.e. Coulombic and van der Waals interaction) energies,  $N_s$  is the number of sorbate molecules. The addition is accepted if the energy change  $\Delta U$ , is negative or if the Boltzmann factor,  $\exp(-\Delta U/kT)$  is greater than a random number generated between 0 and 1.

The solubility coefficient  $S$ , is then obtained from the slope of the sorption isotherm as:

$$S = \lim_{p \rightarrow 0} \frac{c}{p} \quad (2.24)$$

where  $c$  is the sorbed gas concentration, units of  $\text{cm}^3(\text{STP})/\text{cm}^3$  polymer, and  $p$  is pressure.

#### 4.3.2 Hildebrand Solubility

The concept of solubility parameter was first introduced by Hildebrand in an attempt to calculate activity coefficients of small molecules in a solution environment [2.30].

It has also been used quite extensively to predict miscibility of binary solutions since the difference in the components' solubility parameters is related to the enthalpy change on mixing. In fact, non-polar small molecules having comparable solubility parameters are found to be thermodynamically miscible.

In atomistic simulations, the cohesive energy is defined as the increase in energy per mole of a material if all intermolecular forces are eliminated:

$$\delta = \sqrt{\frac{\Delta E_{\text{int}}}{V}} = \sqrt{CED} \quad (2.25)$$

Cohesive energies for mixtures of liquids from different classes (i.e., nonpolar, H-bonded, etc.) are still used as an approximate guide in solubility prediction, especially when the

entropy of mixing is largely combinatorial, as is the case in many polymer mixture systems [2.31]. Moreover, the concept of cohesive energy has found uses in predicting other aspects of behavior such as mechanical properties. Consequently, the use of atomistic methods to furnish a first principles calculation of cohesive energy density is a desirable tool. Additionally, evidence is accumulating that simulations on bulk systems of moderate size (1000-5000 atoms) using recent systematically-derived "class II" forcefields such as "COMPASS" of Accelrys Inc. [2.32-2.34] are capable of making predictions with an accuracy that compares favourably with experiment, with precision (measured by reproducibility obtained with a given forcefield) often higher than experiment [2.35].

## 5. Free Volume Analysis

Several definitions of free volume in glassy polymers are employed in the literature, depending on the method of evaluation or the subject under investigation. In this work, the accessible free volume based on the insertion of a test particle is used. To estimate the size distributions of free volume elements (fves), a recently developed computer program [2.36] was applied to the packing models.

The free volume is derived by the superimposition of a fine grid over the cubic packing model. At every grid point a hard sphere is inserted as test particle. If the test particle overlaps with any atoms of the polymer matrix, which are also represented by hard spheres of van der Waals radii, the grid point is classified as 'occupied' (see red circle in Figure 2.2). If there is no overlap (large green circle), the grid point is considered as 'free' and contributes to the free volume (green dots). Neighboring free grid points are collected into groups which represent individual holes. The grouping is done in two ways [2.36, 2.37]:

In the first approach (named Vcon, con for connected), affiliation to a group is defined through next neighborhood: every point of a group has at least one next neighbour which is also member of this group.

This approach identifies holes, which may be of complex shape and of large volume. In Figure 2.2(a) all grid points marked green contribute to one fve according to the Vcon method. In a second approach (named Rmax) for every free grid point the distance to the nearest matrix atom is determined. By calculation of the gradient, the grid points are assigned to the nearest local maximum in this distance.

The Rmax-approach may divide larger free volume regions of elongated or highly complex shape into smaller, more compact regions (as illustrated in Figure 2.2 (b)).

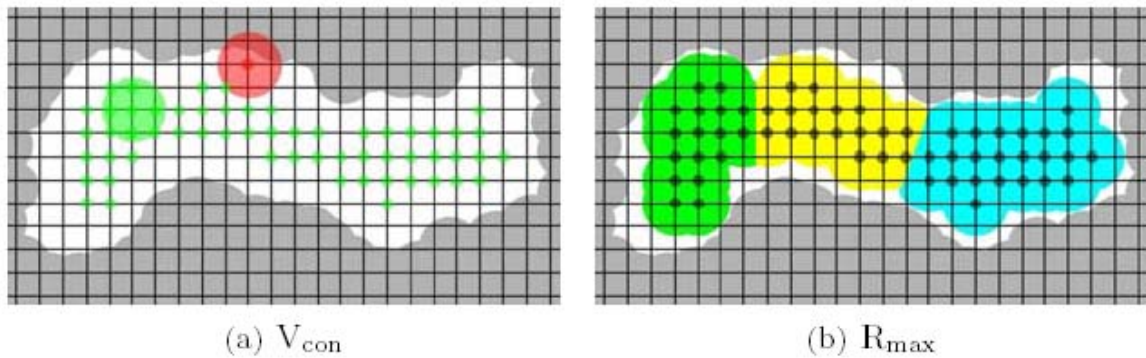


**Figure 2. 2 - 2D-illustration of the free volume analysis: (a) The Vcon-methogroups free gridpoints, where the test-sphere (green) does not overlap the matrix (grey), according to next neighborhood (green dots). (b) The Rmax-method further subdivides these groups by detecting constrictions ('bottlenecks', cf. text)**

Originally introduced to match better the situation in PALS experiments, where the positronium probe can obviously not completely sample very large holes of complex topology [2.36, 2.37] the second approach also seems more adequate to depict the environment of a sorbed molecule [2.38, 2.39] An oblong hole that is constricted at some point would be regarded as a single hole by the Vcon method. However, a penetrant molecule would have to jump an energy-barrier to pass this 'bottleneck' and therefore 'see' two separate sorption sites. By defining a hole according to the Rmax method this separation would be recognized with the help of a small computer program, the grid points of a free volume element are assigned the volume of a cube of edge length according to the grid spacing; corrections are made for grid points that are at the surface of the fve. The volumes of the grid points add up to the total volume of a free volume element.

Results of the free volume analysis and a visualization of the Free Volume will be presented in the VII chapter section 3.6.2.

## REFERENCES

- [2.1] M. Fermeglia, S. Pricl, *Progress in Organic Coatings* 58 (2007) 187–199
- [2.2] J.M. Haile, *Molecular Dynamics Simulations*, Wiley & Sons, New York, 1992.
- [2.3] M.P. Allen, D.J. Tildesley, *Molecular Simulations of Liquids*, Oxford University Press, Oxford, 1987.
- [2.4] K.E. Gubbins, N. Quirke (Eds.), *Molecular Simulations and Industrial Applications*, Gordon & Breach, Amsterdam, 1996.
- [2.5] M. Fermeglia, S. Pricl, *AIChE J.* 45 (1999) 2619–2627.
- [2.6] S. Pricl, M. Fermeglia, *Chem. Eng. Commun.* 190 (2003) 1267–1292.
- [2.7] J.G.E.M. Fraaije, B.A.C. van Vlimmeren, N.M. Maurits, M. Postma, O.A. Evers, C. Hoffman, P. Altevogt, G. Goldbeck-Wood, *J. Chem. Phys.* 106 (1997) 4260.
- [2.8] R.D. Groot, P.B. Warren, *J. Chem. Phys.* 107 (1997) 4423.
- [2.9] J.G.E.M. Fraaije, A.V. Zvelindovsky, G.J.A. Sevink, *Molecular Simulation*, 30 (2004) 225.
- [2.10] A.A. Gusev, *Macromolecules* 34 (2001) 3081.
- [2.11] E. Tocci, A. Gugliuzza, L. De Lorenzo, M. Macchione, G. De Luca, E. Drioli, *J. Membr. Sci.* 323 (2008) 316.
- [2.12] W. Paul and G. D. Smith, *Reports on Progress in Physics*, 67 (2004) 1117.
- [2.13] D. N. Theodorou. Principles of Molecular Simulation of Gas Transport in Polymers. In Y. Yampolskii, I. Pinnau, and B. D. Freeman, editors, *Materials Science of Membranes for Gas and Vapor Separation*, book chapter 2. Wiley, 2006.
- [2.14] A. Hinchliffe *Molecular Modelling for Beginners*. Wiley, 2003.
- [2.15] D. T. Punsalan. A Sorption and Dilation Investigation of Amorphous Glassy Polymers and Physical Aging. Dissertation, University of Texas at Austin, 2001.
- [2.16] Y. Kamiya, T. Hirose, Y. Naito, and K. Mizoguchi. *J. Polymer Sci. Part B: Polym. Phys.* 26 (1988) 159.
- [2.17] G. C. Sarti and F. Doghieri. *Chemical Engineering Science*, 53 (1998) 3435.
- [2.18] *Forcefield-based Simulation, General Theory & Methodology*, Copyright (1997).
- [2.19] D. N. Theodorou and U. W. Suter, *Macromolecules*, 18 (1985) 1467.
- [2.20] H. J. C. Berendsen, J. P. M. Postma, W. F. Vangunsteren, A. Dinola, and J. R. Haak. *J. Chem. Phys.* 81 (1984) 3684.
- [2.21] F. Muller-Plathe, *Acta Ploymer* 45 (1994) 259 .
- [2.22] J.M. Haile, *Molecular Dynamics Simulation*, Wiley, New York, 1992.
- [2.23] L.S. Darken, *Trans. Am. Inst. Min. Metall. Eng.*, 175 (1948) 184.
- [2.24] S. Sunderrajan, C.K. Hall and B.D. Freeman, *J. Chem. Phys.*, 105 (1996) 1621.

- [2.25] A.A. Gusev, S. Arizzi and U.W. Suter, *J. Chem. Phys.*, 99 (1993) 2221.
- [2.26] A.A. Gusev, S. Arizzi and U.W. Suter, *J. Chem. Phys.*, 99 (1993) 2228.
- [2.27] A.A. Gusev, F. Müller-Plathe, W.F. Van Gunstern and U.W. Suter, *Adv. Polym. Sci.*, 116 (1994) 207.
- [2.28] Gsnet & Gsdif Macros, Distributed by Accelrys Inc., San Diego, CA, USA.
- [2.29] N. Metropolis, A.W. Rosenbluth and M.N. Rosenbluth, A.H. Teller and E. Teller, *J. Chem. Phys.* 21 (1953) 1087.
- [2.30] Hildebrand, J.H.; Prausnitz, J.M.; Scott, R.L. *Regular and Related Solutions*, van Nostrand: New York (1970)
- [2.31] Brandrup, J.; Immergut, E.H., eds. *Polymer Handbook*, Third Edition, John Wiley and Sons, Inc.: New York (1989).
- [2.32] H. Sun and D. Rigby, *Spectrochimica Acta Part A Molecular and Biomolecular Spectroscopy*, 53 (1997) 1301.
- [2.33] D. Rigby, H. Sun, and B. E. Eichinger. *Polymer International*, 44 (1997) 311.
- [2.34] *Polymer User Guide*. MSI/Accelrys Inc., San Diego, 1996. Amorphous Cell Section.
- [2.35] B.E. Eichinger, D. Rigby and M.H. Muir., *Comput. Polym. Sci.*, 5 (1995) 147.
- [2.36] D. Hofmann, M. Heuchel, Y. Yampolskii, V. Khotimskii, and V. Shantarovich. *Macromolecules*, 35 (2002) 2129.
- [2.37] D. Hofmann, M. Entrialgo-Castano, A. Lerbret, M. Heuchel, and Y. Yampolskii, *Macromolecules*, 36 (2003) 8528.
- [2.38] M. Heuchel, M. Böhning, O. Hölck, M. R. Siegert and D. Hofmann, *J. of Polym. Sci. Part B: Polym. Phys.*, 44 (2006) 1874.
- [2.39] O. Hölck, M. R. Siegert, M. Heuchel and M. Böhning, *Macromolecules*, 39 (2006) 9590.



### III. TRANSPORT PROPERTIES OF A COPOLY(AMIDE-12-B-ETHYLENEOXIDE) MEMBRANE: A COMPARATIVE STUDY BETWEEN EXPERIMENTAL AND MOLECULAR MODELING RESULTS

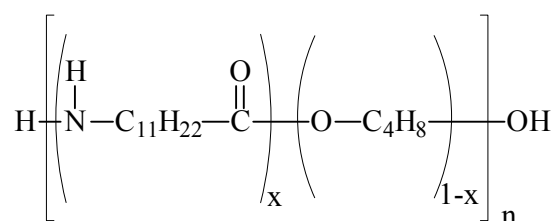
#### 1. MATERIALS: Poly(ether-b-amide) Copolymer Membranes

##### 1.1. Introduction

Elastomeric block co-polyamides and polyurethanes have gained a unique position in many industrial applications for different reasons, mainly related to their good physical properties such as high processability, notable strength and interesting permselectivities both to gases and vapours. Currently the main commercial applications of this class of co-polymers range from sporting goods [3.1], industrial equipment, functional films [3.2-3.4] and electrochemical devices [3.5] to membrane separation processes [3.6-3.11] and biomaterials [3.12, 3.13].

The history of polyether block amide (PEBA) resin can be dated to 1972 research initiatives by Atochem in which the goal was a “soft” nylon material. The actual polyether block amide polymer was commercialized in 1981 [3.14]. Polyether block amide (PEBA) resin is best known under the trademark PEBA<sup>®</sup> and is a thermoplastic elastomer combining linear chains of rigid polyamide segments interspaced with flexible polyether segments. It is produced by polycondensation of a dicarboxylic polyamide and a polyether diol in the presence of heat, vacuum, and a catalyst [3.15].

The structure of the PEBA<sup>®</sup> repeating unit is:



**Scheme 3. 1 - Chemical structure of the repeating unit in PEBA<sup>®</sup>2533 [80PTMO/PA12], [PA12: poly(imino(1-oxododecamethylene)]; PTMO: poly (tetramethylene oxide)].**

where PA is an aliphatic polyamide “hard segment” (i.e., Nylon-6 [PA6], or Nylon-12 [PA12]), and PE is an amorphous polyether “soft segment”. The soft segment is either poly(ethyleneoxide), or poly(tetramethylene oxide). This crystalline/amorphous structure creates a blend of properties of thermoplastics and rubbers. In application to permeation, the hard amide block provides the mechanical strength, whereas gas transport occurs primarily in the soft ether segments [3.16].

Currently, the main commercial applications range from sporting goods (shoe soles), industrial equipment (conveyor belts), as well as functional films (breathable clothing, drying films) and various other materials.

## 1.2. Gas transport across PEBA membrane

Only in recent years membranes based on PEBA polymer have been investigated in separation processes. In the pulp and paper industry, recovery of methanol from water wet air streams is crucial to control hazardous air pollutant emissions.

Many experimental studies have been devoted to understanding the relations between structural characteristics of PEBA copolymers [3.17-3.24] and their transport properties [3.25-3.31].

Rezac et al. [3.25, 3.26] evaluated the sorption and diffusion characteristics of water and methanol in a series of PEBA® copolymers. Their results indicated that PEBA® materials can be used to selectively separate methanol from air, but not methanol from water. The PEBA® series in their study consist of Nylon-12 and polytetramethylene oxide of varying ratios. Among the four grades of PEBA® (2533, 3533, 5533, and 6333), the 2533 grade was the most promising due to high permeation rates.

Djebbar et al. [3.27] studied the pervaporation of three aqueous ethyl ester solutions with PEBA® membranes of different polyamide composition ranging from 25 to 80 weight percent. PEBA® was chosen as the material of interest due to its hydrophobicity and high selectivity of aromatic organic compounds from water. The separation is considered to be an alternative for the extraction of volatile organic compounds (VOCs) from aqueous media.

It was shown in this study that the use of PEBA® membranes of high polyether content is most advantageous for VOCs extraction, as long as the polymer swelling from the penetrant is not excessive.

Bondar et al. [3.16, 3.28] found that in applications such as the removal of CO<sub>2</sub> from mixtures of hydrogen in syngas, PEBA was found to have high selectivity on polar or quadrupolar/nonpolar systems (e.g. CO<sub>2</sub>/H<sub>2</sub> or CO<sub>2</sub>/N<sub>2</sub>). Bondar's group evaluated membranes made from four grades of PEBA®, which range from 80 to 53 weight percent of polyether (PE) in the blockcopolymer. The PEBA® grades are 2533, 4011, 1074, 4033 in depending PTMO weight percent.

Their sorption and permeation results suggest strong interaction between the polar gas CO<sub>2</sub> and the PE blocks in the copolymer. They found that PE composition and CO<sub>2</sub> permeability were directly correlated.

Kim et al. [3.8, 3.9] reported the particular selectivity of CO<sub>2</sub> over N<sub>2</sub> is 61 and that of SO<sub>2</sub> over N<sub>2</sub> is 500. Strong affinity of polar species to the PE block is attributed to the high permeability and permselectivity of polarizable gases through PEBA® copolymer.

Barbi et al. [3.29] studied the nanostructure of different PEBA membrane materials and found that the domain diameters of the hard domains are almost the same for all the studied materials; copolymers of the series with a low hard block content (such as PEBA®2533) appear to reproduce an almost constant domain topology (size and arrangement of domains).

An improvement of gas was observed for increasing size of the soft domain and SAXS experiments indicated that samples with poor phase separation showed decreased gas permeability and diffusivity.

In the last decade polymer modeling methods have been enough powerful to predict diffusion coefficients, permeability and selectivity for specific polymer - penetrant systems by relating these properties to the chemical structure of the polymer under investigation. Fresh insights into the diffusion mechanism of small molecules in a membrane have been provided by molecular dynamics (MD) methods. This method has been extensively used to investigate different types of polymeric

matrices [3.32-3.46]. A better insight into the gas permeation mechanism could be gained by computer simulation for the study of materials at the microscopic and mesoscopic levels.

This paper describes permeation experiments through Pebax membranes performed for six permanent gases, N<sub>2</sub>, O<sub>2</sub>, CH<sub>4</sub>, He, H<sub>2</sub> and CO<sub>2</sub> at different operating conditions.

Molecular dynamics simulations (MD) were used both to study the transport-properties relationships for pure PEBAX<sup>®</sup>2533 dense membranes and to identify the role played by the soft ether block (PTMO) in gas permeability. The predicted values were then compared with experimental data in order to validate the investigative approach.

An accurate fully atomistic study on the bulk amorphous pure PEBAX<sup>®</sup>2533 and on the soft poly(tetramethylene oxide) (PTMO) polyether block were carried out using Gusev -Suter Transition State Theory (TST) [3.47-3.49] and Monte Carlo methods. For semi-crystalline polymers the comparison of theoretical and experimental data is generally limited to the amorphous part of the materials: the diffusivity in the crystallites is of a smaller order of magnitude than in amorphous regions [3.50, 3.51].

In this chapter a detailed fully-atomistic investigation of the separation of polar/non polar pair gas through co-poly(ether/amide) block membranes has been provided. An assessment of the structure/property relationships is included, highlighting the role of diffusivity and solubility selectivities for various penetrant species.

### **1.3. Atomistic Packing Models.**

The amorphous atomistic bulk structures of the copolymer PEBAX<sup>®</sup>2533 and of the homopolymer PTMO were constructed and simulated by using three-dimensional cubic periodic boundary conditions and by using the InsightII (400P+) molecular modelling package of Accelrys [3.52] and the COMPASS force field [3.53]. The process was implemented in four steps :

1. The structure of each single chain of the copolymer was modelled by alternating the comonomers polyamide-12 (PA-12) and poly(tetramethylene oxide) (PTMO) segment, in such a way as to respect the experimental relative weight percentages of 20 wt % of PA-12 and of 80 wt % of PTMO [3.26].
2. The structures of polyamide-12 (PA-12) and poly(tetramethylene oxide) (PTMO) comonomers were constructed using the polymer BUILDER module of Insight II (400P+) molecular modelling package [3.52]. Charge groups were assigned to fragments of each repeat unit and used for their energy minimisation. It was employed a standard algorithm starting with a steepest-descent stage, switching to conjugate gradient when the energy derivative reaches  $1000 \text{ kcal}\cdot\text{mol}^{-1}\text{\AA}^{-1}$  followed by a Newton-Raphson optimisation algorithm. For the final convergence a derivative of less than  $0.001 \text{ kcal}\cdot\text{mol}^{-1}\text{\AA}^{-1}$  was accepted. All the atoms in the copolymer chains were treated explicitly.
3. The isolated initial chain configurations of the copolymer were then constructed [3.52], based on the indication provided by Rezac et al. [3.26] about the molecular weights of each component of the block copolymer 2533, i.e. the PA12 moiety with a  $M_w = 530$  and the PTMO with an  $M_w = 2000$ , the single chain of PEBAX<sup>®</sup>2533 was produced by alternating 3 comonomers of PA-12 and 28 of PTMO. A polymerization degree of 16 was chosen taking into account the dimension of a typical simulation box side (40–50 Å) and the experimental density of pure PEBAX<sup>®</sup>2533, that is  $1.012 \text{ g}\cdot\text{cm}^{-3}$  [3.54]. The backbone dihedral angles were set to random and the copolymer chains were rapidly optimised (500 steps).

4. Bulk amorphous polymer structures were filled with segments of a growing chain under periodic boundary conditions following the Theodorou-Suter [3.55] chain-generation approach and reproducing the natural distribution of conformation angles. The structures were generated using Amorphous Cell, at 303 K. [3.52]. In order to minimize chain end effects, each simulation box contained only one minimized copolymer sequence rather than several confined to the same volume, which would lead to increased density of chain ends. On the same line of thought, the use of single-chain polymers representing bulk amorphous systems is common and has been proven to be quite accurate in replicating the behaviour of experimental polymeric systems [3.43, 3.44, 3.45, 3.56].

Several argon atoms were placed in each packing cell. These objects served as obstacles preventing the growing polymer chains from the overlapping of the same chains.

Choosing an initial density of the models lower than the experimental one and the introduction of argon molecules were sufficient to generate chain overlapping-free structures. Later the obstacle molecules were removed in three steps. Cycles of energy minimizations and dynamic runs - with a force field parameter downscaled (Table 3.1) - were performed after each removal [3.46].

Equilibration stage	Scaling factor for the conformation of energy terms in the forcefield	Type of non-bonded interaction energy terms ( <i>EvdW</i> )	Type of non-bonded interaction energy terms ( <i>ECoulomb</i> )
1	0.001	0.001	0.001
2	0.01	0.001	0.01
3	0.01	0.01	0.01
4	0.1	0.1	1
5	1	1	1

**Table 3. 1-Scaling procedure of FF energy terms torsion, non-bonded and Coulomb interactions.**

The packing models, with a reduced density in comparison to the experimental value, were subjected to extensive equilibration procedures made of sequences of energy minimization and NpT and NVT-MD and annealing simulations (NVT-MD refer to a MD simulation at a constant number of particles (atoms) *N*, volume of the simulation cell *V*, and temperature *T*, whereas at NpT-MD, the pressure *p* is held constant instead of the volume). In order to reach the experimental density the cells were pressurized at 300 K via NpT-MD simulations with increasing values of pressure up to a density greater than the experimental one. The cells were refined by employing three temperature

cycle NVT runs (annealing), with temperatures up to the glass-transition temperature ( $T_g$ ) of the polymer. NVT dynamics at 303 K were used to further relax the polymer structure. The system was then cooled back to 500, 400 and finally 298 K, with NVT–MD simulations alternating energy minimizations. The duration of the NVT dynamics simulations at each temperature was of 5000 fs. The final equilibration stage was carried out using a NVT run at 300K for 300ps duration time, a time recognised to be sufficient for systems reaching an almost constant value of total energy. One cell, with a lower density than the experimental one (about 8 %), was equilibrated via NpT-MD dynamics at a pressure of 1 bar for a total duration of 300 ps (timestep = 1 fs) whereas the NVT-MD ensemble was used for the other cells. NVT simulations at  $T = 298$  K were then performed for 1.5 ns. In all runs the simulation used the following conditions: (a) minimum image boundary condition to make the system numerically tractable and to avoid symmetry effects and (b) a cut-off distance of 15 Å with a switching function in the interval of 13.5–15 Å. Through the dynamics the Andersen [3.57] and the Berendsen [3.58] pressure control methods were applied. Three models for each composition were constructed.  $N_2$ ,  $O_2$  and  $H_2$  molecules were used as inserted gas molecules in one simulation box for the fully atomistic MD simulation. In a second box He and  $CH_4$  were inserted and in a third box only  $CO_2$  molecules were considered. The side length of the bulk models was 40 Å. The procedure of construction and equilibration of a 3D PEBAx is shown step by step in Figure 3.1

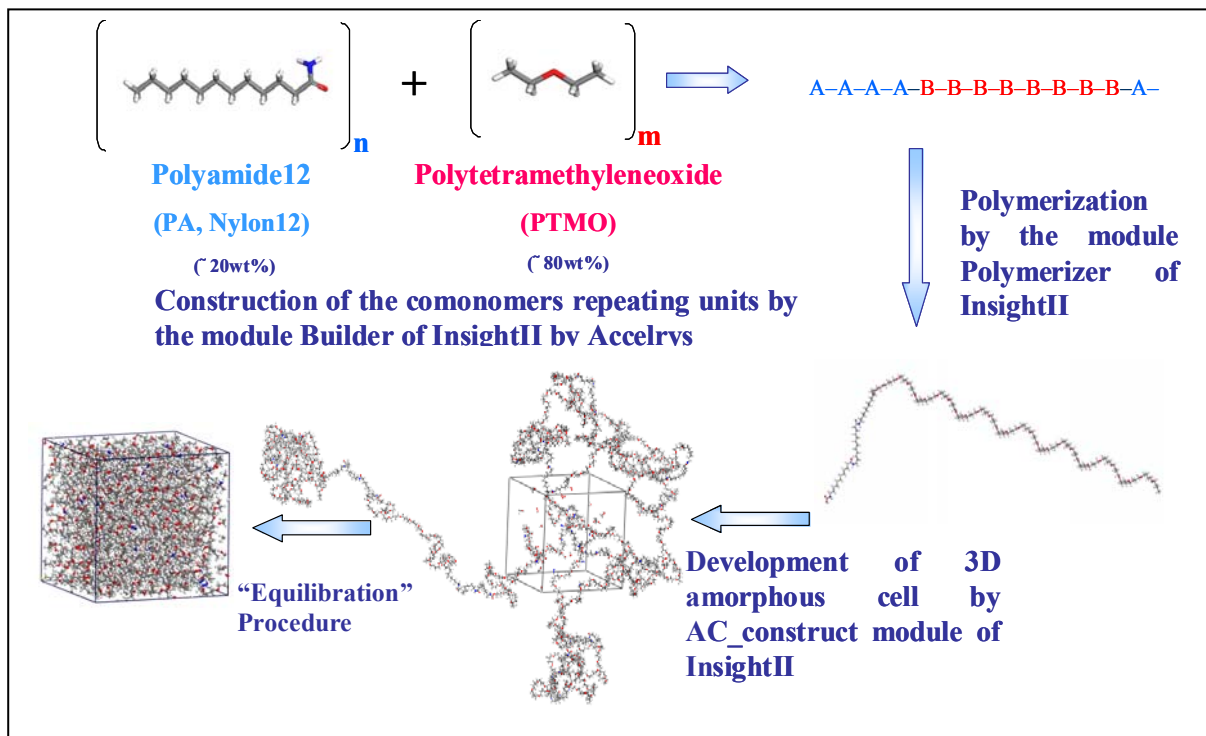


Figure 3. 1 - Construction and equilibration procedure of PEBAx<sup>®</sup>2533 3D cell at the density of 1.01 g/cm<sup>3</sup>.

In a parallel process to the preparation of PEBAx<sup>®</sup>2533 two boxes of pure PTMO were built at the  $d = 1.00$  g·cm<sup>-3</sup> [3.59]. The polymerization degree used was of 688 repeat units with about 9000 atoms. The procedure to prepare and equilibrate the polymeric models was the same as described above.  $N_2$ ,  $O_2$  and  $H_2$  molecules were used as inserted gas molecules for the MD run. The dimension of the two boxes of PTMO were of 44 Å. Details for the simulation are summarized in Table 3.2:

System	DP	N atoms	$\rho$ exp <sup>a</sup>	$\rho$ sim.	Cell length (Å)
PEBAX 1	16	7780	1.01	1.0356	41.18
PEBAX 2	16	7780	1.01	1.0107	41.52
PEBAX 3	16	7780	1.01	1.0107	41.52
PTMO 1	688	9019	1.00	1.0127	43.53
PTMO 2	688	9019	1.00	1.0127	43.53

<sup>a</sup>PEBAX: [3.54]

<sup>a</sup>PTMO:[3.59]

**Table 3. 2 - Details of the simulations**

## 2. Results and Discussion

### 2.1. Structural Properties – WAXD

To obtain reliable results for the diffusion and solubility coefficients of penetrants in polymeric matrices it is very important to demonstrate that the host polymer is simulated consistently. Information about the structural features of the PEBA<sup>®</sup>2533 models at the atomic level was provided by simulating X-ray structure factors: COMPASS was used to obtain the wide-angle X ray diffraction (WAXD) pattern of PEBA<sup>®</sup>2533 using the diffraction module of Insight II [3.51].

The wide-angle X-ray (WAXD) pattern for each single cell was simulated and averaged as presented in Fig. 1 and was compared with the experimental WAXD data [3.28]. The data are presented in the form of normalized intensity (intensity at each angle divided by the intensity of the strongest peak) as a function of angle. The simulated spectrum contains a relatively broad halo centered near 20° (2 $\theta$ ) that can be ascribed to diffraction from amorphous regions of these samples. The calculated spectrum resembles quite well the spectrum measured by Bondar et al. [3.28] where the curve gives a diffuse halo centered around 2 $\theta$  ~ 20°.

The corresponding experimental  $d$ -spacing of 4.4 Å of the amorphous content of the material, calculated by Bragg's relation ( $n\lambda = 2d \sin(\theta_{\max})$ ), coincides with the calculated value.

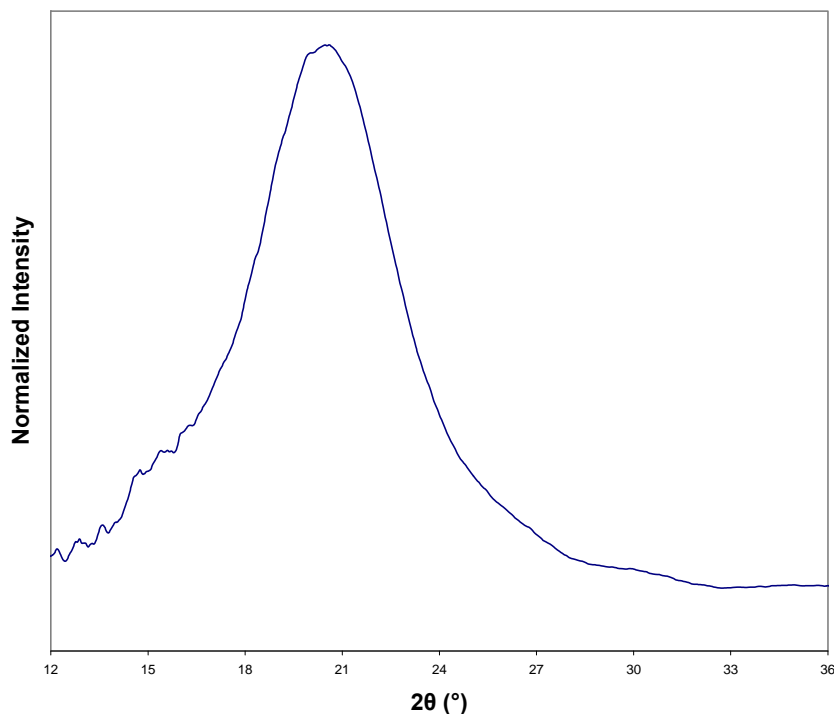


Figure 3. 2 - Simulated Wide Angle X-ray (WAXD) pattern of a PEBA<sup>®</sup>2533 three-dimensional box.



**2.2. Experimental transport properties**

Permeation and Diffusion coefficients were estimated for He, H<sub>2</sub>, N<sub>2</sub>, O<sub>2</sub>, CO<sub>2</sub>, CH<sub>4</sub>. at different operating temperatures (Fig 3.3 (a-b)).

The solubility coefficients were derived from the Permeability and Diffusion coefficients ratio, since swelling or plasticization phenomena were not observed for any gases. Ideal selectivities were calculated for all gases in order to investigate the various contributions of both diffusivity and solubility selectivities to the overall transport through PTMO80/PA12 membranes and were listed in Table 3.3.

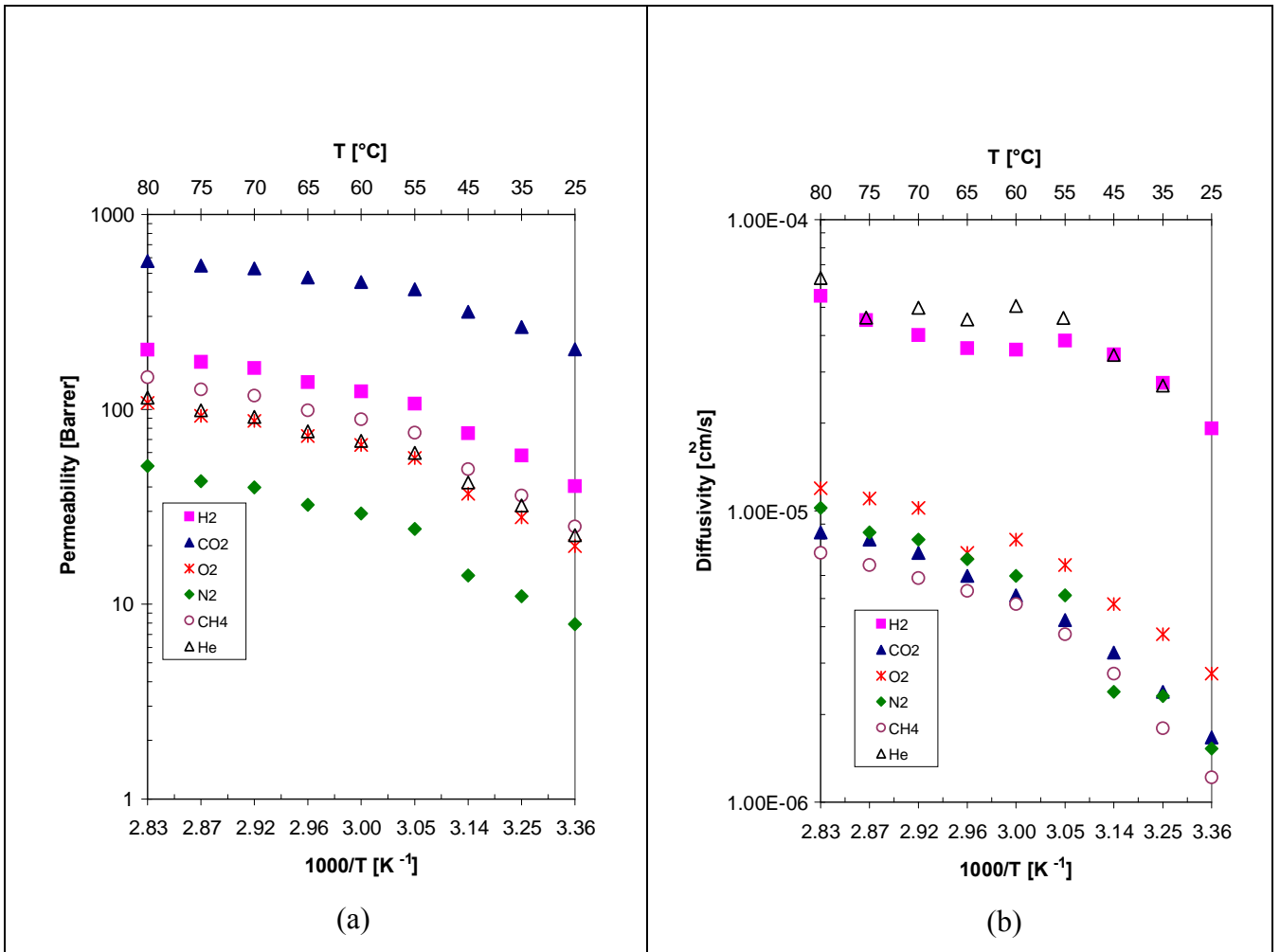


**Figure 3. 3 - Temperature dependence of experimental permeability and (b) experimental diffusivity, ranging both from 25 °C to 80°C of six gases for the solution-cast membrane of PEBA 2533.**

A lowering of the energy barriers was estimated for all penetrants. The activation energies of permeation, E<sub>p</sub>, and of diffusion, E<sub>d</sub>, were derived from two constant slopes across 60°C. These were obtained plotting both the permeability and diffusion coefficients versus the temperature. In Table 3.3 the activation energies below and above 60°C are indicated. This is



an intermediate temperature between the melting points of the two hard and soft blocks. The break points observed in Fig.3.3 a , b can be ascribed to the softness of the segment chains whose thermal mobility enhances the mass transfer. A similar behaviour was observed by Kim *et al.*[3.8] for other polyether blocks containing polymers

Gas	Activation energy of Diffusion		Activation energy of Permeation		Selectivity at 25°C			Selectivity at 55°C			Selectivity at 80°C		
	Ed <sub>1</sub>	Ed <sub>2</sub>	Ep <sub>1</sub>	Ep <sub>2</sub>	P <sub>f</sub> /P <sub>N<sub>2</sub></sub>	D <sub>f</sub> /D <sub>N<sub>2</sub></sub>	S <sub>f</sub> /S <sub>N<sub>2</sub></sub>	P <sub>f</sub> /P <sub>N<sub>2</sub></sub>	D <sub>f</sub> /D <sub>N<sub>2</sub></sub>	S <sub>f</sub> /S <sub>N<sub>2</sub></sub>	P <sub>f</sub> /P <sub>N<sub>2</sub></sub>	D <sub>f</sub> /D <sub>N<sub>2</sub></sub>	S <sub>f</sub> /S <sub>N<sub>2</sub></sub>
	(KJ)	(KJ)	(KJ)	(KJ)	(-)	(-)	(-)	(-)	(-)	(-)	(-)	(-)	(-)
He	20,42	25,07	25,96	22,72	2.87	11.75	0.24	2.46	8.75	0.28	2.24	7.00	0.32
H <sub>2</sub>	17,45	40.79	25,91	21,66	5.13	11.19	0.46	4.39	5.18	0.84	3.95	3.50	1.13
CO <sub>2</sub>	26,23	16,38	18,19	8,41	25.80	1.09	23.61	17.02	0.82	20.66	11.26	0.82	13.67
O <sub>2</sub>	22,04	15,51	28,07	21,42	2.52	1.81	1.39	2.32	1.27	1.82	2.11	1.16	1.81
N <sub>2</sub>	32,38	25,23	30,95	25,22	1	1	1	1	1	1	1	1	1
CH <sub>4</sub>	31,45	20,02	29,59	21,80	3.18	0.80	3.99	3.12	0.74	4.23	2.86	0.70	4.08

**Table 3.3** -Experimental data of solution-cast PEBAX<sup>®</sup> 2533 membrane: activation energies of diffusion and permeation for various gases below (Ed<sub>1</sub>, Ep<sub>1</sub>) and above (Ed<sub>2</sub>, Ep<sub>2</sub>) 60°C; permeability, diffusivity and solubility selectivities at different temperatures.

Three experimental diffusion coefficients of CO<sub>2</sub> were calculated at three different times of the transient state and measured at different temperatures, ranging from 25 °C to 80°C (Fig. 3.4).

Differences can be appreciated at lower temperature values. These can be partly attributed to measurement errors. However, this behaviour may also be explained because of the affinity of quadrupolar carbon dioxide to accessible polar groups of both the hard and soft polymer blocks. Theoretical analysis, i.e. calculated radial distribution functions discussed in the following session 2.3.5 and shown in Fig. 3.9, suggest also a strong association between CO<sub>2</sub> and the various polar groups of the polymer.

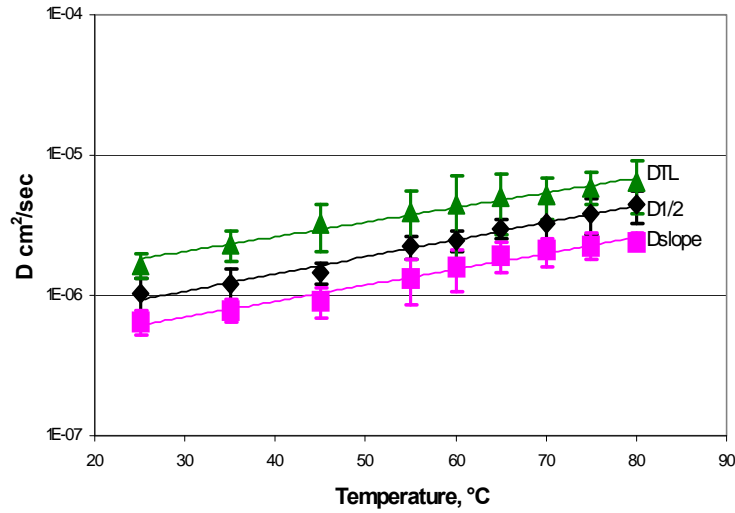


Figure 3. 4- The three experimental diffusion coefficients calculated at three different times of the transient state and measured at different temperatures, ranging from 25 °C to 80°C of CO<sub>2</sub> for the solution-cast membrane of PEBAX 2533.

The solubility data calculated are in reasonable agreement with those estimated at 35 °C by Bondar et al. who used independent sorption experiments [3.28].

Membranes based on PTMO80/PA12 exhibit high permeation values as the penetrant species is a gas with high condensability characteristics, that is a gas with a high critical temperature (Table 3.4). Because molecules become more condensable with increasing diameter, penetrant solubility in typical polymers increases with increasing penetrant condensability [3.64].

Gas	Critical Temperature (K) <sup>a</sup>	Lennard-Jones Diameters d <sub>LJ</sub> (Å) <sup>a</sup>
H <sub>2</sub>	33.2	2.93
O <sub>2</sub>	154.6	3.46
N <sub>2</sub>	126.2	3.698
CO <sub>2</sub>	304.2	4.00
CH <sub>4</sub>	190.6	3.817

Table 3. 4 - Physical properties of six permanent gases used in the experimental and theoretical characterization.

For polar/non polar gases such as for CO<sub>2</sub>/N<sub>2</sub> the permeability and solubility selectivities decreased significantly at elevated temperatures (Table 3.3). These effects are typical for PTMO based films: at elevated temperature the reductions in  $\alpha_{\text{CO}_2/\text{N}_2}$  are due to the decrease of solubility selectivity, the diffusivity selectivity being almost constant in this range. On the other hand the permselectivity of small and nonpolar gases, i.e. H<sub>2</sub>/N<sub>2</sub>, at 80°C decreased only 23% of that at 25°C.

From a comparison of the different permeation data, CO<sub>2</sub> exhibits the highest permeability value owing to the highest contribution of the solubility, resulting in 1-2 orders of magnitude larger than other gases. The solubility selectivity appears to be the key controlling factor in the transport of some species according to the following order CO<sub>2</sub>>>CH<sub>4</sub>>O<sub>2</sub>>>N<sub>2</sub> (Table 3.3). A further confirmation of the strong effect on the transport exercised by the solubility is given by the comparison of the CO<sub>2</sub> and N<sub>2</sub> transport parameters. CO<sub>2</sub> exhibits a permeability value (P) of 203 barrer and a diffusion coefficient (D<sub>0</sub>) of 1.67 cm<sup>2</sup>/s at 25°C, whereas permeability and diffusivity estimated for N<sub>2</sub> are 7.89 barrer and 1.53 cm<sup>2</sup>/s. This means that these two species diffuse through the matrix at a comparable speed. The difference in permeability has to be ascribed, therefore, to the condensability of CO<sub>2</sub> that is 2.41 times higher than that of N<sub>2</sub>, resulting in its higher dissolution in the polymer matrix. Strong interactions between the carbon dioxide and the ether segments of the polymer are expected. Studies related to series of poly(ether-b-amide) block co-polymers have highlighted increasing solubility of CO<sub>2</sub> with rising content in PE-containing blocks [3.10, 3.16, 3.28].

Extremely small molecules like He and H<sub>2</sub> are an exception as a result of their smaller kinetic diameters. These two penetrants permeate faster through the membranes exhibiting a diffusivity selectivity higher than the solubility selectivity as compared with the bulkier N<sub>2</sub> (Table 3.3). The estimated diffusivity values for both gases were one order of magnitude higher than those measured for the other gases (Fig. 3.3 b). As expected, these molecules easily find location in gaps interspaced between the polymer chains, whose distribution changes frequently due to the elastomeric character of the matrix. The transport of this single species through Pebax membranes, however, is strongly affected by its low solubility in the polymer matrix as compared with a more polar and condensable gas such as CO<sub>2</sub>. In this case, the contribution of the diffusivity is overshadowed by its limited affinity to the segment chains. The best selectivities of these membranes were estimated for polar/nonpolar pair of penetrants such as CO<sub>2</sub>/H<sub>2</sub> and CO<sub>2</sub>/N<sub>2</sub> (Table 3.5), confirming the better performance of this class of poly(ether-b-amide) block co-polymers than that of conventional rubbery polymers. The predominance of the solubility contribution appears, therefore, to be the driving force of the selective process.

Gas1/ Gas2	S(Gas1)/S(Gas2)			
	Exp.	Exp. <sup>a</sup>	TST	GCMC
O <sub>2</sub> /N <sub>2</sub>	4.0	4.6	3.75	3.1
CH <sub>4</sub> /N <sub>2</sub>	1.39	2.0	2.12	4.5
CO <sub>2</sub> /N <sub>2</sub>	23.6	28.8	14.9	6.0
CO <sub>2</sub> /H <sub>2</sub>	51.5	43	38.2	32.5

**Table 3.5 - Solubility selectivity for several gas pairs in PEBAX<sup>®</sup> 2533 at 25°C**

Another noteworthy aspect is the satisfactory O<sub>2</sub>/N<sub>2</sub> selectivity exhibited by the PTMO80/PA20 membranes. A value of 2.5 is analogous to that of a high permselective glassy membrane such as the Hyflon AD 60X melt-pressed membrane [3.63] which shows an O<sub>2</sub>/N<sub>2</sub> selectivity of 3.3. Values lower than 2.5 were also estimated for traditional rubbery and some glassy polymers.

The higher condensability as well as the lower kinetic diameter of oxygen in comparison to nitrogen concurs to optimise both the diffusivity and solubility selectivities.

### 2.3. MD simulations

#### 2.3.1 Diffusion coefficients

The reliability of the three equilibrated PEBAX<sup>®</sup>2533 models was also tested by comparing simulated and experimental diffusivity and solubility coefficients of five gas molecules, H<sub>2</sub>, O<sub>2</sub>, N<sub>2</sub>, CH<sub>4</sub> and CO<sub>2</sub>. Equilibrated amorphous cells were used in order to estimate the diffusion coefficients using direct molecular dynamics and TST calculations, and the solubility coefficients with Grand Canonical Monte Carlo (GCMC) and TST calculations.

Two equilibrated amorphous PTMO boxes were used for comparison with the PEBAX<sup>®</sup>2533 models in order to extrapolate the influence of the soft component on the transport properties of the copolymer material. Molecular dynamics simulations for O<sub>2</sub> and N<sub>2</sub> molecules and TST calculations for the five gases mentioned above were performed. The diffusion coefficients of H<sub>2</sub>, O<sub>2</sub>, N<sub>2</sub>, CH<sub>4</sub>, CO<sub>2</sub> calculated with TST in PEBAX<sup>®</sup>2533 and in PTMO were averaged on three theoretical models, and two, respectively. In Table 3.6 are summarized the theoretical transport parameters and the selectivity values estimated for PEBAX<sup>®</sup>2533 and for PTMO. The diffusivity and solubility selectivities for all gases are also indicated. The theoretical diffusivity selectivities are better reproduced by the MD method

that by the TST. On the other hand calculated solubility selectivities are in the same order of magnitude as the experimental ones apart from some exceptions such as for CO<sub>2</sub>.

**2.3.2 Compared theoretical and experimental diffusion data**

Figure 5(a) shows the comparison of the diffusion coefficients obtained via MD simulations with the experimental data presented in Table 3 (at 25°C). It should be noted that the diffusion coefficient defined by Eq. (2.12) is a self-diffusion coefficient obtained under equilibrium dynamics while diffusion coefficients, typically reported in the literature, are transport coefficients obtained from time-lag measurements.

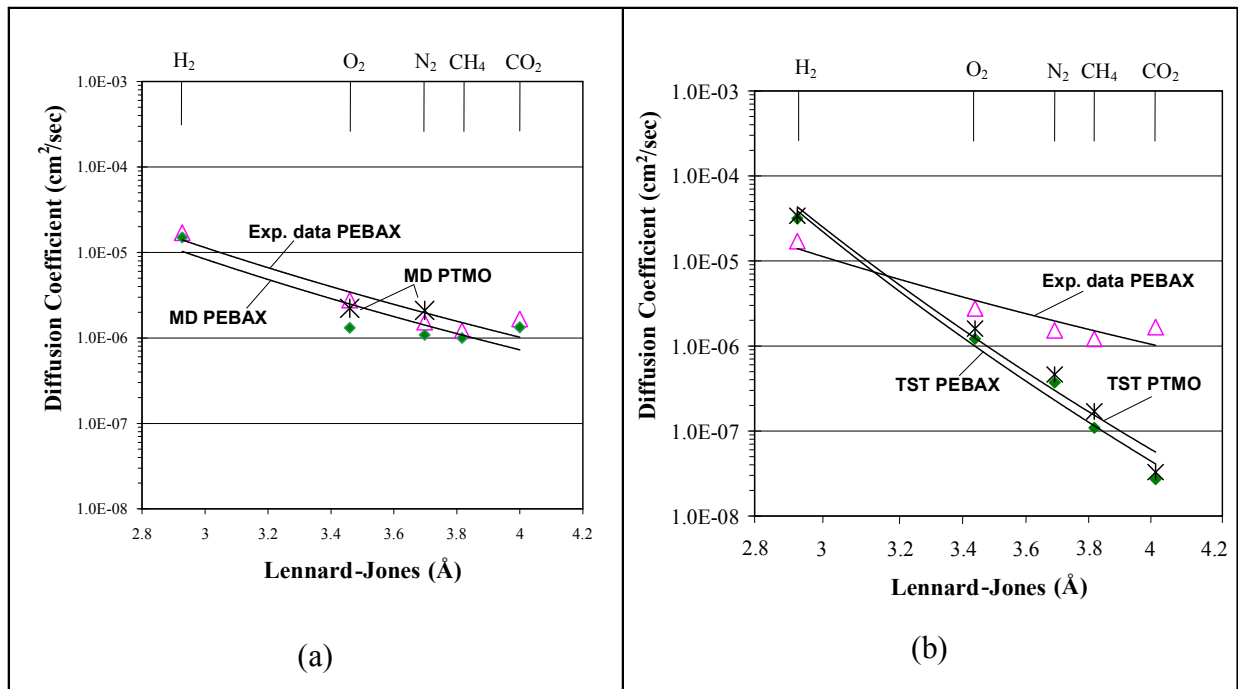


**Figure 3. 5 - (a) Semilogarithmic plot of experimental (time – lag) diffusion coefficients at 25°C of the five gases for the solution-cast membrane of PEBAX<sup>®</sup> 2533 (△) and theoretical data from MD simulations (Eq.(1)) of PEBAX (◆) and of PTMO (\*). (b) Comparison between experimental (time – lag) diffusion data (△) with theoretical data from TST simulations of PEBAX(◆) and PTMO (\*). The lines represent the least-squared fit of experimental (R= 0.9034) and theoretical data**

	Gas	TST	TST	TST	MD	GCMC	Selectivity			
		Permeability coefficient, P barrer <sup>a</sup>	Diffusion coefficient, D (cm <sup>2</sup> /sec)*10 <sup>-6</sup>	Solubility coefficient, S (cm <sup>3</sup> /cm <sup>3</sup> cmHg)*10 <sup>-4</sup>	Diffusion coefficient, D (cm <sup>2</sup> /sec)*10 <sup>-6</sup>	Solubility coefficient, S (cm <sup>3</sup> /cm <sup>3</sup> cmHg)*10 <sup>-4</sup>	D/D <sub>N<sub>2</sub></sub> (-)		S/S <sub>N<sub>2</sub></sub> (-)	
							TST	MD	TST	GCMC
PEBAX 2533	H <sub>2</sub>	186.0 ± 55.0	31.79 ± 9.46	6.16 ± 2.1	15.03	5.37 ± 1.8	85.92	13.92	0.37	0.19
	CO <sub>2</sub>	77.23 ± 33.1	0.027 ± 0.005	321.7 ± 180	1.34	173.1 ± 50	0.073	1.24	19.26	5.99
	O <sub>2</sub>	39.10 ± 15.6	1.21 ± 0.55	35.4 ± 19.3	1.31	43.32 ± 15.7	3.27	1.21	2.12	1.50
	N <sub>2</sub>	5.55 ± 2.4	0.37 ± 0.15	16.7 ± 11.0	1.08	28.9 ± 10.5	1	1	1	1
	CH <sub>4</sub>	6.18 ± 3.6	0.11 ± 0.06	62.63 ± 44.8	1.02	89.74 ± 24.6	3.36	0.94	3.75	3.10
PTMO	H <sub>2</sub>	210.0 ± 41.0	34.4 ± 9.46	0.054 ± 0.01	-	-	74.78	-	0.005	-
	CO <sub>2</sub>	4.2 ± 2.0	0.033 ± 0.02	155.7 ± 60	-	-	0.072	-	-	-
	O <sub>2</sub>	41.99 ± 12.0	1.59 ± 0.7	27.24 ± 4.2	2.23	-	3.46	1.06	13.31	-
	N <sub>2</sub>	5.03 ± 1.0	0.46 ± 0.26	11.71 ± 2.7	2.10	-	1	1	1	-
	CH <sub>4</sub>	6.12 ± 3.0	0.17 ± 0.1	39.93 ± 12.0	-	-	0.37	-	3.41	-

<sup>a</sup> 1 barrer = 10<sup>-10</sup> cm<sup>3</sup><sub>STP</sub> cm/(cm<sup>2</sup> s cmHg)

**Table 3. 6- Theoretical data: permeability, diffusion and solubility coefficients, diffusivity and solubility selectivity data of PEBAX<sup>®</sup>2533 and PTMO membranes at 25 °C.**

The self diffusion coefficients for both PEBAX<sup>®</sup>2533 and PTMO polymers have been calculated from the slope of the mean square displacement curves of the MD runs via averaging over all simulated penetrant molecules of a given kind. The theoretical values are in the same order of magnitude as the experimental values, also when gas of large dimension are simulated. The errors of the diffusion coefficients in PEBAX<sup>®</sup>2533 range between 25% and 30%, moving to bigger variation for O<sub>2</sub> whose error is around 50%. In PTMO membrane the averaged diffusion coefficients of O<sub>2</sub> and N<sub>2</sub> range from 35 to 40%.

The experimental and the theoretical (MD) diffusivities are almost constant with the increasing molecular size of gases, indicating that they have some ability to sieve penetrant molecules based on their size. This is confirmed by the satisfactory O<sub>2</sub>/N<sub>2</sub> selectivity exhibited. Only H<sub>2</sub> is much faster. Values calculated for amorphous PEBAX<sup>®</sup>2533 and for amorphous PTMO are nearly identical with MD simulations., Computed values for PEBAX<sup>®</sup>2533 are slightly smaller than experimental ones, despite the overall good agreement with the experiments. The respective selectivity factors are ( $\alpha = D_{\text{exp}}/D_{\text{calc}}$ ) shown in Table 3. 7 indicate a general good agreement. Density, length of the simulation run, free volume distribution are amongst the main factors considered as responsible. The densities of the models employed are similar to the experimental values.

Gas	D <sub>exp</sub> /D <sub>calc</sub>	S <sub>exp</sub> /S <sub>calc</sub>
	(-)	(-)
	MD	GCMC
H <sub>2</sub>	1.14	0.44
CO <sub>2</sub>	1.25	0.71
O <sub>2</sub>	2.1	0.17
N <sub>2</sub>	1.4	0.18
CH <sub>4</sub>	1.2	0.23

**Table 3. 7-Comparison of experimental and calculated data of PEBAX<sup>®</sup>2533 membrane at 25 C**

Diffusion coefficients can be calculated from the Einstein relationship Eq. (2.12) if a random-walk motion for the diffusing particles is assumed. At very short times of simulation, of the order of ps, penetrants execute, indeed, ballistic motion as they rattle in cavities. Anomalous diffusion, in which molecules still follow correlated paths, depends on how fast the penetrant diffuses. The slope of the mean square displacements curve vs time starts off steeply, since fast jumps present an easy way for a gas molecule to move some distance, and

then gradually levels off to a straight line, as slower jumps now can only help the penetrant move further. The Fickian domain is reached when the  $\langle (r(t) - r(0))^2 \rangle$  is proportional to  $t$ . In the present work the simulation times of the molecular dynamics simulations were long enough, as shown in (Fig. 3.6(a)), and the slopes of the mean square displacements as a function of time were close to unity [3.33] revealing that normal diffusion regime was reached also for the CO<sub>2</sub> gas molecule (Fig. 3.6(b)).

The agreement found gives the indication that the simulation of a purely amorphous PEBAX<sup>®</sup>2533 represents a good (suitable) model for the more complex micro-phase separated real polymer structure. The amount of crystallinity of PEBAX<sup>®</sup>2533 not included in the atomistic amorphous structure is, indeed, the 3% w/w.

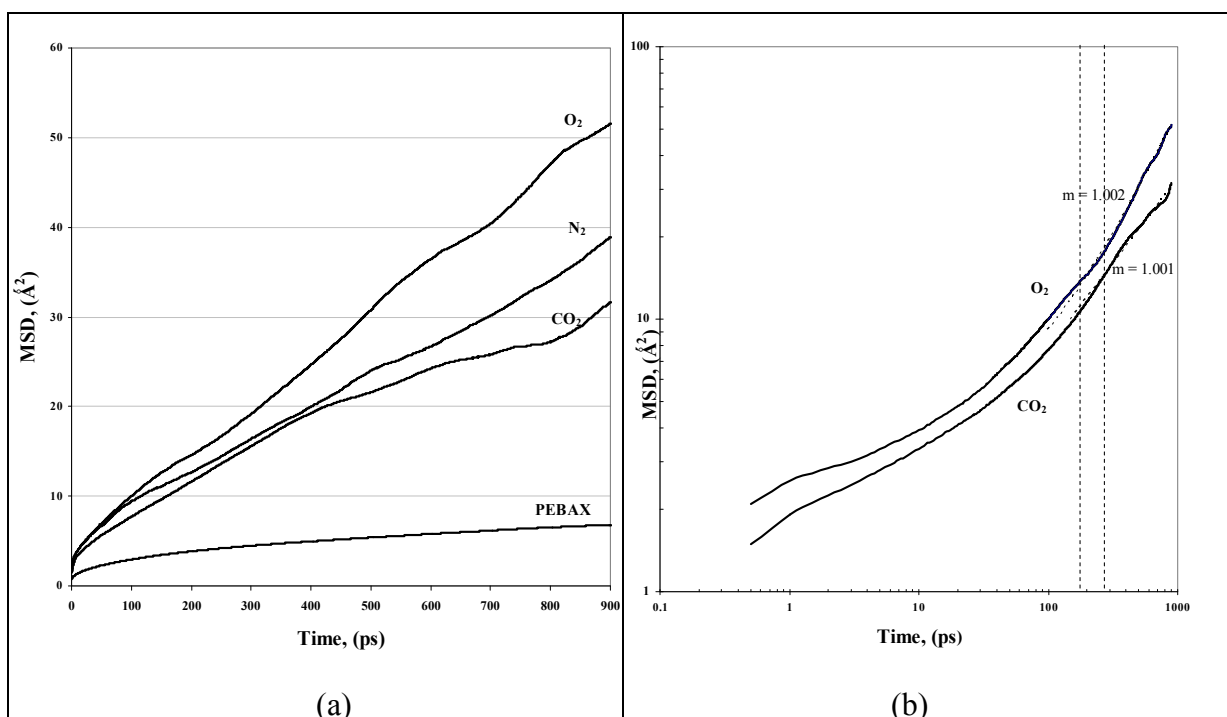


**Figure 3. 6 - (a) Mean square displacements for O<sub>2</sub>, N<sub>2</sub> and CO<sub>2</sub>, and the polymer chain of PEBAX<sup>®</sup>2533 model obtained from a completely atomistic MD run. (b) log  $s(t)$  vs. log  $t$  plot for the diffusion of O<sub>2</sub> and CO<sub>2</sub> (solid line) with  $m$  = slope. The dashed lines indicate that the Fickian domain is reached.**

The experimental diffusivity data were also compared to TST calculations of the five gases for both the PEBAX<sup>®</sup>2533 and the PTMO models (Fig. 3.5(b)). The simulated values, on the basis of the TST method, correspond in principle to constant diffusion coefficients  $D_0$  at infinite dilution which should be observed in permeation experiments at very low upstream pressures. The TST calculations performed using the Gsdif/Gsnet software code [3.61] assume that the penetrant molecules are spherically united atoms characterized by effective Lennard–Jones parameters,  $\sigma, \epsilon$  (expressed in Angstroms and kcal/mol). In all the calculations were used the default values of these parameters, i.e., O<sub>2</sub>(3.460, 0.2344), N<sub>2</sub>(3.698, 0.1889),



H<sub>2</sub>(2.93,0.0735), CH<sub>4</sub>(3.82,0.2945) and CO<sub>2</sub>(4.000, 0.4500). Furthermore, it is assumed that the polymer packing does not have to undergo structural relaxation to accommodate the inserted particle, i.e. resulting from torsion transitions. The thermal fluctuations of the atoms in the polymer matrix are only included through the use of the smearing factor.

By running short MD simulations (in the order of 100 ps) first was calculated the mean square displacement averaged over all atoms of the polymer matrix. The Gsnet code was then used in order to calculate the smearing factor. As already observed for the experimental results, the diffusion coefficients of all gases in PEBAX<sup>®</sup>2533 and in PTMO, calculated by the TST method, show the same trend, namely a reduction as a function of the molecular dimensions of the gases. In addition, the values for PEBAX<sup>®</sup>2533 are nearly identical to those of amorphous pure PTMO.

A closer inspection of Fig. 3.5(b) indicates a systematic underestimation of the diffusion coefficients from TST with respect to that from MD calculations, except for H<sub>2</sub>, which is overestimated. The diffusion coefficients in both PEBAX<sup>®</sup>2533 and PTMO matrixes for nitrogen and oxygen agree within a factor of 3-5 with the respective experimental average values. A notable discrepancy is observed, indeed, between TST and experimental data for methane and carbon dioxide. In both gases the TST values are at least one order of magnitude lower than the experimental values. The discrepancy between the experimental and theoretical data may have several reasons. The deviations for CO<sub>2</sub> and CH<sub>4</sub> may be explained by their relatively large dimensions, necessitating a certain dilation of the polymer matrix for their insertion. The TST method gives good results only for molecules of small dimension since they are gas molecules represented as spherically symmetric molecules. For this reason CO<sub>2</sub>, whose anisotropic shape and large size, causes no negligible segmental rearrangements in the polymer matrix that cannot be captured by Gusev-Suter's smearing factor [3.48, 3.49]. Similar results were found by several other authors [3.39, 3.43-3.45], who used the TST method in order to predict the permeability, diffusivity and solubility coefficients of small gas molecules in different polymeric membranes and whose data are promising except for CO<sub>2</sub>. Another possible source of error is an incomplete equilibration afforded for polymer structures.

It is immediately clear that MD gives a much better reproduction of the experimental transport data than TST because reproduces the chain mobility. For critical applications this justifies the much higher computational effort needed for the MD simulations. TST overestimates diffusion coefficients for H<sub>2</sub>, but it predicts a much stronger decrease of diffusion coefficient with increasing penetrant size than MD and than the experimental values. As a result, the diffusion coefficients of the largest molecules, CH<sub>4</sub> and CO<sub>2</sub> are underestimated by more than one order of magnitude.

### 2.3.3 Solubility coefficients

Theoretical gas solubility coefficients were obtained by using the TST and the GCMC simulation methods. Isotherms were determined for five gases at six pressures over a pressure range from 0.05 to 0.3 atm using the SORPTION module [3.52]. At each pressure, 10<sup>6</sup> steps of GCMC calculations were performed using an initial equilibration period of 5000 steps. The charge interaction was considered and the nonbond cut-off was set to 12Å. The GCMC solubility coefficient of each gas at infinite dilution was computed by fitting the sorption

isotherm obtained from every simulated box, to a straight line through the origin and taking the slope to be the solubility coefficient.

**2.3.4 Compared theoretical and experimental solubility data**

The effective solubility coefficients ( $S= P/D$ ) and the calculated ones of the gases in PEBAX<sup>®</sup>2533 are plotted against the critical temperatures of the gases (Fig. 3.7).

The gas solubility increases with increasing critical temperature ( $T_c$ ) and generally the logarithm of the solubility is a linear function of  $T_c$ . This trend, found for both the experimental and the theoretical values, is commonly observed in both glassy and rubbery polymers [3.64] if polymers do not undergo strong specific interaction with penetrants. TST and GCMC both overestimate the experimental solubility.

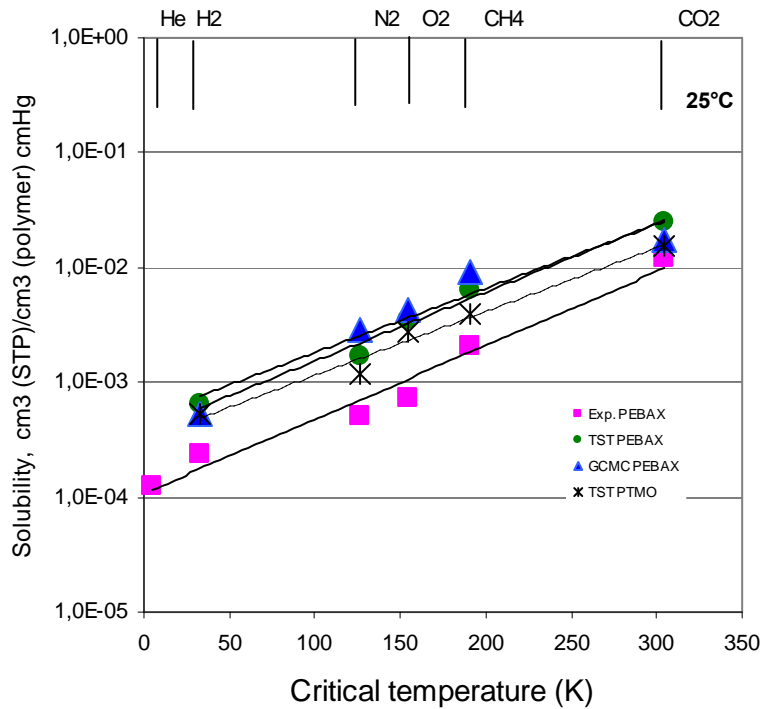


**Figure 3. 7 -Semilogarithmic plot of effective solubility coefficients of six gases in a solution-cast membrane of PEBAX<sup>®</sup>2533 (□) and comparison with theoretical data from GCMC simulation (△) and from TST simulations (○). Also are indicated the solubility coefficients from TST of PTMO (\*). The lines represent the least-squared fit of experimental and of all theoretical data**

The differences between predicted and experimentally determined solubilities fluctuate between 2.0 and 4.9 using TST, and between 0.7 and 3.8 employing GCMC. Similar differences between experimental and calculated solubility values were also observed in previous TST studies [3.37, 3.38]. The solubility coefficient of CO<sub>2</sub> obtained from GCMC simulation is significantly lower than the effective solubility coefficients measured and than the TST calculated data. This could be explained considering that for the GCMC simulations it is assumed that the polymer matrix is rigid, so the free volume elements of the matrix are exclusively used as a sorption site of the membrane. The relatively small dimension of the boxes does not permit also a correct statistic to be reached. The CO<sub>2</sub> insertion necessitates a certain dilation of the polymer matrix.

Solubility is basically a thermodynamic property and an its overestimation suggests that a polymer-penetrant interaction too high it is assumed in the simulations. It is also possible to attribute the discrepancy to the inaccuracy of the interaction potentials, although the good agreement between the experimental and calculated solubility parameters suggests an overestimation of the polymer flexibility. Both techniques determine  $S$  independently, in contrast to the indirect determination of the experimental value of  $S$  from  $P$  and  $D$  as indicated in Eq. (1.2).

The trend of the theoretical data is the same as that found for experimental solubility selectivities: the indication is a high polar/nonpolar ratio (Table 3.5). For gas pairs such as O<sub>2</sub>/N<sub>2</sub> or CH<sub>4</sub>/N<sub>2</sub>, the comparison of calculated and measured selectivities is good. For solubility selectivity values involving quadrupolar CO<sub>2</sub>, however, the solubility selectivity value is sensitive to the theoretical method used. GCMC underestimates the CO<sub>2</sub> solubility, so also the CO<sub>2</sub>/N<sub>2</sub> and the CO<sub>2</sub>/H<sub>2</sub> solubility selectivities are approximately four times and twice times lower than the experimental ones.

In Fig. 3.7 are plotted also the solubilities calculated for PTMO membrane *via* TST. The theoretical solubility coefficients in PTMO are more similar to the experimental solubility of PEBAX®2533. This should suggest the significant role of PTMO segments in the transport through the co-poly(amide/ether) blocks.

The calculated CO<sub>2</sub> value of 1.18 (cm<sup>3</sup>(STP)/(cm<sup>3</sup>(PTMO) atm) is, really, in good agreement with the extrapolated value of 1.12 (cm<sup>3</sup>(STP)/(cm<sup>3</sup>(PTMO) atm) by Bondar et al.[3.28]. In calculating the solubility value in PTMO the authors took into consideration the contribution of each separate phase, i.e., polyamides and polyethers, to the overall sorption.

The fundamental contribution to the transport of CO<sub>2</sub> in PTMO80/PA20 is given by the solubility, i.e. the interaction between the gas and the polymer matrix. The soft block of the co-polymer (PTMO) plays the main role in the solubility of CO<sub>2</sub> in PEBAX®2533. In order to explain the high CO<sub>2</sub> solubility, were investigated associations between CO<sub>2</sub> and possible sites of interactions of the polymeric chains. Nitrogen atoms of amide groups, carboxylic groups and ester linkages in PEBAX®2533 and oxygen atoms of PTMO block have been explored by the radial distribution function  $g(r)$  (RDF). The RDF analysis is defined as the probability of finding an atom at distance  $r$  from another atom compared to the ideal gas distribution.

### 2.3.5 Radial distribution function (RDF) analysis

The average RDF for CO<sub>2</sub> with different atoms was evaluated for distances up to 10 Å in intervals of 0.1 Å as:

$$g_{CO_2,i} = \frac{N_i(r)}{\rho_i N_{CO_2} N_f 4\pi r^2 dr} \quad (3.1)$$

Where  $N_i(r)$  is the number of atoms of type  $i$  in a spherical distance between  $r$  and  $r + dr$  from another atom,  $\rho_i$  the bulk density of atoms of type  $i$  in the polymer,  $N_f$  is the total number of frames used in the analysis and  $N_{CO_2}$  the number of CO<sub>2</sub> molecules.

The calculated radial distribution functions, averaged over all atom pairs are plotted in Fig. 3.8. Results indicates a strong association (a large peak between 2.5 and 6.75 Å) between CO<sub>2</sub> and the oxygen atoms of polyether (PTMO). The association effect is weakened at positions along the amidic component of the chain, resulting in a lower contribution of the hard segments to the quadrupolar CO<sub>2</sub>. These MD simulation results support the hypothesis of CO<sub>2</sub> – polar group moieties affinity as responsible for the experimental differences estimated in diffusion coefficients. Quantum chemical calculations could offer new insight into these phenomena.

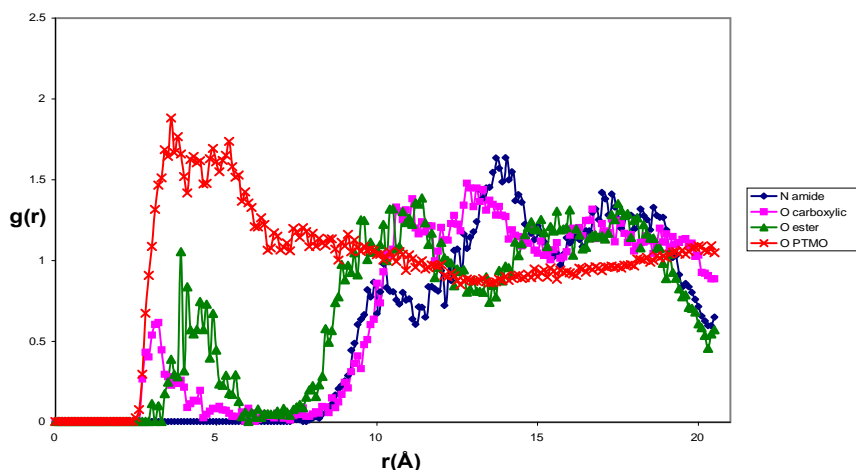


**Figure 3. 8 - Plot of the pair correlation function,  $g_{i,j}(r)$  versus the separation distance,  $r(\text{Å})$ , between CO<sub>2</sub> and the oxygen atoms of PTMO, the nitrogen atoms of amide groups, carboxylic groups, and ester linkages, of the side chains of PEBAX.**

### 2.3.6 Permeability coefficients

Theoretical gas permeability coefficients have been obtained by using the TST method for both PEBAX<sup>®</sup> 2533 and PTMO membranes. From a comparison of the different permeation data for the PTMO80/PA20 membrane, theoretical permeabilities follow the experimental ones: CO<sub>2</sub> exhibits the highest value of permeability (due to the highest contribution of the solubility). O<sub>2</sub>, CH<sub>4</sub> and N<sub>2</sub> then follow in the same order of experimental data. H<sub>2</sub> is an exception exhibiting the highest value of permeability due to the increased values of both theoretical diffusivity (H<sub>2</sub> is an extremely small molecule) and solubility coefficients.

### 3. Conclusions

Molecular simulations using COMPASS force field were successful in predicting the gas-transport properties of a PEBAX<sup>®</sup>2533 block copolymer and for a pure PTMO homopolymer. Experimentally, the diffusivities and the permeation properties of He, H<sub>2</sub>, N<sub>2</sub>, O<sub>2</sub>, CO<sub>2</sub>, CH<sub>4</sub> were determined for PEBAX<sup>®</sup>2533 membranes at various temperatures.

MD simulations give a good representation of the WAXD pattern of the membrane and of the transport of different gas molecules, confirming the representative model boxes. Calculated values for amorphous PEBAX<sup>®</sup>2533 and for amorphous PTMO are nearly identical, both with MD and with TST simulations. MD gives a much better reproduction of the experimental transport data than TST does. MD tends to underestimate D, but the discrepancy over the whole range of gases is not more than a factor 2-3. Grand Canonical Monte Carlo (GCMC) and TST simulations adequately represent solubility coefficients. Interactions between CO<sub>2</sub> and PTMO component of the block copolymer have been detected by radial distribution function.

## REFERENCES

- [3.1] A. Jonquière, R. Clément and P. Lochon, *Prog. Polym. Sci.*, 27 (2002) 1803.
- [3.2] A. Gugliuzza and E. Drioli, *Polymer*, 44 (2003) 2149.
- [3.3] A. Gugliuzza, G. Clarizia, G. Golemme and E. Drioli, *Eur. Polym. J.*, 38 (2002) 235.
- [3.4] A. Barbucci, M. Delucchi and G. Cerisola, *Prog. Org. Coatings*, 30 (1997) 293.
- [3.5] A. Mokrini, J.L. Acosta, *Polymer*, 42 (2001) 9.
- [3.6] K. H. Hsieh, C.C. Tsai and S.M. Tseng, *J. Membrane Sci.*, 49 (1990) 341.
- [3.7] G. Chatterjee, A.A. Houde and S.A. Stern, *J. Membrane Sci.*, 135 (1997) 99.
- [3.8] J.H. Kim and Y.M. Lee, *J Membrane Sci.*, 190 (2001) 179.
- [3.9] J.H. Kim and Y.M. Lee, *J. Membrane Sci.*, 193 (2001) 209.
- [3.10] S. J. Metz, V. Mulder and M. Wessling, *Macromolecules*, 37 (2004) 4590.
- [3.11] A. Gugliuzza and E. Drioli, *Eur. Polym. J.*, 40 (2004), 2381.
- [3.12] P. Minghetti, F. Cilurzo, V. Liberti and L. Montanari, *Int. J. Pharm.*, 158 (1997) 167.
- [3.13] B.O. Jung, T.J. Kim, S.S. Park and J.J. Kim, *J. Ind. Eng. Chem.*, 8 (2002) 57.
- [3.14] G. M. Dennis, G. O'Brien, *Polyether Block Amide Resins: Bridging the Gap between Thermoplastics and Rubbers*; ACS Rubber Division Meeting Cincinnati; ATOFINA Chemicals Inc.: Philadelphia, Oct 2000.
- [3.15] R. Flesher, *Pebax polyether block amide: a new family of engineering thermoplastic elastomers*, in: *Proceedings of the Symposium on the History of High Performance Polymers at the ACS Meeting in New York, April 1986*, pp. 401–408.
- [3.16] V. I. Bondar, B. D. Freeman and I. Pinnau, *J Polym. Sci. Part B: Polym. Phys.*, 38 (2000) 2051.
- [3.17] J.P. Sheth, J. Xu and G.L. Wilkes, *Polymer*, 44 (2003) 743.
- [3.18] M. Xie and Y. Chamberlain, *Makromol. Chem.*, 187 (1986) 383.
- [3.19] N. Alberola *J. App. Polym. Sci.*, 36 (1988) 787.
- [3.20] G.R. Hatfield, Y. Guo, W.E. Killinger, A. Andrejak and P.M. Roubicek, *Macromolecules*, 26 (1993) 6350.
- [3.21] Y.C. Yu and W.H. Jo *J. Appl. Polym. Sci.*, 56 (1995) 895.
- [3.22] Y.C. Yu, W.H. Jo and M.S. Lee, *J. Appl. Polym. Sci.*, 64 (1997) 2155.
- [3.23] McLean and B.B. Sauer, *J. Polym. Sci.*, 37 (1999) 85.
- [3.24] B.B. Sauer, R.S. McLean, D.J. Brill and D.J. Londono, *J. Polym. Sci. Part B: Polym. Phys.*, 40 (2002) 1727.
- [3.25] M.E. Rezac and T. John, *Polymer*, 39 (1998) 599.
- [3.26] M.E. Rezac, T. John and P.H. Pfromm, *J. App. Polym. Sci.*, 65 (1997) 1983.
- [3.27] M.K. Djebbar, Q.T. Nguyen, R. Clement and Y. Germain, *J. Membr. Sci.* 146 (1998) 125.
- [3.28] V. I. Bondar, B. D. Freeman and I. Pinnau, *J. Polym. Sci. Part B: Polym. Phys.*, 37 (1999) 2463.
- [3.29] V. Barbi, S.S. Funari, R. Gehrke, N. Scharnagl and N. Stribeck, *Macromolecules*, 36 (2003) 749.
- [3.30] J.C. Chen, X. Feng and A. Penlidis, *Sep. Sci. and Tech.*, 39 (2004) 149.
- [3.31] A. Gugliuzza and E. Drioli, *Polymer*, 46 (2005) 9994.
- [3.32] P.V.K. Pant and R.H. Boyd, *Macromolecules*, 26 (1993) 679.
- [3.33] F. Mueller-Plathe, *J. Chem. Phys.*, 96 (1992) 3200.

- [3.34] Y. Tamai, H. Tanaka and K. Nakanishi, *Macromolecules*, 27(1994) 4498.
- [3.35] R.H. Gee and R.H. Boyd, *Polymer* 36 (1995) 435.
- [3.36] J. Han and R.H. Boyd, *Polymer* 37 (1996) 1797.
- [3.37] E. Kucukpinar and P. Doruker, *Polymer*, 44 (2003) 3607.
- [3.38] M. Heuchel, D. Hofmann and P. Pullumbi, *Macromolecules*, 37 (2004) 201.
- [3.39] D. Pavel and R. Shanks, *Polymer*, 44 (2003) 6713.
- [3.40] E. Kucukpinar and P. Doruker, *Polymer*, 47 (2006) 7835.
- [3.41] F. Mueller-Plathe, *J. Membr. Sci.*, 141 (1998) 147.
- [3.42] J.R. Fried, M. Sadat-Akhavi and J.E. Mark, *J. Membr. Sci.*, 149 (1998) 115.
- [3.43] D. Hofmann, M. Entrialgo-Castano, A. Lerbret, M. Heuchel and Y. Yampolskii, *Macromolecules*, 36 (2003) 8528.
- [3.44] J.R. Fried and P. Ren, *Comput. Theor. Polym. Sci.*, 10 (2000) 447.
- [3.45] E. Tocci, D. Hofmann, D. Paul, N. Russo and E. Drioli, *Polymer*, 42 (2001) 521.
- [3.46] E. Tocci and P. Pullumbi, *Molecular Simulation*, 32 (2) (2006) 145.
- [3.47] A.A. Gusev, S. Arizzi and U.W. Suter, *J. Chem. Phys.*, 99 (1993) 2221.
- [3.48] A.A. Gusev, S. Arizzi and U.W. Suter, *J. Chem. Phys.*, 99 (1993) 2228.
- [3.49] A.A. Gusev, F. Müller-Plathe, W.F. Van Gunstern and U.W. Suter, *Adv. Polym. Sci.*, 116 (1994) 207.
- [3.50] P. V. K. Pant and R. H. Boyd, *Macromolecules*, 26 (4) (1993) 679.
- [3.51] M. Meunier, *J. Chem. Phys.*, 123 (2005) 134906.
- [3.52] Accelrys Inc., InsightII 4.0.0.P+, POLYMERIZER, DISCOVER, AMORPHOUS CELL, BUILDER SORPTION Modules 2001, San Diego, CA, USA; 2001.
- [3.53] D. Rigby, H. Sun and B.E. Eichinger, *Polymer International*, 44 (1997) 311.
- [3.54] ELF Atochem Inc., PEBAX® Technical Brochure (2000).
- [3.55] D.N. Theodorou and U.W. Suter, *Macromolecules*, 18 (1985) 1467.
- [3.56] R. H. Gee, L.E. Fried and R.C. Cook, *Macromolecules*, 34 (2001) 3050.
- [3.57] T. A. Andrea, W. C. Swope and H. C. Andersen, *J. Chem. Phys.*, 79 (1983) 4576.
- [3.58] H.J.C. Berendsen, J.P.M. Postma, W. F. Van Gunsteren, A. Di Nola and J. R. Haak, *J. Chem. Phys.*, 81 (1984) 3684.
- [3.59] S. Pauly, *Polymer Handbook*, 3rd ed., J. Brandrup, E. Eds. Immergut, Wiley, New York, 1989, VI/435-VI/449.
- [3.60] J.M. Haile, *Molecular Dynamics Simulation*, Wiley, New York, 1992.
- [3.61] Gsnet & Gsdif Macros, Distributed by Accelrys Inc., San Diego, CA, USA.
- [3.62] N. Metropolis, A.W. Rosenbluth and M.N. Rosenbluth, A.H. Teller and E. Teller, *J. Chem. Phys.* 21 (1953) 1087.
- [3.63] M. Macchione, J.C. Jansen, G. De Luca, E. Tocci, M. Longeri and E. Drioli, *Polymer*, 48 (2007) 2619.
- [3.64] Y. Yampolskii, B.D. Freeman, I. Pinnau and S. Matteucci, *Transport of Gases and Vapors in Glassy and Rubbery Polymers*, in Y. Yampolskii, I. Pinnau, and B.D. Freeman (Ed.), *Materials Science of Membranes for Gas and Vapor Separation*, John Wiley & Sons, New York, NY, 2006, pp. 1-445.

## IV. WATER TRANSPORT PROPERTIES OF MODIFIED PEBAX MEMBRANES.

### 1. Modified Poly(ether-b-amide) Copolymer Membranes

#### 1.1. Introduction

In the field of gases separation the modern material science has been tuned increasing attention to design new functional polymeric membranes in order to control interfacial phenomena, traditionally affecting separation and purification processes.

A useful strategy for changing and improving the performance of raw materials consists of suitably incorporation of new structural and chemical elements into the polymer matrixes in order to control structure–property relationships [4.1–4.8]. One of the most flexible methods for achieving this goal is to blend different compounds, selected on the basis of their intrinsic chemical and morphological characteristics [4.9–4.11]. The possibility to manipulate the membrane affinity appears to be a promising strategy for enhancing the efficiency of a process, especially when the sorption selectivity is the predominant parameter on the overall transport [4.12, 4.13].

Gugliuzza et. Al. [4.1-4.4] functionalised the block *co*-poly(ether/amide) 80PTMO/PA12 (PEBAX®2533, Atofina) by dissolving each chemical additive [triethylcitrate (TEC), *N*-ethyl-*o*/*p*-toluene sulfonamide (KET), and sucrose benzoate (SB)] in a mixture of *n*-butanol/*n*-propanol (99.5%, Carlo Erba) 3/1 v/v, ranging in modifier concentration from 20 to 70 wt%.

Vapour permeability, solubility, diffusivity, and hydrophobicity/hydrophilicity measurements were performed for testing the efficiency and performance and for providing a detailed understanding of the vapour permeation mechanism, influence of temperature, component hydrophilicity and additive concentration in these systems. The membrane permeability to polar and non-polar penetrating molecules was remarkably affected by the chemistry and the content of the modifier selected.

The vapour transport through dense PEBAX®2533 films obeys to the solution-diffusion mechanism. The solubility into the polymer matrix depends on the favourable chemical interactions between permeant and polar chemical groups of the polymer, whereas the diffusivity is strictly connected to the mobility of the polymer chain, low packing density and hence the presence of microcavities with sufficient dimension to allow the passage of the vapour molecules.

Figure 4.1 shows the chemical structure of KET:



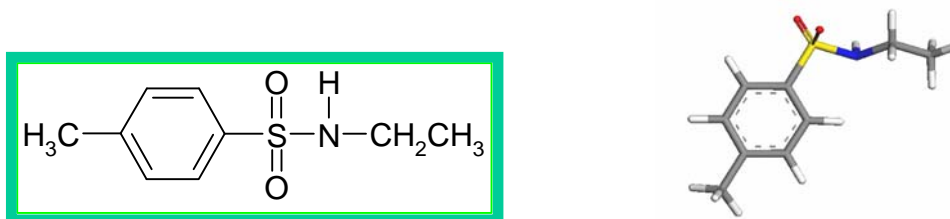


Figure 4. 1 - Chemical formula and 3D structure of *N*-ethyl-*p*-toluene sulphonamide (KET)

Within this context, it is interesting to study the microscopic structure and transport properties of complex systems using molecular dynamics simulations, which in recent years have been used to describe the transport of small molecules in polymer matrices amorphous membrane especially for gas separations [4.14-4.17]. Recently, the MD technique was also used for the detailed analysis of polymer-solvent interface in the case of swelling and water transport in polymer systems, pure or modified by providing useful information on the distribution of hydrogen bonds, solubility, and diffusion of water and on polymer-solvent interactions and distribution of free volume [4.18, 4.19]. In the present chapter the results on fully atomistic investigations of water transport properties across modified PEBAX/KET systems will be presented and discussed to provide useful correlations between the microscopic structure of the materials object of study and the performances of these systems in terms of water diffusivity and solubility.

## 1.2. Computational Details

Three-dimensional boxes of PEBAX®2533 were constructed with periodic boundary conditions and simulated using the commercial software Insight II-Discover ACCELRY'S of [4.20]. The COMPASS force field was used for all simulations [4.21, 4.22].

A single chain of copolymer PEBAX ® 2533 was constructed by alternating comonomers of polyamide-12 (PA-12) and polytetramethyleneoxide (PTMO) according to the experimentally observed weight percentages of 20 wt.% of PA-12 and 80 wt% of PTMO [4.23, 4.24].

PA-12 and PTMO homopolymers were constructed using the BUILDER module of Insight II [4.20]. Single chains of PEBAX ® 2533 copolymer of right composition and length were built by using the module POLYMERIZER of Insight II [4.20].

The degree of polymerization ( $n = 8$ ) was estimated by taking into account the size of a typical simulation box (40-50 Å), and the experimental density of pure PEBAX ® 2533 ( $d_{\text{exp}} = 1.01 \text{ g} \cdot \text{cm}^{-3}$  [4.25]). To avoid the overlap of the polymer chain in each cell large number of molecules of Argon was included.

The chemical additives and the solvent were introduced in the simulation boxes: a number of molecule of *N*-ethyl-*p*-toluenesulfonamide (KET in a racemic mixture of 50 wt% ortho-KET and 50 wt% para-KET) was added to the model containing the polymer in order to get three boxes for each of the following copolymer / additive weight compositions: 70-30 %wt; 50% -50% and 30-70 %wt. The number of water molecules corresponding to the experimental observed amount of absorbed water in the modified membrane for different PEBAX/KET weight percentages [4.1] was added in each simulation box.

Amorphous cells were constructed using the method of Theodorou and Suter [4.26]. The molecules were removed in three stages and after each removal cycles of energy minimization and dynamics were conducted according to the downscaling procedure [4.27], as described in the previous chapter.

The models were then subjected to compression at temperatures of 300K through NPT-MD runs to get the initial density similar to the experimental one.

The cells were completed using procedures known as annealing, which is to heat the system at temperatures well above the  $T_g$  of the polymer ( $T = 700$  K) and then cool the system at 500 K, 400 K and finally at 298 K through simulations NVT ensemble MD on alternate energy to minimize. The final equilibration was carried out by a MD simulation of 300 ps (NPT,  $P = 1$  bar), having verified that this time is sufficient to allow the system to reach an almost constant value of total energy.

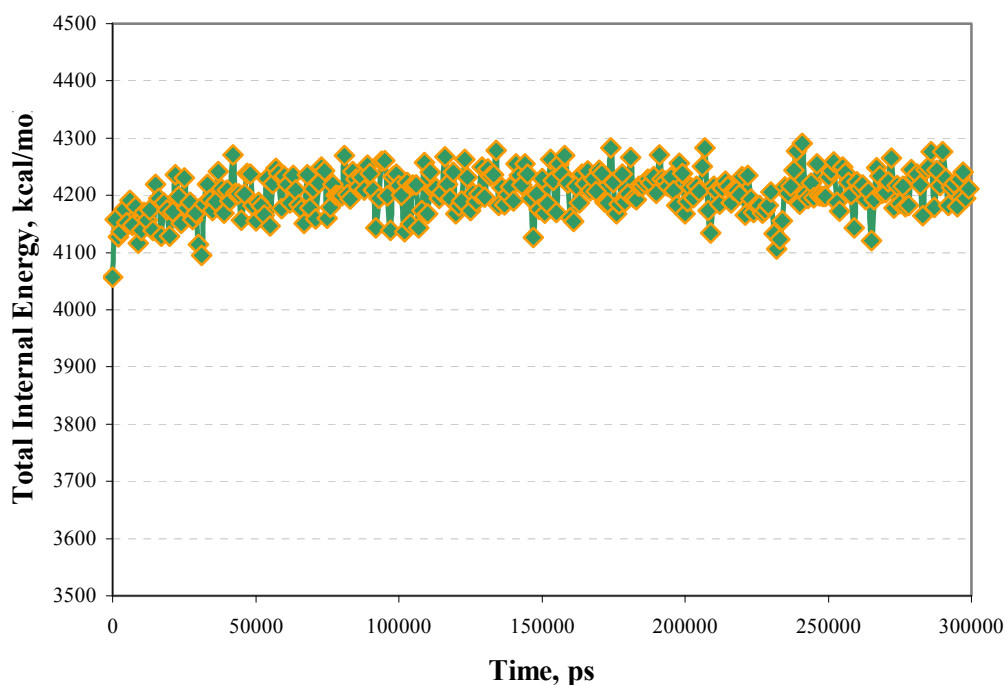


**Figure 4. 2- Plot of the Total Internal Energy of a simulated 3D periodic PEBA/KET cell during 300 ps of simulation.**

All the simulations runs were conducted under periodic boundary conditions to avoid the effects of symmetry and with a distance of  $15 \text{ \AA}$ .

The dynamics were subjected to the temperature control by the method of Andersen [4.28] and to the pressure control by the method of Berendsen [4.29].

Figure 4.3 shows the equilibration procedure of three 3D periodic cells of PEBA modified with 30 %wt, 50 %wt, 70 wt % KET

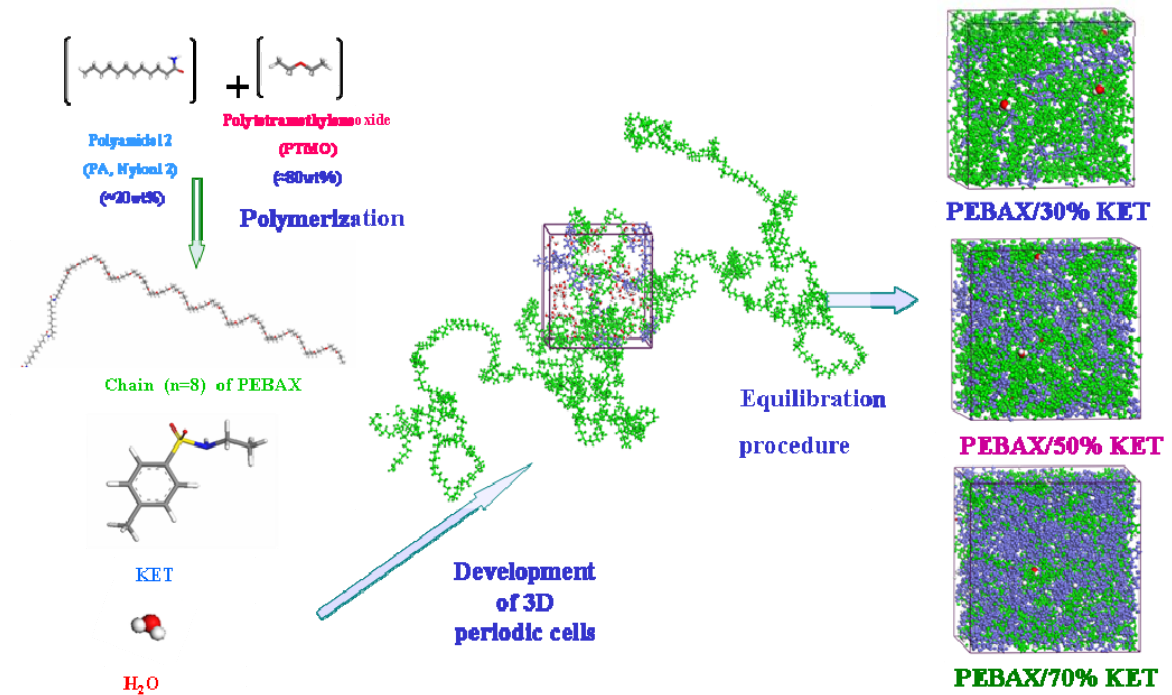


Figure 4. 3 - Construction and equilibration procedure of 3D PEBAX/KET cells with additive compositions of 30 %wt, 50 %wt, 70 %wt

Details of simulation systems are summarized in Table 4.1;

The equilibrated amorphous cells were used in order to estimate the diffusion coefficients using direct molecular dynamics and TST calculations, and the solubility coefficients with Grand Canonical Monte Carlo (GCMC) and TST calculations.

System	DP	N° Atoms	N° KET	N° H2O	$\rho$ sim.	Cell length (Å)
PEBAX 70/KET I 70/30	8	5037	46	5	0.9603	37.480
PEBAX/KET II 70/30	8	5037	46	5	0.9532	37.520
PEBAX/KET III 70/30	8	5037	46	5	0.9659	37.470
PEBAX/KET I 50/50	8	6609	106	9	1.008	42.147
PEBAX/KET II 50/50	8	6609	106	9	1.0150	41.366
PEBAX/KET III 50/50	8	6609	106	9	1.0120	41.323
PEBAX/KET I 30/70	8	10286	248	4	1.0708	48.316
PEBAX/KET II 30/70	8	10286	248	4	1.0692	48.330
PEBAX/KET III 30/70	8	10286	248	4	1.0715	48.293

**Table 4. 1 - Details of Simulations of assembled 3D PEBAX/KET amorphous cells.**

## 2. Results and discussions

### 2.1. Morphological Investigations

#### 2.1.1 Chain Mobility

Gugliuzza et Al. [4.1-4.4] outlined that the incorporation of functional bulky modifiers into the polymer matrix has two effects: it is responsible for the destruction of the packing density of crystalline domains in the block copolymer, but also it causes a decreasing rotational freedom of the segment chains. The H-bonding formation between donors and acceptors as well as the inter-segmental agglomeration of the modifiers, especially at higher content, produce a rising amorphous character and slow down the free volume content. Differential scanning calorimetry, by monitoring position and magnitude of glass transition temperatures and endothermic melting in events for the crystallinity, yielded indicative information on the extent of these two phenomena [4.3]. Consequently, the stiff and bulky structure of some modifiers as well as the higher cohesive energy of the modified polymer matrixes prevented segmental mobility.

By means of MD simulation, through the Einstein equation of motions it's possible to follow the displacements of all the atoms inserted in the simulated system.

The displacements of the polymer chain were calculated on the equilibrated 3D models of pure PEBAX and at different KET compositions by performing dynamic runs on NPT *ensemble* (time of simulation =1 ,5 ns); the polymer mean squared displacements curves (MSD) vs time of simulation are showed in Figure 4.4.

It's evident from the showed MSD curves that the presence of KET reduces the mobility of PEBAX chain increasing the stiffness of the systems.

In PEBAX/KET system, due mainly to the bulky aromatic structure and partial double-bond character of the amide linkage, the overall stiffness of the systems mixed gave rise to the reduction of the rotational freedom; for the system with 70 %wt in KET there's a slight decrease in chain mobility is observed: probably due to rising amorphous character and the destruction of crystallinity domain of PA-12 outlined by DSC analysis in the membrane with 70 %wt in KET [4.2]

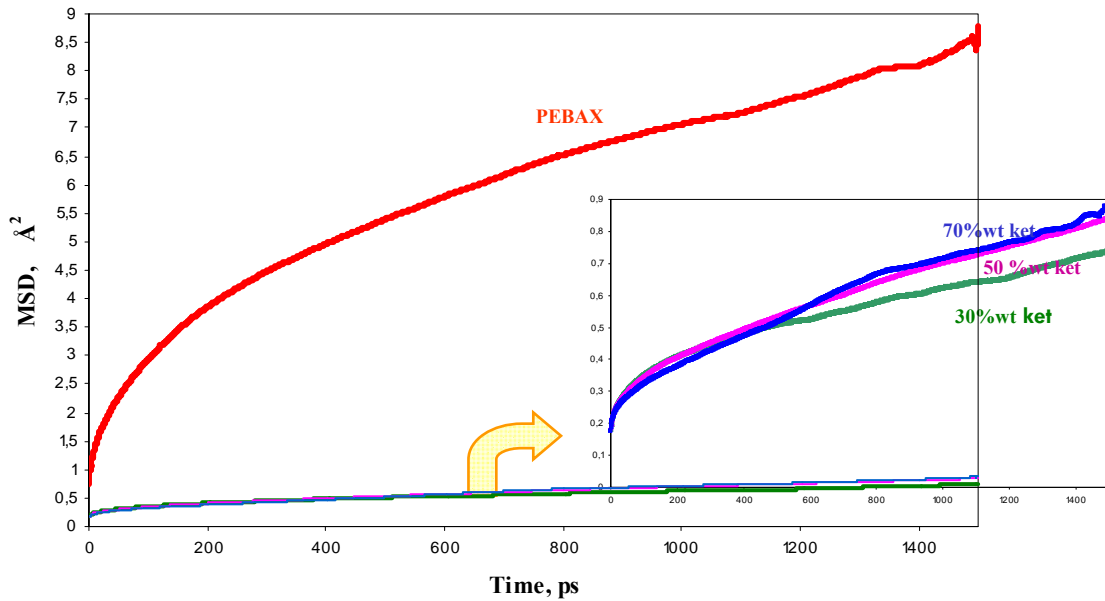


**Figure 4. 4-** Polymer chain mean squared displacements curves (MSD) of pure PEBAX and PEBAX/KET systems during 1,5 ns of simulation.

### 2.1.2 Homogeneity of the layers: Interactions Polymer-Additives

Gugliuzza et Al. [4.3] outlined that all assembled PEBAX/KET layers have shown, on relevant length scale, a good miscibility and compatibility, as the thermal and the infrared analysis have confirmed. The thermal analysis showed the strong interactions between the mixed systems: both the transitions related to soft (PTMO) and hard (PA) blocks of the copolymer were shifted on higher and lower values than those measured for the pure polymer, respectively. This confirmed the migration of each modifier towards both the polymer domains. The increase in  $T_m$ -PTMO of the polyether segments (PTMO) was due to the increasing reduction in mobility of the polymer chains, because of hydrogen bonding of polar groups, bulky and stiff aromatic structures.

We have analyzed the interactions between KET and copolymer chain by using radial distribution functions between atoms of polar and aliphatic chemical groups of KET and of PTMO/PA-12 domains of PEBAX chain.

In Figure 4.5 (a,b) the Radial Distributions Functions (RDFs) between H-N of KET sulphonamidic group and N of PA12 amidic group (a) and O of PTMO ether group (b) in 3D PEBAX models at different weight percentages of KET are showed.

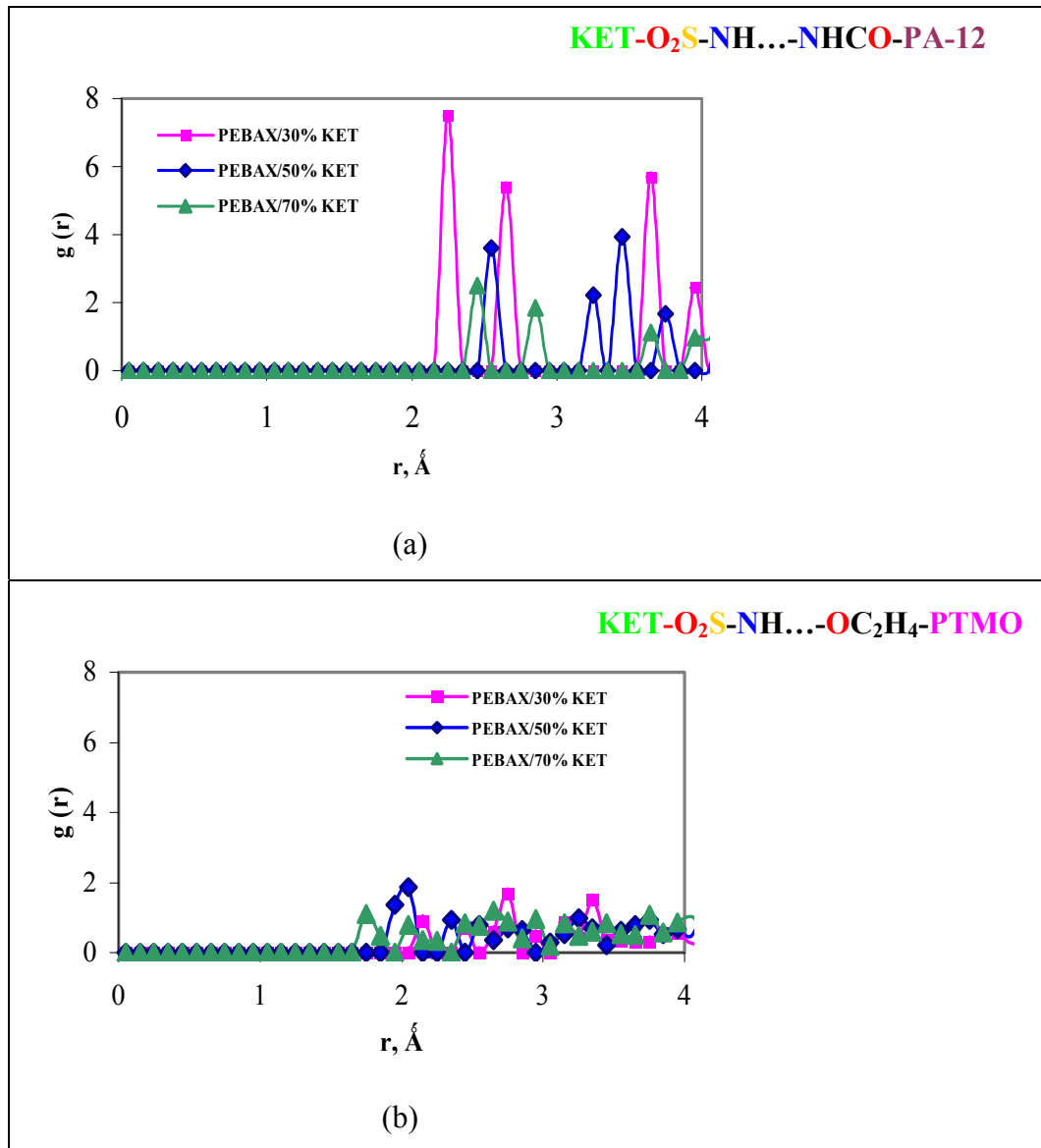


**Figure 4.5- Radial Distributions Functions (RDFs) between H-N of KET sulphonamidic group and N of PA-12 amidic group (a) and O of PTMO ether group (b) in 3D PEBAX/KET models.**

From the analysis of figure 4.5 (a), (b) it's possible to notice that there are strong interactions between the polar part of KET and the amidic group of PA-12 domain of polymer chain, which are of higher intensity respect to the interactions between KET sulphonamidic group and PTMO group of PEBAX, even if the latter are of rather shorter range; it's possible to notice a slight decrease in intensity and a shift to larger interatomic distance of the peaks correspondently to the system with a 70 %wt in KET.

This behaviour suggests that there's a good miscibility between additives and PEBAX, confirmed also by similar radial distributions analysis conducted between C of KET aromatic ring and carbons of PEBAX aliphatic chain, which presents peak of high intensity and short range.

The analysis of the interactions in a fully atomistic range confirms the good compatibility between KET and PEBAX, which leads to homogeneous modified membranes on macroscopic scale and the MD analysis further outlined the strong contributions of the interactions between the apolar, hydrophobic groups, as well as those of polar, hydrophilic chemical moieties of KET and PEBAX, to their miscibility.

## 2.2. Water Transport Properties

Equilibrated amorphous cells were used in order to estimate the diffusion coefficients using direct molecular dynamics and TST calculations, and the solubility coefficients with Grand Canonical Monte Carlo (GCMC) and TST calculations.

The water self diffusion coefficients for the PEBAX<sup>®</sup>2533 modified at varying weight percentages of KET (0 %wt, 30 %wt, 50 %wt, 70 %wt) have been calculated from the slope of the mean square displacement curves of the MD runs, considering a time of simulation of 4ns, via averaging over all simulated water molecules inserted in the simulation box.. The theoretical values are in the same order of magnitude as the experimental values.

The solubility of water by TST method was determined considering a spherical shape of the water and small non bonded interactions expressed by Lennard-Jones Potential in the form:

$$V_r^{LJ} = 4\varepsilon_{ij} \left[ \left( \frac{\sigma}{r_{ij}} \right)^{12} - \left( \frac{\sigma}{r_{ij}} \right)^6 \right] \quad (4.1)$$

with  $\sigma = 3.166 \text{ \AA}$  and  $\varepsilon_{ij} = 0.650 \text{ KJ mol}^{-1}$  [4.30, 4.31].

The averaged results of three cells for each composition PEBAX/KET (100/0 %wt, 70/30 %wt, 50/50 %wt, 30/70 %wt) are reported in the Table 4.2.

H <sub>2</sub> O	THEORETICAL DATA				EXPERIMENTAL DATA		
	TST	TST	TST	MD	GCMC		
	Permeability coefficient, P [barrer * 10 <sup>3</sup> ]	Diffusion coefficient, D (cm <sup>2</sup> /sec)*10 <sup>-6</sup>	Solubility coefficient, S(cm <sup>3</sup> /cm <sup>3</sup> cmHg)	Diffusion coefficient, D (cm <sup>2</sup> /sec)*10 <sup>-6</sup>	Solubility coefficient, S(cm <sup>3</sup> /cm <sup>3</sup> cmHg)	Diffusion coefficient, D (cm <sup>2</sup> /sec)*10 <sup>-6</sup>	Solubility coefficient, S(cm <sup>3</sup> /cm <sup>3</sup> cmHg)
PEBAX/0%KET	5.55 ± 2.54	6.50 ± 2.3	0.08 ± 0.02	0.57 ± 0.32		0.517	4.84
PEBAX/30%KET	28.70 ± 7.43	5.09 ± 3.4	0.57 ± 0.04	0.007 ± 0.005	0.222 ± 0.001	0.473	7.93
PEBAX/50%KET	28.00 ± 3.43	4.46 ± 2.45	0.63 ± 0.02	0.012 ± 0.008	0.238 ± 0.005	0.228	8.90
PEBAX/70%KET	0.17 ± 0.03	2.97 ± 0.94	0.57 ± 0.05	0.0005 ± 0.0001	0.294 ± 0.003	0.107	2.29

**Table 4. 2 - Theoretical Water Transport data of 3D assembled cells PEBAX/KET at different additives composition.**



Figure 4.6 shows the comparison between the theoretical and experimental water diffusivity of water for varying PEBAX/KET compositions.

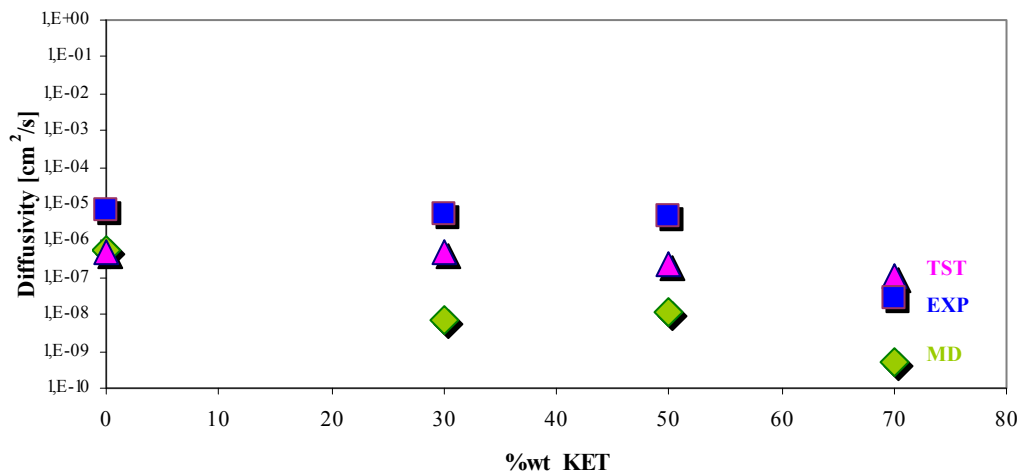


**Figure 4. 6- Experimental and Theoretical Diffusivity of H<sub>2</sub>O in PEBAX membrane with different %wt of KET.**

From the comparison with the experimental data of Gugliuzza et al. [4.4] an acceptable agreement with the calculated diffusion coefficients is observed, taking into account the limitations of the method for calculating the diffusion coefficients: the TST method gives good results only for molecules of small dimension since they are gas molecules represented as spherically symmetric molecules. For this reason H<sub>2</sub>O, whose anisotropic shape and large size, causes no negligible segmental rearrangements in the polymer matrix that cannot be captured by Gusev-Suter's smearing factor [4.32]. Another possible source of error is an incomplete equilibration afforded for polymer structures.

On the other hand MD gives better reproduction of the experimental water diffusivity than TST only for pure PEBAX system because the introduction of an additives like KET with a rigid aromatic rings lead to a reduction of the chain mobility as seen in the previous section thus slowing down the transport of water across the matrix; the reason for this is the immobilization of polymer chains due to the hydrogen bond formation or steric hindrance by aromatic structures. The observed effect increases at increasing %wt of KET in PEBAX membranes so the value of water diffusivity by MD is undervalued especially for the system with the 70 %wt of KET.

Figures 4.7 shows the comparison between the theoretical and experimental water solubility [4.2] observed for different PEBAX/KET membranes.

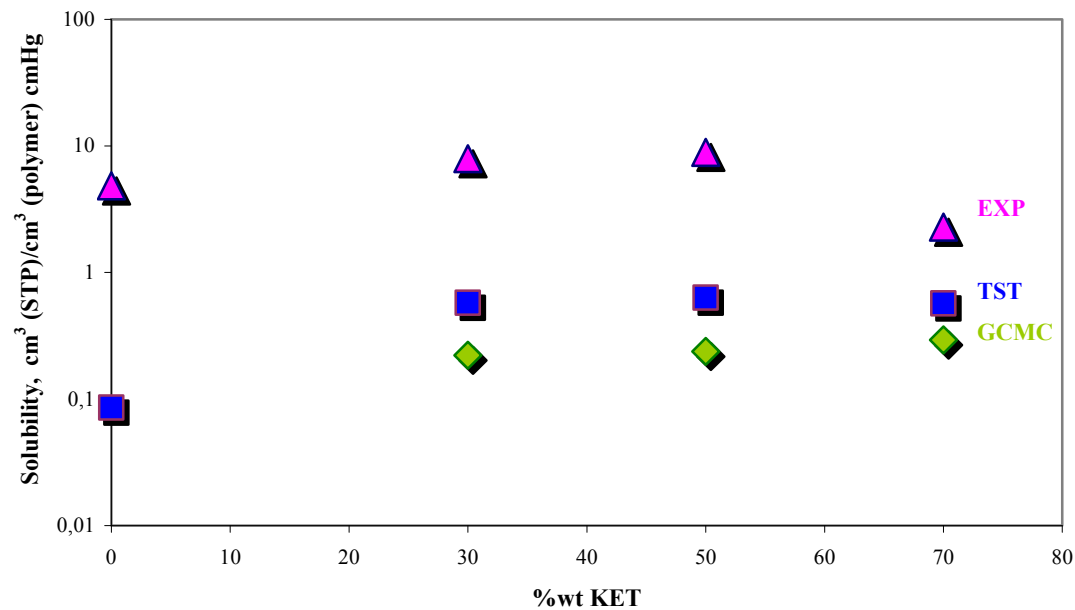


**Figure 4. 7- Experimental and Theoretical solubility of H<sub>2</sub>O in PEBAX membrane with different %wt of KET.**

From the comparison between experimental and theoretical water solubility coefficients an acceptable agreement is observed in spite of the intrinsic limitations of the TST and GCMC methods in evaluation the water solubility. An increase of water solubility is observed for additive concentrations up to 50 %wt, while decreasing for the membranes with the 70% on weight of KET.

Further the Hildebrand Solubility [4.33] parameter was calculated on systems PEBAX/KET at various compositions after the removal of the inserted water molecules as the square root of the cohesive energy densities of the cell when all the intermolecular forces are eliminated the increase in energy.

Figure 4.8 shows the comparison between the theoretical and experimental water solubility parameter  $\sigma$  [4.3] evaluated for different PEBAX/KET membranes:

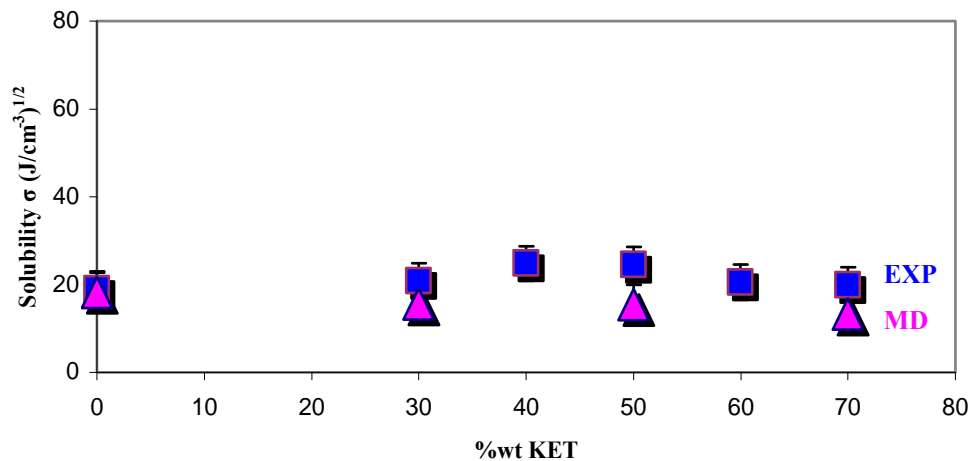


**Figure 4. 8- Experimental and Theoretical Hildebrand solubility parameter  $\sigma$  for  $\text{H}_2\text{O}$  in PEBAX membrane with different %wt of KET.**

Both experimental and theoretical trends show a decrease of solubility parameter of water for higher concentrations of additive up to 50% in weight, as previously observed for the water solubility coefficients in Figure 4.7.

The solubility is influenced by the hydrophilicity of the materials in a significant way: the surface solubility contribution has a large weight on the total solubility.

When adding polar organic compounds, the surface becomes more hydrophilic with respect to that of the pure polymer, promoting favourable interactions with water vapour at the interface feed-membrane.

Polarizable and polar penetrating molecules, such  $\text{H}_2\text{O}$ , interacted favourably with polar matrix, and the presence of a hydrophilic additive as KET lead to an increased absorption of water in the modified membranes, although its permeability behaviour was affected in different way by specific intermolecular interactions, when polarity and concentration of the chemical moieties in the polymer membrane increased.

### **2.3. Intermolecular Interactions as Controlling Factor for Water Sorption into Polymer Membranes**

A multidisciplinary approach, that is experimental (by dr. Annarosa Gugliuzza of ITM-CNR) and with two theoretical methodologies, quanto-mechanical QM (by Dr. Giorgio de Luca of ITM-CNR) and MD (by us), was used for delineating the mechanisms controlling water sorption into modified block co-poly-(ether/amide) (PEBAX) membrane [4.34].

The infrared analysis of modified PEBAX membranes revealed a different availability and accessibility of free polar groups supporting the formation of hydrogen bonding as a function of modifier concentration. This means that the N–H bond of the sulphonamide linkage becomes more and more strong, resulting in weakening of the strength of the hydrogen bond ( $\text{N-H} \cdots \text{Y}$ ) between donor and acceptor. Due to higher concentration of

aromatic moieties of the KET and lesser availability of polar groups, a decrease in the attractive interfacial forces at membrane–feed interface results lowered.

A combination of both experimental and theoretical procedures was used to analyze the molecular processes of water sorption on PEBAX membranes.

MD simulations yielded indications about the modifier distribution in the polymer membranes by evaluating the polymer-modifier as well as the modifier-modifier distances. Bulk equilibrated models of PEBAX with three different amounts of KET (10 %wt, 30 %wt, 60 %wt) were prepared and equilibrated according to the computational procedure described in section 2.2; The side length of the bulk models was 33 Å for the polymer with 10 wt % of KET, 36 Å for 30 wt % of KET, and 43 Å for 60 wt % of KET.

Each 3D simulation box was cut into slides with a dimension of about 8-9 Å along the z-axis (Figure 4.9 (a, b)). The distribution of the modifier molecules inside the box was visualized, and intermolecular distances were indicated. In Figure 4.9 (c), the number of KET dimers found in the boxes with N...H...O bond lengths smaller than 3 Å is reported. Furthermore, the number of modifiers, exhibiting distances from the PEBAX functional groups smaller than 3 Å, was also reported.

The first check was performed on the distribution of KET molecules in the polymeric matrix. In models with 10 wt % of KET, the molecules were randomly dispersed in the bulk of the copolymer. Because of the reduced number of KET molecules in the boxes containing the 30 wt %, few dimers forming hydrogen bonds were found. The interactions between both the amine and sulphur groups of two molecules of KET are present in relevant numbers in the models with 60 wt % of modifier, confirming a large presence of dimers, as shown in Figure 4.9 (c). KET molecules were found to be close to the amide, the carboxyl residues, the ether, and the ester groups of the PEBAX (Figure 4.9(c)).

Independently of modifier concentrations, the number of modifiers close to the ether group of PTMO segments was larger. No distances less than 3 Å between -SO<sub>2</sub> groups and the amide moiety of the polymer were found. The number of proximal modifiers rose with KET concentrations more than the number of modifiers close to polymeric groups. In other words, the distances between KET and copolymer segment chains changed slightly with increasing modifier content, as expected for the distances from the ether moieties. All data were in qualitative agreement with the indications extracted from the infrared analysis [4.34] Particularly, a proportional shift of the vibrational stretching  $\nu_{\text{CO-NH}}$  was not observed in correspondence to the significant shift of the  $\nu_{\text{as-SO}_2\text{-NR}_2}$ . This was confirmed by the lack of bond lengths between SO<sub>2</sub>...CONH moieties as reported in the histogram (Figure 4c). As a consequence, the shift of the  $\nu_{\text{as-SO}_2\text{-NR}_2}$  should be ascribed to interactions between modifier molecules.

Three different dimers linked together by hydrogen bonding were extracted from the model containing 60 % wt of KET and were subjected to density functional calculations to obtain the corresponding stable wave function and interaction energies.

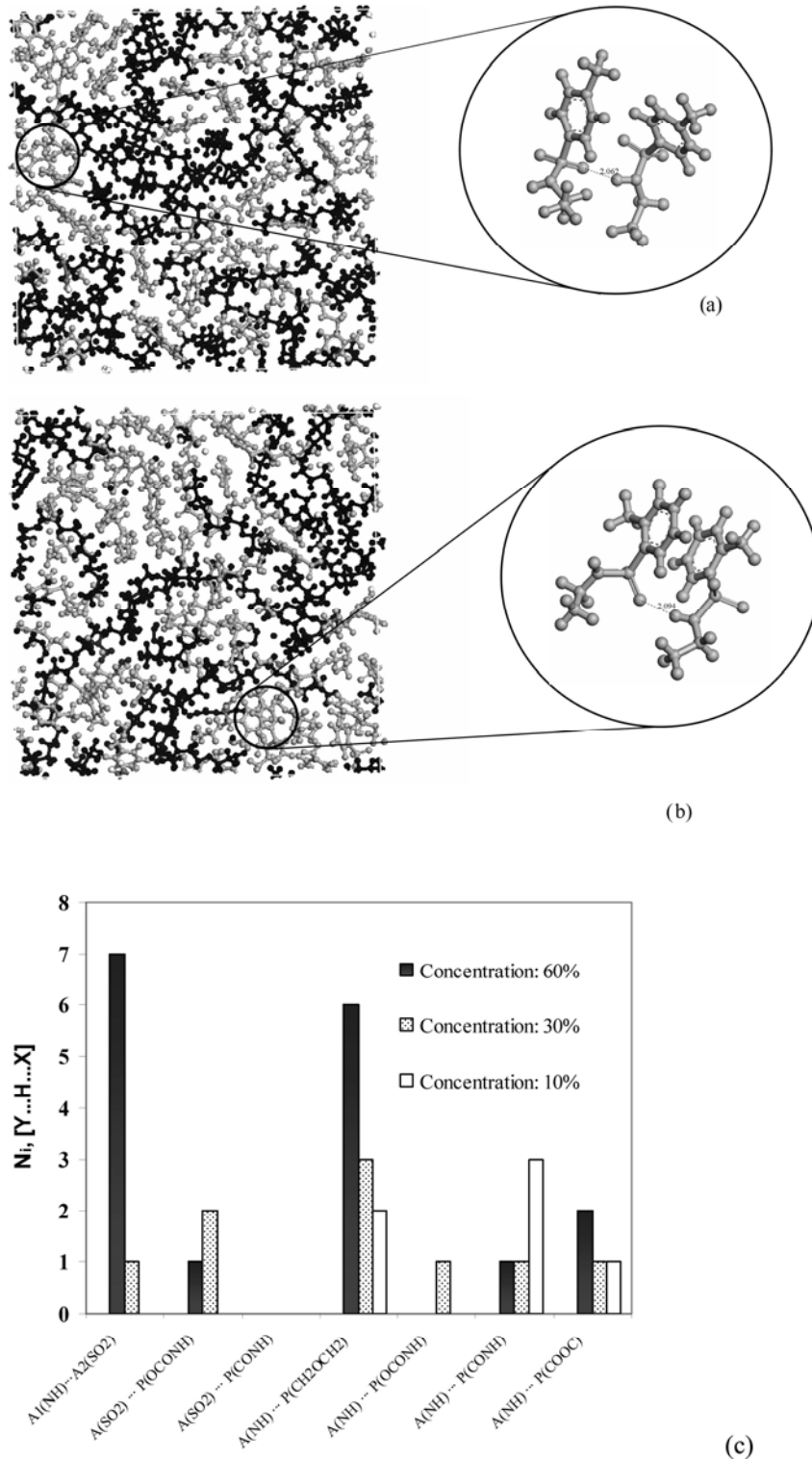


Figure 4. 9- (a) (p-KET)2 and (b) (o-KET)2 dimers extracted from slides of an amorphous box at 60 wt %. The polymer chain is depicted in black and the additive is depicted in gray. (c) Number of interactions involving hydrogen between modifier-polymer and modifier-modifier at a distance of  $\approx 3$  Å.

The key indication derived from theoretical analysis highlighted the geometries involving two linked modifiers and established the intermolecular interaction N-H...O-S-O underlying the polymer influence on this interaction. This information is significant because it explains how a second water molecule interacts less with the  $[\text{H}_2\text{O}\dots(\text{o-KET})_2]$  complex than a separate o-KET. In addition, the dipole moments of  $[\text{H}_2\text{O}\dots(\text{o-KET})_2]$  and  $[(\text{H}_2\text{O})_2\dots(\text{o-KET})_2]$  complexes are almost equal to the dipole moment of the o-KET and  $[\text{H}_2\text{O}\dots(\text{o-KET})]$ . This means that the increase in modifier molecule number does not produce a corresponding increase in the overall dipole moment and, consequently, in the polymer polarization.

The established intermolecular interaction indicated the way by which the KET can be assembled in clusters that could be responsible for changes in the polymer packing and in the hydrophilic/hydrophobic domains.

Experimental and theoretical approaches suggest, therefore, plausible explanations of the sorption phenomenon that can be controlled as a function of the final utilization of modified PEBAX membranes. A reciprocal validation of experimental evidence and theoretical structural models was possible, since the information extracted from multi approach evaluations provided similar interpretations.

### 3. Structural Analysis

#### 3.1. Interactions KET-KET

For better understanding the positions of additives and polymer in the simulated systems the radial distribution functions between H-N and O-S-O of KET sulphonamidic groups were analyzed in the PEBAX/KET 3D cells at different additives compositions (Figure 4.10)

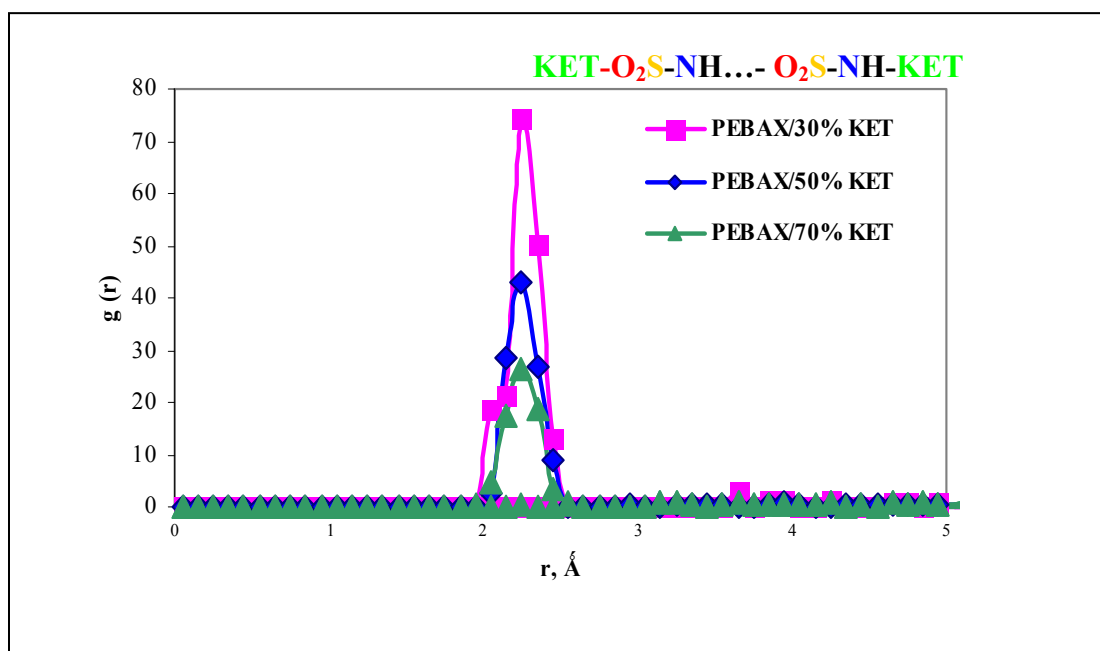


**Figure 4. 10- Radial distribution functions between H-N and O-S-O of KET sulphonamidic groups PEBAX/KET 3D cells.**

In figure 4.10 (a) intense peak in the range of 2,5-2,7 Å is detected for all the modified PEBAX membranes, thus giving evidence of the formations of strong hydrogen bonds between additives linked together in form of dimers.

The intensity of the peak decreases passing from the composition of 30 %wt KET to 70 %wt KET: the observed trend could be an effect of the normalization of the  $g(r)$  on the number of KET in each model.

A further analysis of the hydrogen bonds between all the possible donor and acceptor groups of KET-KET and KET-Polymer in the simulated systems at different KET composition was performed and the data are collected in the histogram of Figure 4.11:

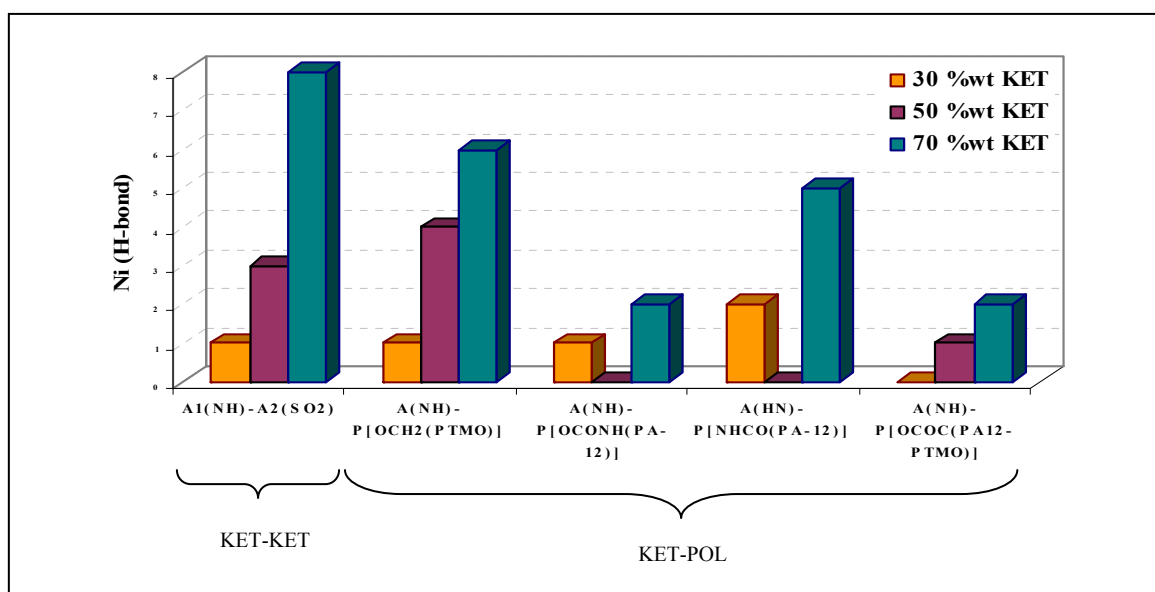


**Figure 4. 11- Distributions of hydrogen bonds between all the possible donor and acceptor groups of KET-KET and KET-Polymer in PEBAX/KET systems.**

From the analysis of Figure 4.11 the number of hydrogen bonds between the Hydrogen of sulphamide group and the oxygen of sulphamidic groups of KET (formation of dimers KET-KET) increases for the system with 70 %wt KET; also the number of hydrogen bond between KET and polar groups of polymer increase for high percentage of KET : in the system PEBAX/ 70 % wt KET the high number of KET molecules (248) leads to higher possibility to form hydrogen bonds for the major availability of polar groups.

3.2. Interactions  $H_2O$ -PEBAK and  $H_2O$ -KET

Figure 4.12 shows the radial distribution functions between H of water molecules and N of amidic group (a) and O of PTMO group (b) of PEBAK chain in 3D PEBAK model with different weight percentage of KET.

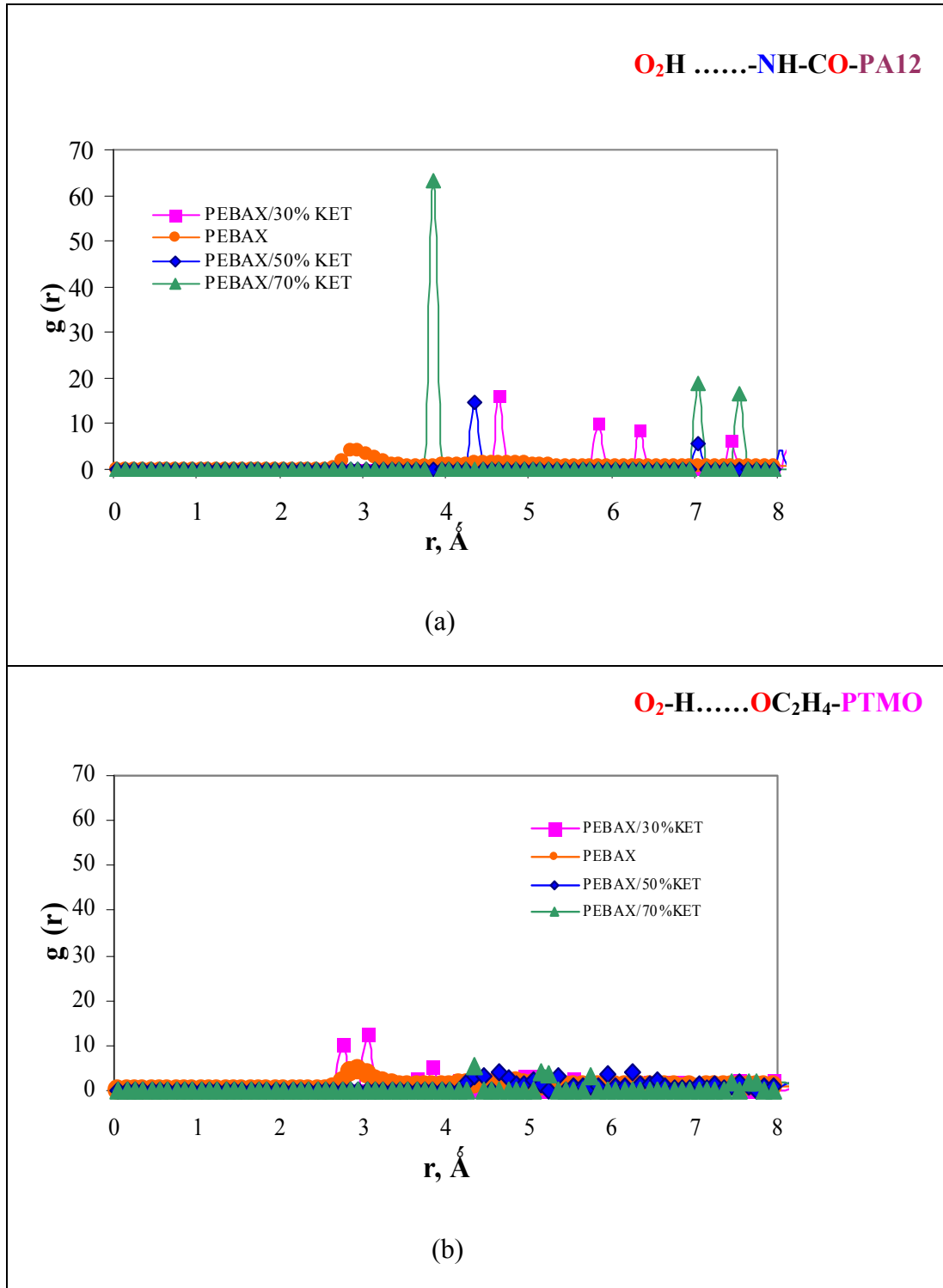


Figure 4.12- Radial distribution functions between H of water molecules and N of amidic group (a) and O of PTMO group (b) of PEBAK chain in PEBAK/KET 3D boxes.



From the analysis of the RDF's, an intense interaction of the water molecules with the PA-12 domain of PEBAX can be detected for the system PEBAX/ 70 %wt KET. The water interacts at short range ( $\approx 3 \text{ \AA}$ ) with the Oxygen of PTMO domain for 30 %wt of ket, and seems more distant to the PA-12 domain ( $30 \text{ %wt} \approx 4,7 \text{ \AA}$  ;  $50 \text{ %wt} \approx 4,5 \text{ \AA}$ ).

In both Figure 4.12(a) and 4.12(b) the increase of intensity of the modified PEBAX peaks respect to the pure system is obsr, thus suggesting stronger interactions between water and polymer in presence of KET: this behaviour is probably responsible for the higher vapours solubility observed in PEBAX/KET membranes.

Finally the RDF between Hydrogen of water and N of sulphonamidic group of KET in the assembled 3D PEBAX/KET models were analyzed and reported in Figure 4.13:

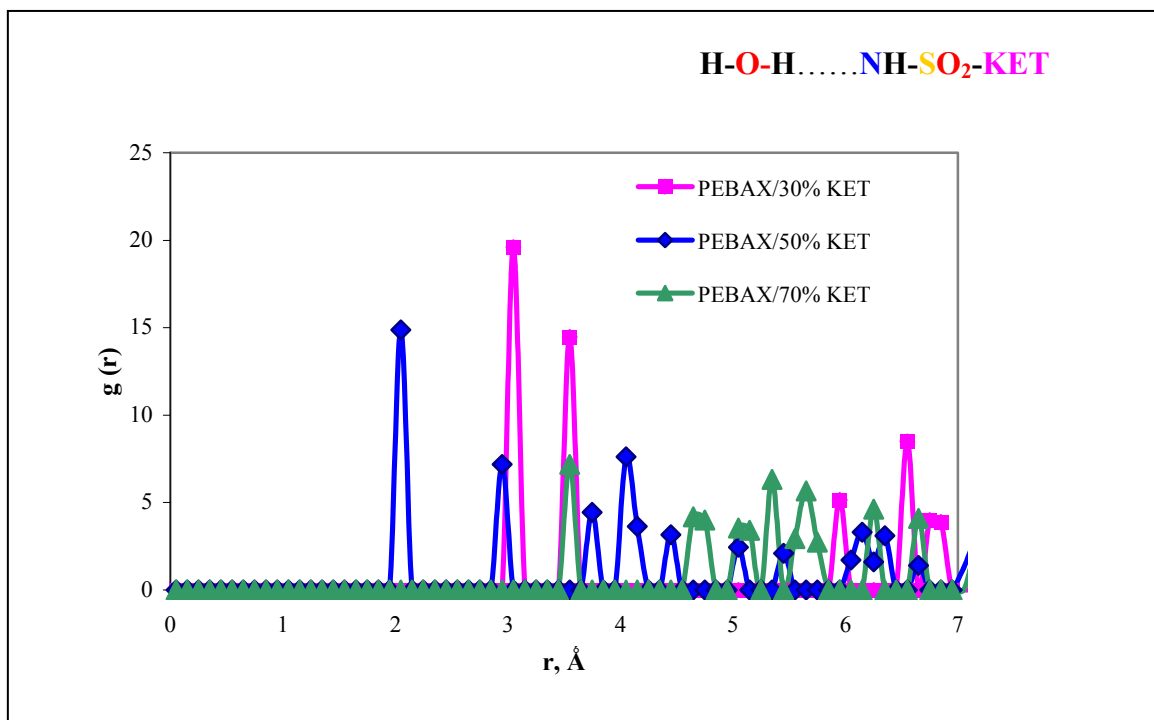


**Figure 4. 13- RDF between Hydrogen of water and N of sulphonamidic group of KET in the assembled 3D PEBAX/KET models.**

In Figure 4.13 the height of the first peaks for PEBAX with 50 %wt of KET are centred at about  $2,3 \text{ \AA}$ : this indicates the occurrence of hydrogen bonds between water molecules and sulphonamidic group of KET at this composition. Strong interactions of high intensity are detected also for the system with 30 %wt in KET at  $\approx 3 \text{ \AA}$ .

The intensity of the peaks for higher concentrations of 70 %wt of KET is decreased and the radial distance is shifted to higher value. The observed trend is in agreement with the IR analysis and the quantum mechanical calculations [4.34] according to which the N–H bond of the sulphonamide linkage in modified PEBAX membrane with 70 %wt in KET becomes more and more strong: the detected presence of KET-KET dimers linked together by strong hydrogen bond obstacles the formation of hydrogen bond between water and KET, probably

responsible for the higher solubility of water observed up to 50%wt; this leads to a macroscopic reduction of water solubility in PEBAX/70%wt KET membranes.

#### 4. Conclusions

In this Chapter Molecular Dynamics (MD) simulations has been successfully used to provide a deeper knowledge of the correlations between water transport properties and structural features of the polymeric membranes materials in microscopic scales.

Three-dimensional models of PEBAX/KET with different copolymer/additive composition have been assembled and equilibrate in order to represent realistic models of the systems object of study,

Fully atomistic investigations of the morphology of the modified PEBAX membranes have been performed to study in details:

- ◆ the PEBAX chain mobility in presence of various KET compositions from the analysis of MSD polymer chain in PEBAX/KET 3D models.
- ◆ the homogeneity of the modified membranes by detailed analysis of RDF's between KET and PEBAX polar and hydrophobic chemical groups.

The water solubility (by TST, GCMC and Hildebrand methods) and diffusivity (by TST and MD methods) of PEBAX<sup>®</sup>2533 block copolymer membranes with different concentrations of an aromatic sulphonamide (KET) have been calculated and compared with experimental data in order to obtain reciprocal validations and useful correlations.

Radial distribution functions between KET-KET, H<sub>2</sub>O-PEBAX and H<sub>2</sub>O-KET at increasing additive compositions have been analyzed for investigating the possible formation of clusters of additives and the short range interactions between water, polymer matrix and additives in these complex systems.

## REFERENCES

- [4.1] A. Gugliuzza, E. Drioli, *Polymer* 44 (2003) 2149.
- [4.2] A. Gugliuzza, E. Drioli, *J. Eur Polym*, 40 (2004) 2381.
- [4.3] A. Gugliuzza, E. Drioli, *Polymer*, 46 (2005) 9994.
- [4.4] Gugliuzza, R. Fabiano, M.G. Garavaglia, A. Spisso, E. Drioli, *Journal of Colloid and Interface Science*, 303 (2006) 38.
- [4.5] WO 99640077.
- [4.6] WO 9964505.
- [4.7] WO 9964078.
- [4.8] K. Nagai, B.D. Freeman, A. Cannon, H.R. Allcock, *J. Membr. Sci.*, 172 (2000) 167.
- [4.9] C.C. Hu, Y.C. Wang, C.L. Lib, K.R. Leeb, Y.C. Chen, J.Y. Lai *Desalination*, 144 (2002) 103.
- [4.10] C.C. McDowell, J.M. Partin, B.D. Freeman, G.W. McNeely, *J. Membr. Sci.*, 163 (1999) 39.
- [4.11] M.E. Rezac, E.T. Sorensen, H.W. Beckham, *J. Membr. Sci.*, 136(1997) 249.
- [4.12] M.E. Rezac, B. Schöberl, *J. Membr. Sci.*, 156 (1999) 211.
- [4.13] T.M. Su, I.J. Ball, J.A. Conklin, S.C. Huang, R.K. Larson, S.L. Nguyen, *Synth Met* 84 (1997) 801.
- [4.14] M. Heuchel, D. Hofmann and P. Pullumbi, *Macromolecules* 37 (2004) 201.
- [4.15] D. Pavel and R. Shanks, *Polymer* 44 (2003) 6713.
- [4.16] E. Kucukpinar and P. Doruker, *Polymer*, 47 (2006) 7835.
- [4.17] E. Tocci, A. Gugliuzza, L. De Lorenzo, M. Macchione, G. De Luca, E. Drioli *J. Membr. Sci.* 323 (2008) 316.
- [4.18] M. Entrialgo-Castaño, A. Lendlein and D. Hofmann, *Advanced Engineering Materials* 8 (2006) 434.
- [4.19] G. Marque, S. Neyertz, J. Verdu, V. Prunier and D. Brown, *Macromolecules*, 41 (2008) 3349.
- [4.20] *Polymer User Guide, Builder Section, Polimerizer Section, Amorphous Cell Section, Discover Section, Version 4.0.0, Molecular Simulation, San Diego* (1996).
- [4.21] H. Sun, D. Rigby, *Spectrochim. Acta*, 53 (1997) 1301. D. Rigby, H. Sun and B.E. Eichinger, *Polymer International*, 44 (1997) 311.
- [4.22] JP, Sheth J. Xu, *Polymer*, 44 (2003) 743.
- [4.23] M.E. Rezac, T. Jhon, *Polymer* 39, (1998) 599.
- [4.24] M.E. Rezac, T. John and P.H. Pfromm, *J. App. Polym. Sci.*, 65 (1997) 1983.
- [4.25] D.N. Theodorou, U.W. Suter., *Macromolecules* 18, (1985) 1467-1478.
- [4.26] D. Hofmann, M. Entrialgo-Castano, A. Lerbret, M. Heuchel and Y. Yampolskii, *Macromolecules*, 36 (2003) 8528.
- [4.27] T. A. Andrea, W. C. Swope and H. C. Andersen, *J. Chem. Phys.*, 79 (1983) 4576.
- [4.28] H.J.C. Berendsen, J.P.M. Postma, W. F. Van Gunsteren, A. Di Nola and J. R. Haak, *J. Chem. Phys.*, 81 (1984) 3684.
- [4.29] Y. Wu, H.L. Tepper, G. A. Voth, *J Chem. Phys.*, 124 (2006), 024503.
- [4.30] B. Nick, U.W. Suter, *Comp. Theor. Polym. Sci.* 11 (2001), 49.
- [4.31] A.A. Gusev, S. Arizzi and U.W. Suter, *J. Chem. Phys.*, 99 (1993) 2228.
- [4.32] J.H. Hildebrand, *J. Am. Chem. Soc.* 51 (1929) 66.

- [4.33] A. Gugliuzza, G. De Luca, E. Tocci, L. De Lorenzo, and E. Drioli J. Phys. Chem. B 111 (2007) 8868.

## **V. MOLECULAR INVESTIGATIONS OF GAS AND VAPOURS TRANSPORT PROPERTIES IN A MODIFIED CO-POLY(AMIDE 12-B-ETHYLENE OXIDE) MEMBRANE**

### **1. Introduction**

The modern science material for gases separation is focused on the preparation of new membrane materials that combines higher permselectivity and higher selectivity for specific gases separation applications.

In the new upper bond published by Robeson [5.1] the selectivity of CO<sub>2</sub>/N<sub>2</sub> for a very large series of polymers commercially in use are considered: polymers containing poly(ethylene oxide) units have interesting CO<sub>2</sub>/N<sub>2</sub> (polar-non polar gases) and the copolymer of the series PEBAX are very close to the upper bond high selectivity polar/non polar gases and high processability (see Figure 1.3).

A useful strategy for changing and improving the performance of raw materials consists of suitably incorporation of new structural and chemical elements into the polymer matrixes in order to control structure–property relationships [5.2–5.7].

One of the most flexible methods for achieving this goal is to blend different compounds, selected on the basis of their intrinsic chemical and morphological characteristics [5.8–5.10].

Membranes based on PEBAX®2533 were functionalised by incorporating chemical compounds containing free N-alkyl sulphonamide in various weight percentage; With this respect, the supra-molecular chemistry can be addressed to manipulate specific interactions, improving the compatibility between polymer surface and chemical species to be separated [5.2-5.7, 5.11]. The possibility to manipulate the membrane affinity appears to be a promising strategy for enhancing the efficiency of a process, especially when the sorption selectivity is the predominant parameter on the overall transport

An increase in polar moieties resulted in enhanced permeability and selectivity with respect to the pure polymer CO<sub>2</sub> transport through functional assembled mono-layers was evaluated in relation to H<sub>2</sub>O and non polar gases such as CH<sub>4</sub>, O<sub>2</sub>, N<sub>2</sub>. It can be observed a good performance in terms of permeability and selectivity of the membranes considered in this work, since high permeability was combined with high selectivity. CO<sub>2</sub> permeability, CO<sub>2</sub>/N<sub>2</sub> and CO<sub>2</sub>/O<sub>2</sub> selectivities for all of the functional layers were remarkably higher than that exhibited by some rubbers and polymers containing PTMO as reported in Table 5.1 [5.2]:

The subject of this research work was the assessment of the chemistry– transport correlations, which govern the passage of small chemical species, such as vapours and gases, across modified matrixes. Specifically, the behaviour of CO<sub>2</sub> in relation to water vapour and other non polar gases (CH<sub>4</sub>, O<sub>2</sub>, N<sub>2</sub>) was evaluated, after introducing different chemical moieties in an elastomeric block co-polyamide Pebax®2533: 80PTMO/PA) [5.2-5.7]. Many studies, devoted to gas separations based on membrane processes, elucidated the importance to correlate the characteristics of polymers, as free volume [5.12], polymer chain packing and inter segmental distance [5.13, 5.14], with their transport properties, emphasising the role of the microstructure of the polymers in gas/vapour permeability and selectivity [5.15]. The MD

simulations represent one of the best tool for obtaining correlation between interaction al molecular level and microscopic structure to the macroscopic transport properties exhibited by polymeric membrane even more complex such us PEBAX®2533 modified with variable weight percentages of a o-p/toluensulphanimide (KET) .

<b>Polymer</b>	<b>PH<sub>2</sub>O [Barrer]</b>	<b>PCO<sub>2</sub> [Barrer]</b>	<b><math>\alpha</math>H<sub>2</sub>O/CO<sub>2</sub></b>	<b><math>\alpha</math>CO<sub>2</sub>/N<sub>2</sub></b>	<b><math>\alpha</math>CO<sub>2</sub>/O<sub>2</sub></b>
NATURAL RUBBER	-	120	-	16.3	-
BUTYL RUBBER	-	4.7	-	16.0	-
PUU(PTMO/PDMS)	-	82	-	24.8	8.1
PU(PTMO)	-	64	-	20.6	10.7
PEBAX100	25030	500	49.2	35.0	14.0
PEBAX /KET 70/30	37500	480	79.0	35.5	12.6
PEBAX /KET 50/50	20330	167	121.7	25.6	12.0
PEBAX /KET 30/70	2455	23	108.1	22.9	8.3

**Table 5. 1- Permeability and selectivity of specific gas pair in various polymers [5.2]**

For this purpose three-dimensional boxes of pure PEBAX®2533 with the insertion of a number of KET molecules corresponding to the following weight percentage: 30%, 50, 70 % were constructed with periodic boundary conditions and simulated using the commercial software Insight II-Discover ACCELRYs of [5.16]: A small amount of gases molecules (10 CO<sub>2</sub>, 10 CH<sub>4</sub>, 10 H<sub>2</sub>, 10 O<sub>2</sub>, 10 N<sub>2</sub>) was inserted in each model in order to prevent mutual diffusion.

The COMPASS force field [5.17] was used for all simulations and the procedure of equilibration was performed as described in section 1.1 of previous chapter in order to obtain 3D models with homogeneous distributions of void and density near to the experimental one (it was considered the density of the pure system 1.01 g/cm<sup>3</sup> [5.18])

Gusev-Suter Transition State Theory (TST) [5.19] are used for simulating the transport of H<sub>2</sub>, N<sub>2</sub>, O<sub>2</sub>, CO<sub>2</sub>, CH<sub>4</sub> and H<sub>2</sub>O for evaluating the selectivity between specific couple of gases and compared with experimental data; Monte Carlo dynamics and calculation of solubility by GCMC method are still in progress.

Structural RDF analysis on the assembled models are performed to investigate in detail the interactions between CO<sub>2</sub>, O<sub>2</sub> and polymeric matrix.

## 2. Results and Discussions

### 2.1. Gases transport properties

Equilibrated amorphous cells of PEBAX/KET at different additive compositions (0, 30%wt, 50 %wt, 70 %wt) were used in order to estimate the diffusion and solubility coefficients using Gusev\_Suter method; the results are shown in Figure 5.1:

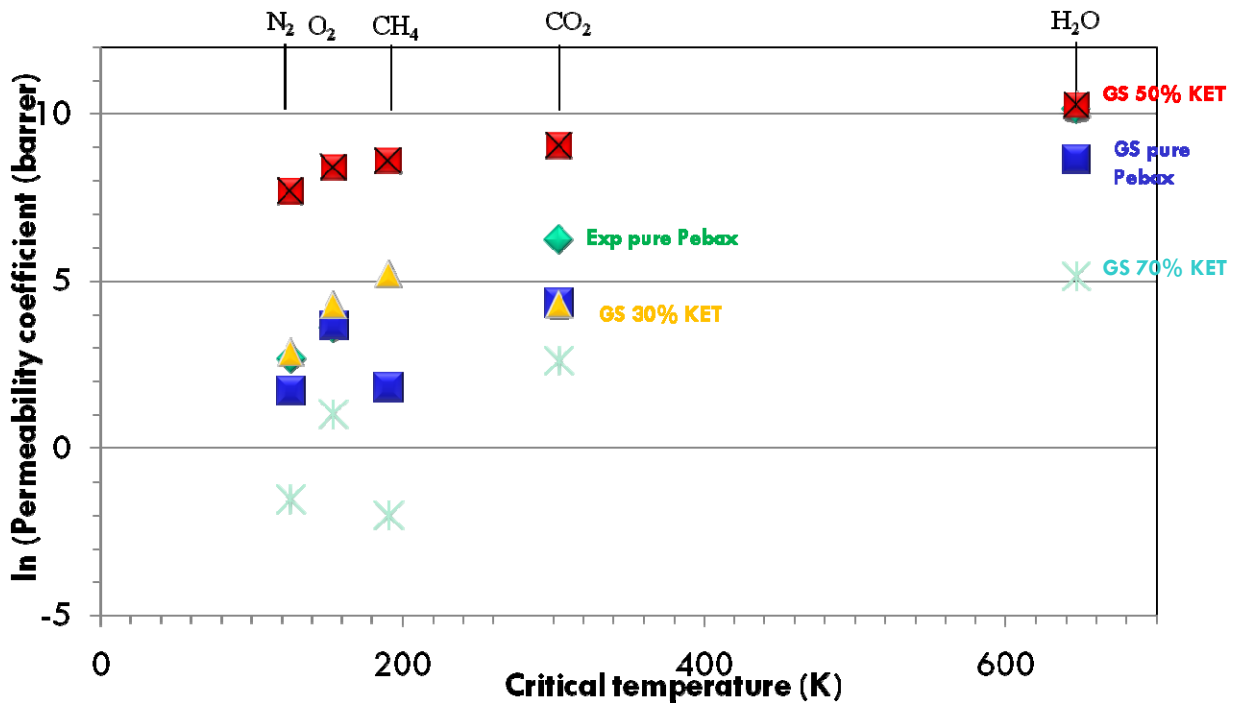
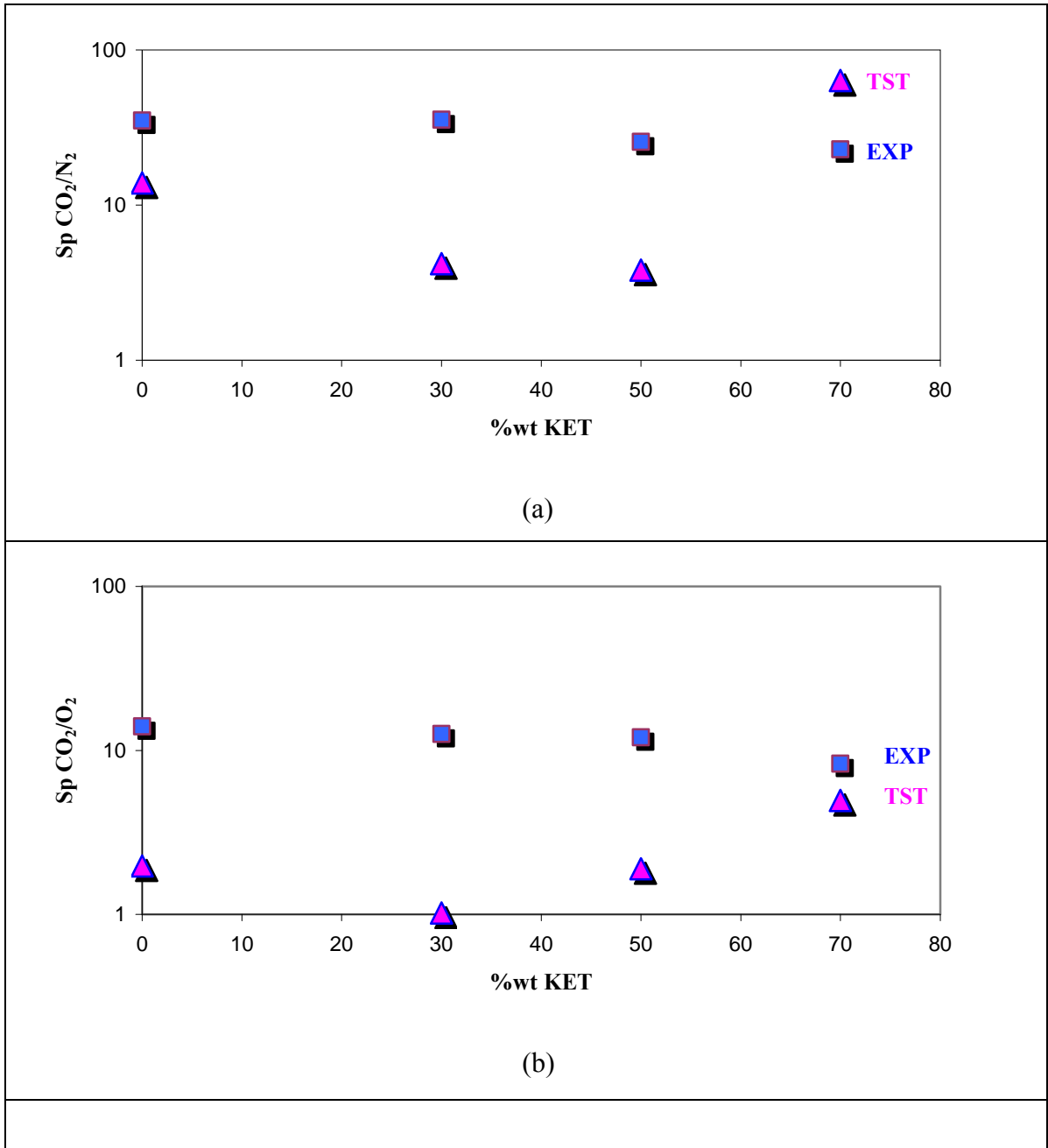


Figure 5. 1 –TST calculated permeability for H<sub>2</sub>O, O<sub>2</sub>, N<sub>2</sub>, CO<sub>2</sub>, CH<sub>4</sub> for modified PEBAX/KET systems.

From the analysis of data reported in Figure 5.1 membranes of PEBAX/KET with amphiphilic sulphonamide were responsible for increase in permeability in the following order: H<sub>2</sub>O>>CO<sub>2</sub>>CH<sub>4</sub>=O<sub>2</sub>>N<sub>2</sub>. The order is mainly due to the different condensability of the penetrant species. Concerning the differences of membranes: the modifiers grouped together in form of clusters have different mobility in comparison to that of the polymer matrix, especially at high modifier content.

For all the gases an increase in permeability is observed for 50 %wt KET while a decrease in permeability is observed for 70 % KET: further investigation of the distributions of voids and of rigidity of chain for these system are in progress to explain the observed trend.

The Permeability Selectivity  $Sp_{CO_2/N_2}$ ,  $CO_2/O_2$ ,  $H_2O/N_2$  and  $H_2O/CO_2$  are analyzed in details and compared with the experimental data; the results are reported in figure 5.2 (a-d).





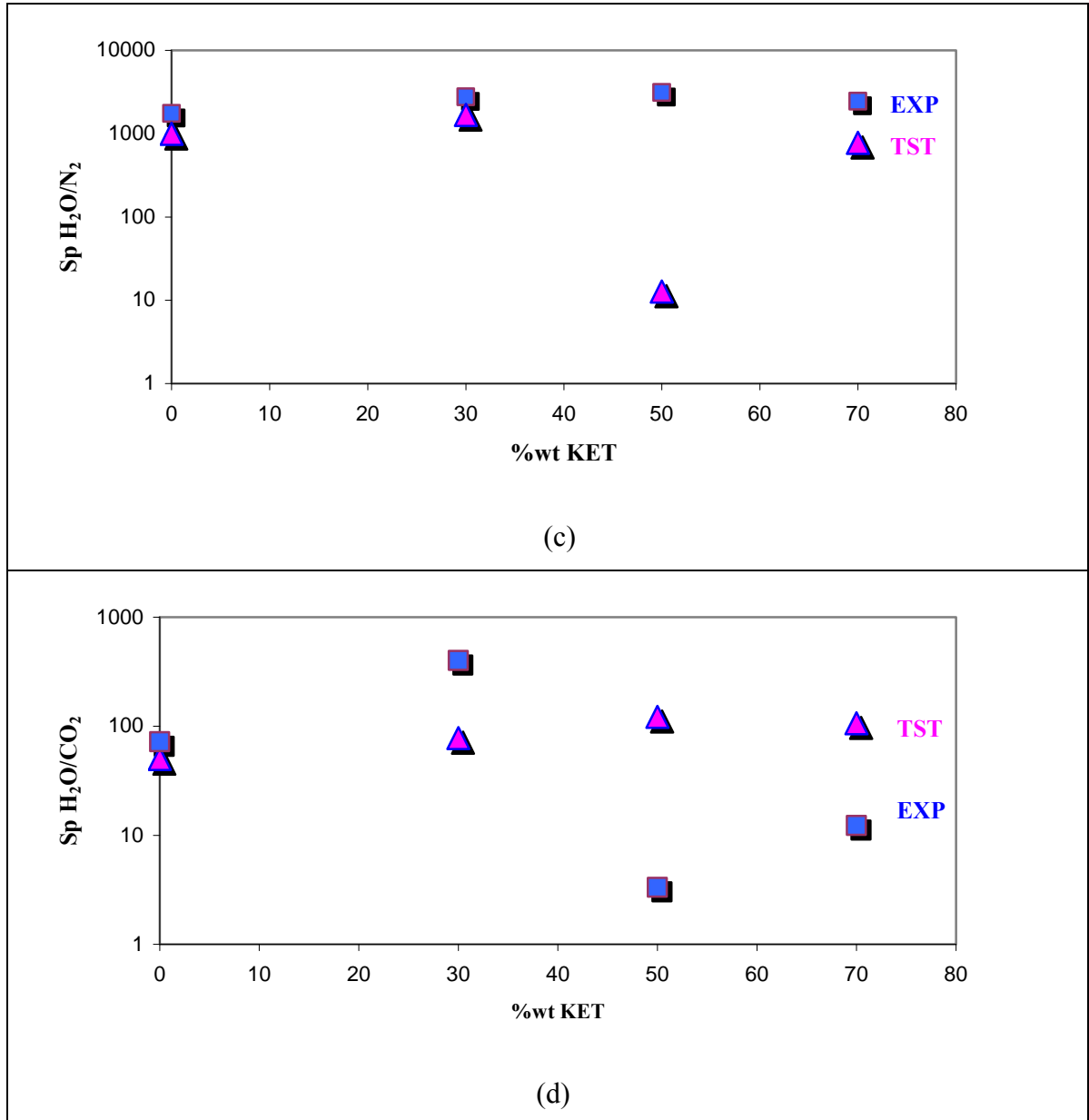
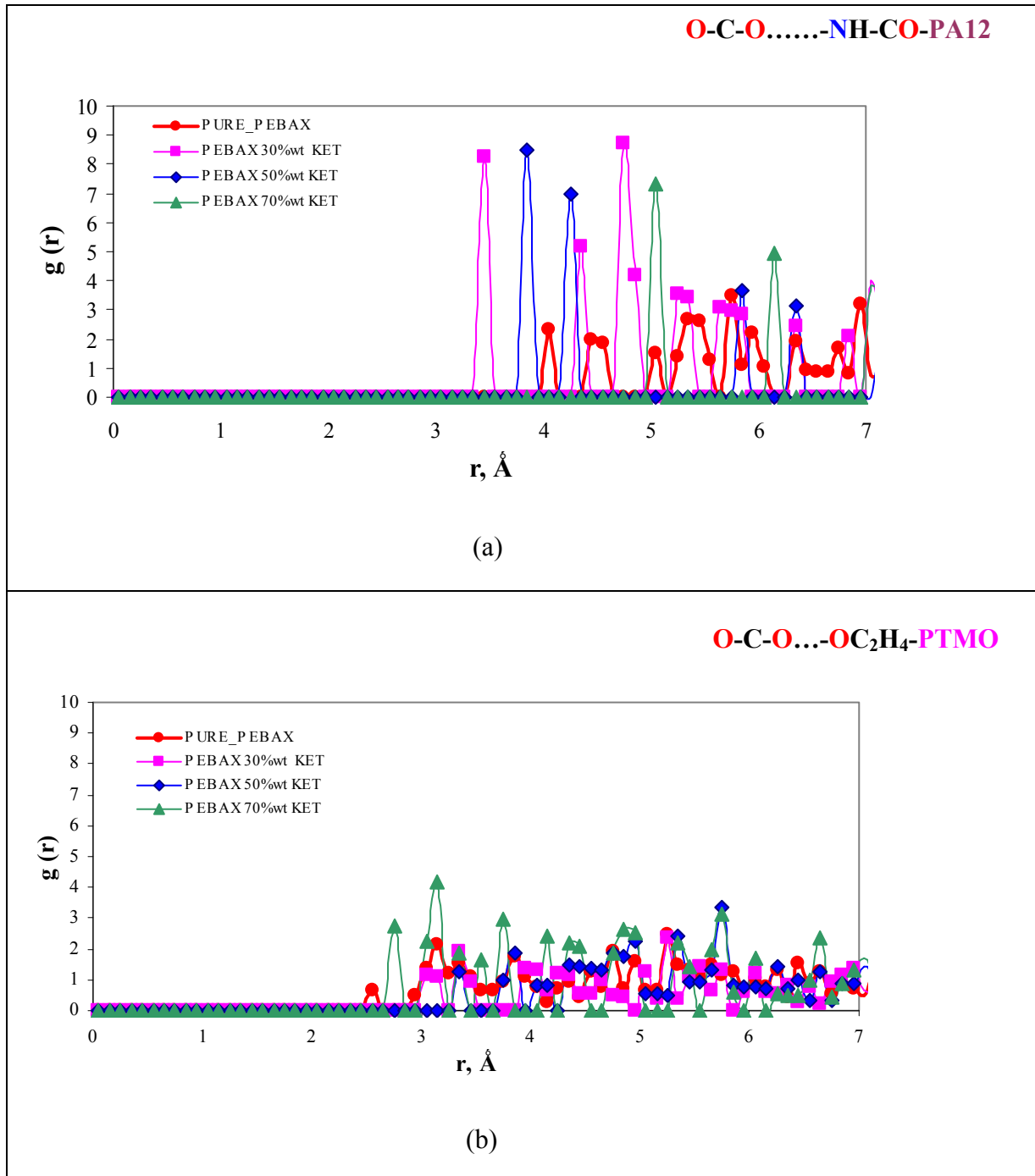


Figure 5. 2- Experimental and theoretical Permeability Selectivity Sp for (a) CO<sub>2</sub>/N<sub>2</sub>, (b) CO<sub>2</sub>/O<sub>2</sub>, (c) H<sub>2</sub>O/N<sub>2</sub> and (d) H<sub>2</sub>O/CO<sub>2</sub>.

An acceptable agreement between experimental and theoretical data is observed in spite of the intrinsic limitations of the GS method in evaluation the transport properties of polar gases; from the analysis of the Figure 5.2 (a-b) the increase of selectivity polar/non polar gases is enhanced in membrane with KET and the highest selectivity can be observed for the separation H<sub>2</sub>O/N<sub>2</sub> Fig 5.2 (b) in the order of 1000.

**2.2. Structural analysis: Radial Distribution Functions**

Radial distribution function between Oxygen of CO<sub>2</sub> and N of PA-12 amidic group (a) and O of PTMO group (b) in PEBAX chain are reported in figure 5.3.



**Figure 5.3 - Radial distribution function between Oxygen of CO<sub>2</sub> and N of PA-12 amidic group (a) and O of PTMO group (b) in PEBAX/KET systems.**

From the analysis of RDF's an increase of the intensity of interactions between CO<sub>2</sub> and amidic group respect to the pure PEBAX is observed; for the pure systems the analysis of the interactions had been outlined that CO<sub>2</sub> interacts most with the ether groups of soft PTMO, (See figure 3.8 Chapter 3,) so the effect of KET is to promote the interaction between quadrupolar CO<sub>2</sub> with NH polar amidic groups of PA12, while in pure system the transport of CO<sub>2</sub> is proved to be vehicled in the soft domain of PTMO.

Stronger short range interactions for the membrane with 30 %wt KET and 50 %wt KET can be observed for the interaction between CO<sub>2</sub> and nitrogen of PA12 amidic group, in agreement with the higher CO<sub>2</sub> solubility experimentally observed at this weight additive percentages in the modified PEBAX membrane. For higher concentrations 70 %wt in KET the CO<sub>2</sub> seems to go far from the PA-12 domain confirmed by the short range peak  $\approx 2,8 \text{ \AA}$  (although of minor intensity) exhibited by the RDF curve between CO<sub>2</sub> and O of PTMO group at this concentration.

### 3. Conclusions

In the research presented in this chapter MD method has been applied for a detailed investigation of gases molecules transport through complex system of PEBAX modified with different weight percentage of KET. Experimental and theoretical approaches suggest plausible explanations of the gases sorption and diffusion mechanisms that can be controlled according to the final utilization of modified PEBAX membranes;

The theoretical data confirms the increase in permeability of all gases and selectivity polar/non polar gases in PEBAX/KET membranes with the exception of 70%wt KET; further calculations of gases diffusion by analysis of MD trajectories and solubility by GCMC method in the assembled 3D amorphous cell of modified PEBAX are still in progress.

Interactions between CO<sub>2</sub> and PA12 and PTMO domain of the block copolymer have been analyzed by radial distribution functions thus providing useful information about microscopic structure of assembled modified PEBAX models.

## REFERENCES

- [5.1] L.M. Robeson J. Membr. Sci. 320 (2008) 390.
- [5.2] A. Gugliuzza, E. Drioli, Polymer, 46 (2005), 9994.
- [5.3] A. Gugliuzza, E. Drioli, Polymer, 44 (2003) 2149.
- [5.4] A. Gugliuzza, E. Drioli, Eur. Polym. J., 40 (2004) 2381.
- [5.5] K. Nagai, B.D. Freeman, A. Cannon, H.R. Allcock, J. Membr. Sci, 172 (2000) 167.
- [5.6] C.C. Hu, Y.C. Wang, C.L. Lib, K.R. Leeb, Y.C. Chen, J.Y. Lai Desalination, 144 (2002) 103.
- [5.7] C.C. McDowell, J.M. Partin, B.D. Freeman, G.W. McNeely, J. Membr. Sci., 163 (1999) 39.
- [5.8] M.E. Rezac, E.T. Sorensen, H.W. Beckham, J. Membr. Sci., 136(1997) 249.
- [5.9] M.E. Rezac, B. Schöberl, J. Membr. Sci., 156 (1999) 211.
- [5.10] T.M. Su, I.J. Ball, J.A. Conklin, S.C. Huang, R.K. Larson, S.L. Nguyen, Synth Met., 84 (1997) 801.
- [5.11] A. Gugliuzza, G. Clarizia, G. Golemme, E. Drioli, Eur. Polym. J. 38 (2002) 235.
- [5.12] M.A. Del Nobile, G.G. Buonocore, L. Palmieri, A. Aldi, A. Acierno J. Food Eng. 53 (2002) 287.
- [5.13] S.J. Metz, W.J.C. van de Ven, J. Potreck, M.H.V. Mulder, M. Wessling, J. Membr. Sci. 251 (2005) 29.
- [5.14] L. Jia, X.F. Xu, H.J. Zhang, J.P. Xu, J. Polym. Sci, Polym. Phys., 35 (1997) 2133.
- [5.15] Z.F. Wang, B. Wang, N. Qia, X.M. Ding, J.L. Hu, Mater. Chem. Phys., 88 (2004) 212.
- [5.16] Accelrys Inc., InsightII 4.0.0.P+, POLYMERIZER, DISCOVER, AMORPHOUS CELL, BUILDER SORPTION Modules 2001, San Diego, CA, USA; 2001.
- [5.17] D. Rigby, H. Sun and B.E. Eichinger, Polymer International, 44 (1997) 311.
- [5.18] ELF Atochem Inc., PEBAX® Technical Brochure (2000).
- [5.19] D.N. Theodorou and U.W. Suter, Macromolecules, 18 (1985) 1467.

## VI. MESOSCALE SIMULATION OF MORPHOLOGY AND TRANSPORT PROPERTIES IN PEBAX MEMBRANES

### 1. Introduction

#### 1.1. Problem Definition

Atom-based simulations such as MD and MM methods have become widely used for materials design. As mentioned above, using atomistic simulation tools, one can analyze molecular structure on the scale of 0.1–10 nm. However, to predict macroscopic properties of materials, one often has to take into account that they result from averaging responses on a much larger length-scales, for structures that are well equilibrated.

In the previous chapters MD simulation of structural and gases transport properties in pure copoly(amide-12b-ethylene oxide) (PEBAX) and modified with variable additive compositions membranes have been described in detail; with fully-atomistic simulation the PEBAX membranes were treated as fully amorphous because at the length scale of the MD modelling the micro-separation between semi-crystalline PA-12 and soft PTMO domains cannot be taking into account.

Here we used mesoscopic techniques to obtain morphology information on the mesoscale and to compliment our atomistic modelling of PEBAX®2533, the polymer in the PEBAX series with the major soft weight percentages and a very low crystallinity percentage ( $\approx 3\%$ ) [6.1].

#### 1.2. Experimental Background

Before conducting any theoretical investigation, a good starting point is a clear experimental description of the properties of the material object of study. Many experimental studies have considered the relations between structural characteristics of PEBAX copolymers [6.1–6.8] and their transport properties [6.9–6.15].

It's well-known that in the PEBAX series copolymer, the amide blocks is the hard segment and the polyether blocks behave as soft segments. The main contribution to crystallinity comes from the amide block in which the less permeable phase resides, whereas the ether block acts as permeable phase due to its high chain mobility.

Sheth [6.1] placed particular emphasis on better defining the morphological features of commercially available PEBAX copolymers. Compression molded and solution cast samples were studied by the techniques of DMA, DSC, WAXS, SAXS, AFM, SALS, and stress-strain response. The strain induced crystallization behaviour of the soft polyether (PE) segments was also investigated. All samples exhibited a microphase separated morphology over a broad temperature range. As expected, an increase in the interconnectivity of the polyamide hard phase was greatly controlled by the polyamide (PA) content. Due to the crystallization of the PA hard segment, the formation of PA lamellar crystals were noted in both melt and solution cast films. At the higher PA contents, a distinct spherulitic superstructure was also observed but this form of morphological texture was diminished as the PE soft segment content

increased. Limited studies of the deformation/recovery behaviour of the spherulitic superstructure provided further information concerning the interaction between the hard and soft segments. A series of PA-12-PTMO based PEBAX thermoplastic elastomers with a systematic change in their PA content revealed a complex morphology that was strongly influenced not only by the PA content of a given sample but also by the sample's thermal and process history (melt versus solution). These segmented copolymers were found to be microphase separated with a relatively wide service temperature range of ca. 120°, between 0° and 120°C for the relatively soft samples and between 30° and 150°C for the relatively hard (higher PA content) samples. Both the constituent soft and hard segments were found to be crystallizable but the crystalline phase due to the soft PE segments completed the associated melting transition well below ambient temperature. The peak  $T_m$  of the PE crystalline phase was found to be lower than that reported for homopolymeric PTMO, thus indicating the inability of the PE crystals to form well defined folded chain lamellae in these materials. The amount of crystallinity in a given sample, as determined by DSC, was found to increase with increasing PA content. On the other hand, DMA studies indicated the presence of mixed amorphous PE and PA phases. The PE amorphous phase contained a small amount of PA segments whereas the PA amorphous phase became richer in PA content as the overall PA content of the sample increased.

The interconnectivity of the hard phase also increased with PA content and this resulted in a distinct yield point in the stress-strain response of compression molded P6333 and P7033, the samples with the highest PA content within the series investigated [6.1] The Young's modulus and the extension at break exhibited a similar trend and a remarkably high extension at break was seen in the relatively soft samples P2533 and P3533. SALS and tapping-mode AFM revealed the presence of a spherulitic superstructure in the bulk and on the surface respectively, in compression molded samples P6333 and P7033. However, this form of morphological texture was diminished in samples with higher content of the PE soft segment.

Investigation of the surface morphology of PEBAX films cast from solution (5 wt % in dimethyl acetamide) was also undertaken via tapping-mode AFM in order to compare the morphology of the free surfaces of melt versus solution cast films. Sample P2533 was also investigated but attempts to obtain a useful phase image of this specific material were not successful. Recall that P2533 is highly dominated by the soft PTMO component, nevertheless with very low crystallinity ( $\approx 3\%$ ) [6.1].

### **1.3. Aim of the work**

Despite the great deal of experimental work, there's a lack of information about the morphological behaviour of PEBAX@2533. From the analysis of the experimental data there's no evidence of microphase separation on relevant scales for this system due to the very low weight percentage of PA-12.

The aim of the study described in this chapter is to analyze in detail the morphology of PEBAX@2533 by mesoscale methodology. For giving a realistic description of the copolymer a degree of crystallinity due to the presence of PA-12 rigid segment must be taken into account and modelled in an appropriate way. Our ultimate challenge is to set up a hierarchical approach via several interconnected mathematical models.

The onset of an integrated experimental/theoretical multilevel approach to PEBAX@2533 was developed during a stage in the Soft matter Chemistry group of Leiden Institute of

Chemistry, in the framework of a scientific collaboration which has been undertaken since last year between the ITM - CNR modelling group and the Soft Matter Chemistry laboratory. The software used for is Culgi, developed in the same host institute, which contains a variety of mesoscopic methods, including Dissipative Particle Dynamics (DPD) and Dynamic Density Functional Theory (DDFT).

In the next sections the employed methods and modelling procedure will be described, followed by a brief discussion of the preliminary results.

## 2. Methods

### 2.1. Dissipative Particle Dynamics (DPD)

All mesoscopic methods apply some averaging over ‘fast’ degrees of freedom, to come up with an effective description on the mesoscale (1-100 nm).

The basic idea is to lump groups of atoms into coarse-grained beads, as shown in Figure 6.1.

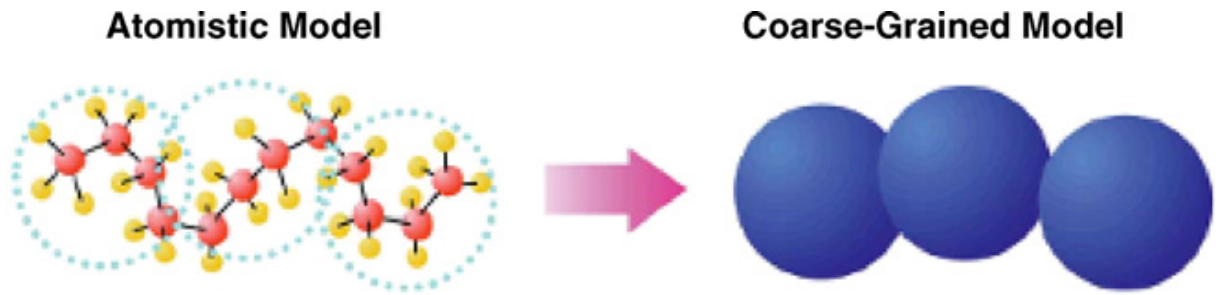


**Figure 6.1 - Coarse grained modeling from atomistic model.**

In DPD, collections of connected soft-core repulsive particles move according to Newton’s equations of motion and interacts dissipatively through simplified force laws (e.g. Groot and Warren [6.16]). In this way, a full hydrodynamics description is recovered.

Setting the masses of all particles equal to 1, the time evolution of the positions ( $r_i(t)$ ) and velocities ( $v_i(t)$ ) is given by:

$$\frac{dr_i}{dt} = v_i(t) \quad , \quad \frac{dv_i}{dt} = f_i(t) \quad (6.1)$$

The force acting on the particles is a combination of three contributions:

$$f_i(t) = \sum_{j \neq i} (F_{ij}^C + F_{ij}^D + F_{ij}^R) \quad (6.2)$$

The conservative force between two beads  $i, j$  separated by a distance  $r_{ij}$ :

$$F_{ij}^C = \begin{cases} a_{ij}(1 - r_{ij}/r_c)\hat{r}_{ij} & r_{ij} < r_c \\ 0 & r_{ij} \leq r_c \end{cases} \quad (6.3)$$

where  $a_{ij}$  is the maximum of the linear potential between particles  $i$  and  $j$ ,  $r_{ij} = r_i - r_j$ ,  $r_{ij} = |r_{ij}|$ ,  $\hat{r}_{ij} = r_{ij}/|r_{ij}|$ , and  $r_c$  is the cut-off radius.

Note that the conservative force is always finite even at zero separation. The other two forces are the dissipative and the random force, which are given by:

$$F_{ij}^D = -\gamma w^D(r_{ij})(\hat{r}_{ij} \cdot v_{ij})\hat{r}_{ij}$$

$$F_{ij}^R = -\sigma w^R(r_{ij})\theta_{ij}\hat{r}_{ij} \quad (6.4)$$

where  $\hat{v}_{ij} = \hat{v}_i - \hat{v}_j$ ,  $w^D$  and  $w^R$  are weight functions tending to zero for  $r = r_c$  and  $\theta_{ij}$  is a randomly fluctuating variable with zero mean and unit variance. Español and Warren [6.17] showed that the weight functions and constants  $\gamma$  and  $\sigma$  (denoting the friction coefficient and the noise amplitude for all particles, respectively) in Eq. (6.4) can be chosen arbitrarily, but should obey:

$$[w^R(r_{ij})]^2 = w^D(r_{ij}), \quad \sigma^2 = 2k_B T \gamma \quad (6.5)$$

where  $k_B$  is the Boltzmann constant and  $T$  the temperature of the fluid. The equations are solved using the modified velocity-Verlet algorithm as described by Groot and Warren. The random force weight function:  $w^R(r_{ij})$  is defined as  $1 - (r/r_c)$ , where  $r_c = 1.0$ .

Since DPD is a coarse-grained model and individual atoms or molecules are not represented directly by the particles but they are grouped together into beads (see Figure 6.1), these beads represent local ‘fluid packages’ able to move independently.

Connections between beads, i.e. a polymer molecule, are established by adding a spring between beads. Thus, beads can be interconnected to highly complex topologies, e.g. branched architectures, and additional spring forces should be added to Eq. (6.2).

Choosing the correct spring force deserves closer examination. Two types of spring force have been considered in literature. Groot and Warren advocated the use of the harmonic spring:

$$F_{ij}^{spring} = k \cdot r_{ij} \quad (6.6)$$

where  $k$  is the spring constant. In this way the mean distance between two consecutive chain beads is governed by the spring force and the repulsive interaction. The value of the spring constant is chosen such that the mean spring distance corresponds to the distance found at the maximum of the pair correlation function of the polymer beads when the spring constant is equal to zero. However, in this manner connected beads are not prevented to be located far more than  $r_c$  apart. This is highly undesirable as hydrodynamic interaction between beads within the same polymer chain is lost and it would be easy for polymer chains to cross each other without ever experiencing any mutual interaction. This is comparable to neglecting the Zimm corrections [6.18] on the dynamical chain behaviour as predicted by the Rouse model [6.19]. Of course, a stiffer spring could be modelled by choosing a larger spring constant, but, essentially, this would also imply an increase in the density of the polymers.



In order to overcome these problems, the Fraenkel spring, as applied by Schlijper et al. [6.20], is used in our simulations:

$$F_{ij}^{spring} = k \cdot (r_{ij} - r_{eq}) \cdot \hat{r}_{ij}$$

$$U_{ij} = \frac{1}{2} k (r_{ij} - r_{eq})^2 \quad (6.7)$$

Here  $r_{eq}$  is the equilibrium spring distance (chosen as  $(r_{eq} = 1/(\sqrt[3]{\rho}))$ ), which is independent from the stiffness of the polymer spring. The spring constant is determined by simulating polymer chains at the relevant conditions for demixing simulations. The distance between two consecutive beads in the polymer chains is sampled for several spring constants. The spring constant value at which 98% of the cumulative spring distance distribution lies within one  $r_c$  is chosen as the correct value.

Chain stiffness is modelled by a three-body potential acting between adjacent bead triples in a chain:

$$U_{i-1,i,i+1} = k_2 [1 - \cos(\phi - \phi_0)] \quad (6.8)$$

Where the angle  $\phi$  is defined by the scalar product of the two bonds connecting the pairs of adjacent beads  $i-1, i, i+1$ : in general, the bending constant  $k_2$ , and preferred angle  $\phi_0$  may be specified independently for different bead type triples allowing the chain stiffness to vary along a molecule's length. A preferred angle of zero means that the potential minimum occurs for parallel bonds in chain.

## 2.2. Dynamic Density Functional Theory (DDFT)

To study the phase separated domains on mesoscopic scales, another useful tool, involving one additional coarse-grained step, is Dynamic Density Functional Theory (DDFT) [6.21-6.27]. Here the phase separated domains are described in terms of density distributions fields of monomers and solvents. One of the important features of DDFT is that it can take into account the conformational entropy of polymer chains with any molecular architecture, i.e. the monomer sequence and the branching structures. Moreover it provides both thermodynamic and kinetic properties of the system. Using DDFT, the equilibrium state of polymeric systems with mesoscopic structure can be assessed, which is not always accessible by particle simulations or fluid dynamics simulations. The advantage of DDFT over DPD is its enhanced efficiency. Although they should sample the same equations-states, DDFT applies a diffusive model for the dynamics.

In DDFT a polymer system is modelled as a collection of flexible chains in a mean field environment; the simulation procedure is described only briefly [6.28, 6.29, 6.30].

The free energy functional has the form:

$$\begin{aligned}
 F[\rho] = & -kT \ln \frac{\Phi^n}{n!} - \sum_I \int_V U_I(r) \rho_I(r) dr \\
 & + \frac{1}{2} \sum_{I,J} \int_{V^2} \varepsilon_{IJ}(|r-r'|) \rho_I(r) \rho_J(r') dr dr' \\
 & + \frac{k_H}{2} \int_V \left[ \sum_I v(\rho_I(r) - \rho_I^0) \right]^2 dr
 \end{aligned} \tag{6.9}$$

where  $n$  is the number of polymer molecules,  $\Phi$  is the intramolecular partition function for ideal Gaussian chains,  $\rho_I$  is the density of the copolymer component  $I$  (in our case A and B), and  $V$  is the system volume. The external potentials  $U_I$  are conjugate to the densities  $\rho_I$  via the Gaussian chain density functional [6.25]

Bead– bead interactions have a Gaussian kernel:

$$\varepsilon_{IJ}(|r-r'|) = \varepsilon_{IJ}^0 \left( \frac{3}{2\pi a^2} \right)^{3/2} e^{-3/2 a^2 (r-r')^2} \tag{6.10}$$

where  $a$  represents the bond length. The epsilon parameter is directly related to the conventional Flory-Huggins parameter by  $\chi_{IJ} = \varepsilon_{IJ}^0 / n_A k_B T$  (with  $n_A$  Avogadro's number,  $k_B$  the Boltzmann constant, and  $T = 300$  the temperature in Kelvin) [6.32]. The extrema of the free energy functional  $F$  are found in a dynamic fashion. The time evolution of the density fields is described by the time dependent Landau–Ginzburg-type of equation [6.25, 6.27, 6.29]:

$$\frac{\partial \rho_I}{\partial t} = M_I \nabla \cdot \rho_I \nabla \mu_I + \eta_I \tag{6.11}$$

where  $M_I$  is the mobility of the different components of the chain,  $\mu_I$  are the chemical potentials and  $\eta_I$  is a noise field that satisfies the fluctuation–dissipation theorem.

The key assumption of DDFT is that the diffusive process is slow, so that the polymer conformation always adjusts itself so that the free energy  $F(\rho)$  is minimised. The external potentials  $U_I(r)$  are determined by the density fields  $\rho_I(r)$  via the one-to-one DFT relation.

### 3. Parameter derivation

#### 3.1. Flory–Huggins parameter estimation

Both theories, DPD and DDFT, contain a number of parameter that represents the specificity of the system. They reflect the coarse graining procedure (the molecular architecture) as well as the effective interactions of the coarse grained beads ( $\varepsilon$  in DDFT,  $a$  in DPD). Both latter parameters can be related to the conventional Flory-Huggins parameter  $\chi$ . Before we estimate these variables for our system, we first review the standard mean field, Flory Huggins theory [6.33].

The general expression for the free energy of mixing of a binary system is:

$$\frac{\Delta G}{RT} = \frac{\phi_h}{n_h} \ln \phi_h + \frac{\phi_s}{n_s} \ln \phi_s + \chi \ln \phi_h \phi_s \quad (6.12)$$

where  $\Delta G$  is the free energy of mixing (per mole),  $\phi_i$  is the volume fraction of component  $i$ ,  $n_i$  is the degree of polymerization of component  $i$ ,  $\chi$  is the interaction parameter,  $T$  is the absolute temperature, and  $R$  is the gas constant. The interaction parameter  $\chi$  is the only variable in this theory that contains material specific information.

The first two terms represent the combinatorial entropy. This contribution is always negative, hence favoring a mixed state over the pure components. The last term is the free energy due to interaction. If the interaction parameter,  $\chi$ , is positive, this term disfavors a mixed state. The balance between the two contributions gives rise to various phase diagrams.

The interaction parameter,  $\chi$ , is defined as:

$$\chi = \frac{E_{mix}}{RT} \quad (6.13)$$

where  $E_{mix}$  is the mixing energy; that is, the difference in free energy due to interaction between the mixed and the pure state.

The phase behavior of a given AB-diblock is determined by two main factors: composition parameter,  $f_A$ , and the ‘‘incompatibility’’ parameter,  $\chi_{AB}(N_A + N_B)$ , where  $\chi_{AB}$  is the Flory–Huggins parameter, and  $N_{A,B}$  are the chain lengths (degrees of polymerization) of A and B blocks.

The determination of  $\chi$  is one of the most crucial steps in our procedure. Several methods have been suggested in the literature but we rely on a simple strategy based on the matching of volumes. We note that more explicit procedures are available in literature [6.34], however, volume matching is the simplest and most straightforward strategy.

Due to the lack of experimental data the interaction parameter between PTMO and PA-12 has been estimated following the theoretical procedure of Ginzburg et Al. [6.35].

This procedure is valid for copolymer with low percentage of hard phase.

As a result PEBAX®2533 has been modelled as a multiblock copolymer of the  $(AB)_n$  type, where A is referred to the hard domain (in our case PA-12) and B to the soft segment (PTMO). According to the experimental weight percentage (PA-12 21.6 %wt; PTMO 78.4 %wt), the number  $N_h$  of PA-12 and  $N_s$  of PTMO monomers is obtained as  $N_h=2.68$ ,  $N_s=27.80$  [6.12]. Consequently PEBAX®2533 has been modelled as  $AB_4$  chain.

Hence, we estimate  $\chi N$  as [6.35]:

$$\chi N = \chi_{hs} [N_h + N_s] = \frac{(\delta_h - \delta_s)^2}{RT} \left[ \frac{\bar{M}_H}{2\rho_H} + \frac{\bar{M}_s}{\rho_s} \right] \quad (6.14)$$

Here,  $\delta_{h,s}$  is the van Krevelen [6.35] solubility parameter of the hard or soft segment;  $\bar{M}_{H,s}$  indicates the mean molar mass of hard, soft segment;  $\rho_{h,s}$  denotes density of the hard

PA-12 or soft segment in our case respectively PA-12 and PTMO ( $\rho_{PA-12} = 1.002 \text{ g/cm}^3$   $\rho_{PTMO} = 1.000 \text{ g/cm}^3$  [6.36]).

To challenge our result from resolving Eq (6.14) we consider the calculated phase diagram in Figure 6.2, for full flexible molecules as a function of block function  $f$  vs  $\chi N$ .

The calculated value of  $\chi N$  (Eq. 6.14) for PEBAX®2533 is 9.66; the weight fraction  $f_A$  of PA-12 segment domain is 0.216 [6.12]: according to these values the phase diagram shows that PEBAX®2533 is in the disordered, completely amorphous phase.

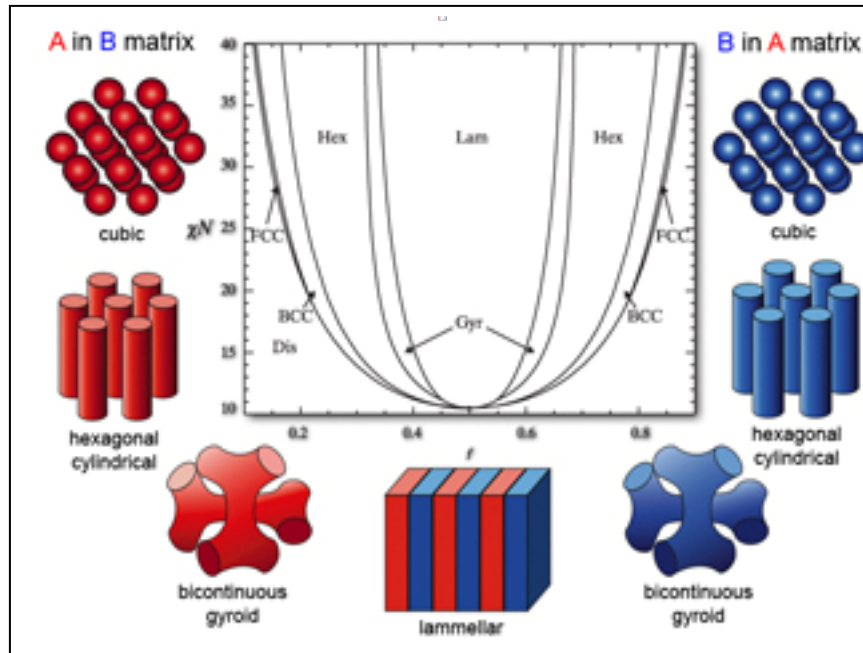


Figure 6. 2- A-B block copolymer phase diagram.

### 3.2. Volume Matching Details

We shortly review the mapping procedure from the full atomistic to the coarse grained representation, which is based on the notion that packing constraints are most important in pattern formation, hence, it relies on matching atomic and coarse grained volumes. In general one should keep in mind that bead radii are constraint below by the persistence length at atomistic resolution.

The volume of the sphere of a single segment of amorphous PTMO,  $V_{PTMO}$ , has been calculated from geometric considerations on structural data extracted by MD models: a single segment has been considered as one bead.

According to the estimated volume  $V_{PTMO}$ , the PA-12 aliphatic chain has been divided into 3 beads of similar volume (calculated from geometric considerations on structural data of crystal of PA-12 in ref [6.37]), while the stiff part (amidic group) of polyamide is been considered as one bead of smaller volume (see Figure 6.3).

Although this representation is rather fine grained from a mesoscopic perspective, this detail is considered essential for capturing intricate properties of the system.

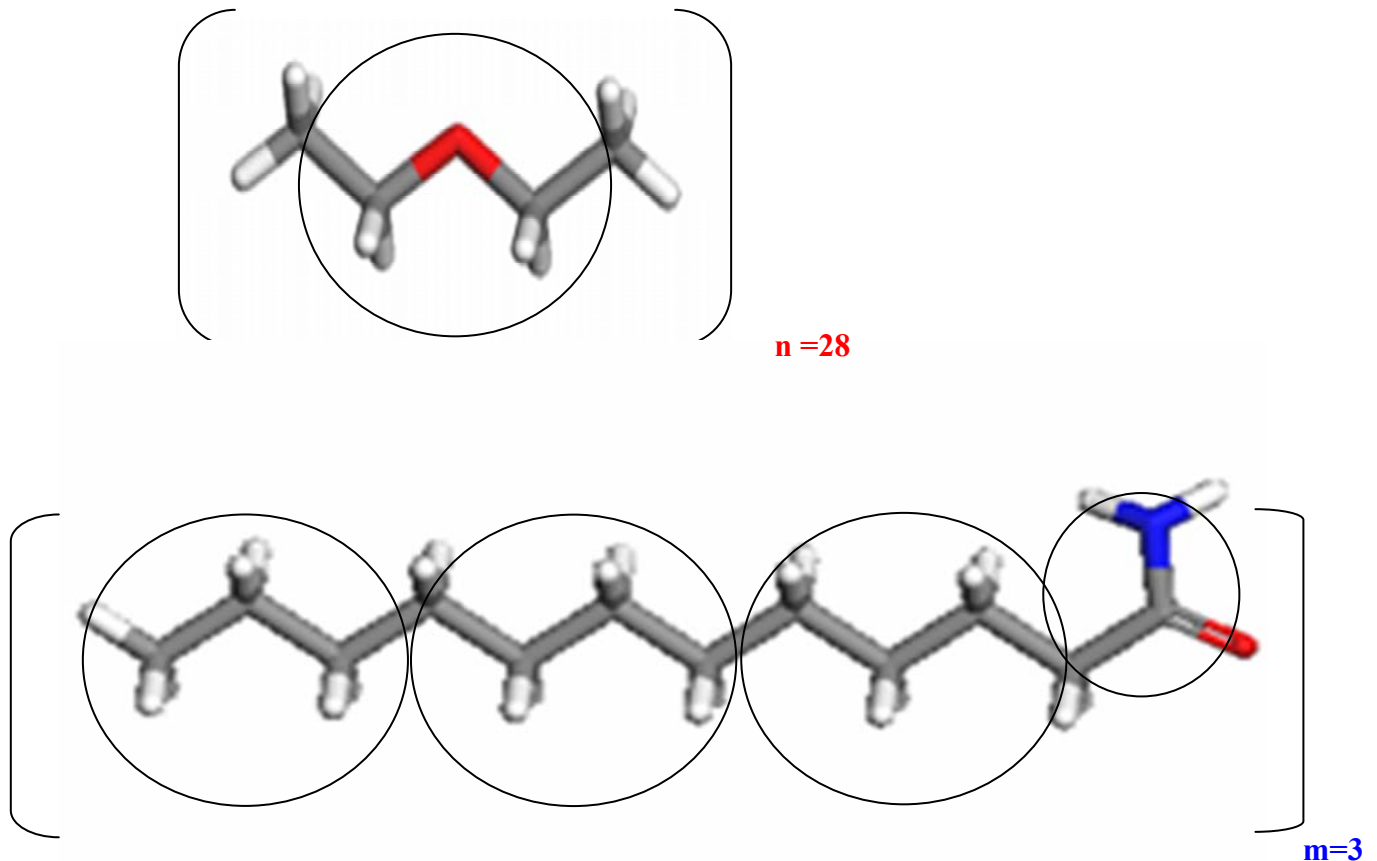


Figure 6.3 - Coarse grained modelling of PTMO and PA-12 monomers from atomistic model.

## 4. Results and discussion

### 4.1. DDFT and DPD simulations

DDFT simulations (Figure 6.4 (a,b)) have been conducted by modelling collections of flexible chains  $AB_4$  and setting  $\chi$  to the calculated value 9.66; the results show a disordered system as predicted in phase diagram (see Figure 6.2). We conclude that the DDFT method, based on a fully flexible representation of molecules, is not suited to address the properties of PEBAX®2533, as expected.

We conclude that it's necessary to introduce a certain degree of stiffness, owing to the presence of PA-12, into the method, which is most easily done in DPD.

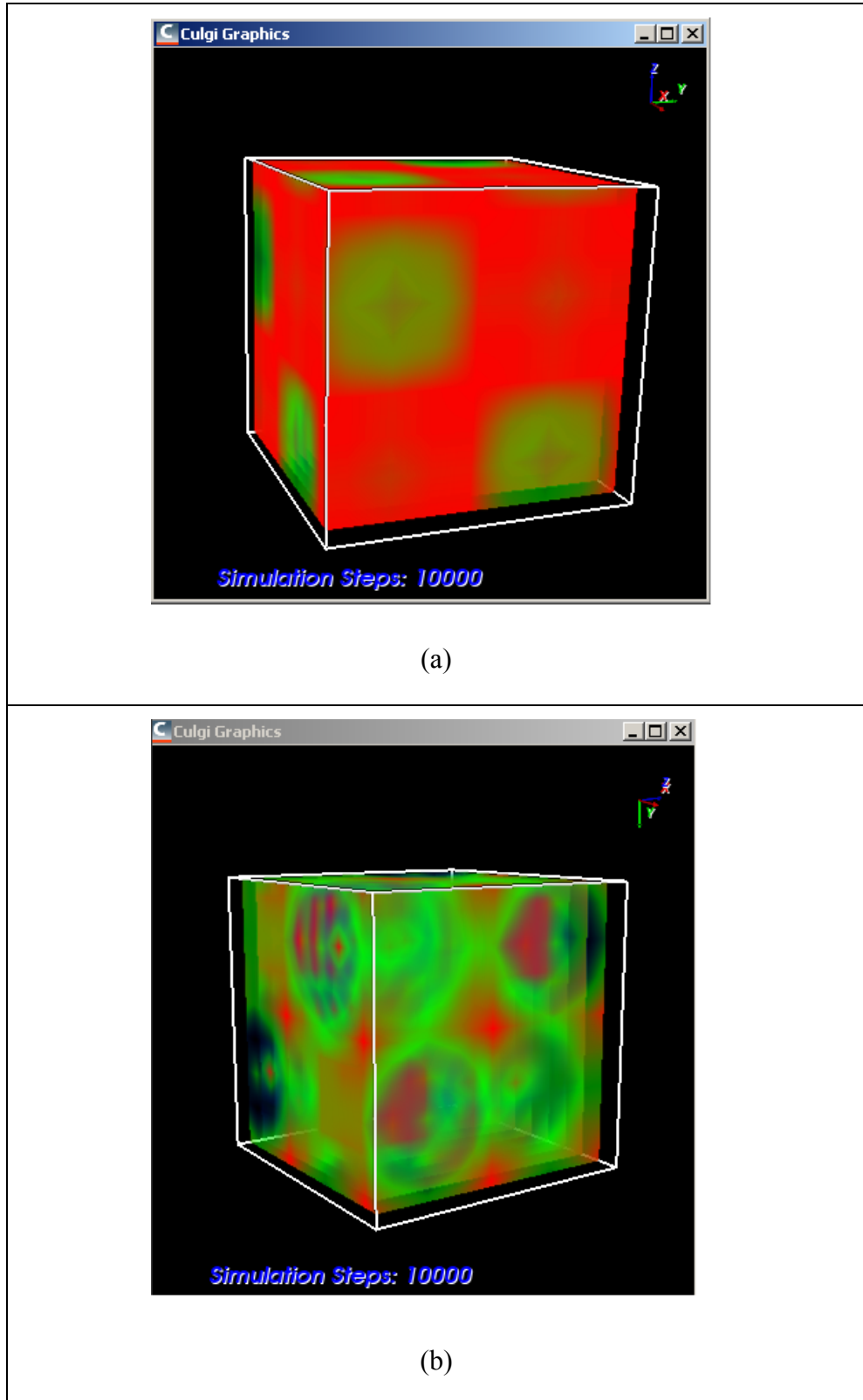


Figure 6. 4-Last frame of PEBAX®2533 DDFt simulations: (a) Density field of B domain coloured in red; (b) Relative density field: B domain coloured in green, A domain coloured in red.

From experimental data it's known that the most stable crystalline phase of PA-12 is  $\alpha$  phase [6.38] consisting of planar sheets of hydrogen-bonded chains with sheets stacked upon one another and displaced along the chain direction by a fixed amount.

Consequently we carried out DPD simulations of PA12 and PEBAX®2533: the incorporation of a certain degree of crystallinity is unprecedented in this respect. PA-12 has been modelled as a collection of rigid rods of compositions  $A_3B \{R\}D$ , where A represents the aliphatic chain bead, B the polar amidic group bead;  $\{R\}D$  are perpendicular to the segment bond and do not represent physical entities but play the role of acceptor and the donor groups. They are introduced in order to define the interchain interactions between different PA-12 chains.

A number of 20 chains with three repetitive units  $A_3B \{R\}D$  is inserted in the simulated volume and stiffness is introduced by making use of angle potential of Eq. 6.8, setting  $k_2 = 130$  and  $\theta = 0$ .

The interaction parameter  $a_{ij}$  (see Eq 6.3) is a measure of the repulsion between every pair of bead; this captures the chemical nature of the molecules, or segments of molecules, that each bead represents. The  $a_{ij}$  parameters as they are used in Culgi (and as reported in most DPD papers) are the dimensionless  $a_{ij}^* = (a_{ij} / k_B T) \cdot h$  [6.39]

The interaction parameters  $a_{ij}^*$  between AA and AB type beads are set to high values, and to low values for  $\{R\}D$  groups (respectly 130 and 2) in order to ensure repulsion between beads of the same type and of the same chain and strong interactions between different chains. Temperature has been set to low value for “freezing” the system and to decrease the entropy.

DPD simulations have been conducted for 10000 iterative steps and the final frame is reported in Figure 6.5:

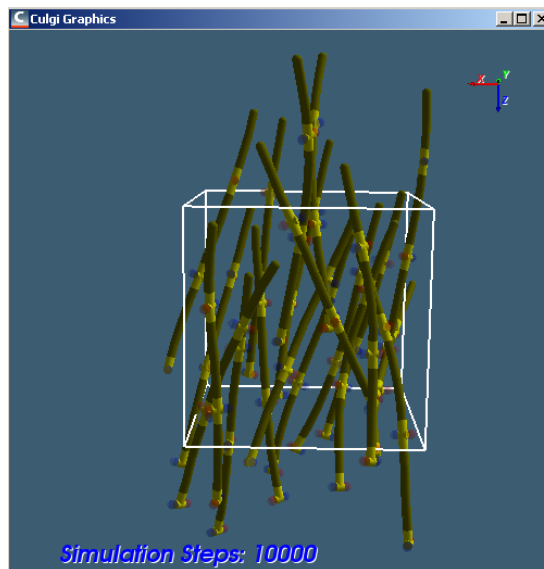


**Figure 6. 5- Last frame of PA-12 DPD simulation: a PA-12 chain is modelled as  $A_3B \{R\}D$ , with A coloured in grey, B in yellow,  $\{R\}$  in red,  $\{D\}$  in blue.**

From a quick visual analysis of Figure 6.5 PA-12 chains are evidently “rigid” rods in an almost parallel reciprocal orientations. We note that the simulation is small and in absence of the flexible ‘spacer’.



To estimate the degree of alignment of PA12-beads with respect to the main direction more quantitative and for a comparison to experimental data, we are currently developing an algorithm to measure the order parameter  $S$  for correlating it to the degree of crystallinity.

DPD simulations of PEBAX®2533 are also in progress (see Figure 6.6); the composition of repeating unit is set to be  $[A_3B \{R\}D]_3 C_{28}$ , having taken into account the number of repeat units of PTMO (C) and PA-12 ( $A_3B \{R\}D$ ) in PEBAX®2533.

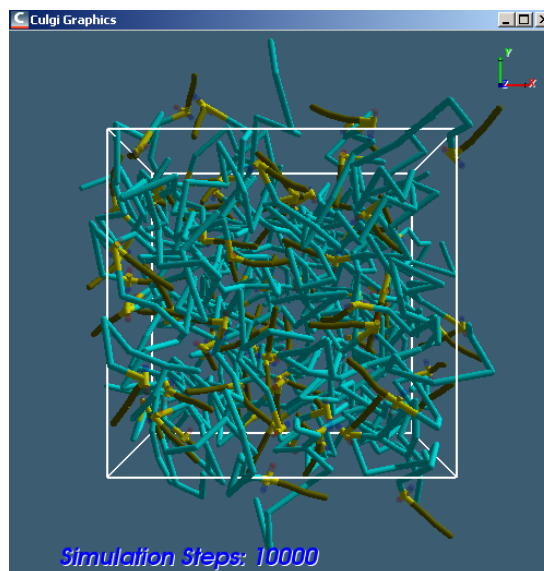


**Figure 6. 6-** Last frame of PEBAX®2533 DPD simulation; a single chain of PEBAX®2533 is modelled as  $[A_3B \{R\}D]_3 C_{28}$ ; PA-12 domain is modelled as  $A_3B \{R\}D$  with A coloured in grey, B in yellow,  $\{R\}$  in red,  $\{D\}$  in blue; PTMO domain is modelled as one bead of type C coloured in light blue.

## 5. Conclusions

The collaboration and on-site training at the Soft Matter Chemistry Group of Leiden Institute of chemistry, Leiden University, The Netherland, aimed at complimenting experimental-theoretical studies with mesoscopic techniques, has led to an initial investigation of the PEBAX®2533 morphology, thus widening the length and temporal range of simulation effort with respect to the fully atomistic investigation by MD methodology described in the previous chapters.

DDFT and DPD simulations will be carried on, based on the crystallinity incorporated in PA-12 coarse grained model, in order to provide a better insight in the microphase separations between hard PA-12 and soft PTMO domains.

The Flory Huggins parameters calculations and parameterization procedure, to introduce different weight percentages of toluensulphonamides (KET) in the system, are in progress in order to study the effect of modification in PEBAX®2533 phase behaviour and permeability properties.



## REFERENCES

- [6.1] J.P. Sheth, J. Xu and G.L. Wilkes, *Polymer*, 44 (2003) 743.
- [6.2] M. Xie and Y. Chamberlain, *Makromol Chem.*, 187 (1986) 383.
- [6.3] N. Alberola, *J. App. Polym. Sci.*, 36 (1988) 787.
- [6.4] G.R. Hatfield, Y. Guo, W.E. Killinger, A. Andrejak and P.M. Roubicek, *Macromolecules*, 26 (1993) 6350.
- [6.5] Y.C. Yu and W.H. Jo, *J. Appl. Polym. Sci.*, 56 (1995) 895.
- [6.6] Y.C. Yu, W.H. Jo and M.S. Lee, *J. Appl. Polym. Sci.*, 64 (1997) 2155.
- [6.7] R.S. McLean and B.B. Sauer *J. Polym. Sci.*, 37 (1999) 85.
- [6.8] B.B. Sauer, R.S. McLean, D.J. Brill and D.J. Londono, *J. Polym. Sci. Part B: Polym. Phys.*, 40 (2002) 1727.
- [6.9] V. Barbi, S.S. Funari, R. Gehrke, N. Scharnagl and N. Stribeck, *Macromolecules*, 36 (2003) 749.
- [6.10] V. I. Bondar, B. D. Freeman and I. Pinnau, *J Polym. Sci. Part B: Polym. Phys.*, 37 (1999) 2463.
- [6.11] V. I. Bondar, B. D. Freeman and I. Pinnau, *J Polym. Sci. Part B: Polym. Phys.*, 38 (2000) 2051.
- [6.12] M.E. Rezac and T. John, *Polymer*, 39 (1998) 599.
- [6.13] J.C. Chen, X. Feng and A. Penlidis, *Sep. Sci. and Tech.*, 39 (2004) 149.
- [6.14] A. Gugliuzza and E. Drioli, *Polymer*, 46 (2005) 9994.
- [6.15] M.E. Rezac, T. John and P.H. Pfromm, *J. App. Polym. Sci.*, 65 (1997) 1983.
- [6.16] R.D. Groot, P.B. Warren, *J. Chem. Phys.* 107 (1997) 4423 .
- [6.17] P. Español, P. Warren, *Phys. Rev. E* 52 (1995) 1734.
- [6.18] B.H. Zimm, *J. Chem. Phys.* 24 (1956) 269.
- [6.19] P.E. Rouse, *J. Chem. Phys.* 21 (1953) 1272
- [6.20] A.G. Schlijper, C.W. Manke, W.G. Madden, Y. Kong, *Int. J. Mod. Phys. C.*, 8 (1997) 919.
- [6.21] K. S. Lyakhova, G. J. A. Sevink, A. V. Zvelindovsky, A. Horvat and R. Magerle, *J. Chem. Phys.*, 120 (2004) 1127.
- [6.22] A.V. Zvelindovsky, Editor, *Nanostructured soft matter*, Springer, Dordrecht (2007)
- [6.23] G.J. Fleer, M.A. Cohen Stuart, J.M.H.M. Scheutjens, T. Cosgrove and B. Vincent *Polymers at interfaces* : Chapman & Hall, London, 1993.
- [6.24] G. J. A. Sevink, J. G. E. M. Fraaije, and H. P. Huinink, *Macromolecules*, 35 (2002) 1848.

- [6.25] J. G. E. M. Fraaije, B. A. C. van Vlimmeren, N. M. Maurits, M. Postma, O. A. Evers, C. Hoffmann, P. Altevogt, and G. Goldbeck-Wood, *J. Chem. Phys.*, 106 (1997) 4260.
- [6.26] N. M. Maurits, B. A. C. van Vlimmeren, and J. G. E. M. Fraaije, *Phys. Rev. E.*, 56 (1997) 816
- [6.27] B. A. C. van Vlimmeren, N. M. Maurits, A. V. Zvelindovsky, G. J. A. Sevink, and J. G. E. M. Fraaije, *Macromolecules*, 32 (1999) 646.
- [6.28] N. M. Maurits and J. G. E. M. Fraaije, *J. Chem. Phys.*, 15 (1997) 5879.
- [6.29] G. J. A. Sevink, A. V. Zvelindovsky, B. A. C. van Vlimmeren, N. M. Maurits, and J. G. E. M. Fraaije, *J. Chem. Phys.*, 110 (1999) 2250.
- [6.30] K. S. Lyakhova, A. V. Zvelindovsky, and G. J. A. Sevink, *Macromolecules*, 39 (2006) 3024.
- [6.31] G. J. A. Sevink and A. V. Zvelindovsky, *Macromolecules*, 42 (2009) 8500.
- [6.32] P. J Flory *Principles of Polymer Chemistry*, Cornell University Press: Ithaca (1953).
- [6.33] F. Müller-Plathe, *ChemPhysChem.*, 3 (2002) 754.
- [6.34] V.V. Ginzburg, J. Bicerano, C. P. Christenson, A. K. Schrock, A. Z. Patashinski *J. Polym. Sci.: Part B: Polym. Phys.*, 45 (2007) 2123.
- [6.35] J. Bicerano, *Prediction of Polymer Properties*, 3<sup>rd</sup> ed.; Marcel Dekker: New York, 2002.
- [6.36] S. Pauly, *Polymer Handbook*, 3rd ed., J. Brandrup, E. Eds. Immergut , Wiley, New York, 1989, VI/435-VI/449.
- [6.37] S. Dasgupta, W. B. Hammond, W. A. Goddard , *J. Am. Chem. Soc.*, 118 (1996) 12291.
- [6.38] M. I. Kohan, *Nylon Plastics*, Wiley-Interscience, John Wiley andSons: New York, 1973.
- [6.39] Culgi Version 4.0.0 Scientific Manual: Copyright 2004-2009 Culgi B.V The Netherlands.



## VII. ANALYSIS OF THE FREE VOLUME DISTRIBUTION IN AMORPHOUS GLASSY PERFLUOROPOLYMERS

### 1. Materials: Perfluoropolymers

#### 1.1. General Characteristics

The discovery of polytetrafluoroethylene (PTFE, Table 7.1) in 1938 by Roy Plunkett [7.1] at DuPont spurred the development of a wide variety of rubbery and glassy perfluoropolymers (PFPs) such as Teflon® AF by DuPont [7.2, 7.3], Cytop™ by Asahi Glass [7.4]. The chemical structures and selected properties of these polymers are shown in Table 7.1. For comparison, semicrystalline polytetrafluoroethylene is included in this table as well.

Glassy polymers, based on copolymers of tetrafluoroethylene and 2,2-bis(trifluoromethyl)-4,5-difluoro-1,3-dioxole, can be readily dissolved in and cast from perfluorinated solvents. The large, bulky dioxole monomer hinders efficient polymer chain packing, thereby preventing crystal formation and yielding a completely amorphous polymer. Monomers used for the synthesis of fluorinated polymers can be briefly classified into two categories,

- 1) base monomers;
- 2) special monomers.

The former are represented by those monomers that constitute the basic structure of modern fluoropolymers and the latter by those other monomers that add specially desired characteristics to match specialty application requirements.

Fluoropolymer materials are capturing greater and greater interest in industrial applications because of the remarkable combination of properties that they exhibit when compared to other polymeric materials [7.5-7.11]. The most well-known property for which fluoropolymers are employed in high-demanding applications is their outstanding thermal and chemical resistance. However, the peculiar nature of the carbon-fluorine bond confers on these materials other unique physical properties (e.g., electrical, optical, and superficial) that can be valuably exploited in the most variegated fields. Perfluoropolymers represent the ultimate in resistance to hostile chemical environments and high service temperature because of the high bond energy of C-F and C-C bonds of fluorocarbons, equal to 485 kJ/mol and 360kJ/mol, respectively [7.12].

Fluoropolymers also possess exceptional optical, electrical and surface properties [7.12, 7.13] that have resulted in the commercial use of fluoropolymers in numerous areas, including the automotive, electronic, aerospace, chemical, specialty packaging and medical industries [7.12-7.14].

Polymer	Chemical structure	Density (g/cm <sup>3</sup> )	T <sub>g</sub> [9] (°C)	N <sub>2</sub> Permeability (barrer)
PTFE		2.1	30	1.3 [7.10]
Teflon® AF		1.74	240	480 [7.11]
Cytop®		2.03	108	5.0 [7.11]
Hyflon® AD		1.92	130	24 <sup>l</sup> [7.12]

Table 7. 1- Chemical structures and selected properties of perfluoropolymers

The discovery in the past 20 years of amorphous, solvent-processable perfluoropolymers, such as Teflon®AF, Cytop®TM and Hyflon®AD [7.11], has created new opportunities for perfluorinated materials in membrane separations [7.12-7.23]. Indeed, the high gas permeability of these polymers [7.2, 7.3, 7.23], due to the great amount of free volume, combined with the usual perfluoropolymer chemical and thermal stability, makes them intriguing membrane materials for gas and vapor separations.

Amorphous perfluoropolymers show glass transition temperatures (T<sub>g</sub>) greater than room temperature [7.17], a thermal decomposition temperature exceeding 400°C and are highly transparent to light from far UV to near infrared. TFE–TTD copolymers, commercially known as Hyflon®AD polymers, are synthesized by free radical polymerization. Amorphous polymers of Hyflon®AD are obtained when m/n is less than about 4; that is, when the TTD molar content is higher than about 20%.

Due to the cyclic structure and the effective steric hindrance of the side group, chain motion is severely hindered and high  $T_g$  glassy polymers result. When  $m = 0$ , as is the case with TTD homopolymer,  $T_g = 170^\circ\text{C}$ . At increasing  $m/n$  values (decreasing TTD content),  $T_g$  decreases.

Another important characteristic of the perfluoropolymers in gas separation is their substantial change in the solubility selectivity, therefore they represent materials suited for challenging separations (e.g., olefin/paraffin or natural gas treatment). Hyflon AD60X is a compromise of a moderately high selectivity and a still interesting permeability, in comparison with the more permeable but less selective TeflonAF. It is particularly suitable for use in dense gas separation membranes, especially in the presence of organic vapours.

Experimental gas separation data obtained with membranes prepared with TTD-TFE (Hyflon AD) copolymers and data from the literature on Teflon AF membranes revealed an interesting linear relationship between permeation and  $T_g$  [7.20]. Perfluoropolymers present an unusually low hydrocarbon-vapour sorption, and a high resistance toward swelling and plasticization [7.18]. In the case of Hyflon AD [7.21] very high  $\text{CO}_2$  permeability (260-280 barrer) are reported and  $\text{CO}_2/\text{CH}_4$  selectivity around 9-11 in the case of streams containing 20% of  $\text{CO}_2$  and up to 5.5 MPa. Membranes prepared using Cytop and Hyflon AD present selectivity factors  $\text{CO}_2/\text{CH}_4$  of ca. 10-15 also in presence of important amounts of  $\text{C}^{3+}$  hydrocarbons and/or  $\text{CO}_2$ , and also at high feed pressure values [7.18].

## 2. Introduction

### 2.1. Free volume in polymers

The search for novel polymeric materials with desired combinations of gas permeability and permselectivity to separate gas mixtures is an important challenge in membrane science. Glassy polymers are often the most useful materials for gas separation membranes because of their superior permeability/selectivity balance. Polymeric glasses are in a non-equilibrium state [7.1] with a continuous evolution towards equilibrium through spontaneous, but usually very slow, molecular rearrangements at temperatures far below the glass transition temperature,  $T_g$ . Since macroscopic properties of glassy polymers depend on their inefficiency of packing or free volume [7.2, 7.3], a rational determination of the relationship between chemical structure and transport parameters, such as permeability and diffusion coefficients, becomes important.

The concept that free volume in polymer glasses is composed of local free volume elements of different sizes has a broad theoretical support [7.1-7.4]. Only recently more experimental data on the distribution of local free volume are gradually becoming available. Various studies have demonstrated a direct correlation between free volume and gas transport in polymeric membranes [7.5, 7.6]. Variations of free volume due to physical aging [7.3] may lead to dramatic changes in the gas permeability, for instance for poly[1-(trimethylsilyl)-1-propyne] (PTMSP), for which the permeability decreases more than two orders of magnitude in only 100 days [7.7]. This behaviour depends strongly on the nature of the polymer, because another high free volume polymer, Teflon AF, is reported to be highly stable towards physical aging [7.8].

Free volume in polymers can be determined by numerous methods [7.9, 7.10], such as positron annihilation lifetime spectroscopy (PALS) [7.11, 7.12], inverse gas chromatography (IGC) [7.13],  $^{129}\text{Xe}$ -NMR spectroscopy [7.14] and by electrochromic [7.15], spin probe [7.15] or photochromic probe methods [7.16].

Data on high free volume perfluorinated polymers are rather rare [7.17, 7.18, 7.19]. For Hyflon AD polymers only the total void fraction, estimated by the group contribution method [7.20] and the average void size determined by  $^{129}\text{Xe}$ -NMR spectroscopy [7.14] have been published in the literature. The calculated fractional free volume of Hyflon AD60X and Hyflon AD80X see of about 23% poses these polymers near other high FFV polymers such as Teflon<sup>®</sup> AF 2400 and Teflon<sup>®</sup> AF1600 [7.21], and clarifies the reason for the high permeability of these polymers, significantly above those of most conventional glassy polymers [7.22, 7.23] like for instance polysulfone and other polymers commonly used in commercial gas separation membranes, with FFVs ranging from around 12 to 17 %.

## 2.2. Photochromic probing

Photochromism of molecular probes is a phenomenon which is sensitive to the distribution of local free volume in polymer glasses [7.16]. Photochromic molecular probes in glassy polymers were first used by Gardlund [7.24] Since then they have been successfully used in evaluating the free volume distribution of various matrices, including polycarbonate [7.25, 7.26] polystyrene [7.16, 7.27], poly(vinyl acetate) [7.26], poly(methyl methacrylate) [7.28], epoxy resin [7.29, 7.30] and other polymers [7.31] (see Table 7.2).

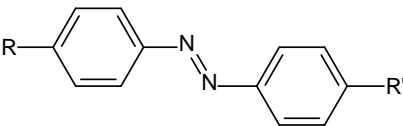
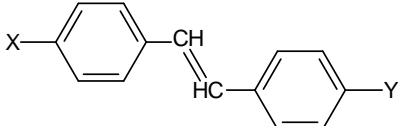
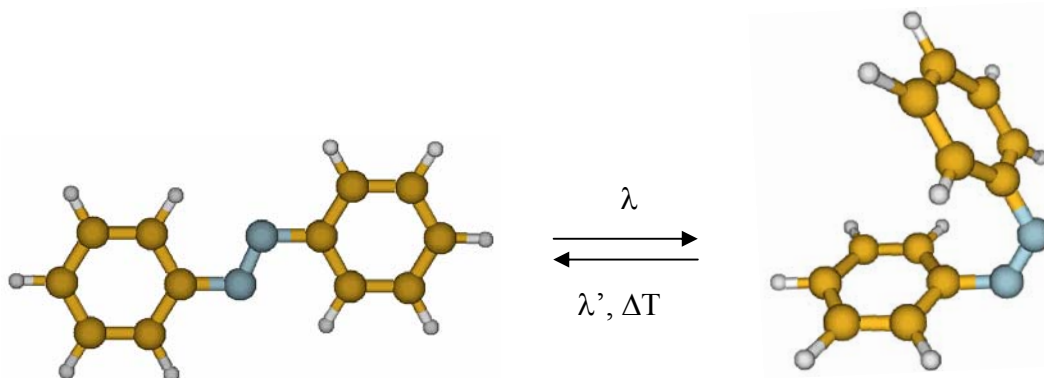
	Azobenzene derivatives		Stilbene derivatives	
Probe molecules				
	R	R'	X	Y
Azobenzene	H	H	-	-
Disperse orange 3	NO <sub>2</sub>	NH <sub>2</sub>	-	-
Disperse red 1	NO <sub>2</sub>	N(CH <sub>2</sub> CH <sub>3</sub> )CH <sub>2</sub> CH <sub>2</sub> OH	-	-
Disperse orange 25	NO <sub>2</sub>	N(C <sub>2</sub> H <sub>5</sub> )CH <sub>2</sub> CH <sub>2</sub> CN	-	-
Stilbene	-	-	H	H
4,4'-dinitrostilbene	-	-	NO <sub>2</sub>	NO <sub>2</sub>

Table 7. 2 - Structure of the azobenzene and stilbene derivatives used as molecular probes in the present Chapter.

For this purpose, photochromic or photo-isomerizable molecules, usually stilbenes and azobenzenes, are dispersed homogeneously within the polymer matrix. Upon irradiation with UV or visible light with the proper wavelength and/or upon heating, the photochromic molecules may undergo trans-cis isomerization and the reverse reaction (Fig 7.1).



**Figure 7.1 - Photochemical isomerization of trans-azobenzene. The reverse reaction can be induced thermally or by irradiation with light of a distinct wavelength.**

In the case of azobenzenes this isomerization involves a rotation around the double bond and the swapping of one of the phenyl groups from one side to the other. In solution the extent of the reaction from the more stable trans-isomer to the cis-isomer depends on the probe structure and on the experimental conditions, such as wavelength, light intensity, irradiation time and on the solvent polarity, but much less on its viscosity [7.32]. Probe isomerization is dramatically slowed down in a glassy polymer matrix and, depending on the specific probe size and volume, also the extent of isomerization is usually lower. Nevertheless, even in glassy polymers the isomerization can be accelerated by creation of a local rubbery environment [7.33]. This principle can be used for sensing glass transitions in polymeric materials [7.34, 7.35].

The difference between the rate and especially the extent of probe isomerization in solution and in a glassy polymer matrix forms actually the basic principle of the photochromic probe method for free volume analysis, originally developed by Victor and Torkelson [7.16] and used in the present paper.

The crucial hypothesis, at the basis of the photochromic probe technique, is that photoisomerization in the glassy state requires a minimum critical size of local free volume in the vicinity of the chromophore. The isomerization requires a certain amount of extra volume during the rotation of the molecule from the trans- to the cis-configuration [7.16] not only because the molecular volume of the cis and the trans isomers may be different, but also because the rotation itself requires some freedom of motion. This is schematically displayed in Fig 7.2:



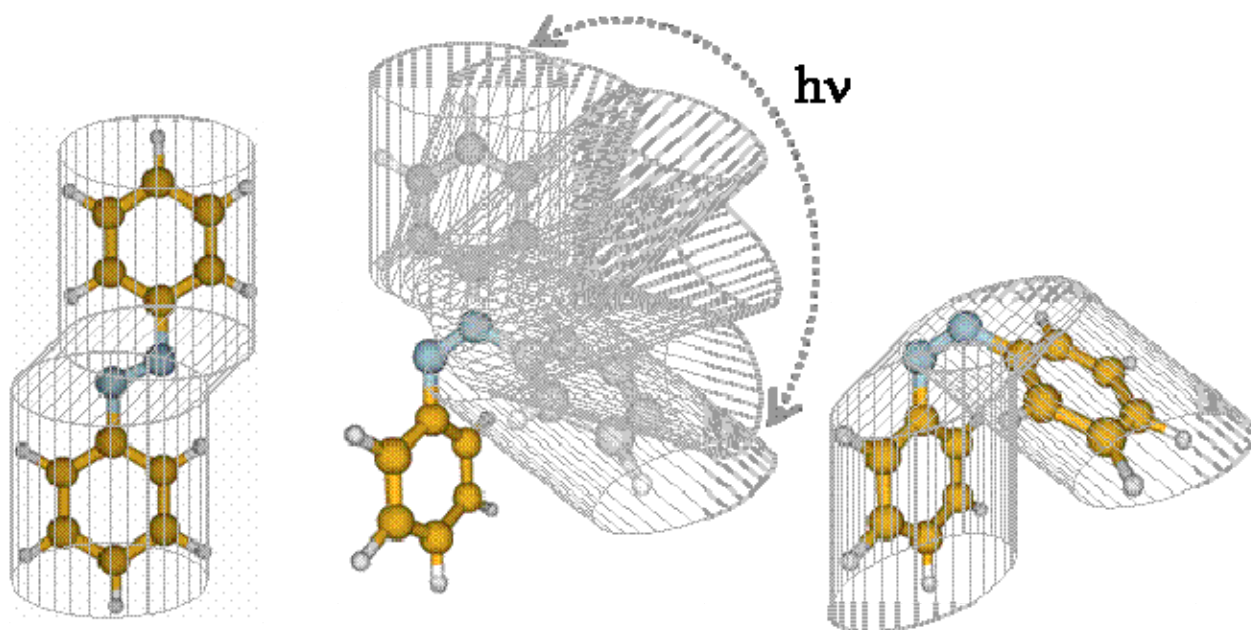


**Figure 7.2-** Schematic representation of the volume occupied by an azobenzene probe molecule in the trans-form (left) and in the cis-form (right), and of the extra volume required for the photo-induced cis-trans isomerization reaction (center).

If this volume is available, i.e. if the photochromic molecule is located in a sufficiently large free volume element, then photoisomerization will occur, otherwise it will not. This procedure thus allows the qualitative determination of the free volume distribution if a series of photochromic molecules is used which require each a different volume for the trans-cis isomerization reaction. An important and generally accepted assumption is that the dye molecule does not influence the free volume itself and that it does not interact with the polymer matrix. Furthermore, the polymer chain dynamics must be sufficiently slow that there is no significant relaxation of the free volume elements on the time scale required to realize the trans-cis transition. In practice the amount of probe photoisomerization in a glassy polymer relative to that in dilute solution in a non-viscous model solvent, where free volume is not a constraint to isomerization, is measured as a function of the volume required for photoisomerization of the probe.

The advantage of the photochromic probe method for free volume determination is the relative simplicity of the experimental procedures and of the equipment required, in contrast to for instance PALS and NMR analysis. However, a critical factor is the knowledge of the volume required for the isomerization reaction. This is usually not known but it can be estimated on the basis of the Van der Waals volume of the probe molecule and on geometric considerations to calculate the volume swept during the isomerization reaction [7.16]. Furthermore, the method is based on several important assumptions, for instance that the probe molecules are homogeneously distributed in the polymer matrix, that no clustering occurs and, most important, that they do not influence the polymer matrix or *vice versa*.

Since it is difficult to check the validity of some of the above assumptions and the fulfilment of these conditions, a comparison with the results of other probe methods is highly

desirable. In the present work the PCP method is compared with results of PALS analysis, MD simulations and with literature data from  $^{129}\text{Xe}$ -NMR spectroscopy.

### 2.3. Positron annihilation lifetime spectroscopy

Among the probe methods to study free volume in polymers, positron annihilation lifetime spectroscopy (PALS) has found the widest application and is considered as the most developed and reliable technique [7.9, 7.10, 7.36]. This method is based on the measurement of the lifetimes of positrons before annihilation in polymers. The most commonly used source that emits positrons is the radioactive  $^{22}\text{Na}$  isotope. The emitted positrons, when getting into condensed matter (polymer) can exist in the form of free positrons ( $e^+$ ) and hydrogen-like Positronium atoms (Ps), combinations of positron and electron, until their annihilation. Depending of the spin of this species, they can form p-Ps (antiparallel spins of  $e^+$  and  $e$ ) and o-Ps (parallel spins). Intramolecular annihilation of p-Ps and annihilation of free positrons proceed with high rate and we shall not discuss them in this paper, since we use the PALS method. Annihilation in the form of o-Ps is characterized by much longer lifetimes. In vacuum the intrinsic lifetime of this bound state is 142 ns. However, in condensed matter the lifetimes are shortened, usually by two orders of magnitude, due to coupling of wave functions of o-Ps and electrons of the atoms of the material that surround o-Ps. In conventional glassy polymers they are in the range of 1.5-3.0 ns [7.37, 7.38, 7.39]. The paradigma of the PALS method is that o-Ps in polymers will move into the regions with reduced density, the free volume elements (FVE), where they will then survive until their annihilation. The principle of the PALS method for free volume evaluation is that the annihilation is slower, the larger the size of the FVE is. The mathematical expression of this statement is the semi-empirical equation, originally proposed by Tao [7.40] for a spherical potential well (spherical pore) and later used by several other authors [7.41, 7.42]:

$$\tau_3 = \frac{1}{2} \left[ 1 - \left( \frac{R_i}{R_0} \right) + \frac{1}{2\pi} \sin \left( \frac{2\pi R_i}{R_0} \right) \right]^{-1} \quad (7.1)$$

where  $\tau_3$  is o-Ps lifetime,  $R_i$  is the corresponding radius of a spherical FVE, and  $R_0 = R + \Delta R$  (where the adjustable parameter  $\Delta R$  is usually fixed at 1.66 Å [7.42]).

The shape of the pore can be also approximated by a channel (cuboid or cylinder, which give results very close to each other for the same width and length [7.39, 7.43], or by a slit. For the cuboid case, the dependence of  $\tau_3$  on the cuboid parameters (sides)  $\alpha_1, \alpha_2, \alpha_3$  is given by [7.43]:

$$\tau_3 \cong 0.5 \left[ 1 - \prod_{i=1}^3 \left( \frac{\alpha_i}{\alpha_i + 2\Delta R} + \frac{1}{\pi} \sin \frac{\pi \alpha_i}{\alpha_i + 2\Delta R} \right) \right]^{-1}, \quad (7.2)$$

where  $\Delta R$  has the same meaning as in Eq. (7.1).

For the same lifetime  $\tau_3$ , channel or slit geometry give smaller pore width. The effect saturates with pore or slit length [7.39].

It is known that dissolved oxygen in polymers can quench o-Ps in the pores or FVEs of a polymer, thus reducing their lifetimes [7.44, 7.45]. This effect is important only for high free volume polymers and virtually disappears for the polymers having smaller sizes of free volume elements [7.46]. Since the Hyflons used in the present work exhibit relatively high gas permeability, the measurements were carried out in the atmosphere of nitrogen.

#### **2.4. Inverse gas chromatography**

Inverse gas chromatography (IGC) is a dynamic method for investigation of the thermodynamic properties of polymers [7.47]. Traditionally, it has been applied for the investigation of polymers above their glass transition temperature. However, studies of polymers with large free volume and high gas permeability showed that it is applicable also for glassy polymers [7.6, 7.7, 7.10]. In such polymers diffusion limitations do not prevent establishing sorption equilibrium, so such characteristics as activity coefficients and the parameters of their temperature dependence  $\overline{H}_1^{E,\infty}$  and  $\overline{S}_1^{E,\infty}$  can be found. It was shown that for series of solutes with widely varying sizes the dependence of  $\overline{H}_1^{E,\infty}$  passes through a minimum when the molecular mass of solutes or their size changes significantly. It was first assumed [7.6] and later confirmed using different polymers as examples [7.10] that the coordinates of these minima can be interpreted as an average size of free volume in the polymers. In these studies, the n-alkane series C<sub>3</sub>-C<sub>13</sub> was used as molecular probes. Critical volume V<sub>c</sub> or molecular volume at boiling point V<sub>b</sub> can be used as a measure of the size of the probe and, hence, of the free volume element (FVE) size. The coordinates of these minima (V<sub>c(min)</sub>) correlate with the gas permeability of different polymers studied using IGC, while the obtained FVE sizes are in a reasonable agreement with the results of other probe methods (see e.g. Ref. 7.11). All this served us an incentive to use also this method for the investigation of the free volume in Hyflon AD samples.

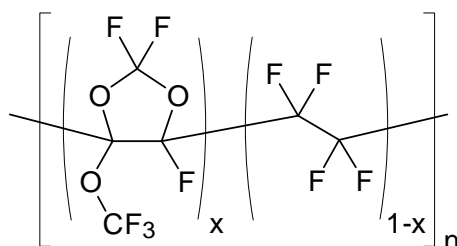
#### **2.5. Molecular dynamics simulations**

With the development of extremely powerful computer hardware and software in the last few decades, computational methods have become an important source of information on the chemical-physical properties of polymers, allowing for instance the analysis of their free volume and transport properties [7.48]. In spite of the advances already made, the development of ever better force fields, calculation algorithms and computer hardware remains a continuous challenge. Nowadays several well established simulation methods exist for the preparation of atomistic packing models, also for high free volume polymers, like PTMSP and Teflon AF, or for polymers containing strongly polar moieties, such as polyimides. Such simulated models allow an accurate determination of geometrical quantities, characterizing the three dimensional structure and chain packing, and represent therefore a valid additional approach to study free volume properties of polymer materials [7.49, 7.50, 7.51].

#### **2.6. Scope**

The aim of the present work is to make a comparison between the most commonly used experimental probing techniques (PALS, IGC, 129Xe-NMR) and photochromic probing for the evaluation of the local free volume and the free volume element size and shape

distribution in Hyflon AD glassy perfluoropolymers. Hyflon AD polymers are amorphous perfluorinated copolymers of tetrafluoroethylene (TFE) and 2,2,4-trifluoro-5-trifluoromethoxy-1,3-dioxole (TTD) (Scheme 7.1). These polymers have a high thermal, chemical, ageing, weathering and solvent resistance which is characteristic for perfluoropolymers (PFPs), like for instance polytetrafluoroethylene (PTFE). In contrast to the semi-crystalline PTFE, Hyflon AD polymers are amorphous glasses with a modestly high  $T_g$ , as a result of the bulky TTD units in the polymer chain. Amorphous glassy PFPs of the Hyflon AD and the Teflon AF family, are known for their relatively high FFV [7.17] or void fraction, which is the reason for their high gas permeability [7.18, 7.20]. In the present work two different grades of Hyflon AD with different copolymer compositions are used.



Scheme 7.1 - Chemical structure of Hyflon® AD60X ( $x=0.6$ ) and Hyflon® AD80X ( $x=0.8$ )

### 3. Results and discussions

#### 3.1. Generation and equilibration of polymer structures

The molecular simulations were performed using the Materials Studio (4.0) software of Accelrys, Inc. (San Diego, CA). Amorphous polymer packings were constructed using the Theodorou/Suter method [7.61] as implemented in the Amorphous-Cell module [7.62]. The MD simulations were performed with the Discover software using the COMPASS force field [7.63]. The Materials Studio (4.0) software was run on a supercomputer (CINECA cluster, Bologna, Italy) and on PC-Hardware.

Both for Hyflon AD60X and for AD80X, three independent atomistic bulk model were prepared. The applied basic techniques of packing and equilibration have been described in detail elsewhere [7.52, 7.64, 7.65]. The procedure is summarized in Fig 7.3. A brief outline of the procedure is given below, where the numbers refer to the different steps in Fig 7.3

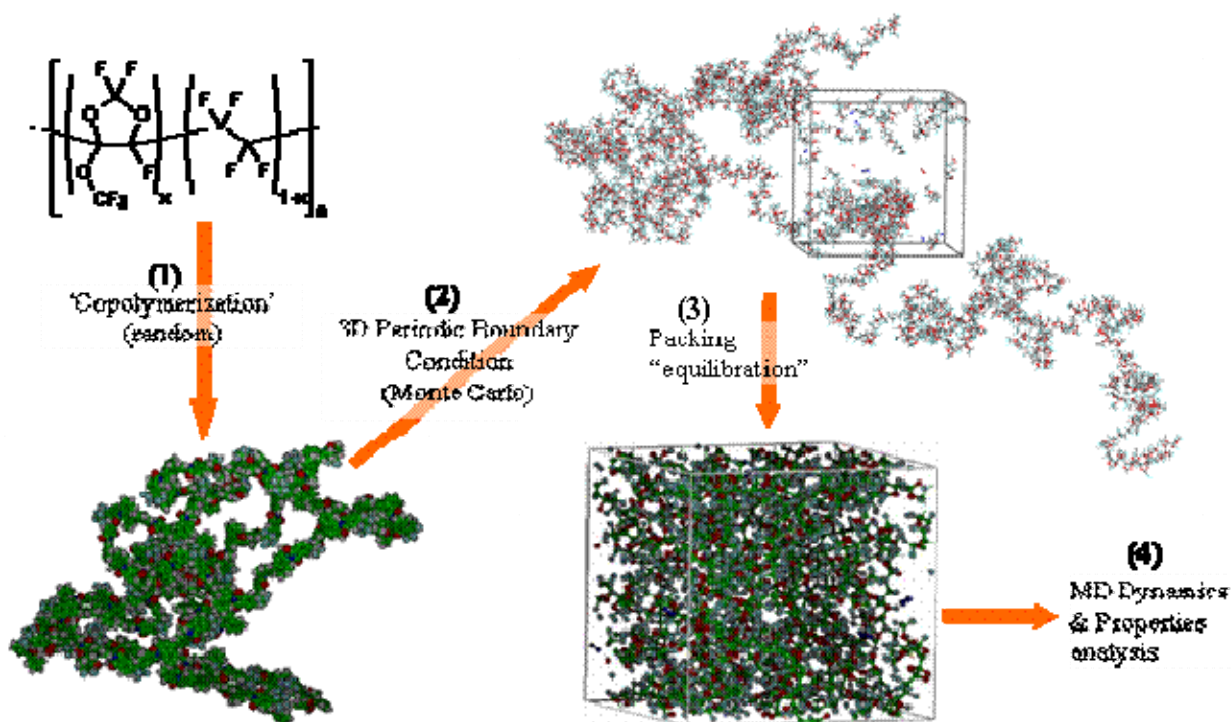


Figure 7.3 - Construction procedure of atomistic packing models for Hyflon AD80X.

(1) After preparing atomistic repeating units of TTD and TFE (see scheme 1), a single copolymer chain with the appropriate molar ratio of TTD and TFE and with 770 repeat units (7856 atoms) for AD60X, and 700 repeat units (8122 atoms) for AD80 was constructed, using conditional statistics. Since the experimental reactivity ratios for TTD and TFE were not available, a series of linear random chains was built by a trial and error procedure until the obtained composition ( $60 \pm 1$  mol.% of TTD and  $80 \pm 2$  mol.% of TTD) was sufficiently close to the specified experimental compositions of Hyflon AD60X and Hyflon AD80X, respectively. For the present work those chains with exactly 60.0% mol of TTD (i.e. with 462 TTD units and 308 TFE units) for AD60X and with 80.0% mol of TTD (i.e. with 560 TTD units and 140 TFE units) for AD80X were selected for the model construction.

(2) For the initial packing of each Hyflon model, a polymer chain was grown under periodic boundary conditions at 308 K and at a density of about 15% of the experimental value in a simulation box. 600 Argon molecules were used as random obstacles to avoid ring catenations of the growing chain. Since solvent-cast films contain significant amounts of residual solvent [7.66] unless they are dried at temperatures above the  $T_g$ , a representative number of 41 solvent molecules were added in the Hyflon AD60X packing model and 26 molecules in Hyflon AD80X. In this way the model should correspond better to the experimental films, which were dried at only 50°C to avoid degradation or thermal isomerization of the probe molecules.



Three independent initial configurations were generated for each polymer. The chain was grown following the Theodorou/Suter method [7.61], based on the Rotational Isomeric State (RIS) model of the Amorphous Cell Program of Material Studio [7.67]. One single long chain was utilized to reduce the influence of chain ends on the simulations. This procedure to represent bulk amorphous systems is common and has been proven to be quite accurate in replicating the behaviour of experimental polymeric systems [7.68, 7.69].

(3) The argon spacers were subsequently removed during the equilibration of the polymer models. The models were subjected to repeated sequences of energy minimization and dynamics runs at constant number of particles, temperature and volume (NVT-MD), combined with force field parameter scaling. Subsequently, compression (runs at constant number of particles, temperature and pressure – NpT-MD) and simulated annealing runs (NVT-MD dynamics at different temperature ) of the initial packing were carried out through a set of successive MD simulations. This procedure yielded well-equilibrated packing models with stable density fluctuations at a density close enough to the given experimental value under the experimental pressure (1 bar). The following simulation conditions were used: periodic boundary condition to make the system numerically tractable and to avoid symmetry effects; a cutoff distance of 22 Å for interaction energy functions with a switching function in the interval 20.5–22 Å. The Andersen thermostat [7.70] was used for temperature control and the Berendsen method [7.71] was applied to control the pressure of the system during NpT-MD simulations.

(4) NpT-MD simulations were performed at  $T=298$  K and  $p=1$  bar for about 1 nanosecond with the Discover package of Accelrys [7.72] employing a time step of 1 fs for the numerical integration.

The obtained packing models have an edge length of about 50 Å, which offers a good compromise between calculation velocity and maximum void size that can be analyzed in comparison with boxes of 40 Å, often used in the literature. The aim of using larger cells in our study is to improve the statistics of the later-derived free volume data. Details are given in Table 7.3 The density of the simulated models deviate less than 2% from the experimental values for both Hyflon samples. These deviations are comparable to other simulated density data in the literature [7.64].

Hyflon Model	No. solvent molecules.	N <sub>atoms</sub> <sup>a)</sup> (-)	Density, $\rho$ <sub>simul.</sub> (g/mol)	Deviation <sup>b)</sup> (%)	Cell edge (Å)
AD60 – 1	41	8594	1.8933	-1.24	49.48
AD60 – 2	41	8594	1.8842	-1.71	49.55
AD60 – 3	41	8594	1.8900	-1.41	48.74
AD80 – 1	26	8122	1.8832	-1.81	49.57
AD80 – 2	26	8122	1.8925	-1.33	49.49
AD80 – 3	26	8122	1.8874	-1.59	49.53

a) Total number of atoms present in the box (polymer + solvent).

b) Experimental densities: 1.917 g/cm<sup>3</sup> for AD60 [7.52] and 1.918 g/cm<sup>3</sup> for AD80 [7.21].

Table 7.3 - Properties of the atomistic packing models for three samples of each Hyflon polymer.

### 3.2. Free volume probing method

Several definitions of free volume in glassy polymers are employed in the literature [7.9, 7.10] depending on the evaluation method or the subject under investigation.

For experimentalists the most common quantity is the FFV, derived from experimental densities. The FFV is the ratio of the "free volume"  $V_f$  of a polymer (cm<sup>3</sup>/g) and the specific volume  $V_{sp}$ , defined as reciprocal density:

$$\text{FFV} = V_f / V_{sp} \quad (7.3)$$

According to the Bondi method [7.73], mostly used for such calculations, the free volume  $V_f$  can be estimated as:

$$V_f = V_{sp} - 1.3 V_{vdW} \quad (7.4)$$

where the van der Waals volume  $V_{vdW}$  is calculated using a group contribution method, and a universal "packing coefficient" equal to 1.3 is used to convert the van der Waals volume of the repeat unit in the "occupied" volume.

In this work, a ‘modified Bondi method’ is also used, in which the *accessible free volume* is based on the insertion of a test particle. A recently developed computer program [7.69] was applied to estimate the size distributions of the FVEs. This gives more accurate information than the original semi-empirical group contribution method to determine the occupied volume [7.73]. The calculation starts by the superimposition of a fine grid of about 0.5 Å over the cubic packing model. At every grid point, a hard sphere of a certain radius is inserted as a test particle. If the test particle overlaps with any atoms of the polymer matrix, which are also represented by respective hard spheres of van der Waals radii, the grid point is classified as “occupied”. If there is no overlap, the grid point is considered as “free” and the respective cublet contributes to the free volume. Neighbouring free grid points are collected into groups that represent individual holes. The grouping is done in two ways. In the first approach (named  $V_{\text{connect}}$ ), affiliation to a group is defined through next neighbourhood: every point of a group has at least one next neighbour that is also member of this group. This approach identifies holes, which may be of complex shape and of large volume. In a second approach (named  $R_{\text{max}}$ ) for every “free” grid point, the “distance” to the nearest matrix atom is determined. Using a gradient procedure, all neighbouring free grid points can be merged to a (local) set where all grid points are assigned to the same nearest local maximum in this “nearest distance” value. The  $R_{\text{max}}$  approach divides larger free volume regions of elongated or highly complex shape into smaller, more compact regions.

The second approach, originally introduced to match better the situation in PALS experiments where the positronium probe can obviously not completely sample very large holes of complex topology, also seems to be more adequate to depict the environment of a sorbed molecule. An oblong hole that is constricted at some point would be regarded as a single hole by the  $V_{\text{connect}}$  method. However, a penetrant molecule would have to jump an energy barrier to pass this bottleneck and therefore it would “see” two separate sorption sites. By defining a hole according to the  $R_{\text{max}}$  method, this separation would be recognized.

The geometrical analysis of packing models allows the determination of a *fractional free volume*. The FFV accessible for a certain test particle in a packing model can be considered as the ratio of “free” grid points to the total number of grid points. This ratio depends very much on the selected radius value of the test particle. The highest value would be obtained for a test particle with vanishing radius. Recently, it was shown that this geometrical analysis of packing models gives FFV values in acceptable agreement with values found by the Bondi method if a hard sphere test particle is used with a radius of 0.473 Å [7.74].

### **3.3. Photochromic probe method.**

#### ***3.3.1 Photoisomerization and UV-Visible characterization***

Photoirradiation of the membranes was performed with a medium pressure mercury UV lamp (GRE 500W, Helios Italquartz). The proper wavelengths were selected by means of band pass filters (OptoSigma). The trans-cis isomerization reaction of all chromophores was realized by means irradiating at 350 nm, using a quartz filter, and the back reaction was induced by irradiation at 440 nm, using a blue glass filter. Studies of the kinetics of the trans-cis photoisomerization recommended an irradiation time of 15 minutes to have the maximum of photoconversion for all types of dye; the lamp to film distance was 15 cm. Band pass filters were placed directly onto the sample surface to avoid irradiation of the films by unfiltered



scattered light from the sides, which may compromise the efficiency of the photoisomerization.

The molar absorption coefficients,  $\epsilon_{\text{trans}}$  and  $\epsilon_{\text{cis}}$ , of photochromic molecules dispersed in a 70/30 w/w mixture of HFE 7100 and DCM at a concentration of  $5.93 \cdot 10^{-3}$  mol/L, were calculated by absorbance measurements, using the Lambert-Beer law:

$$A = C \epsilon d \quad (7.4)$$

where  $A$  is the value of the absorbance peak at the maximum absorption wavelength,  $\lambda$ , of the dye,  $C$  is the concentration and  $d$  is the path length of the UV beam in the cuvette containing the solution. The photochromic solutions were prepared and stored in aluminium foil-wrapped flasks to avoid accidental light exposure leading to uncontrolled photoisomerization. All absorbance measurements were carried out at ambient temperature. The spectrophotometric analysis was performed on a UV-Visible spectrophotometer (Mod. Shimadzu UV 1601), interfaced to a PC for the data elaboration. The resulting cis-fraction or degree of trans-cis isomerization in the films,  $Y$ , was calculated from the following equation:

$$Y = \frac{1 - A / A_{\text{dark}}}{1 - \epsilon_{\text{cis}} / \epsilon_{\text{trans}}} \quad (7.5)$$

where  $A_{\text{dark}}$  is the initial peak absorbance with only trans isomer present,  $A$  is the actual peak absorbance and  $\epsilon_{\text{cis}}$  and  $\epsilon_{\text{trans}}$  are the molar absorption coefficients of the cis and trans isomers, respectively. The maximum isomerization in dilute solution is considered as a reference (100%) for the calculation of the isomerization efficiency in the film. A paradox in this procedure is that  $\epsilon_{\text{trans}}$  and  $\epsilon_{\text{cis}}$  are necessary for the calculation of the degree of isomerization  $Y$  in Eq.(7.4), but if this degree of isomerization is unknown then  $\epsilon_{\text{cis}}$  cannot be calculated with Eq.(7.5). Fischer presented a procedure to overcome this problem and to determine the ratio  $\epsilon_{\text{cis}}/\epsilon_{\text{trans}}$  by absorbance measurements at two different wavelengths [7.54] or through fluorescence measurements if only one of the two isomers shows a distinct fluorescence [7.55].

### 3.3.2 Reaction kinetics and progress of the photoisomerization reaction.

The common characteristic of the azobenzene and its derivatives is the clean and efficient photochemical isomerization that can occur about the azo bond when the chromophore absorbs a photon. The two states are a thermally stable trans, and a meta-stable cis configuration. The cis configuration will then typically relax back to the trans state thermally with a lifetime that depends sensitively on the particular substitution pattern and on local conditions. Irradiation of the cis form with light within its absorption band can also induce the photochemical cis-to-trans isomerization (Figure 7.1). In the present work the extent of isomerization was determined spectrophotometrically, using a pure film without dye as a reference sample.

The extent of the photoisomerization, i.e. the maximum of the trans-cis conversion, depends strongly on the time of exposure at UV light. It is therefore very important to set the proper time of irradiation. For this purpose photochromic Hyflon AD membranes were

irradiated at different times (5, 10, 15, 20 min) and for each time of irradiation, a UV spectrum was recorded. Generally the maximum absorbance was reached within 15 min of irradiation for all photochromic compounds. At room temperature the back reaction in the films was sufficiently slow to allow normal manipulation and characterization of the film, provided that no uncontrolled light exposure occurs. Figure 7.4 shows two examples of the absorption spectra of the Hyflon AD60X membranes containing azobenzene and stilbene before and after irradiation.

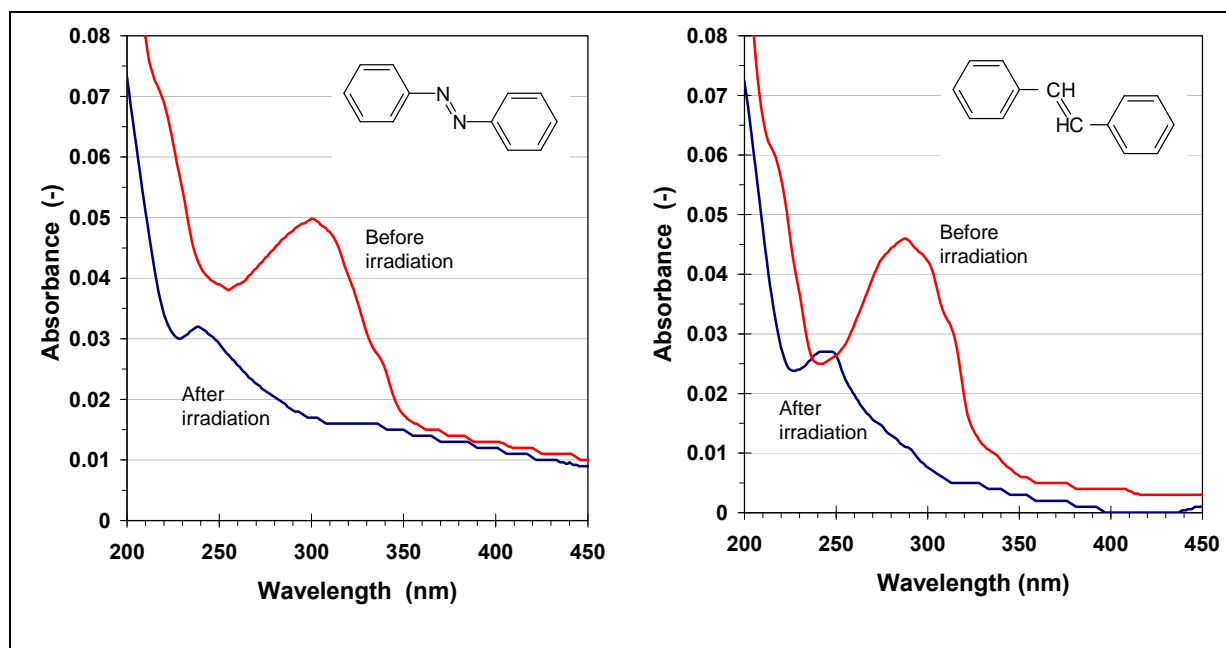


Figure 7. 4 - Absorption spectra of azobenzene and stilbene in Hyflon AD60X membranes, before and after photoirradiation at 350 nm for 15 min.

### 3.3.3 Determination of molar absorption coefficients

In all UV spectra of the photochromic films, the absorbance was sufficiently low for the Lambert-Beer's law to be applicable. If the cis isomer did not have a maximum, its absorbance was read at the same wavelength of the peak maximum of the trans isomer; otherwise the absorbance was read at its own peak maximum. The molar absorption coefficients of the cis and trans isomers in Hyflon AD membranes were thus calculated from Eq. (7.4), using the known dye concentration and optical path length, calculated from the measured membrane thickness and the original dye concentration in the casting solution. The determination of the molar absorption coefficients of the probes in the Hyflon membranes was somewhat sensitive to noise compared to the analysis in solution due to the low probe concentration and the low membrane thickness. This is a common problem reported also for other membrane types [7.16].

The progress of the azobenzene isomerization reaction generally depends strongly on its electronic environment and thus on the type of solvent [7.32] or matrix used. In order to minimize the difference between the absorption measurements in film and in solution, all solution measurements were carried out in the perfluorinated solvent HFE. A certain amount of DCM was always needed for the preparation of the mother solution of the dye molecules and for guaranteeing their solubility also in the perfluorinated solvent.

### 3.3.4 Determination of the total isomerization volume of the photochromic molecules and the FVE size distribution in the films.

A probe molecule has an associated van der Waals volume which represents volume occupied by the molecule, impenetrable for other molecules. This volume can be calculated using van der Waals radii tabulated by Bondi [7.73]. The extra volume needed by a dye molecule to isomerize is the volume swept by the van der Waals area, schematically displayed in Figure 7.2. Trans azobenzene and stilbene are planar molecules and their isomerization to the twisted cis isomer involves a complex series of motions which can only be elucidated by a combination of sophisticated analytical and computational techniques [7.76]. In the case of azobenzene and AZB derivatives the phenyl group is swept through a total angle of  $114^\circ$  during the inversion and it twists  $30^\circ$  to assume the equilibrium conformation of the cis isomer [7.16, 7.77]. The volume required for isomerization consists of two components: the phenyl ring twist and the volume swept by the area comprised of the product of the phenyl thickness and the length. In the case of stilbene and stilbene derivatives, upon irradiation, one of the central carbons twists  $90^\circ$  to the geometry of the excited state. The double bond disappears, allowing rotational diffusion about a single C-C bond [7.16, 7.78, 7.79]. Viktor and Torkelson proposed a method to calculate the extra volume needed for isomerization, based on some simple geometrical considerations [7.16] for a two stage process: from the trans isomer to the excited state and from the excited state to the cis isomer. Table 7.4 lists the Van der Waals volume of the photochromic molecules used in this work and the extra volume needed to isomerize, reported by Viktor and Torkelson or calculated according to their method [7.16].

The size distribution of free volume elements can be derived from the degree of isomerization from the trans- to the cis-isomer ( $Y$  in Eq. (7.5)). The ratio of the cis isomer fraction in the film and that in solution gives a quantitative measure of the efficiency of photoisomerization for each photochromic probe. Figure 7.5 shows this ratio as a function of the total isomerization volume of the dye molecules as defined in Table 7.4.

Probe molecule	Volume of the molecule <sup>a)</sup> , Å <sup>3</sup>	Extra volume for isomerisation, Å <sup>3</sup>	Total volume <sup>b)</sup> , Å <sup>3</sup>	Ref.
Azobenzene	144	127	271	7.16
Stilbene	151	222	373	7.16
Disperse orange 3	171	250	421	This work
4, 4'-Dinitrostilbene	187	262	449	7.16
Disperse red 1	207	310	517	This work
Disperse orange 25	224	350	574	This work

<sup>a)</sup> According to Bondi's method [7.73].

<sup>b)</sup> The sum of the van der Waals volume of the molecule and the extra volume.

**Table 7. 4 - Van der Waals volume of photochromic probes and extra volume needed to isomerize.**

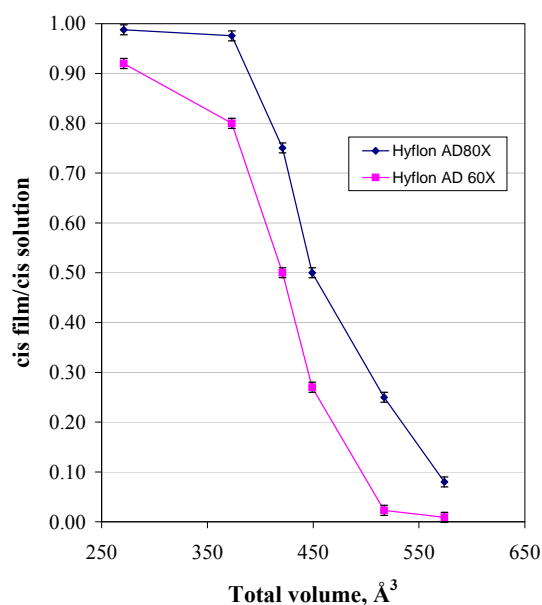


**Figure 7. 5- Ratio of the cis isomer fraction in the film and the cis isomer fraction in solution as a function of the total isomerization volume of the probes in Hyflon AD membranes.**

In both Hyflon grades the isomerization efficiency of the smallest probe, unsubstituted AZB, is nearly 100% and decreases rapidly with increasing probe size, down to about 0% for Disperse Orange 25. Thus, according to this method the size of free volume elements ranges from about 250-520 Å<sup>3</sup> in Hyflon AD60X and from ca. 380-600 Å<sup>3</sup> in Hyflon AD80X. This means that, if we assume a spherical shape of the cavities, the averaged value of equivalent sphere radius ranges between 3.9 and 5.0 Å in Hyflon AD60X and between 4.5 and 5.2 Å in Hyflon AD80X. These values are in line with the results reported on the basis of <sup>129</sup>Xe-NMR studies [7.14]. They confirm that Hyflon AD80X membranes possess only slightly bigger local FVEs than Hyflon AD60X. Arcella et al. reported a three to six times higher permeability of Hyflon AD80X than of AD60X [7.20,7.59]. Recent data of some of the present authors on pure dense films suggest a much smaller difference between the two Hyflon grades [7.60], in line with the small difference in the free volume found here.

### 3.3.5 Comments and critical remarks

The results of the photochromic probe method depends on various assumptions. For instance a critical factor is the actual volume involved in the transition from the cis- to the trans-isomeric form of the probe molecules and vice versa. This volume is obtained by relatively simple approximations [7.16]. A more accurate approach would ideally determine the true Van der Waals volume and shape of the probe molecules by quantum chemical calculations in various stages of the isomerization reaction and in the transition state, requiring detailed knowledge of the excited state. This is beyond the scope of the present paper. Some limitations of the experimental analysis consist in the uncertainty of the isomerization efficiency in solution and in the precision of the determination of the molar absorption coefficient of the least stable isomer in solution when the thermal back reaction is too fast to measure the photostationary state. For a number of different probe molecules the isomerization efficiency in solution varies roughly between 80% and 90% [7.16]. An

estimated average value of 85% was therefore used if no experimental data were available for a specific probe.

An important assumption in this method is that each probe molecule is isolated and that no clusters are formed in the polymer matrix. This requires a molecular solution of the probes in the polymer matrix. Although the probe molecules are in principle insoluble in the polymer matrix the present paper describes an efficient method to circumvent this problem by the smart use of solvent mixtures. The extremely low probe concentration during solution casting and in the final polymer film, in combination with the low dipole moment of the trans-isomeric form of the probe molecules make clustering an unlikely event. The final probe concentration in the polymer film, ca.  $1.7 \cdot 10^{-6}$  mol/cm<sup>3</sup>, is less than 0.1 wt.-% and is negligible compared to the available free volume. Correspondingly, also the total number of probe molecules (ca.  $10^{18}$  cm<sup>-3</sup>) is more than two orders of magnitude smaller than the FVE concentration, generally ranging from about  $2 \cdot 10^{20}$  to  $7 \cdot 10^{20}$  cm<sup>-3</sup> for different polymers [7.10]. We may therefore assume that the probes themselves do not contribute to the formation of free volume and that their distribution in the available free volume elements is completely at random.

### 3.4. Positron annihilation lifetime spectroscopy

Since Hyflons exhibit a relatively high gas permeability, the measurements were carried out in nitrogen atmosphere. This generally gives sufficiently accurate lifetimes compared to measurements carried out under vacuum, even for membrane materials and polymer sorbents with much longer lifetimes like PTMSP [7.80] and cross-linked polystyrenes [7.81]. On the other hand, measurements in air showed significant quenching by oxygen in some samples and could therefore not be used. The PALS analysis was carried out on both grades, Hyflon AD60X and AD80X.

It was found previously that the gas permeability of Hyflon AD60X membranes depends strongly on the sample preparation method, especially for larger penetrant molecules such as methane and CO<sub>2</sub> [7.52]. In particular, residual solvent in solution-cast films increases the gas permeability of these penetrants due to higher diffusion coefficients. The latter is partially due to a certain degree of plasticization of the polymer by residual solvent, evidenced by the strong reduction of the T<sub>g</sub>.

The photochromic probe method requires a solution-casting procedure and the limited thermal stability of some of the probe molecules, in combination with the reluctance to release the residual solvent at low temperatures did not allow the preparation of samples which are completely free of residual solvent.

Therefore the PALS analysis in the present work was used to study the effect of residual solvent and the film formation procedure on the FVE size by comparing the data of solution cast and melt pressed films. Thus, in total 4 different samples were tested. It was shown that a good statistical fit with a maximum variance of about 1.01 can be obtained with the three component PATFIT analyses of the lifetime distributions in all cases. The calculation procedures have been described elsewhere [7.82]. If the statistics are sufficiently large then similar methods (PATFIT, CONTIN, MELT and LT) allow the evaluation of the entire void size distribution [7.46, 7.83, 7.84, 7.85], but for the present analysis smaller statistics were

available and only the average void size was determined by the finite term treatment. The main results are presented in Table 7.5

Several interesting conclusions can be drawn by analyzing this table. Firstly, for films prepared by the same procedure and under the same conditions the lifetimes  $\tau_3$  of the copolymer Hyflon AD80X, and the corresponding radii of FVE computed according to the Tao equation (Eq. (7.1)) are always larger than those of Hyflon AD60X. This observation is in agreement with the higher cyclic dioxole comonomer content in Hyflon AD80X which reduces the packing efficiency of the polymer chains and, assumingly, increases the free volume. Also previous studies that showed a higher permeability of Hyflon AD80X than that of Hyflon AD60X confirm this assumption [7.59].

Secondly, for both copolymers, the films obtained by solution casting showed higher values of  $\tau_3$  and  $R_3$  than the melt pressed films. Thus, the radius of FVE for the solution cast film is more than 10% larger, while the difference in the corresponding spherical volumes amounts more than 30%.

Copolymer	Film preparation	$\tau_3, \text{ns}$	$I_3, \%$	$R_3, \text{\AA}$
AD80X	Solution cast*	5.80±0.14	9.18±0.38	5.22
	Melt pressed	4.58±0.04	10.69±0.18	4.63
AD60X	Solution cast**	5.02±0.06	10.17±0.21	4.78
	Melt pressed	4.36±0.04	12.04±0.21	4.51

\* From the solvent HFE 7100, dried 20 h at 50 °C.

\*\* From the solvent HFE 7100, dried for 20 h at 50 °C in vacuum.

**Table 7. 5- PALS parameters of Hyflons in terms of three components and the equivalent sphere radii,  $R_3$ , of free volume elements (measurements in  $N_2$  atmosphere).**

Some differences were observed in the intensities  $I_3$  for both pairs of samples prepared via the solution casting and the melt pressing procedures. In fact, somewhat higher values of  $I_3$  were observed for the melt pressed samples. In a similar way,  $I_3$  is larger for Hyflon AD60X samples than for Hyflon AD80X. In similar systems where spur processes may be nearly the same it has been suggested [7.86] to use the  $I_3$  values for estimation of the relative fractional free volume from the elementary free volume as:

$$FFV = C v_f I_3 \quad (7.6)$$

where  $C$  is a proportionality factor which must be estimated from independent data.  $I_3$  depends not only on the concentration of FVEs but also the material type, the probability of formation of o-Ps, the rate of capture of o-Ps by FVE and the possible quenching by polar groups e.g. in polyimides.



In very similar materials, as for the two Hyflon grades and for the samples prepared from the same materials but under different conditions, the equation can be used for a qualitative estimation of their relative fractional free volumes. In the samples studied, the differences in  $I_3$  are not big enough to make a final quantitative conclusion for the value of FFV, but nevertheless, these results suggest that the larger FVE size in Hyflon AD80X compared to Hyflon AD60X (for the same membrane preparation procedure) and in the solution cast samples compared to the melt-pressed samples (for the same Hyflon grade), are compensated by a lower FVE concentration. Indeed the density of both grades of Hyflon are reported to be similar [7.21, 7.52], which suggests a more or less equal FFV. Also Bondi's method yields a nearly identical FFV for both samples.

The transport properties depend not only on the FVE size distribution but also on the interconnectivity of the free volume elements and on the chain dynamics. Information on the interconnectivity is obtained from MD simulation studies (see below). The chain dynamics are correlated with, for instance, the  $T_g$  of the polymer, which in turn depends on the dioxole comonomer content and on the presence of residual solvent.

For a solution cast film of the more permeable polymer, Hyflon AD80X, a test for possible oxygen induced quenching was carried out by comparison of measurements in air and in  $N_2$  atmosphere. Indeed, the presence of  $O_2$  induced a noticeable decrease in the observed  $\tau_3$  values: the positronium lifetime in the presence of air was 5.24 ns, about 0.6 ns shorter than in nitrogen atmosphere. Meanwhile the observed intensity  $I_3=9.39\pm 0.11$  was virtually the same in air and in nitrogen atmosphere. Although chemical quenching or conversion of Ps by  $O_2$  generally affects not  $\tau_3$  only but also  $I_3$ , the latter was not observed in the present case, confirming that the results can only be used for a qualitative comparison. As discussed above, a constant value of  $I_3$  would normally suggest that the FVE concentration does not change notably. In any case, only the measurements in  $N_2$  atmosphere were used for the FV analysis.

### 3.5. Inverse gas chromatography

Studies of different glassy polymers indicated that for solutes (n-alkanes  $C_3$ - $C_{12}$ ) having different molecular size the  $\tau_3$  values initially decrease as the molecular size (e.g. its critical volume  $V_c$ ) increases, passing through a minimum at a particular size of the solute molecules (these sizes are different for different polymers) and then increase again [7.9]. It is important that strongly negative values of the enthalpy of mixing are observed. This implies that the process of mixing in glassy polymers (in contrast to rubbers) does not require overcoming the work of chain displacement. Exothermic mixing is consistent with the idea that the solute molecules of certain size can be accommodated within the FVE. This hypothesis is substantiated by establishment of correlations between the minimum  $\tau_3$  values and the diffusion coefficients and gas permeability of glassy polymers [7.9]. Thus, the IGC method allows estimation of the FVE size in glassy polymers.

The dependence of  $\tau_3$  in Hyflon AD80 on the size of the solutes (n-alkanes) is shown in Figure 7.6. For comparison the data for two other glassy polymers (polyvinyltrimethylsilane, PVTMS) [7.13] and amorphous Teflon AF1600 [7.87] and same set of solutes are also shown. It can be noted that the mixing of these molecular probes is strongly exothermic in Hyflon AD80. When the size of the solutes decrease from dodecane to hexane the values of decrease. Unfortunately the solubility of the alkanes lower than  $C_6$  was so small that it was

impossible to locate the minimum of the curve versus  $V_c$ . It can only be stated that the minimum value of  $\bar{H}_1^{E,\infty}$  in this polymer is equal to or smaller than  $368 \text{ cm}^3/\text{mole}$  (critical volume of n-hexane according to [7.58]). Such value is consistent with relatively low gas permeability of Hyflon AD: the largest coordinate of minimum  $\bar{H}_1^{E,\infty}$  is observed for Teflon AF1600 that has a permeability coefficient  $P(\text{O}_2)=170$  Barrer [7.17]; for PVTMS the following values are characteristic:  $V_c(\text{min}) = 368 \text{ cm}^3/\text{mole}$ ,  $P(\text{O}_2)=44$  Barrer. The reported  $P(\text{O}_2)$  value for a solution cast Hyflon AD80X sample is 42 Barrer [7.60], so it can be assumed that its  $V_c(\text{min})$  should indeed be similar to that of PVTMS.

It should be taken into account that the plot shown in Figure 7.6 is a correlation. Different scales can be chosen for the size of the molecular probes. It has been shown that similar correlations can be obtained for the critical volume  $V_c$  and for the molecular volume  $V_b$  in the liquid phase at corresponding boiling point as the scaling parameters [7.88]. Hence, if one supposes that the smallest observed value of  $\bar{H}_1^{E,\infty}$  is the upper limit for the size of FVE in Hyflon AD80, it gives the following upper limits for the radii of spherical FVEs.

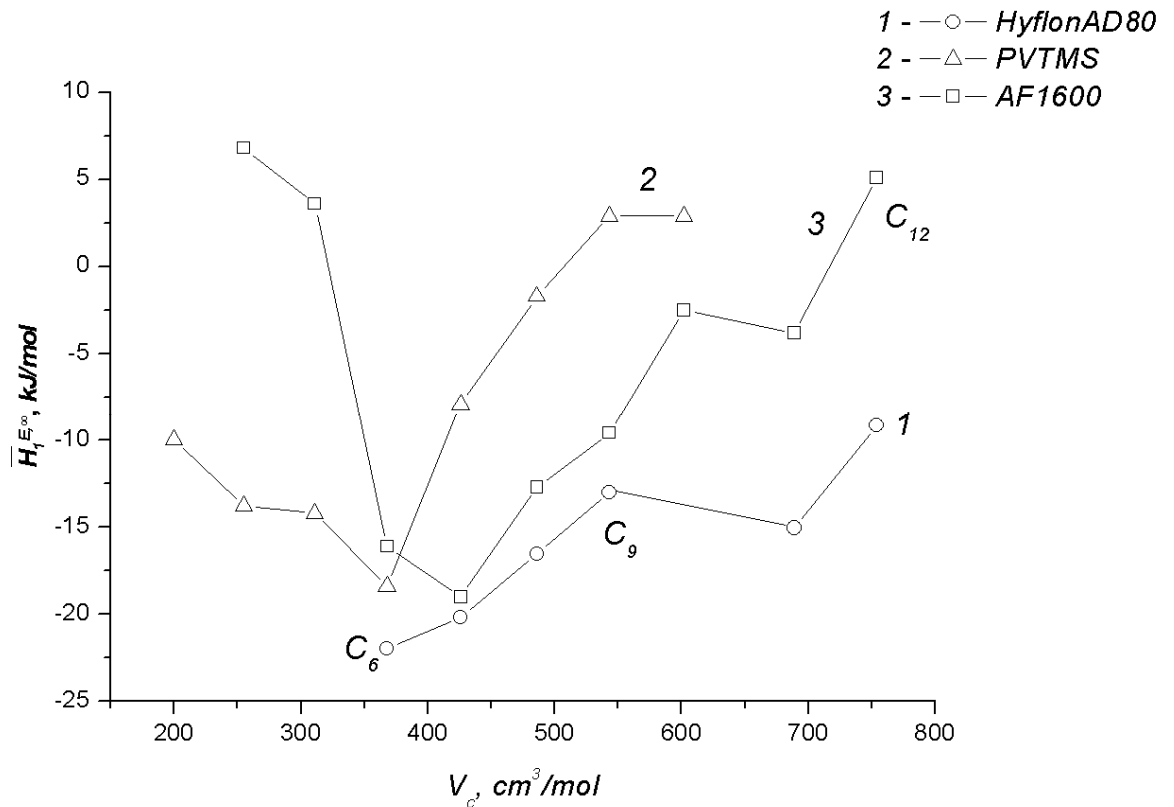


Figure 7. 6 - Dependence of  $\bar{H}_1^{E,\infty}$  on the critical volume of n-alkane solutes in Hyflon AD80X.



### 3.6. Molecular Dynamics Simulations

#### 3.6.1 *Generation and equilibration of polymer structures and qualitative free volume evaluation*

The simulated atomistic bulk models of both Hyflon AD80X and Hyflon AD60X with a representative number of residual solvent molecules allow an accurate determination of the characteristics of the structure of chain packing, the related free volume and their distributions. A qualitative visualization of the free volume distributions for the packing models is shown in Figure 7.7.

The simulation cells of both Hyflon samples have been cut into slices of about 5 Å thickness perpendiculars to the respective z-axis. Eight of the ten slices of the boxes are displayed in Figure 7.7, which gives a qualitative visual impression of the difference between the two copolymers. Hyflon AD80X slices contain larger areas of free volume compared to AD60X. This is in good agreement with the lower gas permeability in AD60X [7.60]. In comparison, the voids are significantly smaller than those found by Hofmann et al. in Teflon AF2400 and AF1600, with lateral void-widths between ca. 5 and 20 Å [7.49]. This corresponds again to the lower gas permeabilities in the Hyflons compared to Teflons AF.

The shape of the free volume elements in each slide is irregular and usually nonspherical. They are rather large and the elongated FVE elements may extend across several slices. This characteristic is more evident in AD80X than in AD60X.

As for other high free volume and high permeability polymers (i.e. PTMSP and aged PTMSP, Teflon AF2400, AF1600) [7.49] the two Hyflon polymers are characterized by the presence of two qualitatively different states. They contain regions of high segmental packing density where the free volume distribution resembles that of conventional glassy polymers [7.89] and regions with rather large voids. In the case of perfluoropolymers these free volume areas show a much smaller tendency to form a continuous hole phase than in PTMSP [7.49].

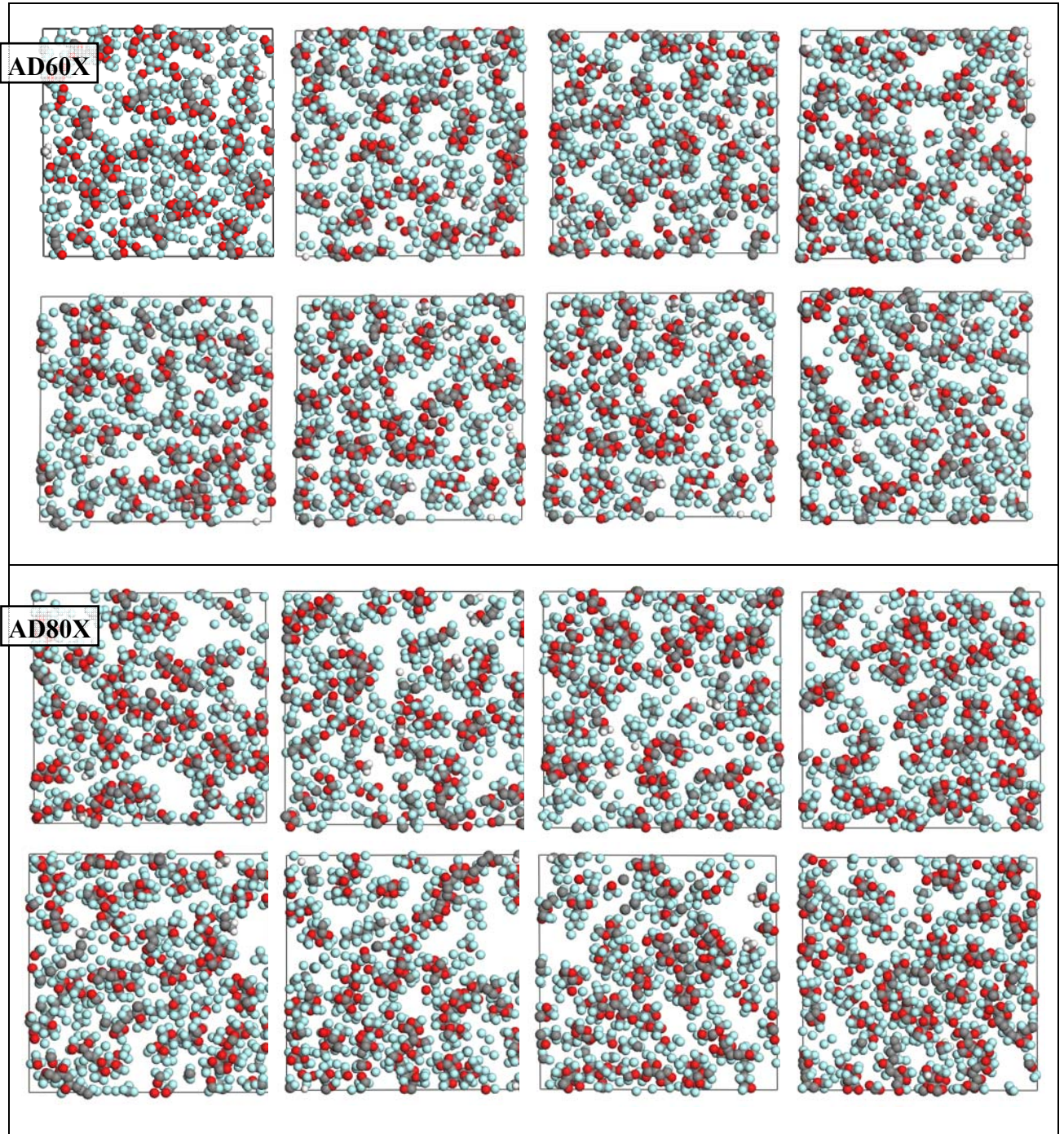


**Figure 7. 7 -  $50 \times 50 \text{ \AA}^2$  sliced box model of Hyflon AD60X (top) and Hyflon AD80X (bottom). Slice order from left to right and from top to bottom.**



The results of the free volume analysis by the  $V_{connect}$  and  $R_{max}$  methods are visualized qualitatively in Figure 7.8 for a representative slice of Hyflon AD80X.

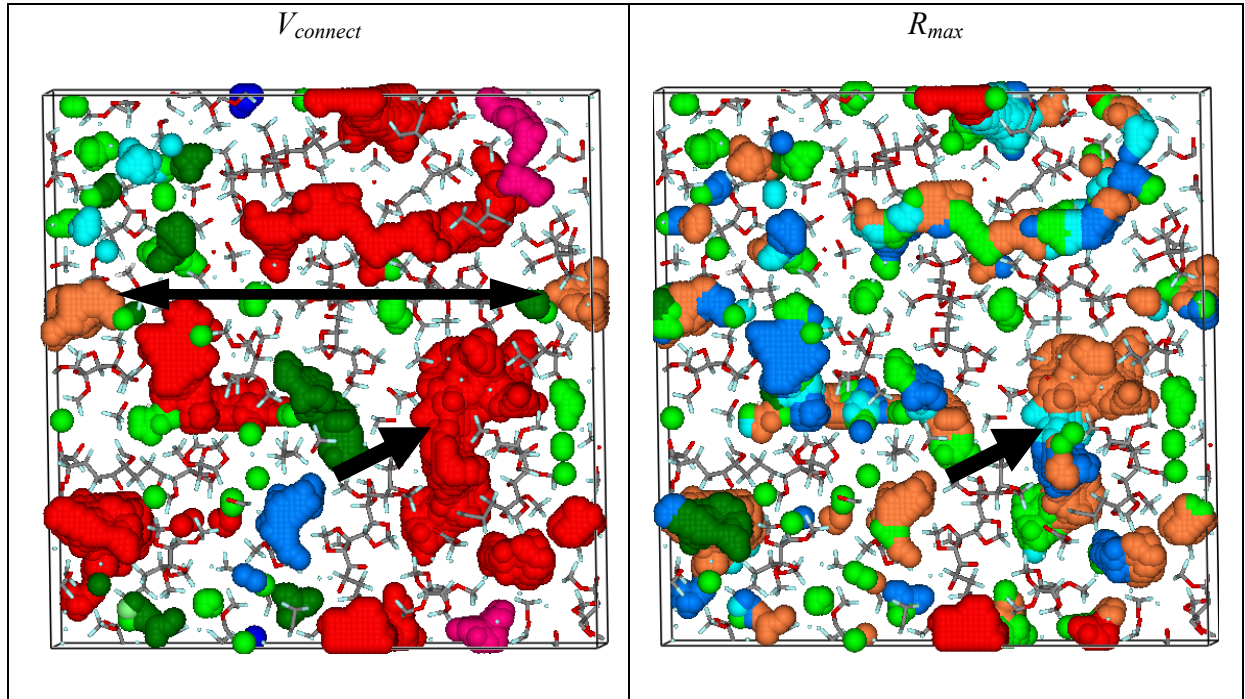


**Figure 7. 8 - Representative slice of about 5 Å thickness of one atomistic packing of Hyflon AD80X, showing the free volume elements according to the  $V_{connect}$  and the  $R_{max}$  method for the positronium probe ( $R = 1.1 \text{ Å}$ ). In the  $V_{connect}$  method (left) each colour indicates one *single* FVE, associated to free grid-points. In the  $R_{max}$  method (right) every single free volume element is subdivided into smaller ones, indicated with different colours. The polymer matrix is represented by the coloured sticks.**

The polymer matrix atoms are displayed in “stick style”. Every free grid point is presented by a sphere of radius of 1.1 Å representing the positronium sized test particle. It should be noted that some matrix atoms as well as FVEs appear fragmented due to the slicing process or continue on the opposite side due to the periodic boundary conditions (double headed arrow).

The left side of Figure 7.8 shows the result for the  $V_{connect}$  analysis. The overlapping spheres build the FVEs. Except for the very small elements in light green, all spheres of one color belong to the same FVE. The largest FVE in this model is indicated in dark red. It seems to consist of eight separate parts, but these parts belong to one single very large interconnected free volume region which extends over the neighboring slices and which would be accessible for the test particle. This single FVE represents about 80 % of the accessible free volume. It is a kind of randomly connected channel and cavity system,

definitely not a big spherical pore. All larger cavities or channel sections can be split into smaller more spherical segments with the  $R_{\max}$  method, as shown in the right graph of Figure 7.8. A good example is again the very large cavity indicated with the single arrow. The  $R_{\max}$  method splits it into about five smaller segments of more compact and nearly spherical shape.

### 3.6.2 Quantitative analysis of the free volume distribution.

The size distributions of FVEs from the packing models have been calculated with the  $V_{\text{connect}}$  and  $R_{\max}$  approach for every packing model. Figure 7.9 shows the distributions for both Hyflon AD60X and Hyflon AD80X as an average of three packing models in comparison with the results of the experimental methods. The analysis was performed using a grid spacing of 0.5 Å and a positronium sized test particle of with a radius of 1.1 Å. The volume of each FVE is represented by the radius of a volume-equivalent sphere,  $R_{\text{eq}}$ , calculated as:

$$R_{\text{eq}} = \sqrt[3]{\frac{3}{4\pi}V} \quad (7.7)$$

where  $V$  is the void volume.

The analysis with the  $V_{\text{connect}}$  method confirms the qualitative impression of the slices in Figure 7.7. For a positronium sized test particle, every packing model contains one large interconnected region, indicated by one of the three single columns in the size range between 14 Å and 21 Å (equivalent sphere radius), plus several more individual large pores of  $\geq 7$  Å. An additional set of smaller independent holes with a radius between 1.1 Å and about 7 Å represents numerically the largest fraction, although their total volume is small. Here, it should be emphasized that a radius of for instance 15 Å does not imply that the packing model contains a single huge spherical hole of this size, because the “radius” of the volume equivalent sphere is only a measure for the total extension of this interconnected “cave and channel system”. From the comparison of the  $V_{\text{connect}}$  distribution of both Hyflons, it follows that the interconnected FVEs in AD80X are a bit larger than in AD60X. A similar bimodal distribution was also found in analogous simulations of Teflons AF [7.49] and with the newly developed alternative CESA algorithm of Willmore et al. [7.90].

Since the  $R_{\max}$  approach splits neighboring FVEs into smaller more compact and more spherical parts, one obtains distributions with radius values between 1.1 Å and 5 Å with a distribution maximum between 2.0-3.0 Å for both Hyflons.

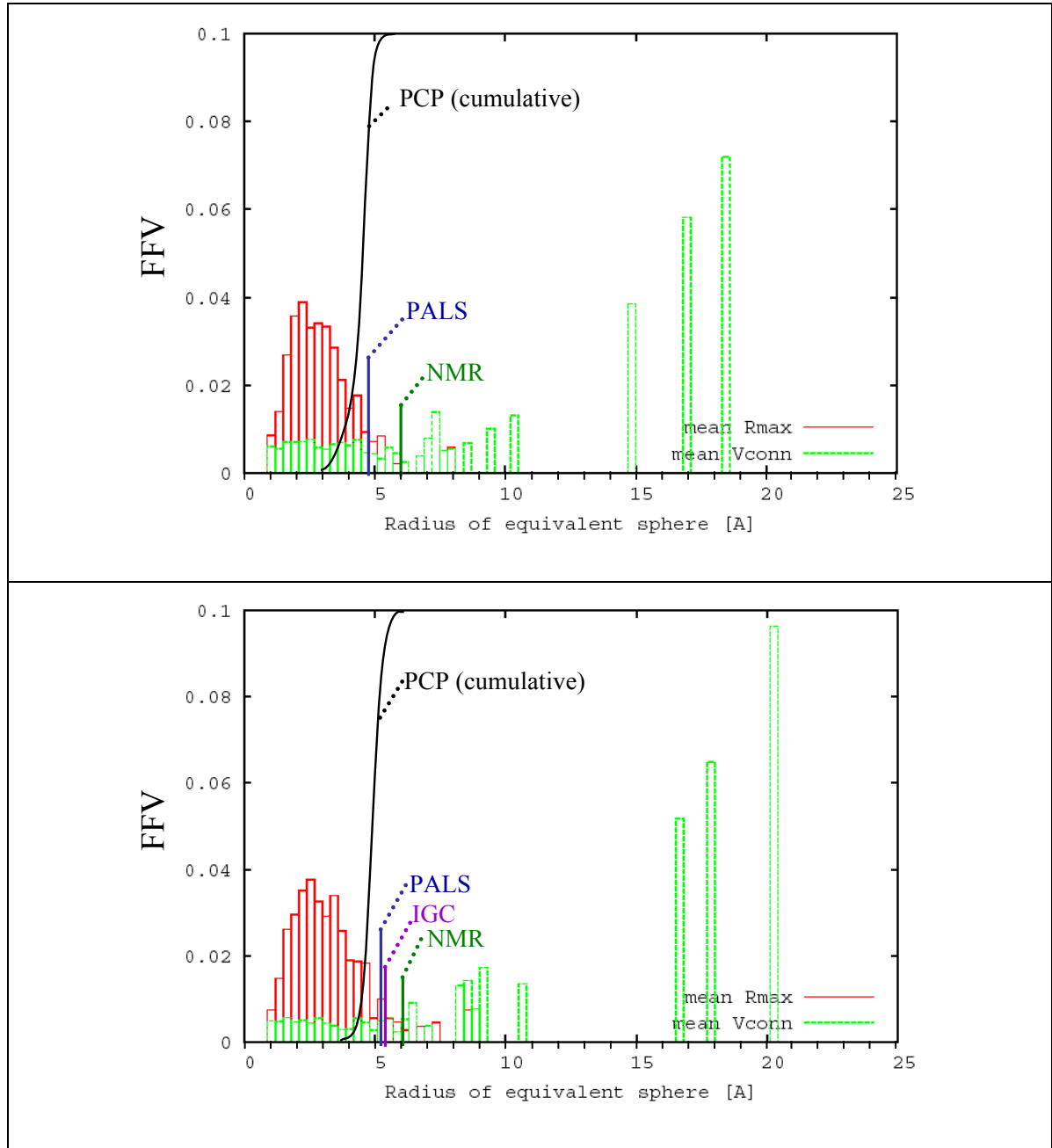


**Figure 7. 9-** Overview of the FVE equivalent sphere radius distribution in Hyflon AD60X (top) and Hyflon AD80X (bottom). Bar chart: FVE distributions by MD simulations with a probe radius of 1.1 Å ( $R_{max}$  and  $V_{connect}$  methods, average of 3 packing models). The average values determined by PALS, the maximum value for IGC based on the probe critical volume and the reference value from  $^{129}\text{Xe}$ -NMR spectroscopy for a spherical void [7.14] are also indicated as a vertical line. The sigmoidal curve represents the cumulative distribution by the PCP method, obtained from the smoothed data of Fig. 7.5.

Recently, some authors argued that the effective size of the o-Ps probe (typically assumed to have a radius of 1.1 Å), is too small to simulate correctly the localization of the o-Ps and they suggested that the effective size should be increased to a radius of about 1.5 Å [7.19]. Therefore the  $V_{\text{connect}}$  and  $R_{\text{max}}$  analysis was also carried out with a probe radius of 1.5 Å. On the basis of the obtained distributions the mean FVE radius was calculated for a quantitative comparison with the experimental results. The total accessible volume and the FFV calculated with both probe sizes are listed in Table 7.6 The FFV obtained by Bondi's method (see next section) is indicated for comparison.

Hyflon	FV	Probe $r_p = 1.1 \text{ \AA}$		Probe $r_p = 1.5 \text{ \AA}$		Bondi's method	
		Value	Std. Dev	Value	Std. Dev	Traditional	Modified
AD60X <sup>a)</sup>	$V_{\text{acc}} [\text{\AA}^3]$	40600	1460	24150	2370		
“	$FFV [-]$	0.338	0.012	0.202	0.023	0.23	0.226
AD80X <sup>a)</sup>	$V_{\text{acc}} [\text{\AA}^3]$	45300	650	33940	2170		
“	$FFV [-]$	0.373	0.005	0.279	0.017	0.23	0.239

<sup>a)</sup> Box size  $119530 \pm 3250 \text{ \AA}^3$  for Hyflon AD60X and  $121510 \pm 294 \text{ \AA}^3$  for Hyflon AD80X (average of 3 packing models).

**Table 7. 6 - Simulated amount of accessible volume and of Fractional Free Volume for AD60X and for AD80X, calculated for a probe equivalent sphere radius of 1.1 Å and 1.5 Å, and estimated with Bondi's methods-**

The mean FVE radius,  $R_{\text{eq}}$ , is determined from the total accessible volume and the mean number of detected holes in the respective packing models.

$$R_{\text{eq}} = \sqrt[3]{\frac{3}{4\pi} \frac{V_{\text{acc}}}{n}} \quad (7.8)$$

where n is the total number of holes.

The results are given in Table 7.7: with a probe of 1.1 Å the  $V_{\text{connect}}$  approach finds in the three packings of AD60X an average of  $395 \pm 41$  holes, forming an accessible free volume of about  $40600 \text{ \AA}^3$  and corresponding to a mean radius of  $2.91 \pm 0.10 \text{ \AA}$ . In AD80X the accessible free volume is 11% higher, but the number of holes is 20% lower than in AD60X, resulting in a larger mean radius of about  $3.25 \text{ \AA}$ . The geometrical splitting of larger free volume regions into smaller parts ( $R_{\text{max}}$  approach) increases the number of pores considerably and results in lower mean pore radii of about  $2.08 \text{ \AA}$  and  $2.21 \text{ \AA}$  for AD60X and AD80X, respectively.

		Void probing $r_p = 1.1 \text{ \AA}$						
		Probing $r_p = 1.1 \text{ \AA}$		Probing $r_p = 1.5 \text{ \AA}$		Evaluation $r_{eq} = 1.5 \text{ \AA}$		
						No. holes <sup>a)</sup>	Eff. no. of	corrected
Hyflon	FV approach	Total no. of holes	mean $R_{eq}$ [ $\text{\AA}$ ]	Total no. of holes	mean $R_{eq}$ [ $\text{\AA}$ ]	with $R_{eq} \leq 1.5 \text{ \AA}$	holes with $R_{eq} > 1.5 \text{ \AA}$	mean $R_{eq}$ [ $\text{\AA}$ ]
AD60X	$V_{connect}$	395±41	2.91±0.10	224±12	2.95±0.13	226±18	169±24	3.87±0.19
“	$R_{max}$	1087±88	2.08±0.05	421±23	2.39±0.10	432±31	655±57	2.46±0.06
AD80X	$V_{connect}$	317±26	3.25±0.10	172±18	3.62±0.20	199±22	119±9	4.50±0.13
“	$R_{max}$	1009±76	2.21±0.06	439±21	2.64±0.10	385±38	624±47	2.59±0.07

<sup>a)</sup> Corresponding to < 8% of the total accessible volume when measured with a 1.1  $\text{\AA}$  equivalent sphere radius probe.

**Table 7. 7-Estimated description of FVEs from the simulated packing models (average values for 3 boxes).**

These values are considerably lower than the experimental values (Figure 7.9 and Table 7.8), while the FFV is significantly overestimated compared to the value of 23% obtained by Bondi's method.

		Average FVE equivalent sphere radius, $R$ ( $\text{\AA}$ )					
Method		PALS	PCP	IGC	<sup>129</sup> Xe-NMR [7.14]		
Sample		$R_3$	$R_{eq}$	$R_{eq,c}$ <sup>b)</sup>	$R_{eq,b}$ <sup>c)</sup>	$R_{eq}$	$R_{eq,cyl}$ <sup>d)</sup>
AD60X solution cast		4.78	4.64	-	-	6.0	4.1
	melt pressed	4.51 <sup>a)</sup>	-	-	-	-	-
AD80X solution cast		5.22 <sup>a)</sup>	4.79	$\leq 5.3$	$\leq 4.5$	6.12	4.16
	melt pressed	4.63 <sup>a)</sup>	-	-	-	-	-

<sup>a)</sup> Measurement in  $N_2$ . <sup>b)</sup> Based on probe critical volume. <sup>c)</sup> Based on probe molecular volume in the liquid at the boiling point. <sup>d)</sup> Value for cylindrical instead of spherical pore shape.

**Table 7. 8 - Overview of the average Free Volume Element sizes according to different experimental probing techniques in Hyflon AD membranes.**

The analysis with a larger probe of 1.5 Å gives some improvement, with an increase of the average FVE size and a strong reduction of  $V_{acc}$  and FFV to a somewhat lower value (AD60X) or a slightly higher value (AD80X) than predicted by Bondi. It is interesting to note that with the  $V_{connect}$  method and the 1.5 Å probe the number of pores in AD80X is lower than in AD60X, while its accessible volume is higher. This reflects a larger number of isolated voids in the latter and the stronger interconnection of the FVEs in AD80X. Nevertheless, the increase of the average FVE equivalent sphere size is still relatively small when a probe with a radius of 1.5 Å is used. Even the values calculated according to the  $V_{connect}$  method, which usually gives the highest results, are still considerably lower ( $R_{eq}$ , AD60X = 2.95 Å and  $R_{eq}$ , AD80X = 3.62 Å, respectively) than the experimental values.

A better correspondence with simulated and experimental results is obtained if the overall free volume is determined with a o-Ps-size probe with a radius of 1.1 Å, whereas the smallest detected voids with an equivalent sphere radius of less than 1.5 Å are excluded for the calculation of the average size (right columns in Table 7.7). The motivation is that o-Ps particles have a too high probability to be annihilated by the wall in so small voids, especially if the latter are relatively thin and elongated. Although the number of excluded pores with  $R_{eq} \leq 1.5$  Å is relatively large, they do not account for more than about 6-8% of the total  $V_{connect}$  void volume because of their small individual volume. Therefore with this procedure the average equivalent sphere diameter of FVEs according to the  $V_{connect}$  method increases to 3.87 Å and 4.53 Å for AD60X and AD80X, respectively. These values are much closer to the experimental data. However, the physical basis of such reasoning is somewhat weak and further improvement of the method is necessary. In any case, all calculations of Table 7.7 show larger mean radii for the FVEs in AD80X than in AD60X.

### 3.6.3 Modified Bondi method.

The modified Bondi method also allowed a quantitative analysis of the FFV of the samples. The FFV according to the modified Bondi method was calculated from the above packing models, using a test particle of a radius of  $r=0.473$  Å. The thus obtained FFV was  $0.239 \pm 0.003$  for AD80X, compared to  $0.226 \pm 0.004$  for AD60X, confirming the slightly higher FFV for Hyflon AD80X.

It must be noted that the FFVs obtained by the computational methods cannot be compared on an absolute scale. In the modified Bondi method, the radius of the test particle ( $r = 0.473$  Å) is smaller than the grid size (0.5 Å), whereas for the calculation with a positronium-like test particle, the radius is much larger than the grid size. In that case a single free grid point may represent a free volume segment that has at least the volume of the test particle. If the same hole is analyzed with the Bondi test particle it may be represented by about 27 free grid points. The calculation procedure tries to account for these effects in approximation. The deviation is larger if a packing model contains many small holes. The FFV determined by the traditional and modified Bondi method are in good mutual agreement (Table 7.6) but considerably higher than the void volume fraction of 9.4-9.5% reported previously [7.20].



#### 4. Comparison of the methods and Conclusions

The present paper describes the investigation of the free volume in amorphous glassy perfluoropolymer films of Hyflon AD. To the knowledge of the authors this is the most extensive comparative study of all actively used experimental methods, namely PALS, IGC and  $^{129}\text{Xe}$ -NMR spectroscopy, for probing of the free volume in a single type of a glassy polymer. The study further includes the photochromic probe method, and it is demonstrated that this method can be successfully used to determine the FVE size distribution in amorphous glassy perfluoropolymers. In addition, the experimental findings are considered jointly with the results of computational studies of the polymer packing and of the free volume and free volume size distribution and spatial arrangement in the investigated Hyflon polymers.

Each of the investigated methods ‘senses’ the free volume in another specific way, with probes of different size and properties, and each method provides a different level of detail in the obtained results. By and large, the agreement between the various experimental methods and between the experimental versus computational is reasonable.

The strengths and weaknesses of the different experimental techniques and computational methods were indicated. PALS allows the best experimental probing of the FV distribution due to the small size of the o-positronium particles, but in contrast to the MD simulations it can only probe the volume and to some extent the shape but not the connectivity of the FVEs. The PCP method has the advantage of its simplicity, but it has also the strongest limitations: the probes have a distinct, non spherical shape, related to the structure of the dye molecule, and the minimum size which can be probed is that corresponding to azobenzene, the smallest available probe molecule. In spite of the differences and limitations of each technique, there is a surprisingly good agreement of the results from all methods if the FVE size is expressed as the radius of an equivalent sphere.

In quantitative terms the results of the photochromic probe method were in rather good agreement with those of the other experimental FV probing techniques PALS and IGC, and with  $^{129}\text{Xe}$ -NMR reported in the literature [7.14], although in the approximation of spherical microcavities PALS gives somewhat higher R values than PCP. On the other hand, the results of IGC may be in better agreement with the PCP data if the FVE size is based on the probe volume at the boiling point, while they are closer to the PALS data if the probe critical volume is considered. With respect to the other techniques, the photochromic probe method revealed a particularly narrow FVE size distribution. This is probably a limit of the PCP method, which not only requires free volume elements of a certain size, but also of a certain shape, in order to have sufficient freedom of motion for the probe molecules to undergo isomerization.

Such information on the shape and interconnectivity of the FVEs was only obtained by MD simulations. These indeed confirmed that many voids have a narrow and extended shape. The MD method revealed a rather wide FVE size distribution. Depending on the calculation method, the MD simulations seem to underestimate the average FVE size found by the other techniques, especially in terms of  $R_{\text{max}}$ . This is related to the fact that experimental techniques are much more sensitive to the void shape than MD, for which an equivalent sphere size can be defined without any physical implications. In real PALS measurements the quenching probability of the probe strongly depends on the void geometry and it is higher in a thin elongated pore than in a spherical pore of the same volume. Very narrow pores may not be detected at all or may be detected as very small, while such pores may be small or large

according to MD, depending on their degree of interconnectivity. The importance of the pore shape is confirmed by the better correspondence of the NMR results with the other experimental methods when a cylindrical pore shape is considered than when a spherical shape is considered. Normally the experimental methods should detect an intermediate average void size compared to the two MD evaluation methods ( $V_{\text{connect}}$  and  $R_{\text{max}}$ ). If this is not the case, this may be due to the approximations used in the MD simulations, for instance in the force field used. In any case, the present study indicates that the pore shape is a fundamental parameter and that a description of the FVE size distribution in terms of the pore size alone is too restrictive. In the PALS experiments, for the same lifetime  $\tau_3$ , processing of the results in terms of channel or slit geometries makes the width of the pore smaller (about 1.2 times for the channel and 1.7 times for the slit) and thus the coincidence with the most probable pore width found by MD simulation ( $R_{\text{max}}$  approximation) better [7.39].

An overview of the main results from the different techniques is given in Table 8. The mean FVE sizes from all experimental techniques are in between the peak maxima from the  $R_{\text{max}}$  and  $V_{\text{connect}}$  MD simulation approaches (Figure 7.9). Summarizing, it may be concluded that all methods detect a slightly higher average FVE size in Hyflon AD80X compared to Hyflon AD60X and this is in agreement with the  $^{129}\text{Xe}$ -NMR data reported in the literature [7.14]. On the other hand there seems to be no substantial difference in the FFV of the two polymer grades according to MD. This is again confirmed by  $^{129}\text{Xe}$ -NMR spectroscopy, which indicates an equal Xenon solubility in both polymers,  $0.19 \text{ cm}^3\text{STP}/(\text{cm}^3\text{atm})$  [7.14].

One of the main conclusions of this work is that for a fair comparison of the different approaches, a discussion on the shape of the FVEs is of fundamental importance. MD is the only method which can provide such information directly. Knowledge of the FVE size and shape distribution is helpful for the understanding of numerous molecular properties of polymeric materials, for instance for the understanding of mass transport in these polymers when used as a membrane material.

## REFERENCES

- [7.1] Y. Huang and D. R. Paul, *Polymer*, 45 (2004) 8377.
- [7.2] R. E. Robertson, *Macromolecules* 18 (1985) 953.
- [7.3] T. S. Chow, *Macromolecules* 17 (1984) 2336.
- [7.4] J. G. Curro, R. R. Lagasse and R. Simha, *Macromolecules*, 15 (1982) 1621.
- [7.5] A. Thran, G. Kroll and F. Faupel, *J. Polym. Sci. B: Polym. Phys.*, 37 (1999) 3344.
- [7.6] C. Nagel, K. Günther-Schade, D. Fritsch, T. Strunskus and F. Faupel, *Macromolecules*, 35 (2002) 2071.
- [7.7] K. Nagai, T. Masuda, T. Nakagawa, B.D. Freeman and I. Pinnau, *Prog. Polym. Sci.*, 26 (2001) 721.
- [7.8] A. M. Polyakov, L. E. Starannikova and Y. P. Yampolskii, *J. Membr. Sci.*, 216 (2003) 241.
- [7.9] Y. P. Yampolskii *Russ. Chem. Rev.*, 76 (2007) 59.
- [7.10] Y. P. Yampolskii, V. Shantarovich, Positron annihilation lifetime spectroscopy and other methods for free volume evaluation in polymers, in: Yu. Yampolskii, I. Pinnau, B. D. Freeman, (Eds.), *Materials Science of Membranes for gas and vapor separation*, Chichester, England, John Wiley & Sons, 2006, Chapter 6, p. 191-210.
- [7.11] D. M. Shrader, Y. C. Jean, *Positron and positronium chemistry*, Elsevier, Amsterdam, 1988.
- [7.12] G. Dlubek, A. P. Clarke, H. M. Fretwell, S. B. Dugdale and M. A. Alam, *Phys. Stat. Sol. A*, 157 (1996) 351.
- [7.13] Y. P. Yampolskii, N. E. Kaliuzhnyi and S. G. Durgaryan, *Macromolecules*, 19 (1986) 846.
- [7.14] G. Golemme, J. B. Nagy, A. Fonseca, C. Algieri and Y. P. Yampolskii, *Polymer*, 44 (2003) 5039.
- [7.15] Y. P. Yampolskii, V. P. Shantarovich, F. P. Chernyakovskii, A. I. Kornilov and N. A. Platé, *J. Appl. Polym. Sci.* 47 (1993) 85.
- [7.16] J. G. Victor and J. M. Torkelson, *Macromolecules*, 20 (1987) 2241.
- [7.17] A. Y. Alentiev, Y. P. Yampolskii, V. P. Shantarovich, S. M. Nemser and N. A. Platé, *J. Membr. Sci.*, 126 (1997) 123.
- [7.18] T. C. Merkel, I. Pinnau, R. Prabhakar, B. D. Freeman, Gas and vapor transport properties of perfluoropolymers, in Yampolskii Yu, Pinnau I and Freeman BD (Eds.), *Materials science of membranes for gas and vapor separation*, Chichester, England, John Wiley & Sons, 2006 (chapter 9).
- [7.19] M. Rudel, J. Kruse, K. Rätzke, F. Faupel, Y. P. Yampolskii, V. P. Shantarovich and G. Dlubek, *Macromolecules*, 41 (2008) 788.

- [7.20] V. Arcella, P. Colaianna, P. Maccone, A. Sanguineti, A. Gordano, G. Clarizia and E. Drioli, *J. Membr. Sci.*, 163 (1999,) 203.
- [7.21] R.S. Prabhakar, B.D. Freeman and I. Roman, *Macromolecules*, 37 (2004) 7688.
- [7.22] L.B. Robeson, *J. Membr. Sci.*, 320 (2008) 390.
- [7.23] C.C. Hu, C. S. Chang, R. C. Ruaan, and J.Y. Lai, *J. Membr. Sci.* 226 (2003) 51.
- [7.24] Z.G. Gardlund, *J. Polym. Sci., Polym. Lett. Ed.*, B6 (1968) 57.
- [7.25] I. Mita, K. Horie and K. Hirao, *Macromolecules*, 22 (1989) 558.
- [7.26] J. Scot Royal and J. M. Torkelson, *Macromolecules*, 25 (1992) 4792.
- [7.27] C. S. P. Sung, I. R. Gould and N. J. Turro, *Macromolecules*, 17 (1984) 1447.
- [7.28] J. Scot Royal, J.G. Victor and J.M. Torkelson, *Macromolecules*, 25 (1992) 729.
- [7.29] M. Ueda, H.B. Kim, T. Ikeda and K. Ichimura, *Chem. Mater.*, 4 (1992) 1229.
- [7.30] M. Ueda, H.B. Kim, T. Ikeda and K. Ichimura, *J. Non-Cryst. Solids*, 163 (1993), 125.
- [7.31] J. Algers, P. Sperr, W. Egger, L. Liskay, G. Kögel, J. de Baerdemaeker and F. H. J. Maurer, *Macromolecules*, 37 (2004) 8035.
- [7.32] F. Serra and E.M. Terentjev, *Macromolecules*, 41 (2008) 981.
- [7.33] R.A. Evans, T.L. Hanley, M.A. Skidmore, T.P. Davis, G.K. Such, L.H. Yee, G.E. Ball and D.A. Lewis, *Nature Materials*, 4 (2005) 249.
- [7.34] C.J. Ellison, J.M. Torkelson, *Nature Materials*, 2 (2003) 695.
- [7.35] C.J. Ellison, J.M. Torkelson, *J. Polym. Sci. B: Polym. Phys.* 40 (2002) 2745.
- [7.36] J. Bartos, *Positron Annihilation Spectroscopy of Polymers and Rubbers*, in: *Encyclopedia of Analytical Chemistry*, Meyres R.A., Ed., Wiley, Chichester, UK, 2000, p.7968.
- [7.37] Y. Kobayashi, W. Zheng, E.F. Meyer, J.D. McGervey, A.M. Jamieson and R. Simha, *Macromolecules*, 22 (1989) 2302.
- [7.38] H.A. Hristow, B. Bolan, A.F. Yee, L. Xie and D.W. Gidley, *Macromolecules*, 29 (1996) 8507.
- [7.39] V.P. Shantarovich *J. Polym. Sci. Part B: Polym. Phys.*, 46 (2008) 2485.
- [7.40] J. Tao *J. Chem. Phys.*, 56 (1972) 5499.
- [7.41] M. Eldrup, D. Lightbody and J.N. Sherwood, *Chem. Phys.*, 63 (1981) 51.
- [7.42] Y.C. Jean *Microchemical J.*, 42 (1990) 72.
- [7.43] B. Jasinska, A.E. Koziel and T. Goworek, *J. Radioanal. Nucl. Chem.*, 210 (1996) 617.
- [7.44] A.D. Mokrushin, A.O. Tatur and V.P. Shantarovich, *Izv. Acad. Nauk SSSR, Ser. Khim.*, 6 (1973) 1216.

- [7.45] G. Consolati, I. Genco, M. Pegoraro and L. Zanderighi, *J. Polym. Sci: Part B: Polym. Phys.*, 34 (1996) 357.
- [7.46] V.P. Shantarovich, I.B. Kevdina, Y. P. Yampolskii and A.Y. Alentiev, *Macromolecules*, 33 (2000) 7453..
- [7.47] J.M. Braun, J.E. Guillet, *Adv. Polym. Sci.*, 21 (1976) 107.
- [7.48] D.N. Theodorou, , Principles of molecular simulation of gas transport in polymers, in: Y. P. Yampolskii, I. Pinnau, B. D. Freeman (Eds.), “Materials Science of Membranes for gas and vapor separation, Chichester, England, John Wiley & Sons, 2006, Chapter 2, 49-94.
- [7.49] D. Hofmann, M. Entrialgo-Castano, A. Le Bret, M. Heuchel and Y. P. Yampolskii, *Macromolecules*, 36 (2003) 8528..
- [7.50] X. Wang, R. D. Raharjo, H. J. Lee, B. D. Freeman and I. C. Sanchez, *J. Phys. Chem. B*, 110 (2006) 12666.
- [7.51] M. Heuchel, D. Hofmann and P. Pullumbi, *Macromolecules*, 37 (2004) 201.
- [7.52] M. Macchione, J.C. Jansen, G. De Luca, E. Tocci, M. Longeri and E. Drioli, *Polymer* 2007, 48, 2619.
- [7.53] J.C. Jansen, M. Macchione and E. Drioli, *J. Membrane Sci.*, 255 (2005) 167.
- [7.54] E. Fischer, *J. Phys. Chem.*, 71 (1967) 3704.
- [7.55] J. Blanc, D. L. Ross, *J. Phys. Chem.*, 72 (1968) 2817.
- [7.56] Y.C. Jean, P. E. Mallon, D.M. Schrader, (Eds), Principles and applications of positron and positronium chemistry. World Scientific. New Jersey, London, Singapore, Hong-Kong 2003.
- [7.57] V. Shantarovich, *J. Nucl. Radiochem. Sci.*, 7 (2006) 37.
- [7.58] R.C. Reid, T.K. Sherwood, *The Properties of Gases and Liquids*. New York: McGraw–Hill, 1966.
- [7.59] V. Arcella, G. Brinati, P. Colaianna, A. Sanguineti, A. Gordano, G. Clarizia, R. Molinari and E. Drioli, Proceedings of Ravello Conference “New Frontiers for Catalytic Membrane Reactors and Other Membrane Processes”, 1999, p.102.
- [7.60] J.C. Jansen, K. Friess and E. Drioli, in preparation.
- [7.61] a) D.N. Theodorou and U.W. Suter, *Macromolecules* 18 (1985) 1467. b) D.N. Theodorou and U.W. Suter, *Macromolecules* 19 (1986) 139.
- [7.62] *Polymer User Guide, Amorphous Cell Section, Version 4.0.0*. Molecular Simulations Inc.: San Diego, CA, 1999.
- [7.63] a) H. Sun and D. Rigby, *Spectrochim Acta A* 53 (1997) 1301; b) D. Rigby, H. Sun, and B. E. Eichinger, *Polym Int* . 44 (1997) 311.
- [7.64] D. Hofmann, L. Fritz, J. Ulbrich, C. Schepers, and M. Boëhning, *Macromol. Theory Simul.*, 9 (2000) 293.

- [7.65] E. Tocci and P. Pullumbi, *Molecular Simulation*, 32 (2006) 145.
- [7.66] J.C. Jansen, M. Macchione and E. Drioli, *J. Membr. Sci.* 287 (2007) 132..
- [7.67] Material Studio software package. San Diego, CA, USA: Accelrys Inc.; 2004.
- [7.68] R.H. Gee, L.E. Fried and R.C. Cook *Macromolecules* 34 (2001) 3050.
- [7.69] D. Hofmann, M. Heuchel, Y.P. Yampolskii, V. Khotimskii and V. Shantarovich, *Macromolecules*, 35 (2002) 2129.
- [7.70] T. A. Andrea, W.C. Swope and H. C. Andersen, *J. Chem. Phys.* 79 (1983) 4576.
- [7.71] H.J.C. Berendsen, J.P.M. Postma, W.F. Van Gunsteren, A. Di Nola and J.R. Haak, *J. Chem. Phys.*, 81 (1984) 3684.
- [7.72] InsightII 4.0.0.P+, Polymerizer, Discover, Amorphous Cell, Builder Sorption Modules 2001, Accelrys Inc., San Diego, CA, USA, 2001.
- [7.73] A. Bondi *J. Phys. Chem.*, 68 (1964) 441.
- [7.74] O. Hölck, M. Böhning, M. Heuchel and D. Hofmann, *J. Membr. Sci.*, in preparation.
- [7.75] The cis-fraction in solution was not available in the literature for 4,4-dinitrostilbene and therefore a value of 85% was assumed for the isomerization efficiency in dilute solution. This is about the average value of various different probes reported in the literature, most of them lying in the range from about 80% to 90%
- [7.76] S. Takeuchi, S. Ruhman, T. Tsuneda, M. Chiba, T. Taketsugu and T. Tahara, *Science*, 322 (2008) 1073.
- [7.77] M. Traetteberg, I. Hilmo and K. Hagen, *J. Mol. Struct.*, 39 (1977) 231.
- [7.78] G. Orlandi and W. Siebrand, *Chem Phys. Lett.*, 30 (1975) 352.
- [7.79] J. B. Birks *Chem. Phys. Lett.*, 38 (1976) 437.
- [7.80] V. P. Shantarovich, T. Suzuki, Y. Ito, K. Kondo, R.S. Yu, P.M. Budd, Y.P. Yampolskii, S.S. Berdonosov and A.A. Eliseev, *Phys. Stat. Sol. (c)*, 4 (2007) 3776.
- [7.81] V. P. Shantarovich, T. Suzuki, C. He, V.A. Davankov, A.V. Pastukhov, M.P. Tsyurupa, K. Kondo and Y. Ito, *Macromolecules* 35 (2002) 9723.
- [7.82] P. Kirkegaard, N.J. Pederson and M. Eldrup PATFIT-88: A data processing system for positron annihilation spectra on mainframe and personal computers, Risoe-M-2740, Risoe National Laboratory DK-4000, Roskilde, Denmark, February (1989).
- [7.83] A.Yu. Alentiev, A.V.P. Shantarovich, T.C. Merkel, V.I. Bondar, B.D. Freeman and Yu.P. Yampolskii, *Macromolecules* 35 (2002) 9513.
- [7.84] a) G. Dlubek, C. Hübner and S. Eichler, *Nucl. Instr. Meth. Phys. Res. B*, 142 (1998) 191. b) G. Dlubek and S. Eichler, *Phys. Stat. Sol.*, 168 (1998) 333.
- [7.85] G. Dlubek, K. Saarinen and H.M. Fretwel, *Nucl. Instr. Meth. Phys. Res. B*, 142 (1998) 139.
- [7.86] J. Liu, Y.C. Jean and H. Yang, *Macromolecules*, 28 (1995) 5774.

- [7.87] Y. P. Yampolskii, V. Berezkin, T. Popova, A. Korikov, B.D. Freeman, V. Bondar and T.C. Merkel, *Polym. Sci. A*, 42 (2000) 679.
- [7.88] Y. P. Yampolskii, S. Soloviev and M. Gringolts, *Polymer*, 45 (2004) 6945.
- [7.89] E. Tocci, D. Hofmann, D. Paul, N. Russo and E. Drioli., *Polymer*, 42 (2001) 521.
- [7.90] F.T. Willmore, X. Wang and I.C. Sanchez, *J. Polym. Sci. B: Polym. Phys.*, 44 (2006) 1385.

## FINAL CONCLUSIONS

The prospect of assessing the properties of polymer/gas systems by examination of detailed atomistic molecular packing models, selecting only the most promising materials for further investigation, seems a reasonable presumption, given the progress in computing power and availability of CPU time is sustained. However, the large gap of several orders of magnitude in system size and time scales between experiment and simulation will not be bridged by capacity and speed alone. Methods are called for that combine experiment and simulation and make possible a deeper understanding of the mechanisms that govern transport mechanism in polymer/gas systems.

In this thesis the transport properties of small molecules through polymeric membranes using computer simulation methods have been investigated in order to provide useful correlations with the microstructure properties of the materials object of study.

Two different types of materials have been chosen to be investigated by Molecular Dynamics (MD) method for the high performances for gases separation exhibited in the field of membrane technology.

In particular fully atomistic simulations are been used to study:

- ◆ Gases and vapour transport and structural analysis of pure and modified rubbery copolymer with high selectivity for polar/non polar gases; the modification *in situ* of these types of membranes by adding variable percentages of chemical additives led to an enhancement of specific surface and permeability properties.
- ◆ Morphological properties of high free volume glassy polymer by quantitative measure of free volume distributions.

Molecular simulations using COMPASS force field were successful in predicting the gas-transport properties of a PEBAX<sup>®</sup>2533 block copolymer and for a pure PTMO homopolymer.

MD simulations give a good representation of the WAXD pattern of the membrane and of the transport of different gas molecules, confirming the representative model boxes. Calculated values for amorphous PEBAX<sup>®</sup>2533 and for amorphous PTMO are nearly identical, both with MD and with TST simulations. MD gives a much better reproduction of the experimental transport data than TST does. MD tends to underestimate *D*, but the discrepancy over the whole range of gases is not more than a factor of 2-3. Grand Canonical Monte Carlo (GCMC) and TST simulations adequately represent solubility coefficients. Interactions between CO<sub>2</sub> and PTMO component of the block copolymer have been detected by radial distribution function.

Fully atomistic investigations of the morphology of the modified PEBAX membranes have been performed to study in details:

- the PEBAX chain mobility in presence of various KET compositions from the analysis of MSD polymer chain in PEBAX/KET 3D models.
- the homogeneity of the modified membranes by detailed analysis of RDF's between KET and PEBAX polar and hydrophobic chemical groups.

Gases and vapour transport properties of PEBAX<sup>®</sup>2533 block copolymer membranes with different concentrations of an aromatic sulphonamide (KET) have been theoretically



calculated and compared with experimental data in order to obtain reciprocal validations and useful correlations.

Radial distribution functions between KET-KET, H<sub>2</sub>O-PEBAX, CO<sub>2</sub>-PEBAX and H<sub>2</sub>O-KET at increasing additive compositions have been analyzed for investigating the possible formation of clusters of additives and the short range interactions between water, polymer matrix and additives in these complex systems.

Going in the direction of a multidisciplinary approach and interconnections of mathematical theoretical method in the VI chapter of this thesis Mesoscale simulations (Dynamic mean field theory (Mesodyn) and dissipative particle dynamics (DPD) utilizing coarse-grained molecular models) have been performed on PA-12 and PEBAX®2533 systems: crystallinity has been incorporated in PA-12 coarse grained model in order to provide a better insight in the microphase separations between hard PA-12 and soft PTMO domains.

In the final chapter a comparative study of five different experimental and computational methods has been presented for the characterization of the overall free volume (FV) and the free volume element (FVE) size and shape distribution in amorphous glassy perfluoropolymers (PFPs). Experimental results from the photochromic probe (PCP) method, positron annihilation lifetime spectroscopy (PALS) and inverse gas chromatography (IGC) were confronted with literature data from <sup>129</sup>Xe-NMR spectroscopy, and the experimental data have been further compared with molecular dynamics (MD) simulations and a combination of studies and the well-known Bondi method, as well as a modified Bondi method. One of the main conclusions of this work is that for a fair comparison of the different approaches, a discussion on the shape of the FVEs is of fundamental importance. MD is the only method which can provide such information directly. Knowledge of the FVE size and shape distribution is helpful for the understanding of numerous molecular properties of polymeric materials, for instance for the understanding of mass transport in these polymers when used as a membrane material.

### SCIENTIFIC PUBLICATIONS

- Gugliuzza A., De Luca G., Tocci E., De Lorenzo L., Drioli E., “Intermolecular interactions as controlling factor for water sorption into polymer membranes, *J. Phys. Chem. B*, 2007, 111(30), 8868 –8878.
- Tocci E., Gugliuzza A., De Lorenzo L., Macchione M., De Luca G., Drioli E., “Transport properties of a co-poly(amide-12-b-ethylene oxide) membrane : a comparative study between experimental and molecular modelling results” *J. Membr. Sci.*, 2008, 323, 316-327.
- Jansen J.C., Macchione M., Tocci E., De Lorenzo L., Yampolskii Y. P., Sanfirova O., Shantarovich V. P., Heuchel M., Hofmann D. and Drioli E., Comparative Study of Different Probing Techniques for the Analysis of the Free Volume Distribution in Amorphous Glassy Perfluoropolymers, *Macromolecules*, 2009, 42 (19), pp 7589–7604.
- De Lorenzo L., Tocci E., Gugliuzza A. and Drioli E. Molecular investigation of water solubility and structural properties of water solubility and structural properties of pure and modified PEBAX models: in preparation.
- De Lorenzo L., Tocci E., Gugliuzza A., Macchione M. and Drioli E., Molecular investigations of gas and vapors transport properties in a modified co-poly(amide-12-b-ethylene oxide) membrane: in preparation.

### CONGRESS PARTICIPATIONS

- ◆ De Lorenzo L., Tocci E., Drioli E., *Molecular Investigation of water solubility and structural properties of pure and modified Pebax models* in proc of 6th Convegno Nazionale sulla Scienza e Tecnologia dei Materiali, 12th-15th June 2007, Perugia, Italy.
- ◆ Jansen J.C., Macchione M., Tocci E., De Lorenzo L., Yampolskii Y. P., Shantarovich V. P., Heuchel M. and Drioli E, *Analysis of the Size Distribution of Local Free Volume in Hyflon® AD Perfluoropolymer Gas Separation Membranes by Photochromic Probes*, in proc of International Congress on Membranes and Membrane Processes, ICOM 2008, 12th-18 th July 2008, Honolulu, Hawaii, USA
- ◆ De Lorenzo L., Tocci E., Gugliuzza A., De Luca G., *Indagine molecolare delle proprietà di trasporto dell’acqua in matrici di PEBAX puri e modificati*, in proc. Convegno G.R.I.C.U. 2008, 14th-17th September 2008, le Castella (KR), Italy.
- ◆ De Lorenzo L., Tocci E., Gugliuzza A., Macchione M. and Drioli E., *Molecular investigations of gas and vapours transport properties in a modified co-poly(amide-12-b-ethylene oxide) membrane* in proc. of EUROMEMBRANE2009, 06th-10th September 2009, Montpellier, France,

---

## RESEARCH EXPERIENCES AND TRAINING COURSES ABROAD

EC-funded Marie Curie *Nanostructured Materials & Membranes Training Course*, 18th-27th June 2008 in Patras, Greece.

*NaPolyNet Demonstration Course* 13th-15th May 2009, Athens, Greece.

Poster Title: L. De Lorenzo, E. Tocci, J.C. Jansen, M. Macchione, Y.P. Yampolskii, V.P. Shantarovich, M. Heuchel, D. Hofmann, and E. Drioli, Experimental and Theoretical Structural Characterization of free volume in Hyflon®AD glassy perfluoropolymers.

Stage of an one month (June 2009) in the *Soft Condensed Matter Group at Leiden Institute of Chemistry*, Leiden University (The Netherlands), for conducting studies on the morphological and transport properties of polymeric blends of material with innovative properties by using mesoscale modeling.

## DIDACTIC EXPERIENCES

From academic year 2007-2008 to the actual, 2009-2010, I'm attempting support educational activities as teaching assistant of General Chemistry course of Engineering Faculty at the University of Calabria.

## NOMENCLATURE

c	sorbed gas concentration ( $\text{cm}^3(\text{STP})/\text{cm}^3$ polymer)
d	lattice spacing (nm)
dS	surface element ( $\text{m}^2$ )
D	self-diffusion coefficient of gas molecules ( $\text{cm}^2/\text{s}$ )
$D_{1/2}$	diffusion coefficient calculated at $t_{1/2}$ of the transient state ( $\text{cm}^2/\text{s}$ )
$D_{\text{slope}}$	diffusion coefficient calculated at $t_{\text{slope}}$ of the transient state $\text{cm}^2/\text{s}$
$D_0$	diffusion coefficient calculated at $t_0$ of the transient state ( $\text{cm}^2/\text{s}$ )
Ed	diffusivity activation energy ( $\text{kJ mol}^{-1}$ )
Ep	permeability activation energy ( $\text{kJmol}^{-1}$ )
$k_b$	Boltzmann's constant (J/K)
kij	rate constant for the particle transition from site I to a site j
h	Planck Constant ( $6.626 \cdot 10^{-34} \text{m}^2 \text{kg} / \text{s}$ )
l	membrane thickness (nm)
m	mass of the particle (g)
$M_w$	molecular weights of polymer
N	number of atoms in the simulation
$N_\alpha$	number of diffusing molecules $\alpha$
$N_i(r)$	the number of atoms of type i in a spherical distance between r and r + dr
$N_f$	the total number of frames used in the RDF analysis
$N_s$	number of sorbate molecules
p	pressure (cmHg)
P	permeability coefficient ( $\text{cm}^3(\text{STP})/(\text{cm}^2 \cdot \text{s} \cdot \text{cmHg}) \cdot 10^{-10}$ )
R	gas constant ( $8.31 \text{kJ mol}^{-1} \text{K}^{-1}$ )
Qi	partition functions of the molecule in microstate i

## NOMENCLATURE

$t_{1/2}$	time during which the flux rises from its initial value to one-half of its final value (i.e. steady state value)
$t_{\text{slope}}$	time between the onset and end set of the sigmoidal permeation curve.
$t_0$	time obtained by extrapolation of the linear steady state section of the permeation curve to the initial pressure.
T	absolute Temperature (K)
Tg	glass-transition temperature (K)
U	sum of nonbonded Coulombic and van der Waals interaction energies(KJ/mol)
$U(\bar{x})$	interaction potential energy between guest molecule at point $\bar{x}$ and the host matrix atoms
V	volume of the simulation cell ( $\text{\AA}^3$ )
$V_i$	volume of the site i
<i>Greek symbols</i>	
$\mathcal{E}$	Partition Function
$\alpha_{ij}$	ideal selectivity between the penetrants i,j
$\Delta 2$	smearing factor of atoms i
$\Delta \mathbf{r}_i$	displacements of atoms i
$\langle \Delta \mathbf{r}_i^2 \rangle$	mean square displacement from the equilibrium position of atoms i
$2\theta$	scattering angle.
$\lambda$	wave length of the incident X-ray beam.
$\rho_i$	bulk density of atoms of type i in the polymer
$\rho_{ij}$	particle transition probability from site i to a particular adjacent site j
$\rho(\bar{x})$	modified equilibrium Boltzman probability density of finding a solute at the position $\bar{x}$ .
$\tau_i$	mean residence time for the probe molecule at site i
$\Omega_i$	crest surface separating sites i and j.

## ACKNOWLEDGMENTS

The author is gratefully for the financial support to:

“MULTIMATDESIGN: Computer aided molecular design of multifunctional materials with controlled permeability properties”, Contract No: NMP3-CT-2005-013644; Thanks to POR CALABRIA 2000/2006 MISURA 3.7 for the financial support and realization of the excellence stage abroad at the Soft Chemistry Group, University of Leiden, Netherland.

I would like to take this opportunity to thank all the people who have given me the greatest support during my PHD studentship and contributed to the good outcome of this thesis.

First of all I would like to thank my supervisor Dr. Elena Tocci for her guidance and constant support during these three years for almost eight hours to day: she has been always present in planning together the research work as well as sharing opinions, feelings and troubles. Thanks to prof. Enrico Drioli for introducing me to membranes and his diligent guidance throughout the project. Thanks to Dr. Giovanni Golemme for fruitful suggestions and discussions, to Dr. John Jansens and Marialuigia Macchione for their kind help and contributions for interpreting experimental data; to Dr AnnaRosa Gugliuzza for experimental contributions and to Dr. Giorgio De Luca for quantomechanical calculations.

I would like to thank prof. Raffaele Molinari for his careful coordination and the directives during the didactic experience as teaching assistant of Chemistry for Engineering Department. Many thanks to Dr. Andrew Emerson for the ready advices in the understanding why a job doesn't run!

I would like to thank all the people of Soft Matter Group of University of Leiden: especially for 100000<sup>th</sup> time thanks to Dr. Agur Sevink for his insightful guidance and encouraging support, for his fast help and multitasking mind and to prof. Hans Fraaije for his overwhelming energy and contagious optimism.

I'm really grateful to my pc-mates Angela Cairo and to the other PHD and post-doc students of ITM-CNR and Chemical Engineering Department: Carla, MariaConcetta, Alessio, Alfredo, Samuel, Sudip, Fernando, Rosalinda, Emma, Adele, Antonella, Silvia for all the funny breaks, the unforgettable experiences during Impossible Missions Abroad and for sharing with me the “enthusiasm” and the sorrow to be temporary employed of research in Italy.

I would to thank the Chemical friends, Tania S & Gianfranco, Tania C, Donatella, Giovanna, Alessandro, Daniela Mavrici, Mazzottina, Emanuela, Francesca, Martigna, Ciccio Tag for being always close to me and for their genuine and endless friendships born in the Chemistry department among studying, laboratories, exams, laughs and “tresette” playing. I would also to thank my house mates, the Italian friends, all the ESA inter and PHD students who have met in Leiden for the unforgettable evenings of fun and drinking beers.

Outside ITM-CNR my life is kept busy and interesting by my nearest and dearest: I would like to thank them for warm hearts and for being a source of joy and happiness every day.

I'm most gratefully to my parents, Laura e Antonio, and my brothers, Carlo e Giuseppe for fortifying my confidence to do what I love and for believing in me, for their endless support, love, care and trust: they are always close to my heart and this thesis is mainly dedicated to them.

Finally I would to thank the part of me that loves learning, knowing new things, to test myself, to overcome my limitations, to understand and investigate. Thanks to this internal “shove” I have the enthusiasm, ideas, effort and “driving” force for doing research in a country where the most seek the easy way to make career and money: I hope it will stay alive, strong and does not succumb...

*Stuff your eyes with wonder, live as if you'd drop dead in ten seconds.  
See the world. It's more fantastic than any dream made or paid for in  
factories. Ask no guarantees, ask for no security, there never was such  
an animal. And if there were, it would be related to the great sloth  
which hangs upside down in a tree all day every day, sleeping life away...*  
Ray Bradbury “Fahrenheit 451”

<b>I. MEMBRANE FOR GAS SEPARATION.....</b>	<b>- 1 -</b>
1. BASIC PRINCIPLES AND APPLICATIONS.....	- 1 -
2. TRANSPORT THROUGH POLYMER MEMBRANES .....	- 4 -
2.1. <i>Fundamentals</i> .....	- 4 -
2.2. <i>Solution_Diffusion Model and Permeability Equations</i> .....	- 5 -
2.3. <i>Performance of membranes for Gases separation: Robeson Plot</i> .....	- 8 -
3. FREE VOLUME .....	- 10 -
3.1. <i>Definition of Free Volume</i> .....	- 11 -
<b>II. THEORETICAL BASIS OF MOLECULAR SIMULATION.....</b>	<b>- 16 -</b>
1. INTRODUCTION .....	- 16 -
2. FORCE FIELD BASED SIMULATION.....	- 18 -
2.1. <i>The ForceField</i> .....	- 18 -
2.2. <i>Molecular dynamics (MD)</i> .....	- 19 -
3. CONDENSED PHASE SIMULATION .....	- 20 -
3.1. <i>Periodic Boundary Conditions</i> .....	- 20 -
3.2. <i>Amorphous Cell Construction</i> .....	- 21 -
3.3. <i>The Concept of Ensembles</i> .....	- 21 -
4. SIMULATION OF GAS TRANSPORT PROPERTIES .....	- 22 -
4.1. <i>Calculation of diffusion coefficients</i> .....	- 22 -
4.2. <i>TST method</i> .....	- 24 -
4.3. <i>Calculation of solubility coefficients</i> .....	- 26 -
4.3.1 GCMC method .....	- 26 -
4.3.2 Hildebrand Solubility .....	- 26 -
5. FREE VOLUME ANALYSIS .....	- 27 -
<b>III. TRANSPORT PROPERTIES OF A COPOLY(AMIDE-12-B-ETHYLENEOXIDE) MEMBRANE: A COMPARATIVE STUDY BETWEEN EXPERIMENTAL AND MOLECULAR MODELING RESULTS .....</b>	<b>- 31 -</b>
1. MATERIALS: POLY(ETHER-B-AMIDE) COPOLYMER MEMBRANES .....	- 31 -
1.1. <i>Introduction</i> .....	- 31 -
1.2. <i>Gas transport across PEBAX membrane</i> .....	- 32 -
1.3. <i>Atomistic Packing Models</i> .....	- 33 -
2. RESULTS AND DISCUSSION .....	- 37 -
2.1. <i>Structural Properties – WAXD</i> .....	- 37 -
2.2. <i>Experimental transport properties</i> .....	- 38 -
2.3. <i>MD simulations</i> .....	- 42 -
2.3.1 Diffusion coefficients .....	- 42 -
2.3.2 Compared theoretical and experimental diffusion data .....	- 43 -



2.3.3 Solubility coefficients.....	- 47 -
2.3.4 Compared theoretical and experimental solubility data.....	- 48 -
2.3.5 Radial distribution function (RDF) analysis.....	- 50 -
2.3.6 Permeability coefficients.....	- 50 -
3. CONCLUSIONS .....	- 51 -
<b>IV. WATER TRANSPORT PROPERTIES OF MODIFIED PEBAX MEMBRANES.....</b>	<b>- 54 -</b>
1. MODIFIED POLY(ETHER-B-AMIDE) COPOLYMER MEMBRANES .....	- 54 -
1.1. <i>Introduction</i> .....	- 54 -
1.2. <i>Computational Details</i> .....	- 55 -
2. RESULTS AND DISCUSSIONS .....	- 59 -
2.1. <i>Morphological Investigations</i> .....	- 59 -
2.1.1 Chain Mobility .....	- 59 -
2.1.2 Homogeneity of the layers: Interactions Polymer-Additives.....	- 60 -
2.2. <i>Water Transport Properties</i> .....	- 62 -
2.3. <i>Intermolecular Interactions as Controlling Factor for Water Sorption into Polymer Membranes</i> .....	- 65 -
3. STRUCTURAL ANALYSIS .....	- 68 -
3.1. <i>Interactions KET-KET</i> .....	- 68 -
3.2. <i>Interactions H<sub>2</sub>O-PEBAX and H<sub>2</sub>O-KET</i> .....	- 70 -
4. CONCLUSIONS .....	- 72 -
<b>V. MOLECULAR INVESTIGATIONS OF GAS AND VAPOURS TRANSPORT PROPERTIES IN A MODIFIED CO-POLY(AMIDE- 75 -12-B-ETHYLENE OXIDE) MEMBRANE.....</b>	<b>- 75 -</b>
1. INTRODUCTION .....	- 75 -
2. RESULTS AND DISCUSSIONS .....	- 77 -
2.1. <i>Gases transport properties</i> .....	- 77 -
2.2. <i>Structural analysis: Radial Distribution Functions</i> .....	- 80 -
3. CONCLUSIONS .....	- 81 -
<b>VI. MESOSCALE SIMULATION OF MORPHOLOGY AND TRANSPORT PROPERTIES IN PEBAX MEMBRANES.....</b>	<b>- 83 -</b>
1. INTRODUCTION .....	- 83 -
1.1. <i>Problem Definition</i> .....	- 83 -
1.2. <i>Experimental Background</i> .....	- 83 -
1.3. <i>Aim of the work</i> .....	- 84 -
2. METHODS .....	- 85 -
2.1. <i>Dissipative Particle Dynamics (DPD)</i> .....	- 85 -
2.2. <i>Dynamic Density Functional Theory (DDFT)</i> .....	- 87 -
3. PARAMETER DERIVATION .....	- 88 -
3.1. <i>Flory-Huggins parameter estimation</i> .....	- 88 -

3.2. <i>Volume Matching Details</i> .....	- 90 -
4. RESULTS AND DISCUSSION.....	- 91 -
4.1. <i>DDFT and DPD simulations</i> .....	- 91 -
5. CONCLUSIONS .....	- 94 -
<b>VII. ANALYSIS OF THE FREE VOLUME DISTRIBUTION IN AMORPHOUS GLASSY PERFLUOROPOLYMERS .....</b>	<b>- 98 -</b>
1. MATERIALS: PERFLUOROPOLYMERS.....	- 98 -
1.1. <i>General Characteristics</i> .....	- 98 -
2. INTRODUCTION .....	- 100 -
2.1. <i>Free volume in polymers</i> .....	- 100 -
2.2. <i>Photochromic probing</i> .....	- 101 -
2.3. <i>Positron annihilation lifetime spectroscopy</i> .....	- 104 -
2.4. <i>Inverse gas chromatography</i> .....	- 105 -
2.5. <i>Molecular dynamics simulations</i> .....	- 105 -
2.6. <i>Scope</i> .....	- 105 -
3. RESULTS AND DISCUSSIONS .....	- 106 -
3.1. <i>Generation and equilibration of polymer structures</i> .....	- 106 -
3.2. <i>Free volume probing method</i> .....	- 109 -
3.3. <i>Photochromic probe method</i> .....	- 110 -
3.3.1 <i>Photoisomerization and UV-Visible characterization</i> .....	- 110 -
3.3.2 <i>Reaction kinetics and progress of the photoisomerization reaction</i> .....	- 111 -
3.3.3 <i>Determination of molar absorption coefficients</i> .....	- 112 -
3.3.4 <i>Determination of the total isomerization volume of the photochromic molecules and the FVE size distribution in the films</i> .....	- 113 -
3.3.5 <i>Comments and critical remarks</i> .....	- 114 -
3.4. <i>Positron annihilation lifetime spectroscopy</i> .....	- 115 -
3.5. <i>Inverse gas chromatography</i> .....	- 117 -
3.6. <i>Molecular Dynamics Simulations</i> .....	- 119 -
3.6.1 <i>Generation and equilibration of polymer structures and qualitative free volume evaluation</i> .....	- 119 -
3.6.2 <i>Quantitative analysis of the free volume distribution</i> .....	- 122 -
3.6.3 <i>Modified Bondi method</i> .....	- 126 -
4. COMPARISON OF THE METHODS AND CONCLUSIONS.....	- 127 -